Study on Ruthenium Complexes and Methylene Blue Based Photosensitizers for Visible Light Bactericidal Action

THESIS

Submitted in partial fulfilment
of the requirements for the degree of
DOCTOR OF PHILOSOPHY

by

PRIYADARSHINI PARAKH

Under the Supervision of
Prof. HALAN PRAKASH

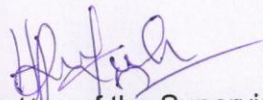
BITS Pilani
Pilani | Dubai | Goa | Hyderabad

BIRLA INSTITUTE OF TECHNOLOGY AND SCIENCE, PILANI

2016

BIRLA INSTITUTE OF TECHNOLOGY AND SCIENCE, PILANI

CERTIFICATE

This is to certify that the thesis entitled **"Study on Ruthenium Complexes and Methylene Blue Based Photosensitizers for Visible Light Bactericidal Action"** and submitted by **Priyadarshini Parakh** ID No **2010PHXF016G** for award of Ph.D. of the Institute embodies original work done by her under my supervision.

Signature of the Supervisor

Name in capital letters: HALAN PRAKASH

Designation: Associate Professor

Date: 14/7/2016

DEDICATED TO............
MY GRANDPARENTS
AND MY PETS

for their constant support and unconditional love.

I love you all dearly.

Acknowledgements

Abstract

The combined use of photosensitizer (PS) and light to kill cancerous and microbial cells has emerged as photodynamic therapy (PDT), and photodynamic antimicrobial chemotherapy (PACT), respectively. PSs are known to generate reactive oxygen species (ROS) on photo excitation that has the ability to kill cells. Moreover, recent studies indicate that PACT agents have been useful for light induced water disinfection. The PSs can be organic compounds, transition metal complexes, bioconjugates or nanoparticle systems. The recovery of homogeneous PS by adsorption from disinfected water is important to obtain water free of microbes and PS. Ruthenium complexes as PSs for visible light water disinfection and their removal from water after disinfection have not been studied. A photostable PS which retains its activity after adsorption, and does not leach is desirable. Furthermore, nano hybrid systems of PS and nanoparticles are known. However, their effect on bacterial photoinactivation has not been well studied. Light emitting diodes (LEDs) are emerging as suitable and promising light sources for photoinactivation of bacteria. A brief introduction on all the above facts is presented in chapter 1. Gap in the literature, on the use of PSs for photoinactivation of bacteria is presented in chapter 1. Two ruthenium complexes namely, $[Ru(bpy)_2(phendione)]^{2+}$, $[Ru(phendione)_3]^{2+}$ have been demonstrated to kill both Gram-positive and Gram-negative bacteria in water using LED as visible light source. These complexes were also effectively removed from water using activated carbon (AC) and silica, and these results are presented in Chapter 2. Further, ruthenium complexes ($[Ru(bpy)_2(phendione)]^{2+}$, $[Ru(bpy)_3]^{2+}$) adsorbed onto AC were shown to inactivate bacteria without leaching of complexes and reused for at least 5 cycles (Chapter 3). Nano hybrid systems consisting of positively charged $[Ru(bpy)_3]^{2+}$ and negatively charged Ag-GSH showed the ability to completely photoinactivate both Gram-positive and Gram-negative bacteria in water. The results reveal that the $[Ru(bpy)_3]^{2+}$ concentration required for photoinactivation in presence of Ag-GSH was significantly reduced as compared to only complex (Chapter 4). Visible light irradiation of both Gram-positive and Gram-negative bacteria in presence of $[RuCl(bpy)_2(ATPh)]^+$ resulted in complete photoinactivation of bacteria (Chapter 5). MB adsorbed onto magnetic hydrogen titanate nano sheets (MB+FHTNS) was shown to completely photoinactivate bacteria for at least 5 cycles (Chapter 6).

Table of Contents

List of Tables

List of Figures

xvii

List of Units, Symbols and Abbreviations

Units:

1.	Å	Angstrom
2.	µg/ml	Microgram per millilitre
3.	cm^{-1}	Per centimetre
4.	J/cm^2	Joules per centimetre square
5.	keV	Kilo electron volt
6.	kV	Kilovolts
7.	mA	Milliampere
8.	mg	Milligram
9.	mg/ml	Milligram per millilitre
10.	ml	Millilitre
11.	mM	Millimolar
12.	mm^2	Millimetre square
13.	mW/cm^2	Milliwatt per centimetre square
14.	nm	Nanometre
15.	µl	Microlitre
16.	µm	Micrometre
17.	µM	Micromolar
18.	µg	Microgram
19.	m/z	mass to charge ratio
20.	ng	Nanogram
21.	ppm	Parts per million
22.	rpm	Revolutions per minute

Symbols:

23.	°C	Degree Celsius
24.	$^1O_2$	Singlet Oxygen
25.	Ag	Silver
26.	Ag^+	Silver ions
27.	$AgNO_3$	Silver nitrate
28.	Au	Gold
29.	$BaSO_4$	Barium sulphate
30.	C	Concentration at a given time
31.	C_e	Equilibrium concentration of adsorbate (mg/l)
32.	Cl	Chlorine
33.	C_o	Initial concentration
34.	H_2O_2	Hydrogen peroxide
35.	HCl	Hydrochloric acid
36.	HNO_3	Nitric acid
37.	K	Potassium

38.	KBr	Potassium bromide
39.	KCl	Potassium chloride
40.	K_F	Freundlich adsorption capacity
41.	m_a	Mass of complex adsorbed by adsorbent
42.	m_d	Mass of desorbed complex into solution
43.	n	Freundlich adsorption intensity
44.	Na	Sodium
45.	$NaBH_4$	Sodium borohydride
46.	$O_2^{\bullet-}$	Superoxide Radical
47.	O_3	Ozone
48.	$^{\bullet}OH$	Hydroxyl Radical
49.	Q^o	Langmuir monolayer adsorption capacity (mg/g)
50.	b	Langmuir constant related to free adsorption energy
51.	q_e	Amount of substance adsorbed per unit weight of adsorbent at equilibrium (mg/g)
52.	Ru	Ruthenium
53.	SiOH	Silanol group
54.	Si-O-Si	Siloxane group
55.	TiO_2	Titanium Dioxide
56.	Φ	Quantum yield
57.	λ	Wavelength

Abbreviations:

58.	AC	Activated Carbon
59.	AHP	2-amino-3-hydroxypyridine
60.	aq	Aqueous
61.	ATPh	4-aminothiophenol
62.	*B. subtilis*	*Bacillus subtilis* (NCIM 2545)
63.	bpy	2,2'-bipyridine
64.	CFU	Colony forming units
65.	Conc	Concentration
66.	DCM	Dichloromethane
67.	DMF	N,N-Dimethylformamide
68.	DNA	Deoxyribonucleic Acid
69.	DPBF	1,3-diphenylisobenzofuran
70.	*E. coli*	*Escherichia coli* (NCIM 2345)
71.	EDS	Energy Dispersive X-ray Spectroscopy
72.	ESI-MS	Electrospray Ionisation Mass Spectrometry
73.	FTIR	Fourier Transform Infrared Spectroscopy
74.	FHTNS	Ferrous Hydrogen Titanate Nano Sheets
75.	GSH	Glutathione
76.	HPLC	High Performance Liquid Chromatography
77.	HTNS	Hydrogen Titanate Nano Sheets

78.	ICP-OES	Inductively Coupled Plasma Atomic Emission Spectroscopy
79.	IR	Infra red
80.	IUPAC	International Union of Pure and Applied Chemistry
81.	LED	Light emitting diode
82.	LMCT	Ligand to metal charge transfer
83.	MLCT	Metal to ligand charge transfer
84.	MB	Methylene Blue
85.	NB	Nutrient Broth
86.	NCIM	National Collection of Industrial Microorganisms
87.	NCL	National Chemical Laboratory
88.	NPs	Nanoparticles
89.	*P. aeruginosa*	*Pseudomonas aeruginosa* (NCIM 2581)
90.	PACT	Photodynamic Antimicrobial Chemotherapy
91.	PBS	Phosphate Buffered Saline
92.	PDT	Photodynamic Therapy
93.	phendione	1,10- Phenanthroline-5,6-dione
94.	PI	Propidium Iodide[®]
95.	PM	Photoactive molecule
96.	PS	Photosensitizer
97.	PTFE	Polytetrafluorethylene
98.	RB	Rose Bengal
99.	ROS	Reactive Oxygen Species
100.	RNA	Ribonucleic Acid
101.	*S. aureus*	*Staphylococcus aureus* (NCIM 2127)
102.	SEM	Scanning Electron Microscopy
103.	SGW	Simulated Ground Water
104.	SODIS	Solar Disinfection
105.	UV	Ultra violet
106.	vis	Visible
107.	WD	Working distance
108.	wt%	Weight percent
109.	XRD	X-ray diffraction

Table of content for chapters

Chapter 1

Introduction

Highlights:

1. Generation of ROS by photoactive molecules.

2. PDT and PACT as methods to kill cancerous cells and microbes.

3. Organic compounds, inorganic metal complexes, bioconjugates and nanoparticle systems as photosensitizers.

4. Charge transfer complexation between photosensitizers and nanoparticles.

5. Water disinfection using homogeneous and heterogeneous photosensitizers.

6. Recovery of photosensitizers by adsorption.

7. LED as light source.
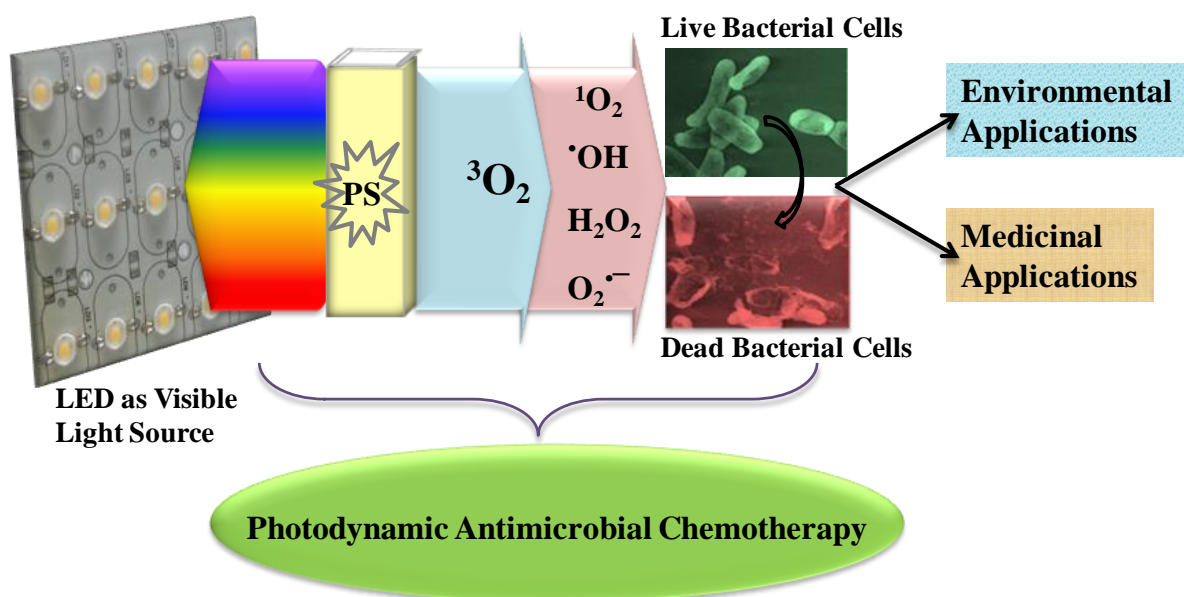
1.1. Introduction:

1.1.1. Photochemistry:

Visible light is part of the electromagnetic radiation (EMR) received from sun (Figure 1.1). Visible spectral region (400-750 nm) of EMR is perceived by human eyes [Stochel et al., 2009] and this energy drives the various photobiological processes on earth i.e., photosynthesis, phototropism, phototaxis, photoperiodism [Szaciłowski et al., 2005, Milgrom, 1997, Wolken, 1998, Suppan, 1994, Bensasson, 1999, Stochel et al., 2009]. Ultraviolet (UV) radiation that fall in the wavelength range of 100-400 nm, have harmful effects, especially UV-C (200-280 nm) can permanently cause cell damage and lead to cell death. Most of UV-C radiation is absorbed by the ozone layer of the earth's atmosphere [Stochel et al., 2009]. The relatively longer wavelength radiation (750-2500 nm), i.e., the infrared (IR) rays are absorbed by earth's surface and clouds and re-emitted to atmosphere. Also, certain gases in atmosphere like CO_2, CH_4, water vapours etc. absorb IR rays and radiate them in all directions that are responsible for maintaining atmosphere and surface of earth warmer [Szaciłowski et al., 2005].
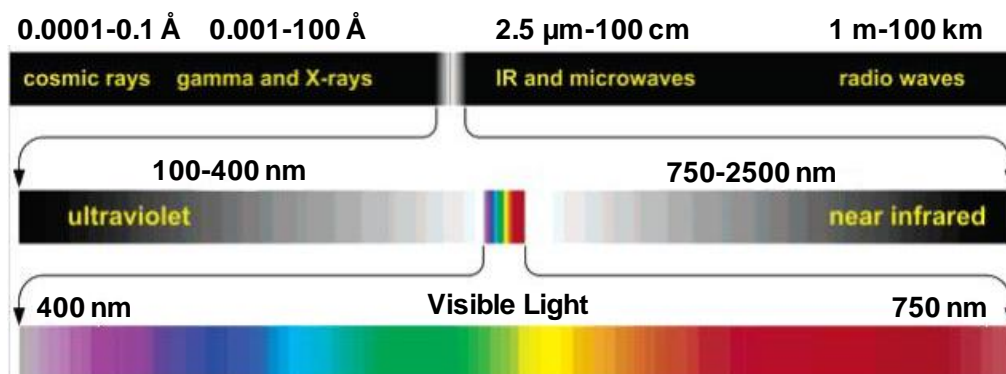
Figure 1.1: Representation of spectrum of electromagnetic radiation (EMR).

In general, molecular photochemistry is a branch of chemistry concerned with the study of physical changes, and chemical reactions of molecules caused by absorption of light [Rohatgi-Mukherjee, 1986, Turro et al., 2009]. Usually, UV (100-400 nm), Visible (400-750 nm) or IR (750-2500 nm) radiations cause the photophysical and photochemical changes of organic and inorganic molecules [Szaciłowski et al., 2005, Balzani et al., 1996, DeRosa et al., 2001, Stochel et al., 2009, IUPAC Gold Book].

The two laws of photochemistry are:

1. First law or Grotthuss-Draper law: Light must be absorbed by a molecule for photochemical reactions to take place.

2. Second law or Stark-Einstein law or photoequivalence law: For each photon of light absorbed by a chemical system, only one molecule is activated for subsequent reaction.

Quantum Yield (Φ) represents the efficiency of a photochemical reaction. It is defined as "number of moles of a reactant disappearing or number of moles of a product forming per einstein of monochromatic light absorbed (1 einstein = 1 mole of photons) [DeRosa et al., 2001, Rohatgi-Mukherjee, 1986, Turro et al., 2009].

$$\Phi(\lambda) = \frac{\text{moles of reactant consumed or product formed}}{\text{moles of photons absorbed}}$$

Where, one mole of photons = 6.023 x 10^{23} photons or 1 einstein.

Quantum yield can vary from 0 to 1. The unity quantum yield represents an ideal photochemical reaction and it is the theoretical maximum [Kornblum, 2010, Bansal, 1998].

1.1.2. Fundamental photochemical processes:

A molecule has quantized electronic energy states. The electronic ground state of the molecule is a singlet state (S_0). Absorption of a photon (hv) causes excited singlet states (Figure 1.2). Photon absorption is followed by a rapid vibrational relaxation (vr). Higher excited states can undergo vr that causes the molecule to reach its first electronic excited state (S_1). S_1 state can return to S_0 state by radiative fluorescence (f) or non radiative internal conversion (ic). S_1 can convert to first excited triplet state (T_1) by intersystem crossing (isc) with high quantum yield. Excited molecule in T_1 state can release energy by radiative phosphorescence (p) or return to S_0 by non radiative (nr) mode. Photon absorption by a molecule changes its electronic distribution and is represented by Jablonski diagram (Figure 1.2) [Szaciłowski et al., 2005, Balzani et al., 1996, DeRosa et al., 2001, Rohatgi-Mukherjee, 1986, Turro et al., 2009, Wainwright, 2009, Stochel et al., 2009, Jablonski, 1933, Elumalai et al., 2002].
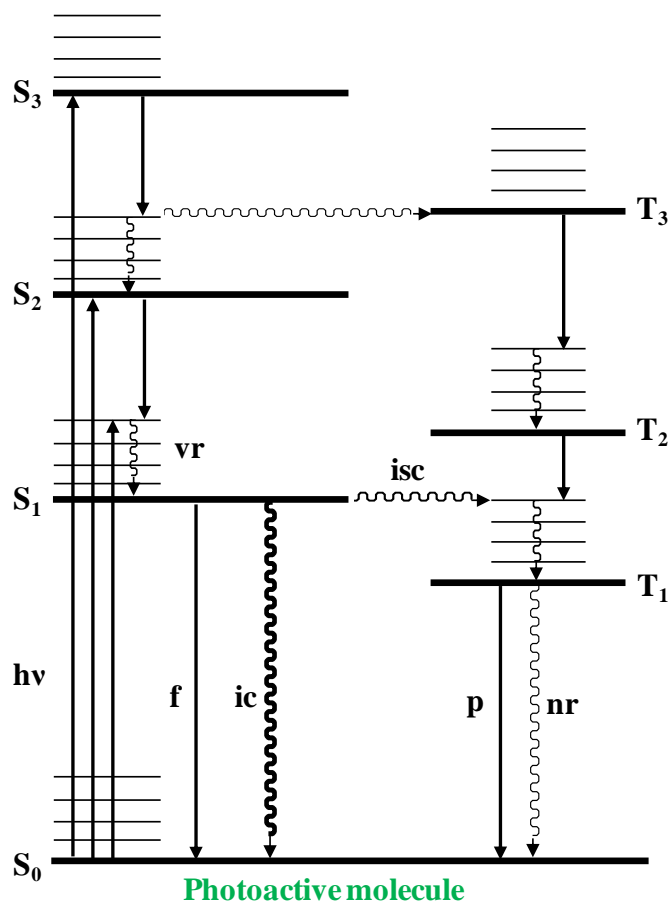
Figure 1.2: Fundamental photochemical and photophysical processes.

1.1.3. Photochemical processes in metal complexes:

The electronic transitions in a metal complex are represented in Figure 1.3. There are four main types of transitions that are possible in metal complexes.

(i)   L-L: Ligand-Ligand transition. In this type of transition, electron is usually excited from ligand π orbital to ligand π^* orbital. LL is also called as ligand-field transition.

(ii) d-d: d-d transition. This represents metal centred transition, where an electron is excited from a metal ion d orbital to an unoccupied metal ion d orbital. d-d transition usually occurs in transition metal complexes.

(iii) LMCT: Ligand to Metal Charge Transfer. In this type of transition electron is excited from ligand to metal.

(iv) MLCT: Metal to Ligand Charge Transfer. This transition is characterised by transfer of electron from metal to ligand.
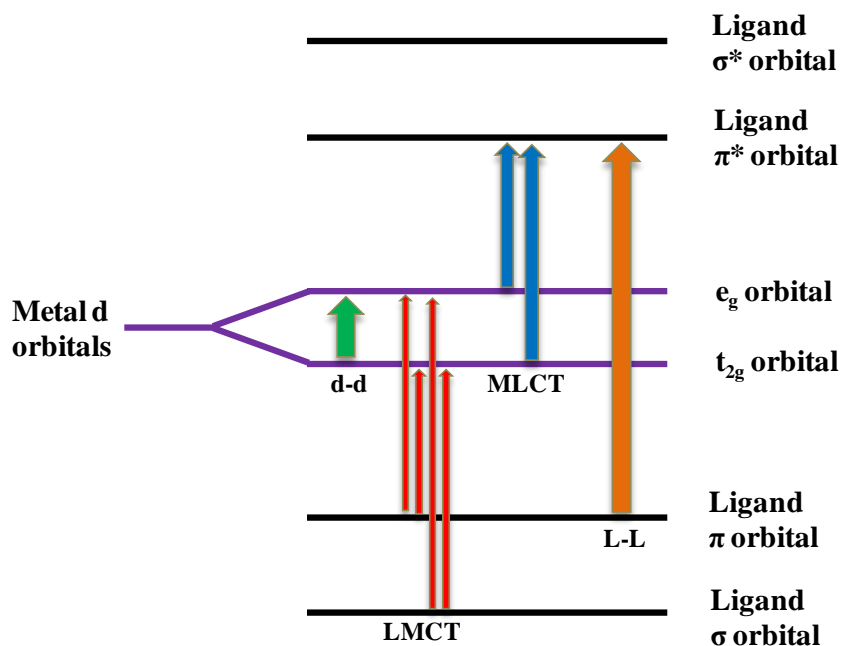
Figure 1.3: Electronic transitions in transition metal complexes.

1.2. Review of literature:

1.2.1. Generation of reactive oxygen species (ROS) by photoactive molecules:

A photoactive molecule (PM) in ground state absorbs light of suitable wavelength and forms singlet excited state ($PM^*(S_1)$) that could also undergo isc to form triplet state ($PM^*(T_1)$), as represented in equation 1 and as shown in Figure 1.2. Usually, T_1 state has relatively longer lifetime (in μs range) as compared to S_1 state (in ns range) [DeRosa et al., 2002]. The T_1 state can transfer electron to oxygen and produce superoxide ($O_2^{\cdot-}$) free radical (equation 2) (Figure 1.4) that is called as Type I mechanism [Bilski et al., 1993, Ma and Jiang, 2001, Huang et al., 2012, Sperandio et al., 2013]. It is important to note that, $O_2^{\cdot-}$ can also undergo secondary reactions, to produce hydrogen peroxide (H_2O_2) and oxygen (equation 3), in presence of an enzyme called superoxide dismutase (SOD) [Castano et al., 2004]. Moreover, $O_2^{\cdot-}$ also reduces metal ions such as iron (Fe^{3+}) and copper (Cu^{2+}) present in cells. These reduced metal ions (Fe^{2+}, Cu^+) break the oxygen–oxygen bond in H_2O_2 to form hydroxyl radical ($^{\cdot}OH$) and hydroxide ion (OH^-) (equation 4) [Castano et al., 2004]. Further, $O_2^{\cdot-}$ itself is not very reactive in biological systems. H_2O_2 in micromolar quantities is also not very harmful [Neyens and Baeyens, 2003, Pignatello et al., 2006]. However, the decomposition to hydroxyl radical is deleterious to cells [Neyens and Baeyens, 2003, Pignatello et al., 2006]. $^{\cdot}OH$ is highly reactive and damage most of the biomolecules. Hydroxyl radicals can cause lipid

peroxidation, mutations in nucleic acids, oxidation of carbohydrates and damage amino acids (e.g. convert phenylalanine to m-tyrosine and o-tyrosine) [Wainwright, 2009, Girotti, 1985, Bachowski et al., 1994, Bachowski et al., 1991, Buchko et al., 1993].

$$PM\ (S_0) \xrightarrow{h\nu} PM^*(S_1) \xrightarrow{isc} PM^*(T_1) \ .... \ \textbf{(1)}$$

$$PM^*(T_1) + O_2 \xrightarrow{e^- \ transfer} PM^+ + O_2^{\bullet-} \ .... \ \textbf{(2)}$$

$$O_2^{\bullet-} + O_2^{\bullet-} \xrightarrow{SOD} H_2O_2 + O_2 \ .... \textbf{(3)}$$

$$H_2O_2 \xrightarrow{M^+} 2HO^{\bullet} + OH \ .... \textbf{(4)}$$
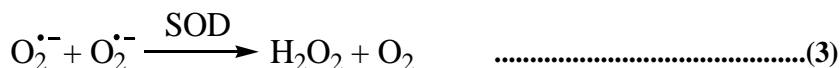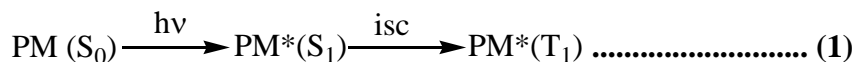
Where $M^+ = Fe^{2+}, Cu^+$
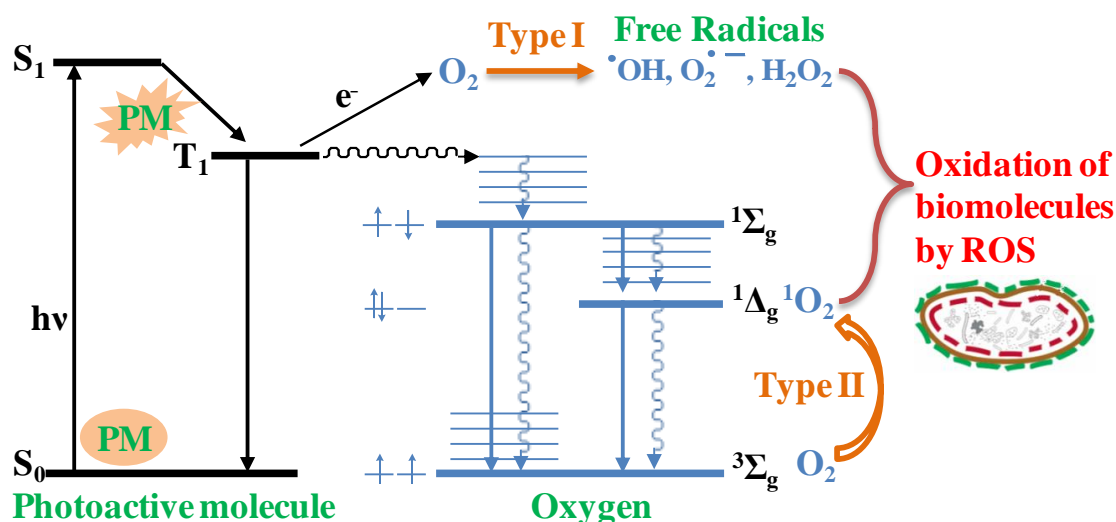
Figure 1.4: Generation of Reactive Oxygen Species (ROS) by photoactive molecule.

Additionally, the T_1 state can transfer energy to oxygen. Dioxygen (O_2) occurs as triplet state naturally in its ground state. Energy transfer from T_1 of PM* to O_2 generates highly reactive singlet oxygen ($^1O_2$) (equation 5) (Figure 1.4). The process of formation of $^1O_2$ via energy transfer is referred as Type II mechanism [Huang et al., 2012, Sperandio et al., 2013, Castano et al., 2004, DeRosa et al., 2002]. $^1O_2$ is a strong electrophile and oxidizes many cellular enzymes leading to protein synthesis inhibition, altering DNA structure and disrupting cell membrane integrity [Grune et al., 2001, Midden and Dahl, 1992, Girotti, 1983, Buchko et al., 1995, Ravanat et al., 1995].

$$PM\ (T_1) + {}^3O_2 \xrightarrow[transfer]{Energy} PM\ (S_0) + {}^1O_2 \ .... \ \textbf{(5)}$$

6
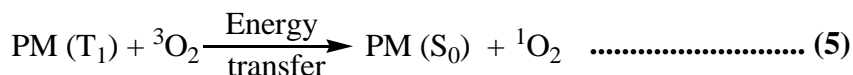
The photoactive molecule can be selectively accumulated in the target tumor tissue, and the light irradiation of the tumours treated with photoactive molecules can be spatially and temporally controlled, which generates ROS and selectively kills cancerous cells [Yoon et al., 2013, Detty et al., 2004]. Thus, the technique of using monochromatic and energetic laser light beams in combination with photoactive molecule to generate ROS that kills the cancer cells is a promising strategy and emerged as photodynamic therapy (PDT) for cancer treatment [Castano et al., 2004]. Importantly, the application of PDT against microbes is called photodynamic antimicrobial chemotherapy (PACT) [Sperandio et al., 2013]. A variety of photoactive molecules have been developed as photosensitizers (PSs) which has the ability to inactivate human cell lines as well as microbes such as bacteria etc. [Szaciłowski et al., 2005, Stochel et al., 2009, Wainwright, 2009].

1.2.2. Cellular damage of bacteria in PACT:

Photo-antibacterial action is extremely destructive for microbes because of two main reasons: (i) multiple sites of attack and (ii) lack of effective microbial defensive mechanisms [Szaciłowski et al., 2005]. ROS lead to non-specific damage to multiple components of bacteria, such as cytoplasmic membrane, intracellular proteins, and DNA [Stochel et al., 2009, Wainwright, 2009]. Damage to the cytoplasmic membrane leads to altered permeability of cellular membranes to potassium and calcium ions, causing leakage of cellular contents or inactivation of membrane transport systems and enzymes [Midden and Dahl, 1992, Girotti, 1985]. There is also evidence that treatment of bacteria with various PS and light leads to nucleic acids (DNA or RNA) damage (Figure 1.5) [Hamblin and Hasan 2004, Grune et al., 2001, Buchko et al., 1993].

Although cells have several natural defenses against ROS, the level of redox imbalance inflicted by PACT is several orders of magnitude larger than the level or protection allowed by enzymatic and molecular antioxidant species in the cell [Demidova and Hamblin, 2004]. Besides, antioxidant cellular enzymes such as catalase and superoxide dismutase are inactivated by singlet oxygen [Hamblin and Hasan 2004]. The above facts reveal that an important benefit of PACT is the absence of microbial resistance and, thus, a similar efficacy against conventional drug-sensitive and drug-resistant microbial strains [Hamblin and Jori 2011].
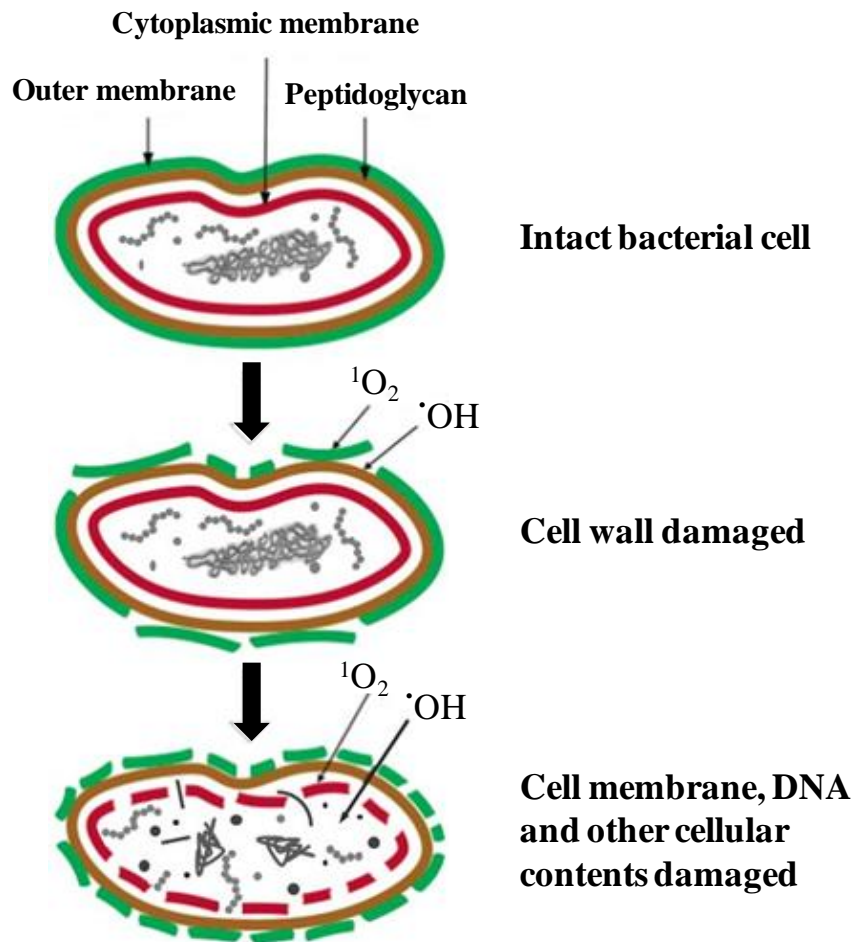
Figure 1.5: Cellular damage of bacteria by ROS.

The highly reactive $^{\cdot}$OH radical can be scavenged by mannitol, melatonin, α-tocopherol and glutathione [Matés et al., 2012, Reiter et al., 2000, Girotti, 2001, Murata et al., 1986, Taylor et al., 1980]. A few $^{1}O_2$ quenchers are sodium azide, histidine, cholesterol, β-carotene, imidazole, α-tocopherol, tryptophan and reduced glutathione [Perotti et al., 2002, Girotti et al., 2000, Song et al., 1999, Henderson and Miller, 1986]. Singlet oxygen can also be spectrophotometrically detected using probes such as 2-amino-3-hydroxypyridine (AHP) and 1,3-diphenylisobenzofuran (DPBF) (Figure 1.6) [Komagoe et al., 2001, Amat-Guerri et al., 1999, Gomes et al., 2013, Pia Donzello et al., 2012]. The absorbance of the probes reduces in the presence of $^{1}O_2$ due to the oxidation and consequent fading of the probe [Wainwright, 2009]. Change in absorbance of AHP and DPBF is monitored at their λ_{max}, 318 nm and 414 nm respectively.
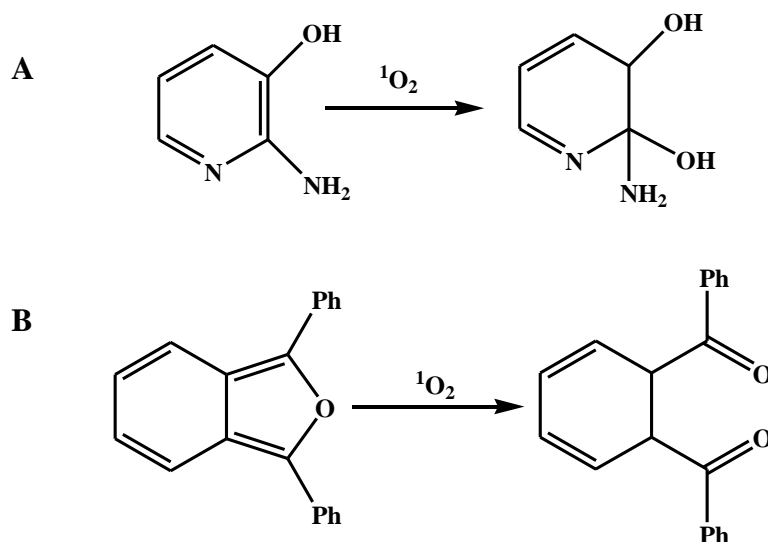
Figure 1.6: Probes for spectrophotometric detection of singlet oxygen and their possible products formed after reaction with singlet oxygen, (A) 2-amino-3-hydroxypyridine and (B) 1, 3-diphenylisobenzofuran.

1.2.3. Effect of photogenerated ROS on Gram-positive and Gram-negative bacteria:

In the 1990s, it was reported that there was distinction in susceptibility between Gram-positive and Gram-negative bacteria towards PACT [Dahl et al., 1988]. The high susceptibility of Gram-positive species was explained based on cell wall composition. The cytoplasmic membrane of Gram-positive bacteria allows PS to cross as it is surrounded by a relatively porous layer of peptidoglycan and lipoteichoic acid (Figure 1.7) [Hamblin et al., 2004, Maclean et al., 2009, Dahl et al., 1988].

On the other hand, in case of Gram-negative bacteria the cell envelope consists of two cytoplasmic membranes that are separated by peptidoglycan-containing periplasm (Figure 1.7). The outer membrane forms a physical and functional barrier between the cell and its environment. In the outer membrane, several different proteins are present; some of them function as pores to allow passage of nutrients, whereas others have an enzymatic function or are involved in maintaining the structural integrity of the outer membrane and the shape of the bacteria. This extra outer membrane may provide resistance to Gram-negative bacteria against ROS generated during photolysis [Hamblin et al., 2004, Maclean et al., 2009, Dahl et al., 1988].

A Structure of Gram Positive bacterial cell wall
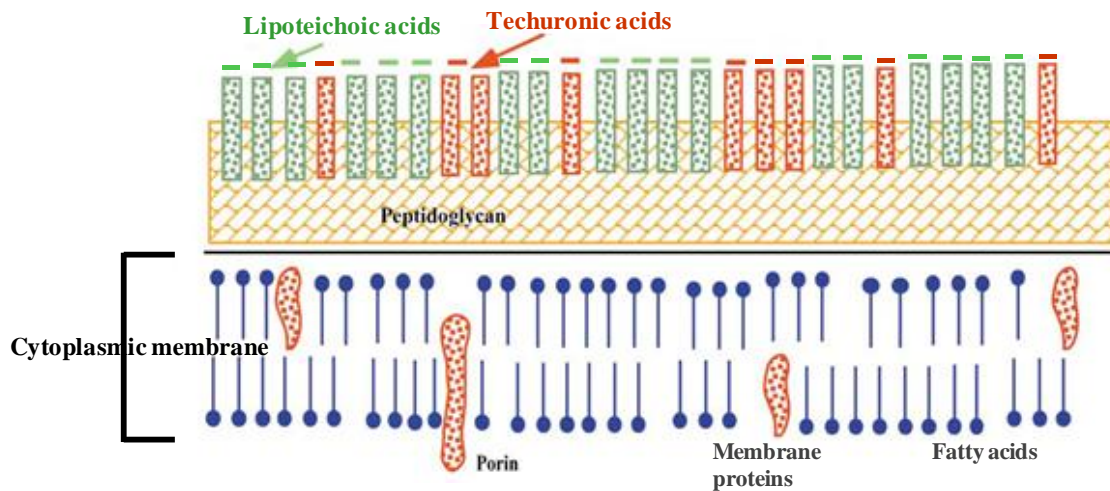
B Structure of Gram Negative bacterial cell wall
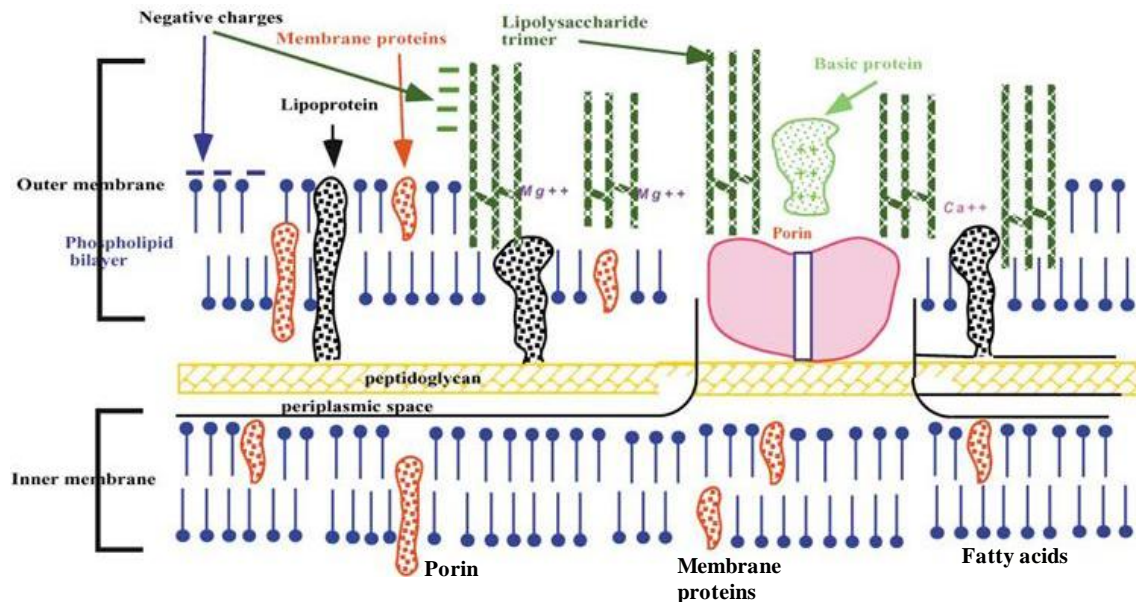
Figure 1.7: Diagrams illustrating differences in membrane structure between (A) Gram-positive and (B) Gram-negative bacteria.

A good photosensitizer for PDT or PACT should be a single substance with constant composition and a high degree of chemical purity, nontoxic in the dark, and sufficiently photostable under physiological conditions [Guo et al., 2010, Li et al., 2011, Szaciłowski et al., 2005, Stochel et al., 2009, Detty et al., 2004]. As the efficiency of photosensitizer depends on the photophysical properties of the first excited triplet state, this state should be generated with a high quantum yield (Φ) and have an appropriate energy and long enough lifetime to allow efficient energy or electron transfer to the

oxygen molecule [Szaciłowski et al., 2005, Stochel et al., 2009]. Each photosensitizer molecule can typically produce 10^3-10^5 molecules of $^1O_2$ before being degraded through photobleaching by $^1O_2$ or by some other process [DeRosa et al., 2002]. Photosensitizers can be both, organic compounds or inorganic metal complexes.

1.2.4. Organic photosensitizers:
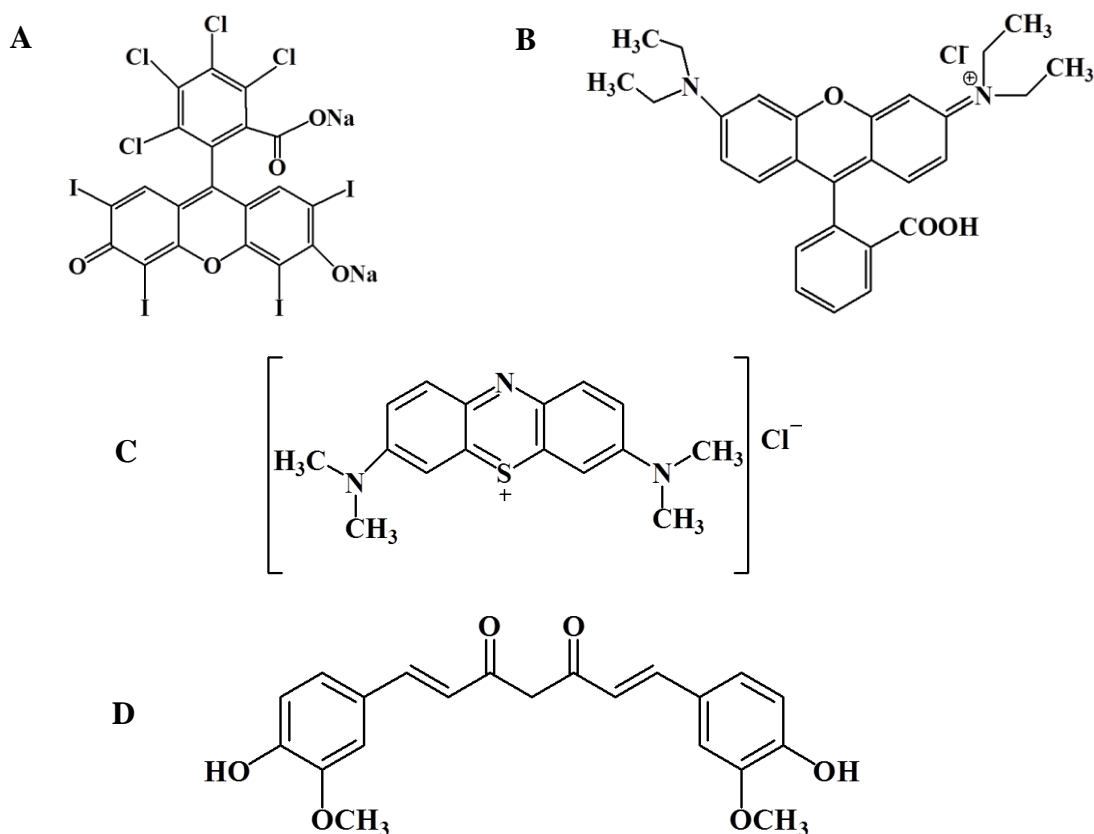
Figure 1.8: A few organic photosensitizers (A) Rose Bengal, (B) Rhodamine B, (C) Methylene Blue, (D) Curcumin.

Organic photosensitizers are molecules with highly conjugated structure that absorb light. Some examples are dyes such as Rose Bengal, Methylene Blue, Rhodamine B and Curcumin and others (Figure 1.8). Photoexcitation of these dyes generate singlet oxygen with appreciable quantum yield. PDT action by these dyes is generally due to singlet oxygen based Type II mechanism. These dyes have also been reported to inactivate microbes. Singlet oxygen destroys conjugation which results in reduction of the ability to absorb visible light, and over the time these photosensitizers undergo bleaching [DeRosa et al., 2002]. It has been shown that stability and water solubility of Curcumin increases when it is bound to polyvinylpyrrolidone (PVP-C). PVP-C can be used for

disinfection of wounds and employed in aseptic production of foodstuffs [Winter et al., 2013].
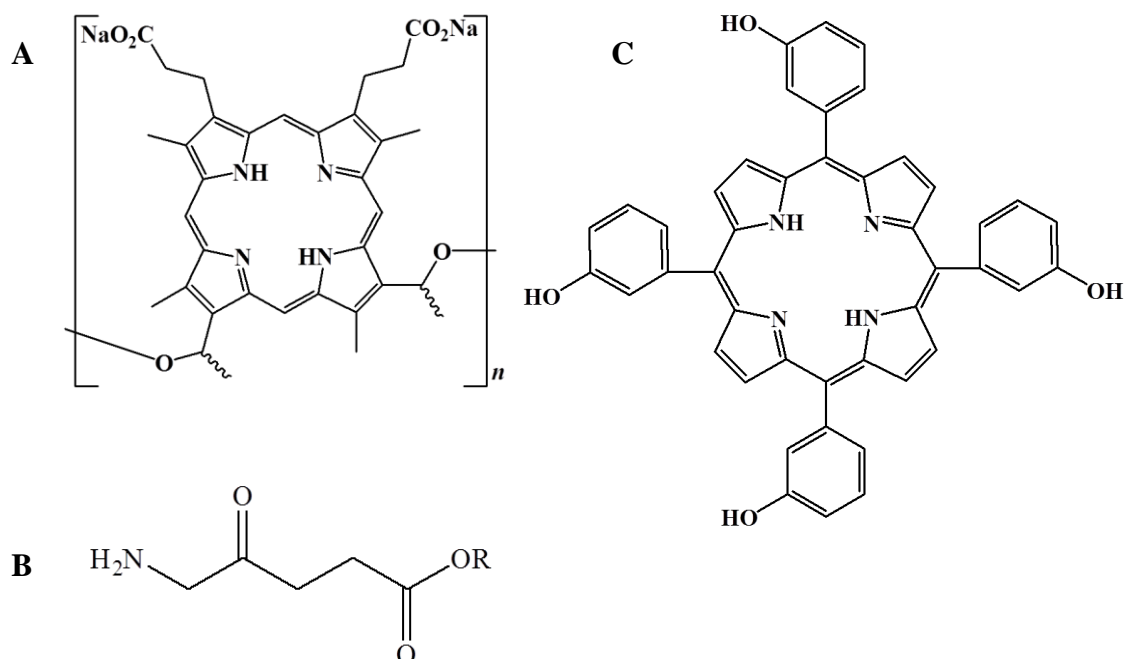
Figure 1.9: Structures of a few clinically accepted photosensitizers. (A) Photophrin, (B) Levulan, where, R= H, methyl, hexyl, benzyl, (C) Foscan.

The first accepted photosensitizer for PDT is Photofrin, which is a mixture of hematoporphyrin monomers, dimers, and oligomers (Figure 1.9 (A)) [Szaciłowski et al., 2005, Stochel et al., 2009, Detty et al., 2004]. 5-aminolevulinic acid (Levulan) and its methyl (Metvix), hexyl (Hexvix), and benzyl (Benzvix) ester derivatives (Figure 1.9 (B)) [Lang et al., 2001, Wachowska et al., 2011, Wan and Lin, 2014] are precursors of protoporphyrin IX. The synthetic *m*-tetrahydroxyphenylchlorin (*m*THPC, Foscan) (Figure 1.9 (C)) [Rezzoug et al., 1998, Coutier et al., 1999, Kniebühler et al., 2013] has been accepted for clinical applications [Szaciłowski et al., 2005, Stochel et al., 2009, Detty et al., 2004]. In general, porphyrins, chlorins, bacteriochlorins, phthalocyanines, naphthalocyanines, and texaphyrins (Figure 1.10) are the various clinically relevant photosensitizers for PDT or PACT [Ali and van Lier, 1999, Nyman and Hynninen, 2004, Detty et al., 2004, Szaciłowski et al., 2005, Stochel et al., 2009].
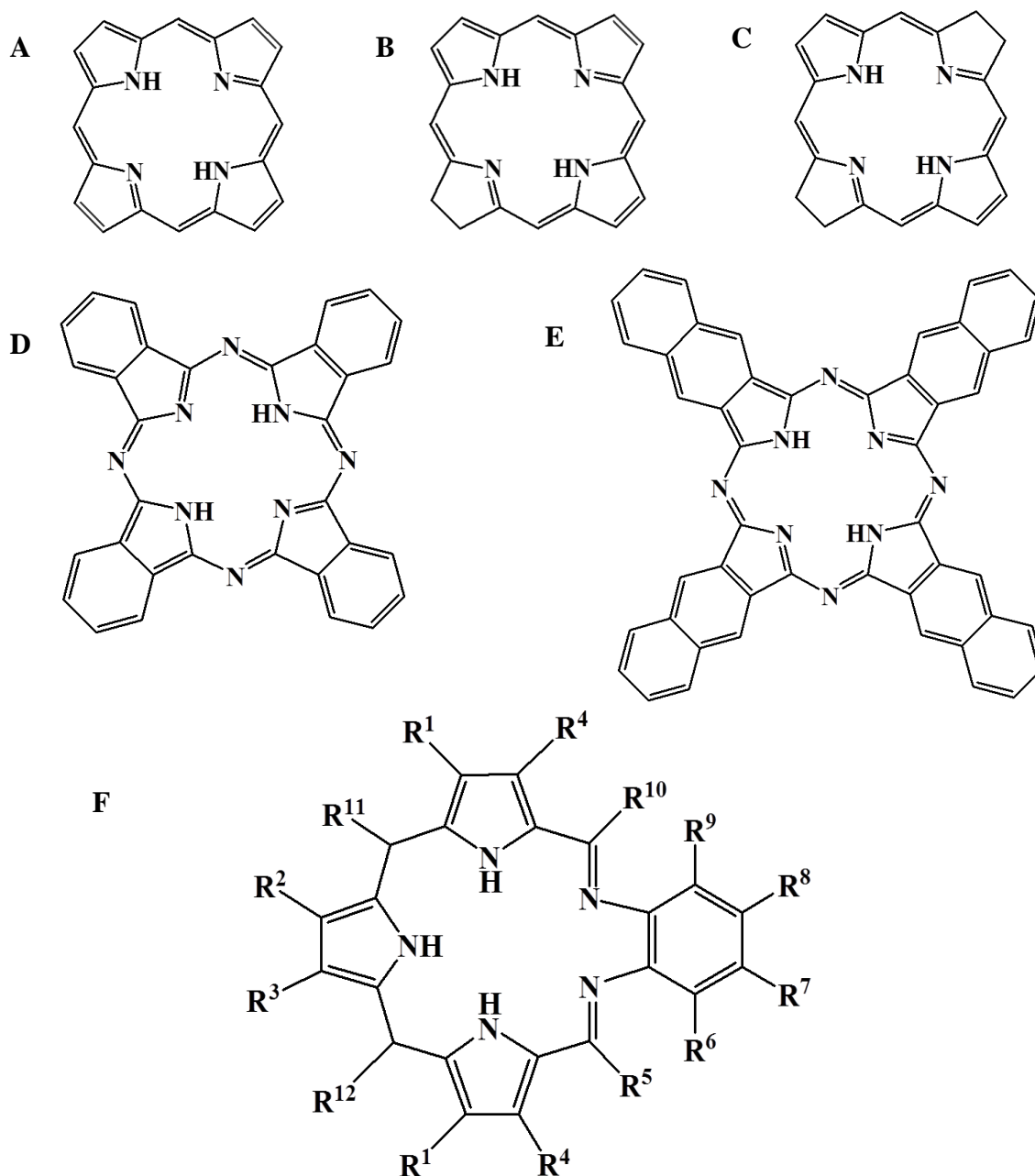
Figure 1.10: Representative figures of clinically relevant photosensitizers (A) Porphyrin, (B) Chlorin, (C) Bacteriochlorin, (D) Phthalocyanine, (E) Naphthalocyanine, (F) Texaphyrin.

1.2.5. Transition metal complexes based photosensitizers:

Metal complexes can act as photosensitizers via both Type I and Type II mechanisms. Photochemical excitation of transition metal complexes by visible and UV light generates electronic excited states under moderate reaction conditions (ambient temperature and pressure) [Hennig et al., 1999].

Some of the transition-metal complexes are photochemically stable, have long lived triplet state and high efficiency of producing ROS on visible light irradiation [Balzani et al., 1996]. In particular, the assembly of ligands around the central metal makes it possible to design transition metal complexes with multiple functions, such as water solubility, biological compatibility, and phototoxicity [Szaciłowski et al., 2005, Stochel et al., 2009, Detty et al., 2004, Balzani et al., 2001, Hammarstroem et al., 2010, Goss et al., 1985, Rengifo-Herrera et al., 2007, Villen et al., 2006]. For example, ruthenium (II) complexes of polypyridyl ligands such as bipyridine and phendione are highly photoactive and have been reported to show energy and electron transfer on excitation. The excited ruthenium complexes can from various ROS as described in equations 5-9 [Lei et al., 2011, Gao et al., 2006, Yavin et al., 2004, Concepcion et al., 2007, Abdel-Shafi et al., 2004, Mulazzani et al., 1994, Garcìa-Fresnadillo et al., 1996].

$$Ru(II) \xrightarrow{h\nu} {}^{*}Ru(II) \qquad \dots\dots\dots\dots\dots(5)$$

$$^{*}Ru(II) + O_2 \longrightarrow Ru(II) + {}^{1}O_2 \quad \dots\dots\dots\dots(6)$$

$$Ru(II) + O_2 \xrightarrow{h\nu} Ru(III) + O_2^{\cdot -} \quad \dots\dots\dots\dots(7)$$

$$O_2^{\cdot -} + O_2^{\cdot -} \xrightarrow{H^+} H_2O_2 \quad \dots\dots\dots\dots\dots\dots\dots(8)$$

$$H_2O_2 \xrightarrow{Ru(III)} 2HO^{\cdot} \quad \dots\dots\dots\dots\dots\dots\dots\dots(9)$$
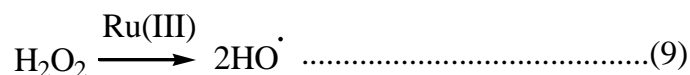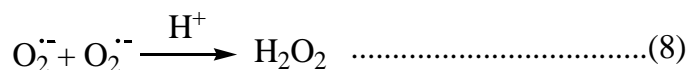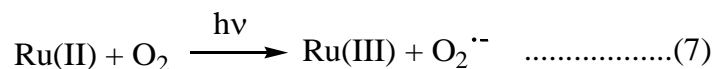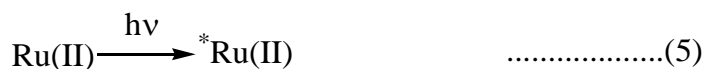
$[Ru(bpy)_3]^{2+}$, where bpy (2,2'-Bipyridine) is polypyridyl bidentate chelating ligand, is a well known photoactive metal complex (Figure 1.11 (A)). The bpy complexes of ruthenium absorb light intensely in the visible part of the spectrum. The electronic transitions are attributed to MLCT [Smith et al., 2003], which could result in photo-redox reactions.

Quantum yield of singlet oxygen formation by $[Ru(bpy)_3]^{2+}$ depends on the solvent. Some of the values described with different solvents are as follows: 0.22 in D_2O, 0.41 in water, 0.56 in acetonitrile, 0.73 in CD_3OD and 0.87 in methanol [DeRosa et al., 2002]. The complex has been studied in many areas such as PDT, water disinfection, and solar (photo voltaic) cells [Lei et al., 2011, Gokulakrishnan et al., 2013, Gao and Bard, 2000].

MLCT visible light excitation of Ru(II) polypyridyl complexes containing phendione as ligand (Figure 1.11 (B, C)), results in charge-separated excited species which generates Ru(III) and ligand centred radicals [Concepcion et al., 2007, Goss et al., 1985, Campagna et al., 1999]. The charge-separated excited species undergo fast radiation-less decay to ground state resulting in quenching or reduced luminescence [Zhou et al., 2010, Chouai et al., 2005], which is not favourable for the formation of singlet oxygen [Garcìa-Fresnadillo et al., 1996, Zhou et al., 2010, Chouai et al., 2005, DeRosa et al., 2002].
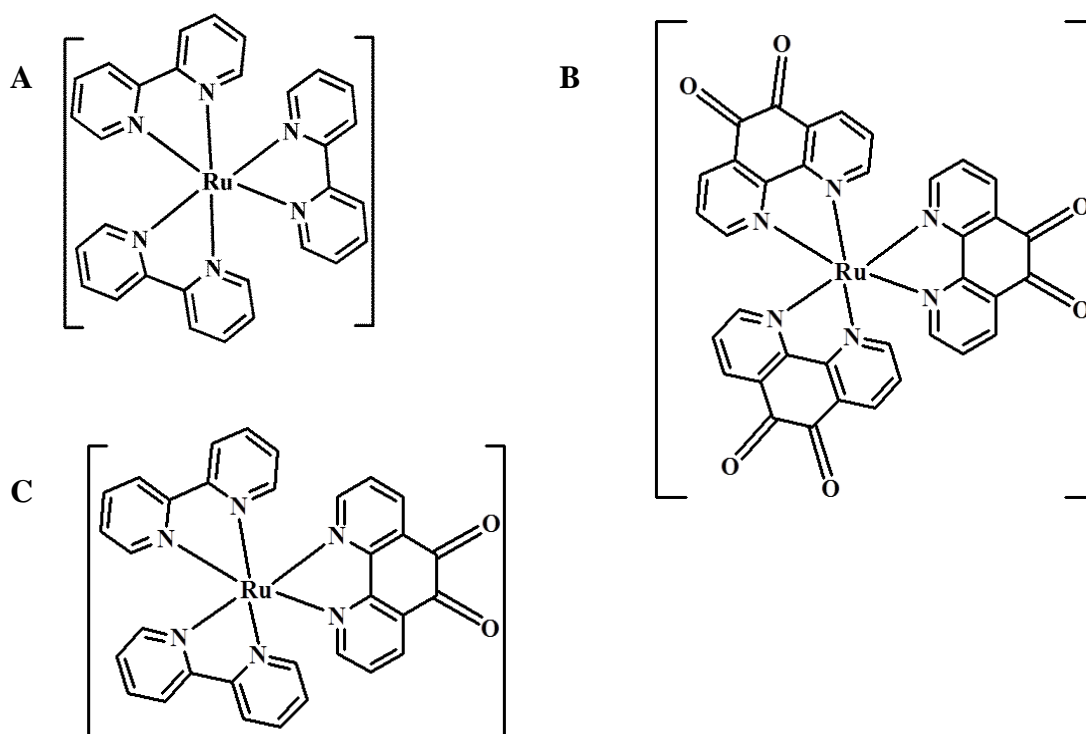
Figure 1.11: Structure of a few Ru polypyridyl complexes showing visible light MLCT excitation, (A) [Ru(bpy)$_3$]$^{2+}$, (B) [Ru(phendione)$_3$]$^{2+}$, (C) [Ru(bpy)$_2$(phendione)]$^{2+}$.

1.2.6. Bioconjugates as photosensitizers:

The third generation of PSs for PDT represent a class of molecules in which a PS is conjugated to carrier molecules for specific targeting to tumor cells. These carrier molecules include monosaccharides [Zheng and Pandey, 2008], peptides [Shadidi and Sioud, 2003], low density lipoproteins (LDLs) [Polo et al., 2002], antibodies [Vrouenraets et al., 2000], nanoparticles (NPs) [Chatterjee et al., 2008] and polymers [Greco and Vicent, 2008]. Developing conjugates of PSs with saccharides help in targeting carbohydrate-binding molecules, which are known to express on the surface of many tumor cells [Zheng and Pandey, 2008, Liu and Rabinovich, 2005]. It was found
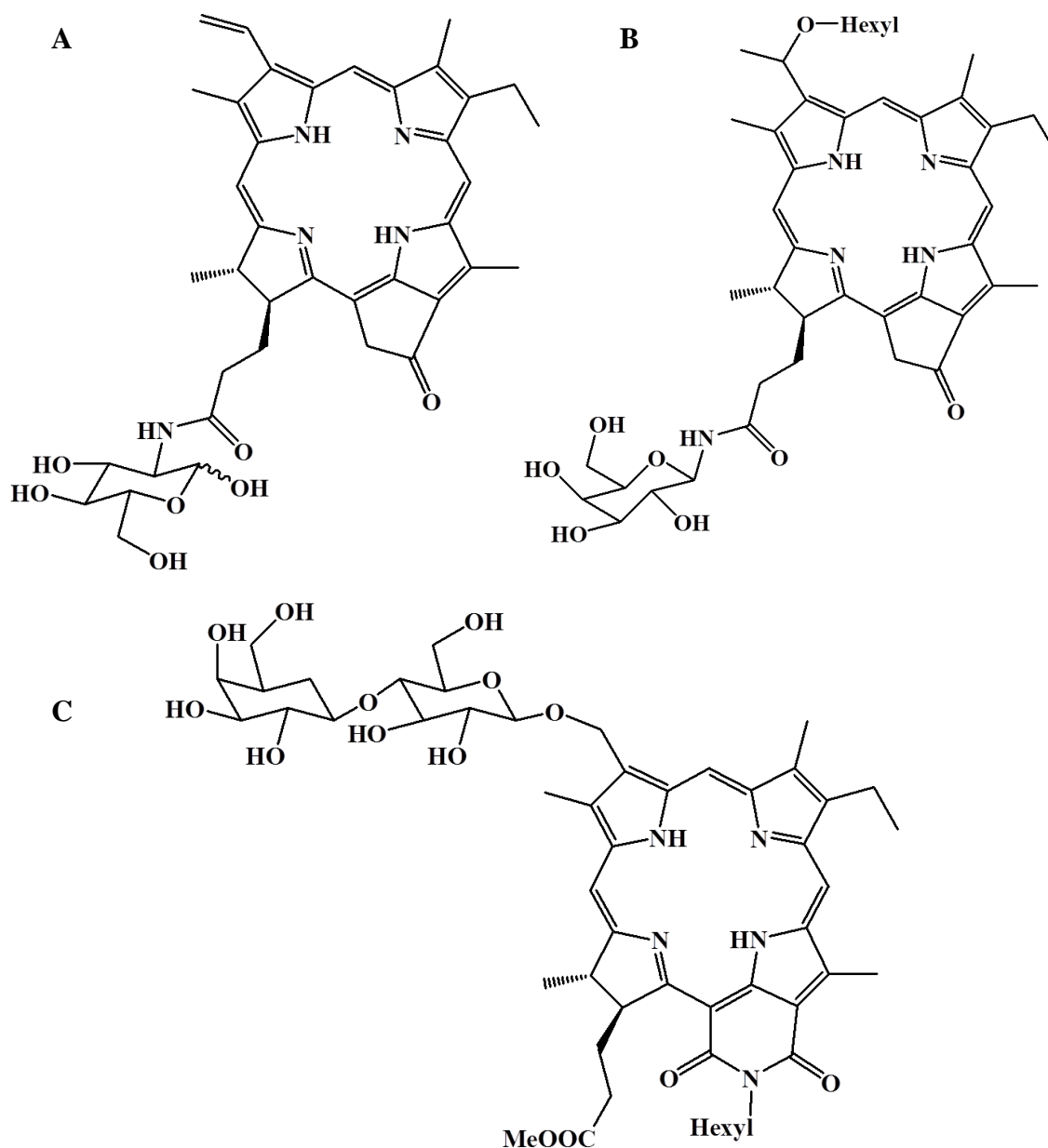
Figure 1.12: Structures of photosensitizer-carbohydrate conjugates. (A) Pyropheophorbide 2-deoxyglucosamide (Pyro-2DG), (B) 2-(1-hexyloxyethyl)-2-devinyl pyropheophorbide-a (HPPH)-Gal, (C) Purpurinimide-lactose.

that carbohydrate conjugates (Pyropheophorbide 2-deoxyglucosamide, Purpurinimide-lactose, HPPH-Gal) showed higher binding affinity than the corresponding non-conjugated PSs (Figure 1.12) [Zhang et al., 2003, Pandey et al., 2007, Zheng et al., 2009]. Additionally, peptides and proteins can also be used to enhance the uptake of PS-carrier conjugates by tumor cells [Gariépy, 2001, Tarragó-Trani et al., 2006]. It was reported that the conjugate with the peptide linker (Pyro-GDEVDGSGK), tended to specifically accumulate into the tumor cells as compared to that without the peptide linker [Stefflova et al., 2007, Chen et al., 2007]. Also, PS have even been targeted to

sub-cellular components like nucleus by conjugating PSs to peptides like poly-L-lysine and nuclear localization sequences (NLS) peptide [Ogura et al., 2005, Tijerina et al., 2003] (Figure 1.13). Moreover, a conjugate of PS Chlorin $_{e6}$ and peptide poly-L-lysine was able to efficiently kill both Gram-positive and Gram-negative bacteria on illumination with red light [Soukos et al., 1998]. Furthermore, LDL conjugated to PS can be used to target membrane of tumor cells that over express LDL receptors [Zheng et al., 2002, Nikolaeva et al., 2010] (Figure 1.14).
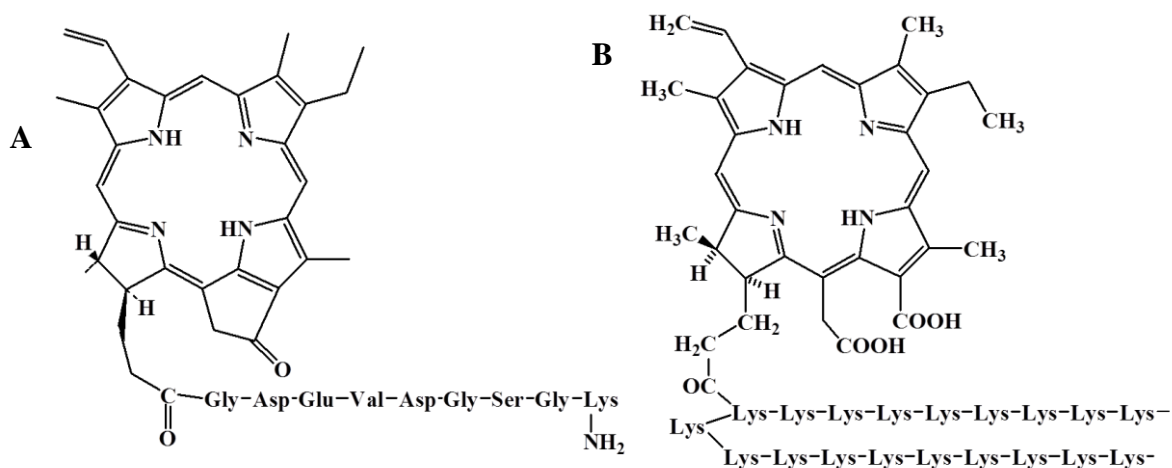
Figure 1.13: Structures of PSs conjugated to peptides. (A) Pyropheophorbide – GDEVDGSGK, (B) Chlorin $_{e6}$ – poly – L – lysine.
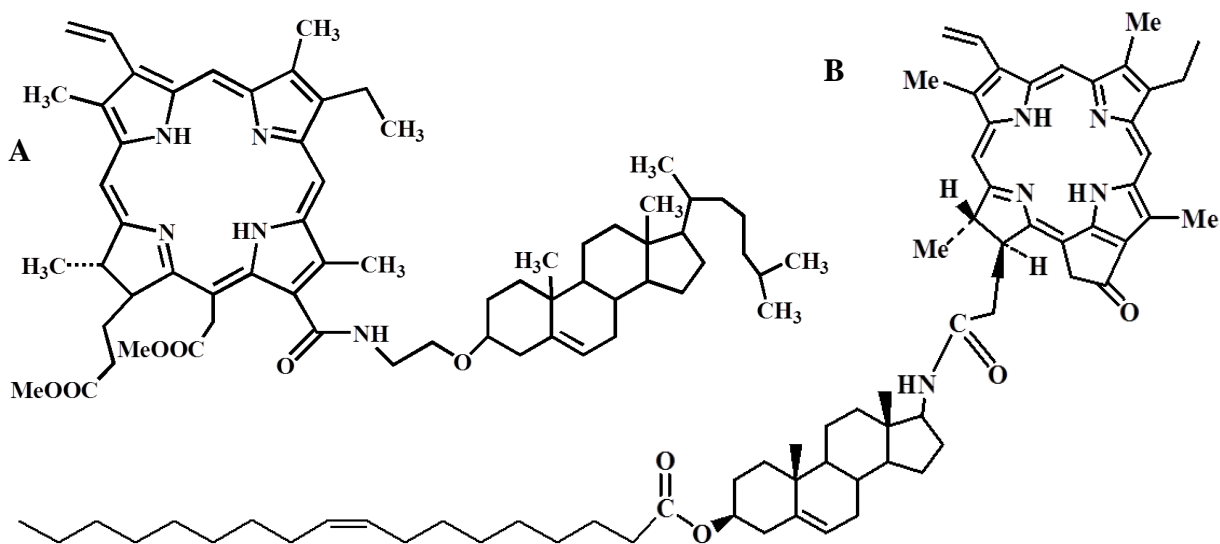
Figure 1.14: Structures of PSs conjugated LDLs. (A) Chlorin $_{e6}$ – cholesterol, (B) Pyropheophorbide – Cholesteryl Oleate Amine 4.

1.2.7. Nanoparticle systems as photosensitizers:

Development of visible light active PSs for water disinfection is important from the view point of utilising a major part of solar spectrum for bactericidal action [Blanco et al., 2009, Boyle et al., 2008]. Solar-driven photocatalytic disinfection systems at the nano-level can be of three types: doped-TiO_2, dye-sensitised TiO_2 and composite inorganic nanomaterials [Zhang et al., 2010].
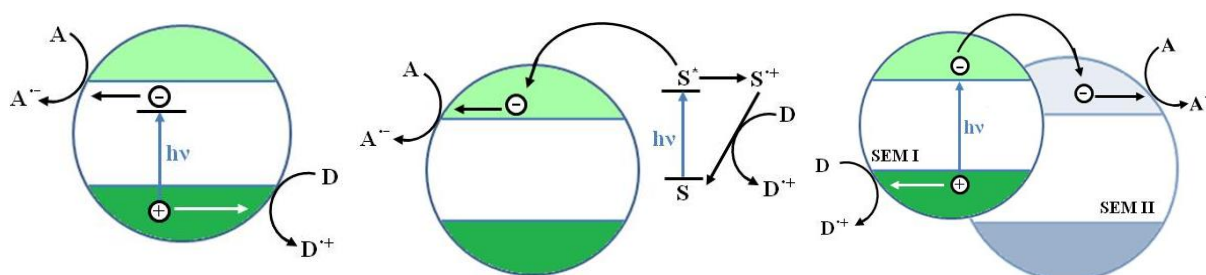
Figure 1.15: Development of visible light active semiconductors. (A) Doping of TiO_2 with ions, (B) Photosensitization of TiO_2 with a photosensitizer, (C) Composite inorganic nanomaterials.

TiO_2 doped with nitrogen, carbon or sulphur absorbs wavelengths in visible region (Figure 1.15 (A)). This is an advantage over neat TiO_2 which absorbs in near UV region (< 400 nm), in utilising sunlight [Li et al., 2009, Sakthivel et al., 2004, Miyauchi et al., 2004, Yu et al., 2005, Huo et al., 2008, Rengifo-Herrera et al., 2008]. Further, in another study, the nitrogen doped TiO_2 was modified with palladium and it was found to enhance visible-light photocatalytic disinfection of bacteria as compared to neat TiO_2 [Wu et al., 2008].

Dye-sensitization is one of the most popular and economical processes for improving the TiO_2 photocatalyst performance [Zhang et al., 2010]. A few sensitizers that have been used are $[Ru(bpy)_3]^{2+}$, Eosin and Safranine. The PSs on excitation, direct electron injection into conduction band of TiO_2 photocatalyst [Jin et al., 2006, Hussein and Alkhateeb, 2007, Jin et al., 2007, Yao et al., 2008, Hashimoto et al., 1988]. The redox potential of the excited state (S*) of PS should be lower than the conduction band edge of the semiconductor. The electron transfer from S* to the conduction band can occur with subsequent reduction of the oxidized form of the sensitizer (S^{+}) by an electron donor, D. The sensitizer is therefore regenerated, and the catalytic cycle is closed. The semiconductor plays only the role of a support, mediating electron transfer to the acceptor, A (Figure 1.15 (B)) [Szaciłowski et al., 2005]. To cite one example, Yao et al. doped TPPN into TiO_2 thin films by a sol–gel method. Such dye-sensitized TiO_2 thin

film exhibited visible light-induced bactericidal effects on phytopathogenic bacteria, killing 90% cells in ~60 min [Yao et al., 2007].

The coupling of a photocatalyst with a metal forms composite inorganic nanomaterials and these can be developed as effective visible light photocatalysts. Visible light irradiation leads to charge separation only in the semiconductor of lower band gap (SEM I). Then an electron can be transferred to the conduction band of the second semiconductor (SEM II) and later used in reduction of the electron acceptor. On the other hand, oxidation of D takes place at the surface of the first semiconductor (Figure 1.15 (C)) [Szaciłowski et al., 2005]. The main advantages of such systems are suppression of the recombination process, efficient charge separation, activity upon visible light irradiation and increased yield of the catalytic reaction. For example, $Ag/AgBr/WO_3 \cdot H_2O$, AgI/TiO_2 and $Ag/AgBr/TiO_2$ are visible-light active photocatalysts and were used to efficiently kill *E. coli* and *S. aureus*. This effect was attributed to combined advantages of a plasmon photocatalyst and a composite photocatalyst. The photogenerated electrons were transferred to Ag NPs and were separated from the holes in the valence bands of AgBr and $WO_3 \cdot H_2O$ or TiO_2. The separated holes thus produced, oxidized the bacteria [Hu et al., 2006, Hu et al., 2007, Wang et al., 2009].

1.2.8. Charge transfer complexation between photosensitizers and nanoparticles:

A charge transfer complex is an association of two or more molecules in which electronic charge is transferred from electron donor to electron acceptor. The resulting electrostatic attraction provides a stabilizing force for the charge transfer molecular complex [Rohatgi-Mukherjee, 1986]. A few examples of charge transfer complexes between photosensitizers and nanoparticles have been reported [Franzen et al., 2002, Glomm et al., 2005, Huang and Murray 2002, Glomm et al., 2004]. Stephen *et. al.,* have reported the photoinduced charge separation between $Ru(bpy)_3$ and capped metallic NP (such as Au, Ag) [Glomm et al., 2002] (Scheme 1). Additionally, combination of photoactive molecules such as porphyrin and chlorophyll, with silver nanoparticle (Ag NP) are also known to produce the charge-separation states upon photoexcitation [Barazzouk et al., 2004, Murphy et al., 2011].

$$[Ru(bpy)_3]^{2+} - NP \longrightarrow [Ru(bpy)_3*]^{2+} (MLCT) - NP \longrightarrow$$

$$[Ru(bpy)_3]^{3+} - NP^- \longrightarrow [Ru(bpy)_3]^{2+} - NP$$
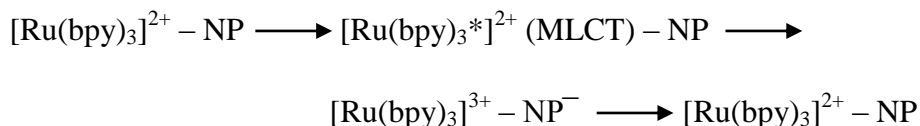
Scheme 1: Electron transfer between $[Ru(bpy)_3]^{2+}$ and NP.

In order to form the electrostatic interaction between $[Ru(bpy)_3]^{2+}$ complex and Ag NP, the Ag NP was quoted with negatively charged species (Figure 1.13). Glutathione (GSH) is one such ideal candidate as it has a thiol functional group which strongly binds to Ag NP surface. This biomolecule also has charged functional groups (carboxylate and amine) which promote water solubility and interaction towards biostructures [Taglietti et al., 2012, Amato et al., 2011, Pallavicini et al., 2010] and $[Ru(bpy)_3]^{2+}$ complex [Franzen et al., 2002]. The biological ligands such as peptides, proteins, oligonucleotides and carbohydrates attract attention due to their well-defined interactions in living systems [Wigginton et al., 2010, Singh et al., 2009].
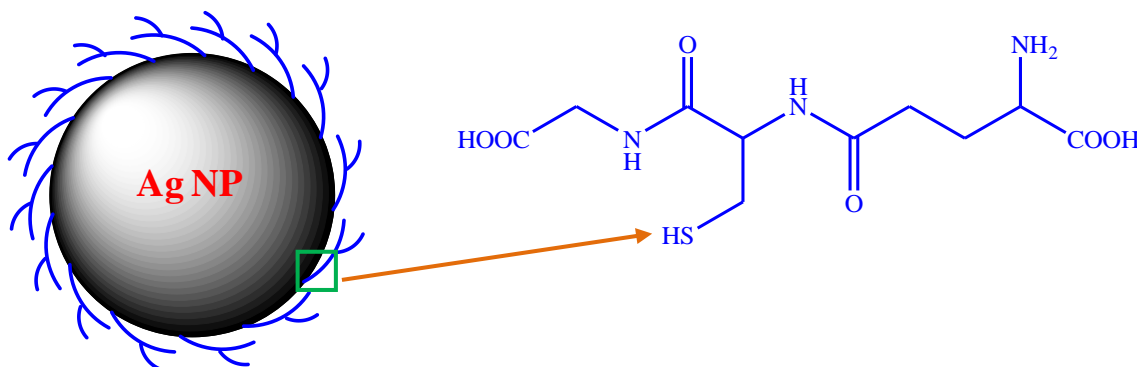
Figure 1.16: Structure of silver nanoparticle bound to glutathione.

1.2.9. Antimicrobial activity of Ag NPs:

Ag NP exhibit enhanced antimicrobial effects due to high surface-to-volume ratio of NPs, which provide a substantial and sustained contact with the bacterial cell [Feng et al., 2000, Jose Ruben et al., 2005, Lee et al., 2007]. However, for biological applications, Ag NPs have to be coated with molecules such as GSH, such that they are soluble in water based systems, do not aggregate in physiological conditions like high salt concentration and favor interactions with biosystems such as bacterial membranes [Wigginton et al., 2010, Singh et al., 2009]. Additionally, surface modifications of NPs improve their targeting and enhance cellular uptake. However, coating with GSH reduces the antibacterial activity of the Ag NP [Amato et al., 2011]. Furthermore, a few studies show that antimicrobial activity of Ag NPs may also be due to slow release of

silver ions in medium of interest [Feng et al., 2000, Wu et al., 2009, Holt and Bard, 2005, Pallavicini et al., 2010]. Interestingly, antimicrobial activity of silver ions has been well known for many years [Silver et al., 1996]. Silver ions kill microbial cells by binding to electron-donor groups in biological molecules including sulphur, oxygen, thiol groups, etc. and inhibiting the essential enzymatic functions such as permeability and respiration [Jain et al., 2009, Leung et al., 1992, Kokura et al., 2010, Roe et al., 2008, Egger et al., 2009, Varghese et al., 2013, Mirjalili et al., 2013, Thanh et al., 2009,].

1.2.10. Photochemical disinfection of water using photosensitizers (PACT and PDT agents for water disinfection):

Availability of clean drinking water is a major concern throughout the world. Contamination in water can be caused by unplanned sewage disposal to surface and ground water [Kemper, 2004, Coetser et al., 2007, Weber et al., 2002]. The sewage contains microbes such as bacteria, viruses, fungi, algae and parasites. Of the above mentioned microbes, bacteria are the cause of most infections and diseases to humans and animals [Montgomery and Elimelech, 2007, Shannon et al., 2008].

The important techniques used for water disinfection of bacteria include UV light, chlorination, ozonation, and chemical treatments using sodium hypochlorite, H_2O_2 etc [Tomas, 1990, Legrini et al., 1993, Sioi et al., 2006, Zhang et al., 2010, Magaraggia et al., 2011]. UV light, especially UV-C is a very potent germicide. UV-C irradiation of nucleic acids leads to formation of dimers of pyrimidine residues that result in RNA and DNA damage with cell death [Gurzadyan et al., 1995]. However, the penetration depth of UV radiation in aqueous medium is very less [Magaraggia et al., 2011]. Additionally, prolonged exposure to UV irradiation is hazardous to human skin. Particularly, UV-C is a potent carcinogen [Yin et al., 2013, Legrini et al., 1993]. Therefore, UV light based disinfection is an energy consuming method, and careful handling is required.

Chlorine is a very potent antimicrobial agent and has low cost [Szewzyk, et al, 2000]. However, exposure to chlorine causes irritation in nose, eyes, throat and skin. If chlorine enters the body, it forms acids further harming the cells [Gopal et al., 2007, Magaraggia et al., 2011]. On the other hand, ozonation is more effective than chlorination against microbes and has a short contact time (~ 10-30 min). However, implementing ozonation on a large scale is not economically favorable [Khan et al., 1985, Francis, 1988,

Magaraggia et al., 2011]. There are also a few mechanistic problems like dissolving ozone (O_3) on a large scale, photolyzing it efficiently and less reactivity of O_3 towards unsaturated compounds [Legrini et al., 1993]. To overcome a few problems, ozonation is coupled with UV photolysis. Oxidative degradation using O_3-UV is better as compared to either using O_3 or UV alone [Khan et al., 1985, Prat et al., 1990, Francis, 1988]. Moreover, chlorination, ozonation and chemical disinfectants produce harmful disinfection byproducts (DBPs) such as endoperoxides or trihalomethanes or haloacetic acids [Legrini et al., 1993, Zhang et al., 2010].

In order to address these problems, novel methods for water disinfection are being actively studied. One of the methods is utilizing full sunlight spectrum, taking advantage of deeper penetration of visible light. Solar disinfection (SODIS) combines the effect of light and heat energy of sunlight and is effective in cleaning water with high turbidity, but is constrained by weather and geography [Lui et al., 2016, Loeb et al., 2016, Hunter, 2009, Fewtrell, et al., 2005, Chaidez et al., 2004, Meierhofer and Wegelin, 2002]. The other method can be the use of photosensitizers for driving photochemical reactions and generation of ROS that are deleterious to cells [Yin et al., 2013, Zhang et al., 2010, Magaraggia et al., 2011]. Photosensitisers were mainly employed as PDT or PACT agents. Recently, PACT agents are gaining attention for water disinfection under visible light. Both, organic and inorganic photosensitizers can be used for disinfection of waste water. Photogeneration of ROS using visible light sensitizers, in both homogeneous and heterogeneous systems has been developed.

1.2.11. Recovery of photosensitizers by adsorption:

The word "adsorption" was coined by a German physicist Heinrich Kayser [Kayser, 1881]. Depending on the type of interactions, adsorption can be of two types: physisorption (usually involving weak Vander Waals interactions) or chemisorption (characteristic of covalent bonding) [Filho and Carmo, 2006, Mohan et al., 2006, Atkins and Paula, 2013].

The adsorbents must have a large surface area that gives the adsorbent a high capacity for adsorption. Some of the common adsorbents used are silica gel, activated carbon (AC), activated alumina and zeolites [Filho and Carmo, 2006]. After disinfection of a water sample is complete, these adsorbents can be used to remove the disinfectant.

Silica gel is chemically inert, non toxic, porous and amorphous form of SiO_2. Silica is used for drying air (remove moisture) and control humidity and in research laboratories for separating compounds using column chromatography. Chemical modifications on the surface of silica with chelating agents are often done to increase its efficiency. Silica surface is covered with hydroxyl groups, SiOH, called silanol groups and its interior is connected by siloxane groups (Figure 1.14) (Si-O-Si) [Peri et al., 1968, Filho et al., 2006]. Moreover, silica can also be used as one of the potential inorganic materials for water treatment [Kannan et al., 2008, Repo et al., 2009, Ahmed et al., 1992].
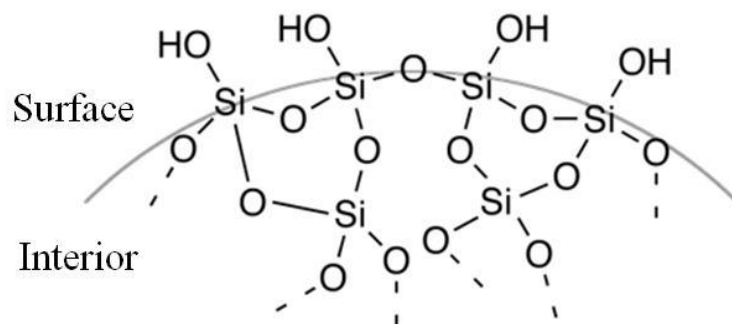
Figure 1.17: Structure of surface and interior of a silica gel particle.

Another example of a versatile adsorbent is Activated carbon. AC is highly porous, non-polar, amorphous cheap solid prepared from carbonaceous material like coal, wood or nutshells. It is the most widely used adsorbent as it has large volume and high surface area. AC is used for making high vacuum, remove impurities from sugar, preparation of gas masks and waste gas and water treatment. It was first used for water treatment in US in 1930 for elimination of taste and odor from contaminated water. The surface of AC has oxides, hydroxyl, aldehyde and carboxyl groups (Figure 1.15). Adsorption capacity depends on AC properties, adsorbate chemical properties, temperature, pH, ionic strength, etc [Moreno-Castilla, 2004, Mohan et al, 2006, Daud et al, 2010].
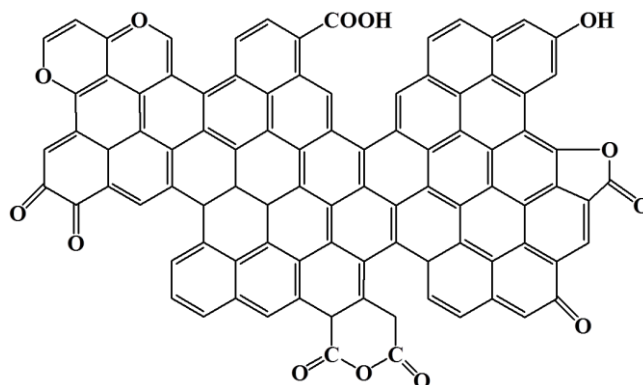
Figure 1.18: Diagrammatic representation of functional groups present on surface of activated carbon.

Apart from the above facts, it is also important to note that activated carbon is generally used as a final filter for purification of water [Kuznetsova et al., 2007, Gonzalez-Serrano et al., 2004, Mohan et al., 2006, Gupta et al., 2009]. Activated carbon treatment can effectively remove taste and odour causing compounds [Gupta et al., 2009, Chen et al., 1997], chlorinated substances [Pavoni et al., 2006, Urano et al., 1991] and transition metal ions and complexes [Mohan et al., 2006, Jusoh et al., 2005, Kasaini et al., 2000, Kim, 2004].

Adsorption isotherms are usually used to describe the process of adsorption (equation 10). An isotherm is a graph between the amounts of adsorbate on the adsorbent as a function of concentration of adsorbate at a constant temperature [Atkins and Paula, 2013].

$$\text{A} \; + \; \text{B} \;\; \underset{\text{Desorption}}{\overset{\text{Adsorption}}{\rightleftharpoons}} \;\; \text{AB} \;\; .... (10)$$

Adsorbate Adsorbent
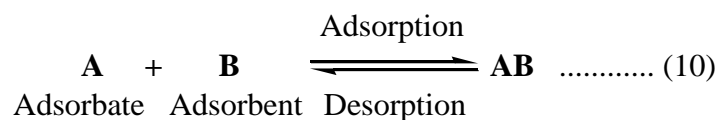
The two main isotherms used to describe adsorption are Langmuir and Freundlich. The Freundlich isotherm was first published by Freundlich and Kuster in 1906 and describes equilibrium on heterogeneous surfaces (equation 11, 12).

$$q_e = K_F C_e^{1/n} \qquad\qquad \text{(non-linear form)} ....(11)$$

$$q_e = \log K_F + \frac{1}{n} \log C_e \qquad \text{(linear form)} ....(12)$$

where, K_F is adsorption capacity constant, n is adsorption intensity constant, q_e is amount of substance adsorbed per unit weight of adsorbent at equilibrium (mg/g) and C_e is equilibrium concentration of adsorbate (mg/l) [Mohan et al., 2006].

Irving Langmuir derived the isotherm in 1918. Langmuir isotherm describes equilibrium on homogeneous surfaces (equation 13, 14).

$$q_e = \frac{Q^o b C_e}{1 + b C_e} \qquad\qquad \text{(non-linear form)} ....(13)$$

$$\frac{C_e}{q_e} = \frac{1}{Q^o b} + \frac{1}{Q^o} C_e \qquad \text{(linear form)} ....(14)$$

where, q_e is amount of solute adsorbed per unit weight of adsorbent (mg/g), C_e is equilibrium concentration of solute in solution (mg/l), Q^o is monolayer adsorption capacity (mg/g) and b is constant related to free adsorption energy [Mohan et al., 2006].

1.2.12. Light emitting diodes:

A large variety of light sources can be used in photochemistry. These can be artificial (lamps, lasers) or natural light (sun), coherent (laser) or non-coherent (sun, lamps), monochromatic or polychromatic, operating continuously or pulsed [Stochel et al., 2009, Calin et al., 2009].

Both coherent and non-coherent light sources are used for PDT and PACT depending upon the application and the target. Some of them are lasers, xenon lamps, mercury lamps, UV lamps, LEDs, etc [Stochel et al., 2009, Calin et al., 2009]. Lasers are coherent sources of light and are monochromatic. They can be used as pulsed or non-pulsed sources of EMR. However, they are expensive. Two main lasers used are He-Ne laser and semiconductor laser. Lamps and LEDs are a source of non-coherent light. Lamps can be further classified as those with continuous spectrum (incandescent or xenon arc lamps) and those with spectrum in bands (gas discharge or metallic vapour lamps). Xenon and mercury lamps produce a lot of heat. They have a high luminosity and a continuous spectrum in UV-Vis-IR region. UV and heat filters have to be applied to study the effect of only Vis region. UV light is harmful as it can damage DNA. Therefore, to handle UV lamps trained personnel are needed [Wainwright, 1998, Calin et al., 2009, St. Denis et al., 2011].

LEDs are light in weight, easy to handle, cost effective, less energy consuming light sources. They don't generate a lot of heat and can be used at room temperature when combined with a heat sink (a metal plate). LEDs can be custom manufactured according to the need or the absorption maxima of the photosensitizer. In other words, they can be tailor-made as either monochromatic or polychromatic [Wainwright, 1998, Maclean et al., 2009, Chen et al., 2011].

1.3. Gaps in existing research:

1.3.1. Ruthenium complexes as PSs for water disinfection:

Ruthenium complexes co-ordinated with polypyridyl ligands such as bypyridine, 1,10-phenanthroline, phendione and dppz are well known. These ligands have been known as very good chelating agents for transition metal complexes. They exhibit MLCT and LMCT transitions in the complex form. *In vitro* DNA damaging studies of some complexes in presence of redox active co-reactants

such as H_2O_2 is known. However, their photoinduced effect on bacteria and DNA is recently being studied in presence of visible light, without the use of any co-reactant. The effect of these metal complexes on photoenhanced antimicrobial, and DNA damaging activities for water disinfection is not known.

1.3.2. Removal of homogeneous PSs from water after disinfection:

Although, photosensitizers have potential for water disinfection at relatively lower concentrations, their removal from water bodies is desirable for obtaining water free of microbes and photosensitizers. Therefore, photoactive molecules capable of inactivating microbes, as well as the removal of photoactive molecules using common adsorbents such as activated carbon and silica are important for water decontamination. Importantly, removal of Ru(II) polypyridyl complexes from aqueous media by activated carbon and silica have not been reported.

1.3.3. Adsorption of PSs on suitable supports to develop heterogeneous PSs for water disinfection:

Homogeneous PSs effectively inactivate bacteria. However, their removal is very important to render water usable after disinfection. To avoid this removal, heterogeneous PSs for water disinfection are preferred and are being recently developed. However, a heterogeneous PS which is photostable, does not leach in water, retains the activity after adsorption and does not need autoclaving after disinfection is not known.

1.3.4. Nano hybrid systems for photoinactivation of bacteria:

$[Ru(bpy)_3]^{2+}$ and Ag NPs are known to form nano hybrid systems. Plasmonic properties and surface functionalization of Ag NPs with biomolecules like GSH improve their targeting and cellular uptake efficiency. However, the effect of nano hybrid of $[Ru(bpy)_3]^{2+}$, and GSH coated Ag NPs (Ag-GSH-Ru) on photoinactivation of bacteria is not known.

1.4. Objectives of the proposed research:

The proposed research aims:

1. Preparation of photoactive ruthenium complexes of polypyridyl ligands.
2. Investigation on photoenhanced antibacterial activity of ruthenium polypyridyl complexes.
3. Development of heterogeneous ruthenium complexes of polypyridyl ligands for visible light water disinfection.
4. Modification of nanoparticles (like TiO_2, Ag, Au) with photosensitizers and peptides and study their antibacterial activity.

1.5. Thesis structure:

Chapter 1: Introduction

Chapter 2: Visible light water disinfection using $[Ru(bpy)_2(phendione)](PF_6)_2.2H_2O$ and $[Ru(phendione)_3]Cl_2.2H_2O$ complexes and their effective adsorption onto activated carbon

Chapter 3: Effective water photodisinfection using ruthenium polypyridyl complexes adsorbed onto activated carbon

Chapter 4: Enhanced photoantibacterial activity of $[Ru(bpy)_3]^{2+}$ complex in presence of glutathione coated silver nanoparticles

Chapter 5: Photo antibacterial activity of $[RuCl(bpy)_2(ATPh)]Cl$

Chapter 6: Heterogenized methylene blue on hydrogen titanate nanosheets as effective visible light active photosensitizer for water disinfection

Chapter 7: Conclusions and future scope of work

Chapter 2

Visible light water disinfection using [Ru(bpy)$_2$(phendione)](PF$_6$)$_2$.2H$_2$O and [Ru(phendione)$_3$]Cl$_2$.2H$_2$O complexes and their effective adsorption onto activated carbon

Highlights:

1. Complete photoinactivation of bacteria by ruthenium polypyridyl complexes.

2. Visible light emitting diode array used for photoinactivation of bacteria.

3. Loss of cell integrity due to membrane damage on photolysis.

4. Effective adsorption of complexes onto activated carbon.

5. Promising photosensitizers for visible light water disinfection.

Graphical abstract figure:
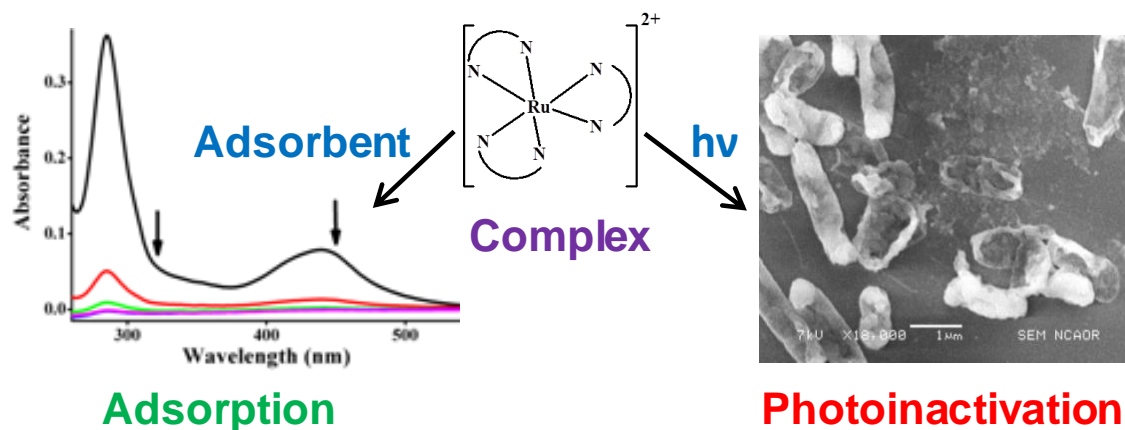
2.1.   Background:

Visible light active photosensitizers such as porphyrins [Caminos et al., 2008, Hamblin et al., 2004, Tavares et al., 2011], phthalocyanins [Hamblin et al., 2004, Spesia et al., 2009], porphycenes [Ragas et al., 2010] and ruthenium polypyridyl metal complexes [Lei et al., 2011, Manjon et al., 2008, Rengifo-Herrera et al., 2007, Villen et al., 2006] show excellent photoantimicrobial activity which is mainly attributed to photochemical generation ROS (chapter 1, section 1.2.4, 1.2.5). These compounds are mainly studied for their applications as PACT agents. On the other hand, potential non-therapeutic applications of photosensitizers have also been indicated in a few reports [Manjon et al., 2008, Rengifo-Herrera et al., 2007, Villen et al., 2006, Kuznetsova et al., 2007, Cooper et al., 2002, Acher et al., 1977, Schäfer et al., 2000]. Recently, M. A. F. Faustino and A. Almeida groups have reported the feasibility of PACT agents as an alternative to inactivate fish pathogenic bacteria in aquaculture systems, and emphasis that cationic porphyrin can cause effective photoinactivation of bacteria in water bodies [Arrojado et al., 2011]. Although, photosensitizers have potential for water disinfection at relatively lower concentrations, their removal from water bodies is desirable for obtaining water free of microbes and photosensitizers [Kuznetsova et al., 2007]. Therefore, photoactive molecules capable of inactivating microbes, as well as the removal of photoactive molecules using common adsorbents such as activated carbon are important for water decontamination. Earlier, it has been reported that irradiation of Ru(II) polypyridyl complexes generate Ru(III) species, and highly reactive hydroxyl radicals that cause non specific DNA damage [Yavin et al., 2004]. Importantly, visible light inactivation of bacteria by ruthenium polypyridyl complexes in aqueous media and adsorption of these complexes by activated carbon and silica have not been reported.

Here we aimed to study the effect of photolysis of $[Ru(bpy)_2(phendione)](PF_6)_2.2H_2O$ and $[Ru(phendione)_3]Cl_2. 2H_2O$ on Gram positive and negative bacteria. Adsorption of $[Ru(bpy)_2(phendione)]^{2+}$, and $[Ru(phendione)_3]^{2+}$ using environment friendly adsorbents, activated carbon and silica were investigated.

2.2.   Materials and methods:

2.2.1. Materials:

Ruthenium trichloride hydrate, 2,2'-bypyridine, 1,10-phenanthroline, lithium chloride, sodium chloride, disodium hydrogen orthophosphate, sodium dihydrogen phosphate,

sodium azide, potassium chloride, ethanol, glutaraldehyde, hydrochloric acid, N,N-Dimethylformamide, Dichloromethane, silica (60-200 mesh) and activated carbon were purchased from SD Fine Chemicals Limited, India. Ammonium hexafluorophospate was purchased from Sigma Aldrich, India. 2-amino-3-hydroxypyridine and 1,3-diphenylisobenzofuran were supplied by Alfa Aesar. Nutrient broth, agar-agar and D-mannitol were obtained from Hi Media, India. DNA isolation kit was purchased from SRL, India. Gel loading buffer and agarose were obtained from Bangalore Genei, India. Filter membranes (0.45 μm) were procured from Millipore, India. Double distilled water was used for all experiments. *Escherichia coli* (NCIM 2345) (*E. coli*), *Pseudomonas aeruginosa* (NCIM 2581) (*P. aeruginosa*), *Staphylococcus aureus* (NCIM 2127) (*S. aureus*) and *Bacillus subtilis* (NCIM 2545) (*B. subtilis*) were obtained from National Collection of Industrial Microorganisms (NCIM), National Chemical Laboratory Pune, India. Phendione was prepared as reported earlier [Goss et al., 1985].

2.2.2. Complex preparation:

$[Ru(bpy)_2(phendione)](PF_6)_2.2H_2O$ and $[Ru(phendione)_3]Cl_2.2H_2O$ were prepared and characterised spectrophotometrically (JASCO V-570 UV/Vis/NIR Spectrophotometer), as reported earlier [Goss et al., 1985]. Appropriate amount of complexes was dissolved in water to get stock solution.

2.2.3. Visible light source:

LED array was used as visible light source, purchased from Kwality Photonics, Hyderabad, India. LED array consisted of 3 x 8 LEDs. Warm white light emitting Polywatt PowerLEDs (KLHP3433WW), having λ_{max} at 450 and 625 nm (Figure 2.1) were used for all studies. Output angle = 120 degree. Average Luminous flux = 60 lumen. Luminous intensity = 19098.59 millicandela. Fluence rate was measured using Ophir PD100 Nova II power meter.

2.2.4. Antibacterial studies:

Cultures were grown in NB at 37 °C to attain log phase in a shaking incubator. Bacterial suspension was then centrifuged at 1000 g for 15 min and supernatant was discarded. Pellet was resuspended in 10 mM phosphate buffered saline (PBS) and used as stock. 2 ml of 10^7 CFU/ml cells in PBS containing appropriate concentration of complex in quartz cuvettes were photolysed (Figure 2.2 (A)). Control had 10^7 CFU/ml cells in reaction mixture without complex. Dark controls (10^7 CFU/ml cells with appropriate

concentration of complex) were covered with aluminium foil to protect from light (Figure 2.2 (B)). 100 µl aliquots of reaction mixture were withdrawn every 20 minutes during photolysis, serially diluted, and plated on NB agar plates. Plates were incubated for overnight at 37 °C and colonies were counted to obtain cell viability Vs time plots. Effect of bacterial cell concentration (10^3 - 10^8 CFU/ml) on photoinactivation of *E. coli* by complexes was also studied. All the tests were done in triplicates. Intensity of light was optimised by adjusting the distance between light source and surface of quartz cuvette containing bacterial cell suspension. *E. coli* and *P. aeruginosa* were exposed to light at the fluence rate of 95 mW/cm^2. *S. aureus* and *B. subtilis* were exposed to light at the fluence rate of 60 mW/cm^2 and 48 mW/cm^2, respectively. Under these photolytic conditions the light alone had no effect on cell viability.
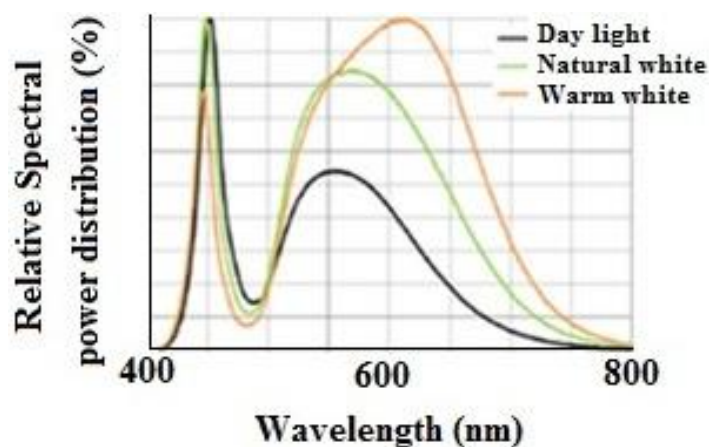
Figure 2.1: Spectral characteristics of the warm white LED (orange line).
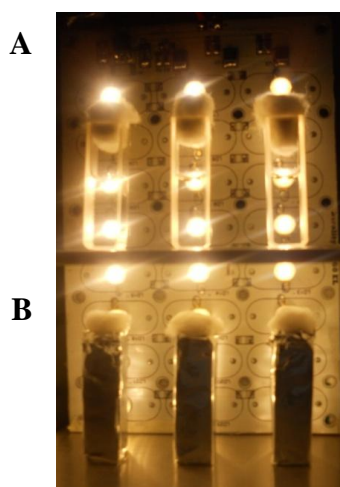
Figure 2.2: Visible light LED array photolysis setup used for photoinactivation of bacteria (A) irradiation condition, (B) dark condition.

Stability of $[Ru(bpy)_2(phendione)]^{2+}$, and $[Ru(phendione)_3]^{2+}$ was spectrophotometrically followed by recording absorption spectra. Briefly, 10^7 CFU/ml *E. coli* cells in PBS containing 10 μM of $[Ru(bpy)_2(phendione)]^{2+}$ or $[Ru(phendione)_3]^{2+}$ were incubated under light and dark conditions for 120 minutes. Absorption spectra of these suspensions were taken after filtering through 0.45 μm PTFE filter. It was observed that complexes were not adsorbed to this filter.

2.2.5. Effect of singlet oxygen quencher and hydroxyl radical scavenger on bacterial inactivation:

Stock solution of sodium azide (a known singlet oxygen quencher) was prepared in distilled water. 2 ml of 10^7 CFU/ml cells in PBS containing 10 μM of complex and 25 mM sodium azide in quartz cuvettes were photolysed for 120 minutes. Only quencher with bacteria was also exposed to light, as controls. Quencher in presence of $[Ru(bpy)_2(phendione)]^{2+}$ and $[Ru(phendione)_3]^{2+}$ was incubated under dark conditions, as dark controls. Similarly, mannitol (a known hydroxyl radical scavenger) was used to study the effect of hydroxyl radicals in presence of $[Ru(bpy)_2(phendione)]^{2+}$ and $[Ru(phendione)_3]^{2+}$. 100 μl aliquots from each reaction mixture were serially diluted and plated to find the effect of quencher/scavenger on cell viability.

2.2.6. Detection of singlet oxygen:

Spectrophotometric detection of singlet oxygen was done as reported, using AHP and DPBF [Komagoe et al., 2001, Amat-Guerri et al., 1999, Gomes et al., 2013, Pia Donzello et al., 2012]. $[Ru(bpy)_2(phendione)]^{2+}$, and $[Ru(phendione)_3]^{2+}$ (10 μM) in PBS containing AHP (200 μM) was exposed to light. Rose Bengal (10 μM) with AHP (200 μM) was studied as positive control for singlet oxygen. Spectra were recorded during photolysis at every 2 minute interval. Change in absorbance of AHP was monitored at its λ_{max} 318 nm. In the case of DPBF, DMF:H$_2$O (9:1) solution containing either $[Ru(bpy)_2(phendione)]^{2+}$ or $[Ru(phendione)_3]^{2+}$ (10 μM) and DPBF (50 μM) was exposed to light. Spectra were recorded during photolysis at every 1 minute interval. Change in absorbance of DPBF was monitored at its λ_{max} 414 nm.

2.2.7. Analysis of cell integrity:

LIVE/DEAD® *Bac*light™ Bacterial Viability Kit (Invitrogen™ Molecular Probes® L7012) has two dyes, SYTO9® (green fluorescence) and propidium iodide® (PI) (red fluorescence), which stain nucleic acids. SYTO9 can enter both live and dead cells and

gives green fluorescence. PI can enter only those cells in which membrane is damaged. Once it enters the cell, PI competitively binds to nucleic acids over SYTO9 and gives a bright red fluorescence. Thus, intact cells give green fluorescence whereas cells with damaged membranes exhibit red fluorescence [Salmi et al., 2008]. *E. coli* cells were treated with $[Ru(bpy)_2(phendione)]^{2+}$, and $[Ru(phendione)_3]^{2+}$ (10 μM), under dark and light conditions, for 120 minutes. Cells were then centrifuged and pellet was resuspended in 0.85% saline and 1:1 (v/v) dye mixture (SYTO9® and PI®) was added. Suspension was incubated in dark for 15 minutes, as per manufacturer's instructions. A small amount (10 μl) of the suspension was then placed on slide and covered with coverslip, avoiding air bubbles. Slides were then visualized under fluorescence microscope (Nikon Eclipse Ti-U, Nikon, Japan) with excitation wavelength of 480 nm (SYTO9) and 490 nm (PI).

2.2.8. Scanning Electron Microscopy (SEM) analysis:

E. coli cells in PBS were exposed to light for 120 minutes with and without (control) complexes (10 μM). Suspensions were then centrifuged at 5000 rpm for 10 minutes and cell pellet was washed with PBS. The obtained cells were resuspended in a minimum quantity of PBS and spread on a coverslip. Coverslips were then incubated for one hour in 2% glutaraldehyde for fixing cells. Smears were then washed with PBS and dehydrated using ethanol series in the order: 10%, 25%, 50%, 75%, 90% and 100% [Cahan et al., 2008]. Dried cells were coated with platinum by JEOL JFC-1600 Autobine sputter. Images were taken using JEOL JSM-6360LV SEM at a voltage of around 10kV.

2.2.9. *in viv*o genomic DNA extraction:

E. coli cells were treated with $[Ru(bpy)_2(phendione)]^{2+}$, and $[Ru(phendione)_3]^{2+}$ (10 μM) in presence of light for 120 minutes. Only cells were also photolysed for 120 minutes, as light control. Bacterial suspensions were centrifuged to obtain cell pellet, followed by extraction of DNA using bacterial genomic DNA isolation kit (SRL, Biolit™ BTK007), according to manufacturer's instructions. Extracted DNA was mixed with gel loading buffer and loaded in agarose gel. Samples were run on a 10 cm, 1% agarose gel for 3 hours at 60V. Gel was stained with Ethidium bromide (1 mg/ml) and visualized using Gel documentation system (Biorad GelDoc™ XR).

2.2.10. Adsorption of complexes by activated carbon and silica:

Activated carbon (0.75 and 1.5 mg/ml) was suspended in aqueous complex solution (10–30 μM range) and was thoroughly mixed. Suspension was then centrifuged at 5500 rpm for 3 minutes to settle the adsorbent. Supernatant was carefully transferred to quartz cuvette, and absorption spectrum was recorded to find the free complex remaining in supernatant and thus, determine adsorption of complex by activated carbon.

Silica (1.5 and 3 mg/ml) was suspended in aqueous solution of complex (5–30 μM range) and thoroughly mixed. Silica was allowed to settle and absorption spectra of the solutions were recorded at different time intervals to find the free complex remaining in supernatant and thus, determine adsorption of complex by silica.

Experiments were carried out at room temperature, in triplicates. Data was fitted to first order decay kinetics using Origin lab 6.1 (at 440 nm for $[Ru(bpy)_2(phendione)]^{2+}$ and at 466 nm for $[Ru(phendione)_3]^{2+}$) and rate constants were determined. Percentage adsorption for adsorbents was calculated by plotting C/C_o Vs time (C = concentration at a given time, C_o = initial concentration). Experimental data for adsorption of $[Ru(bpy)_2(phendione)]^{2+}$, and $[Ru(phendione)_3]^{2+}$ by activated carbon and silica were analysed using Freundlich equilibrium adsorption isotherm (equations 10 and 11, chapter 1) [Mohan et al., 2006]. Adsorption capacity (K_F) and adsorption intensity (n) constants were calculated.

2.2.11. Desorption of complexes:

100 mM KCl, 10 mM KCl and water at pH 4 (adjusted using HCl) were used for desorption studies. Silica saturated with complexes (silica 1.5 mg/ml containing 8.8 μM $[Ru(bpy)_2(phendione)]^{2+}$ or 4.7 μM $[Ru(phendione)_3]^{2+}$) was mixed thoroughly with appropriate solution. Amount of metal complexes desorbed into the solution was determined spectrophotometrically by following the increase in absorbance of complexes over the time. Kinetics of desorption was monitored at 440 nm for $[Ru(bpy)_2(phendione)]^{2+}$ and at 466 nm for $[Ru(phendione)_3]^{2+}$. Equation 1 was used to calculate percentage of desorption.

$$\text{Desorption ratio (\%)} = \frac{m_d}{m_a} \times 100 \quad .... (1)$$

where, m_d is mass of desorbed complex into solution and m_a is mass of complex adsorbed by adsorbent [Laus et al., 2010, Wang et al., 2009].

2.3.   Results and discussions:

2.3.1. Photoinduced antibacterial activity:

Visible light photolysis of bacteria in presence of either $[Ru(bpy)_2(phendione)]^{2+}$ or $[Ru(phendione)_3]^{2+}$ resulted in complete inactivation of bacteria (Figure 2.3, 2.4). Complexes had no effect on cell viability under dark conditions (Figure 2.3, 2.4). Time, fluence rate, total light dosage and effective concentrations for complete photoinactivation of both Gram positive and negative bacteria are summarised in Table1. Based on the above results, order of susceptibility of bacteria towards photolysis in presence of $[Ru(bpy)_2(phendione)]^{2+}$, and $[Ru(phendione)_3]^{2+}$ is given as:

B. subtilis> S. aureus > E. coli> P. aeruginosa
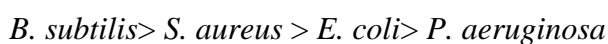
Photolysis of Ru(II) polypyridyl complexes is known to produce singlet oxygen, and generate other ROS (equation 5-8, chapter 1) [Lei et al., 2011, Gao et al., 2006, Yavin et al., 2004, Concepcion et al., 2007]. Singlet oxygen and ROS are known to cause cell damage [Caminos et al., 2008, Hamblin et al., 2004, Tavares et al., 2011, Spesia et al., 2009, Ragas et al., 2010, Lei et al., 2011, Arrojado et al., 2011, Manjon et al., 2009, Manjon et al., 2010]. This fact indicates that reactive species generated on photolysis of Ru(II) complexes could attack cell and cause cell damage.

Importantly, the above results showed that Gram-positive bacteria (*S. aureus* and *B. subtilis*) were more susceptible towards photoinactivation than Gram-negative bacteria (*E. coli* and *P. aeruginosa*). Gram-negative bacteria have a peptidoglycan layer between its outer and inner membrane. Outer membrane acts as a barrier between cell and its environment, maintaining cell integrity. This extra outer membrane may provide resistance to Gram-negative bacteria against reactive species generated during photolysis [Hamblin et al., 2004]. However, in case of Gram-positive bacteria the relatively porous layer of peptidoglycan and lipoteichoic acid surrounding cytoplasmic membrane, lack extra outer membrane, and is more susceptible to reactive species. Earlier, such difference between Gram-positive and Gram-negative bacteria was observed [Hamblin et al., 2004, Maclean et al., 2009]. Thus, the results indicate that photolysis of $[Ru(bpy)_2(phendione)]^{2+}$, and $[Ru(phendione)_3]^{2+}$ have the ability to cause inactivation of both Gram-positive and Gram-negative bacteria by generating reactive radicals.

Table 2.1: Complete photoinactivation of bacterial cells in presence of $[Ru(bpy)_2(phendione)]^{2+}$, and $[Ru(phendione)_3]^{2+}$ using visible light LED at 37 °C.

Name and type of bacteria	$[Ru(bpy)_2(phendione)]^{2+}$				$[Ru(phendione)_3]^{2+}$			
	Time[a]	Fluence rate[b]	Light dosage[c]	Conc[d]	Time[a]	Fluence rate[b]	Light dosage[c]	Conc[d]
Gram-negative								
E. coli	100	95	570	10	120	95	684	10
P. aeruginosa	120	95	684	20	120	95	684	20
Gram-positive								
S. aureus	80	60	288	5	80	60	288	5
B. subtilis	60	48	172.8	5	60	48	172.8	5

[a]min, [b]mW/cm^2, [c]J/cm^2, [d]μM

Effect of concentration of $[Ru(bpy)_2(phendione)]^{2+}$ and $[Ru(phendione)_3]^{2+}$ on photoinactivation:

Effect of concentration of $[Ru(bpy)_2(phendione)]^{2+}$ and $[Ru(phendione)_3]^{2+}$ on visible light inactivation of both Gram-negative bacteria and Gram-positive bacteria in presence of $[Ru(bpy)_2(phendione)]^{2+}$ and $[Ru(phendione)_3]^{2+}$ was studied. 5 μM of either $[Ru(bpy)_2(phendione)]^{2+}$ or $[Ru(phendione)_3]^{2+}$ caused ~4 log reduction, and 10 μM caused 7 log reduction in cell viability of Gram-negative bacteria, *E. coli* within 140 min (Figure 2.3 (A)). Moreover, the other Gram-negative bacteria, *P. aeruginosa* showed ~1.5 log reduction at 5 μM of either $[Ru(bpy)_2(phendione)]^{2+}$ or $[Ru(phendione)_3]^{2+}$, ~3.5 log reduction at 10 μM, and 7 log reduction in cell viability at 20 μM, within 140 min (Figure 2.3 (B)). On the other hand, Gram-positive bacteria, *S. aureus* showed ~5 log reduction at 2.5 μM of either $[Ru(bpy)_2(phendione)]^{2+}$ or $[Ru(phendione)_3]^{2+}$, and 7 log reduction in cell viability at 5 μM, within 140 min (Figure 2.4 (A)). Additionally, 2.5 μM of either $[Ru(bpy)_2(phendione)]^{2+}$ or $[Ru(phendione)_3]^{2+}$ caused ~5 log reduction, and 5 μM caused 7 log reduction in cell viability of Gram-positive bacteria, *B. subtilis* (Figure 2.4 (B)).

Figure 2.3: Cell viability Vs Light dosage (Time) plot of $[Ru(bpy)_2(phendione)]^{2+}$ (C1) and $[Ru(phendione)_3]^{2+}$ (C2) for Gram-negative bacteria (A) *E. coli* and (B) *P. aeruginosa*.
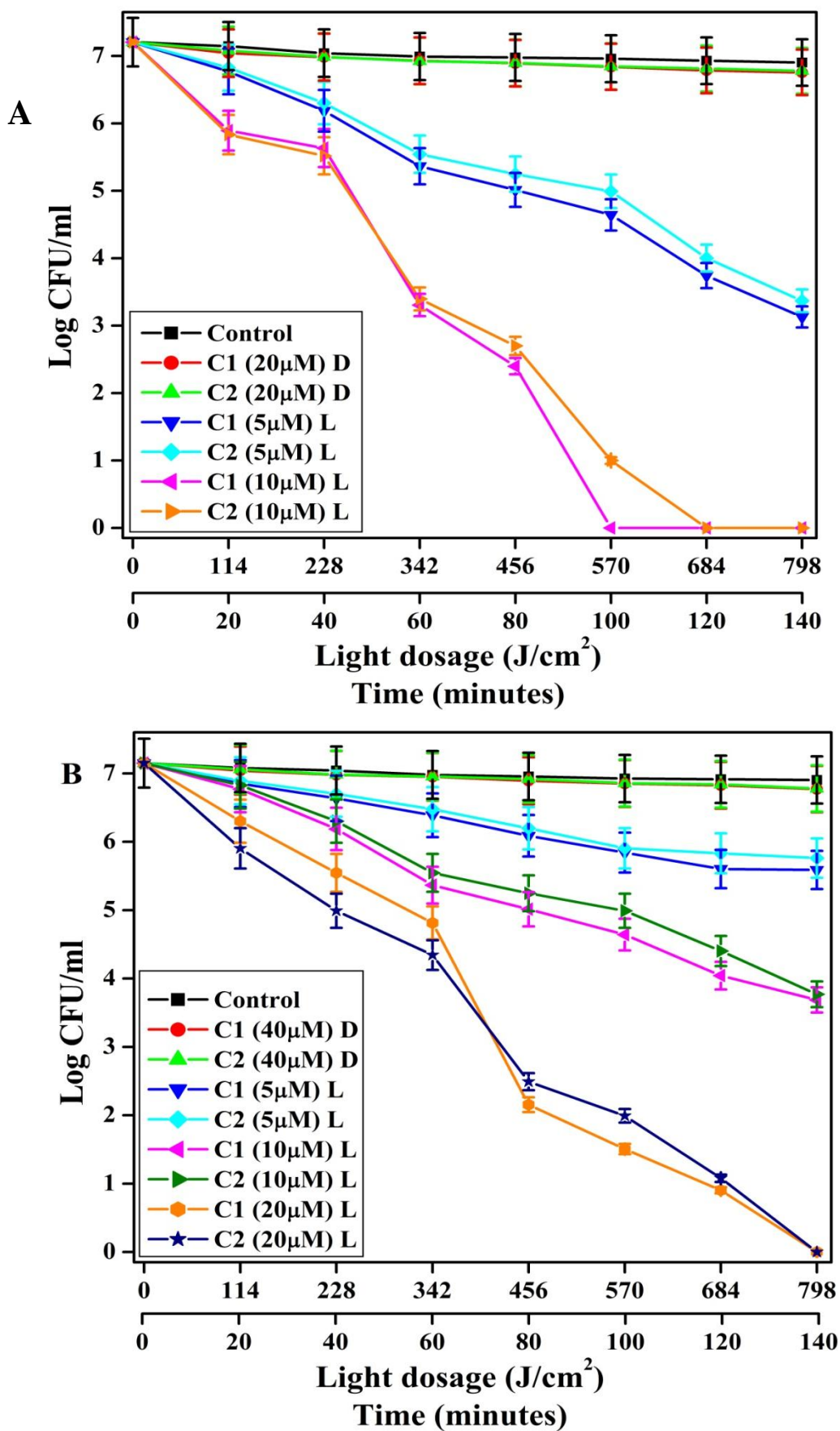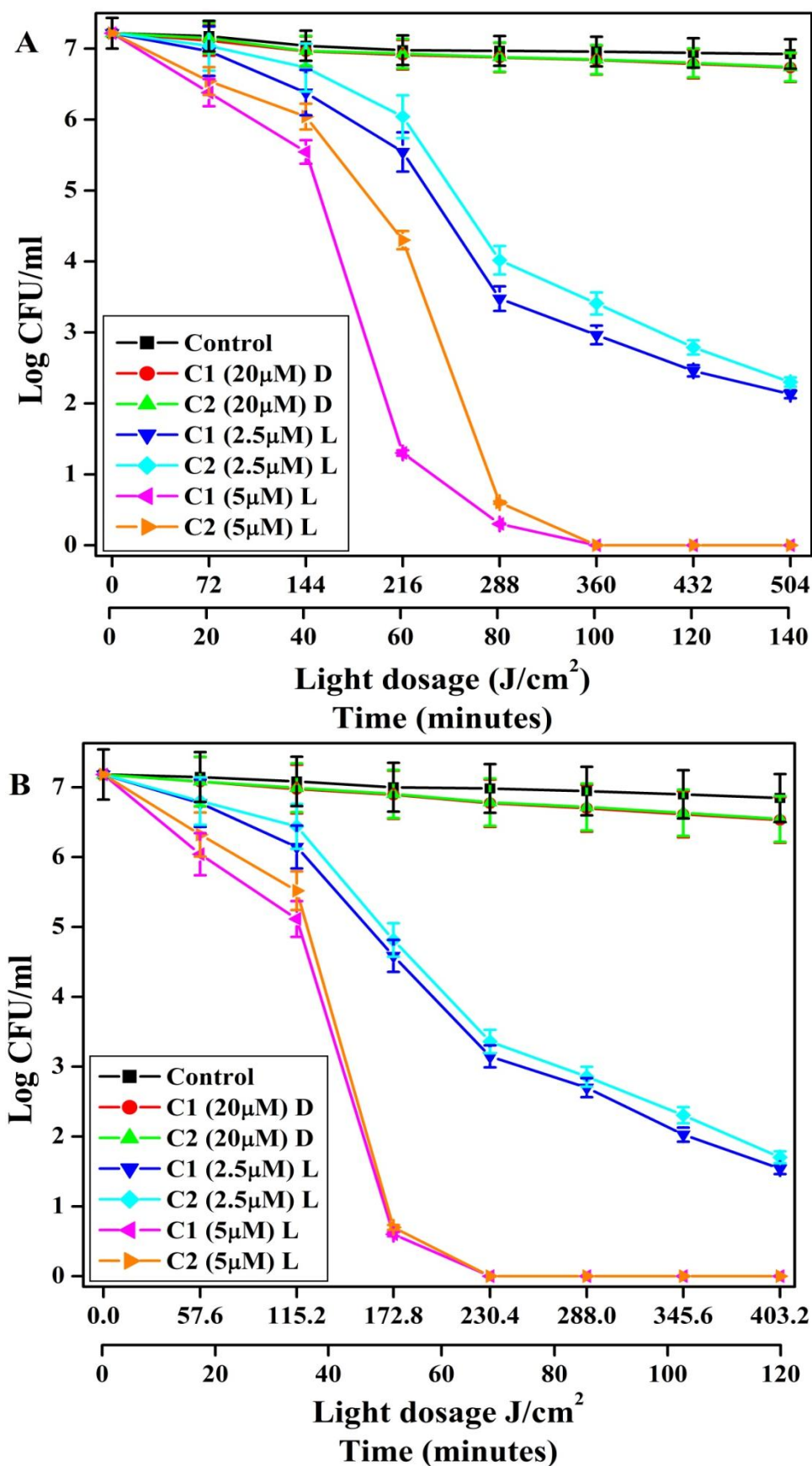
Figure 2.4: Cell viability Vs Light dosage (Time) plot of $[Ru(bpy)_2(phendione)]^{2+}$ (C1) and $[Ru(phendione)_3]^{2+}$ (C2) for Gram-positive bacteria (A) *S. aureus* and (B) *B. subtilis*.

Effect of initial cell concentration on photoinactivation of *E. coli* by [Ru(bpy)$_2$(phendione)]$^{2+}$ and [Ru(phendione)$_3$]$^{2+}$:

Effect of initial concentration of cells on photoinactivation of *E. coli* by [Ru(bpy)$_2$(phendione)]$^{2+}$ and [Ru(phendione)$_3$]$^{2+}$ revealed that complete inactivation was achieved within 120 minutes when initial concentration was 10^7 CFU/ml cells and significant inactivation (~7 log reduction) was achieved within 120 minutes when initial concentration was increased to 10^8 CFU/ml cells (Figure 2.5). The time for complete inactivation was reduced to 60 minutes on decreasing the initial concentration to 10^3 CFU/ml cells (Figure 2.5). These results reveal that the complexes are promising photosensitizers for inactivation of *E. coli* [Demidova et al., 2005].

Photostability of complexes:

Importantly, effective photoinactivation of bacteria was achieved using LED array as visible light source. LEDs are preferred owing to their low energy consumption, and are safe to handle. They are compact, and also known to have long life time [Maclean et al., 2009, Chen et al., 2011]. Under these photolytic conditions, both the complexes were found to be photostable in presence or absence of *E. coli* cells (Figure 2.6, 2.7), indicating that complexes are effective for visible light inactivation of bacteria.
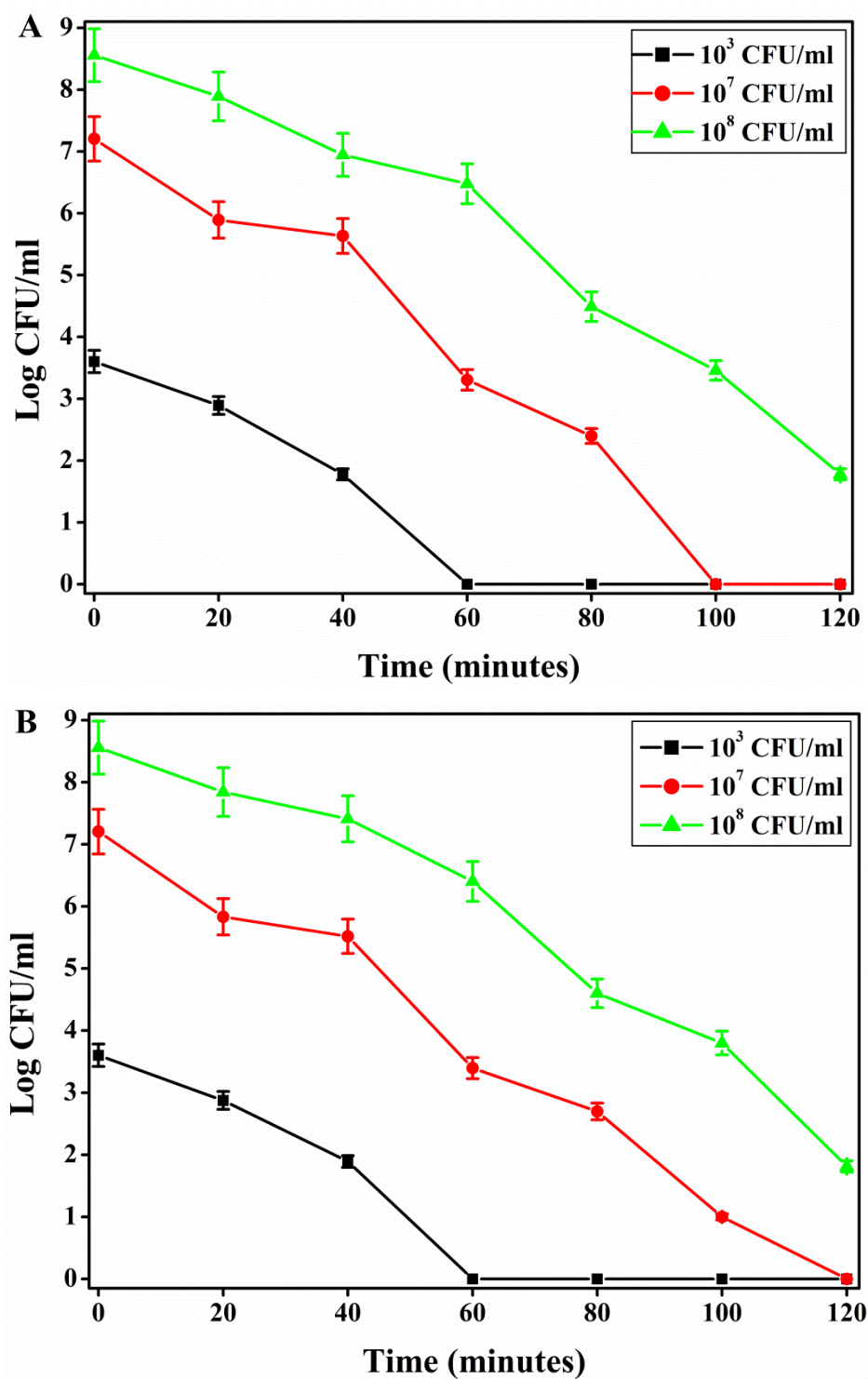
Figure 2.5: Dependence of photoinactivation of *E. coli*, in presence of (A) $[Ru(bpy)_2(phendione)]^{2+}$ and (B) $[Ru(phendione)_3]^{2+}$ on cell concentration.
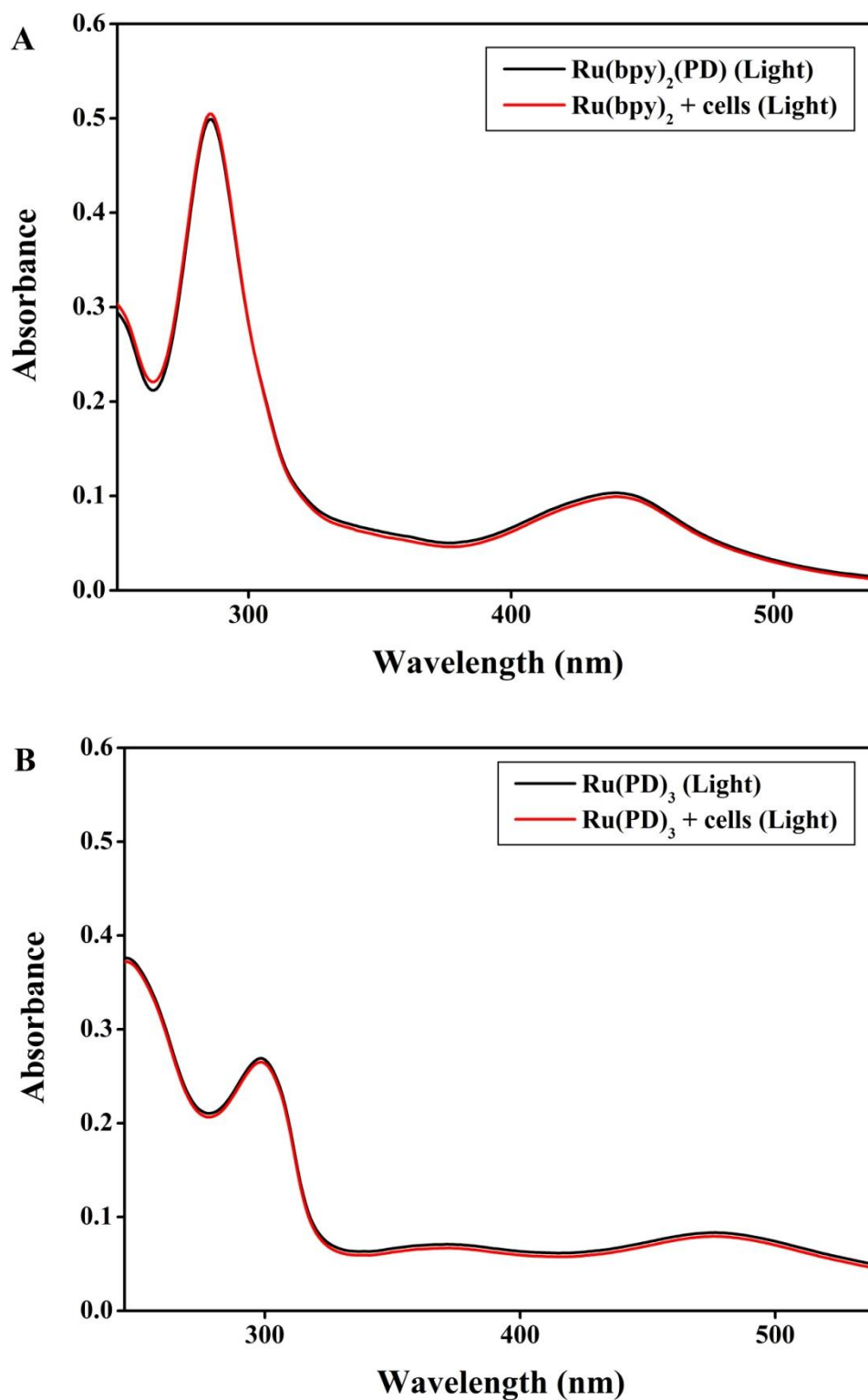
Figure 2.6: Stability of (A) [Ru(bpy)$_2$(phendione)]$^{2+}$ and (B) [Ru(phendione)$_3$]$^{2+}$ under light irradiation. Absorption spectra of the filtered solutions of [Ru(bpy)$_2$(phendione)]$^{2+}$ (10 μM) and [Ru(phendione)$_3$]$^{2+}$ (10 μM), with and without *E. coli* cells.
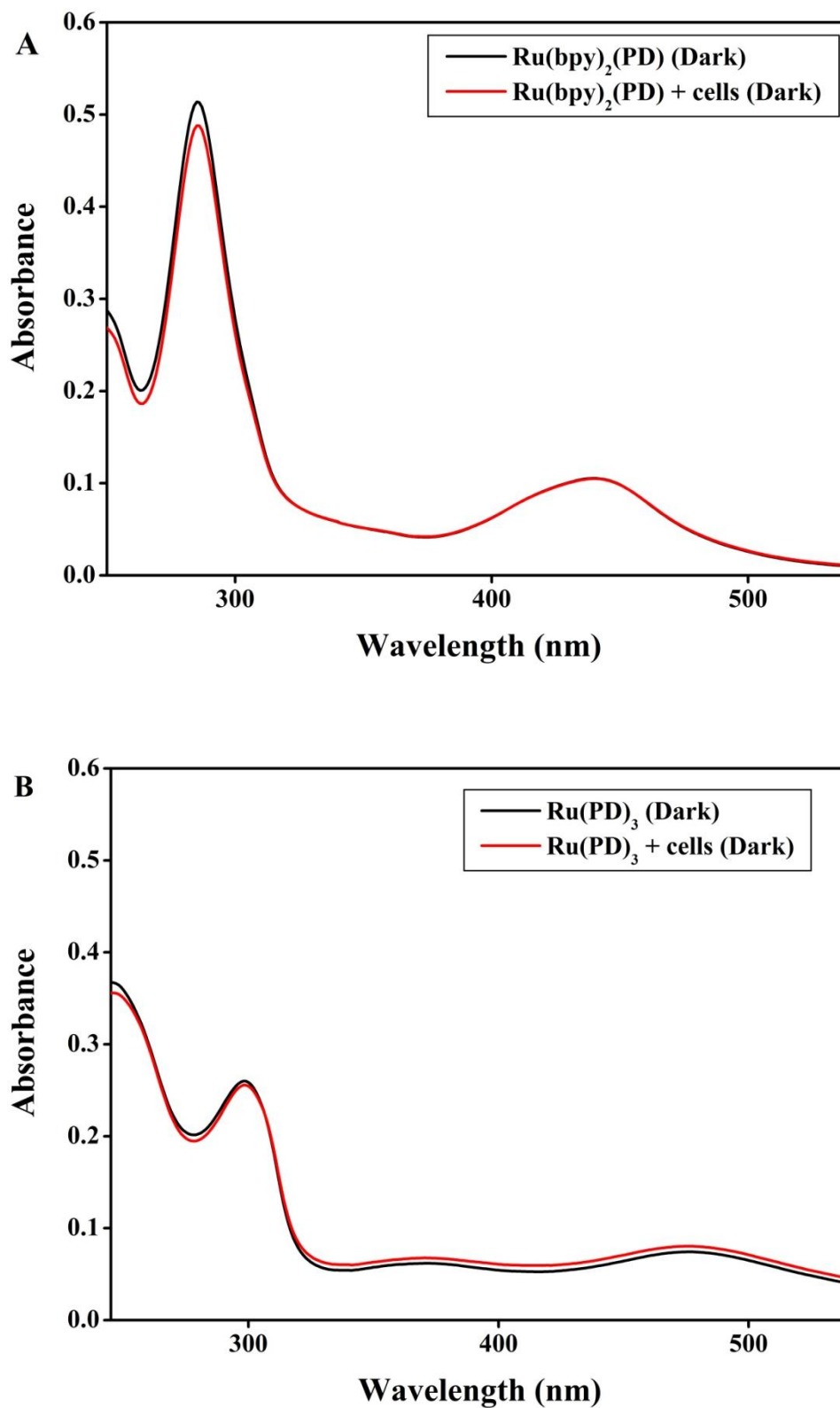
Figure 2.7: Stability of (A) [Ru(bpy)$_2$(phendione)]$^{2+}$ and (B) [Ru(phendione)$_3$]$^{2+}$ under dark conditions. Absorption spectra of the filtered solutions of [Ru(bpy)$_2$(phendione)]$^{2+}$ (10 μM) and [Ru(phendione)$_3$]$^{2+}$ (10 μM), with and without *E. coli* cells.

2.3.2. Effect of singlet oxygen quencher and hydroxyl radical scavenger on photoinactivation of bacteria:

Effect of quencher/scavenger on photoinactivation was studied using *E. coli* as model organism. Photolysis of *E. coli* by $[Ru(bpy)_2(phendione)]^{2+}$ (10 μM), and $[Ru(phendione)_3]^{2+}$ (10 μM) in presence of sodium azide (25 mM) showed complete inactivation (Figure 2.8 (A)), similar to that observed in absence of sodium azide (Figure 2.8 (A)). Importantly, sodium azide (25 mM) alone under light, and also sodium azide in presence of $[Ru(bpy)_2(phendione)]^{2+}$, and $[Ru(phendione)_3]^{2+}$ under dark condition had no effect on viability of *E. coli* (Figure 2.8 (A), 2.9 (A)). Sodium azide is a well known quencher of singlet oxygen [Tavares et al., 2011, Cormick et al., 2011, Maisch et al., 2005]. The above results showed that sodium azide was not able to inhibit photoinactivation, indicating that singlet oxygen is not major reactive species for inactivation of *E. coli*.

In addition, there was no significant decrease in absorbance on photolysis of singlet oxygen probe, AHP (200 μM) in presence of $[Ru(bpy)_2(phendione)]^{2+}$ (10 μM), and $[Ru(phendione)_3]^{2+}$ (10 μM), as compared to standard singlet oxygen generator, rose bengal (10 μM) (Figure 2.8 (B), 2.10) [Komagoe et al., 2001, Amat-Guerri et al., 1999]. Moreover, DPBF (50 μM), singlet oxygen scavenger, was also not degraded effectively on photolysis in presence of $[Ru(bpy)_2(phendione)]^{2+}$ (10 μM), and $[Ru(phendione)_3]^{2+}$ (10 μM) (Figure 2.8 (B)). However, DPBF was significantly degraded in presence of rose bengal (10 μM) (Figure 2.11) [Gomes et al., 2013, Pia Donzello et al., 2012]. This result further emphasize that singlet oxygen is not the major reactive species for photoinactivation of *E. coli* by $[Ru(bpy)_2(phendione)]^{2+}$, and $[Ru(phendione)_3]^{2+}$. Ru(II) complexes containing phendione ligands are known to be non-emissive or have reduced emission at room temperature [Campagna et al., 1999]. MLCT excitation of these complexes results in charge-separated excited species [Concepcion et al., 2007, Campagna et al., 1999]. The charge-separated excited species undergo fast radiation-less decay to ground state resulting in quenching or reduced MLCT luminescence [Zhou et al., 2010 (ii), Chouai et al., 2005], which is not favourable for the formation of singlet oxygen [Garcìa-Fresnadillo et al., 1996, Zhou et al., 2010 (ii), Chouai et al., 2005, DeRosa et al., 2002].
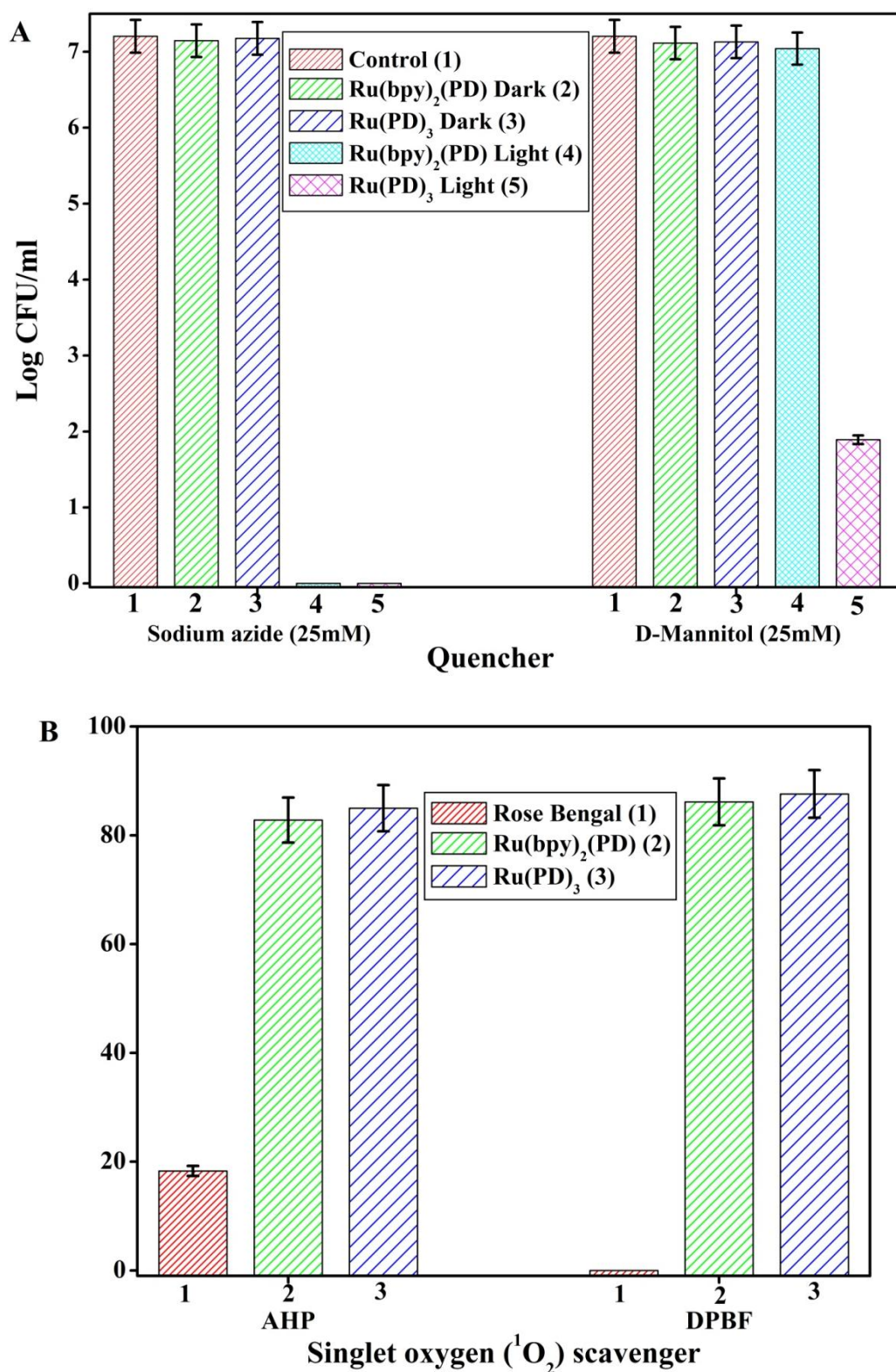
Figure 2.8: (A) Effect of ROS quenchers on photoinactivation of *E. coli* by [Ru(bpy)$_2$(phendione)]$^{2+}$ (10 μM), and [Ru(phendione)$_3$]$^{2+}$ (10 μM). (B) Photodegradation of 2-amino-3-hydroxypyridine (200 μM) and 1,3-diphenylisobenzofuran (50 μM) in presence of [Ru(bpy)$_2$(phendione)]$^{2+}$ (10 μM), [Ru(phendione)$_3$]$^{2+}$ (10 μM) and rose bengal (10 μM).
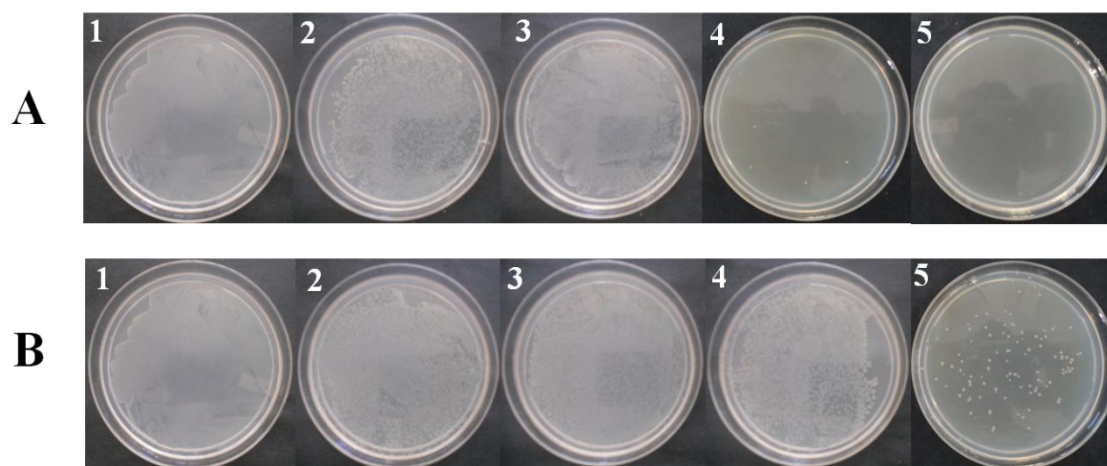
Figure 2.9: Effect of ROS quenchers on photoinactivation of *E. coli* by [Ru(bpy)$_2$(phendione)]$^{2+}$ (10 μM), and [Ru(phendione)$_3$]$^{2+}$ (10 μM). A- In presence of 25 mM Sodium azide, B- In presence of 25 mM of D-mannitol. 1- Light control, 2- [Ru(bpy)$_2$(phendione)]$^{2+}$ (Dark), 3- [Ru(phendione)$_3$]$^{2+}$ (Dark), 4- [Ru(bpy)$_2$(phendione)]$^{2+}$ (Light), 5- [Ru(phendione)$_3$]$^{2+}$ (Light).
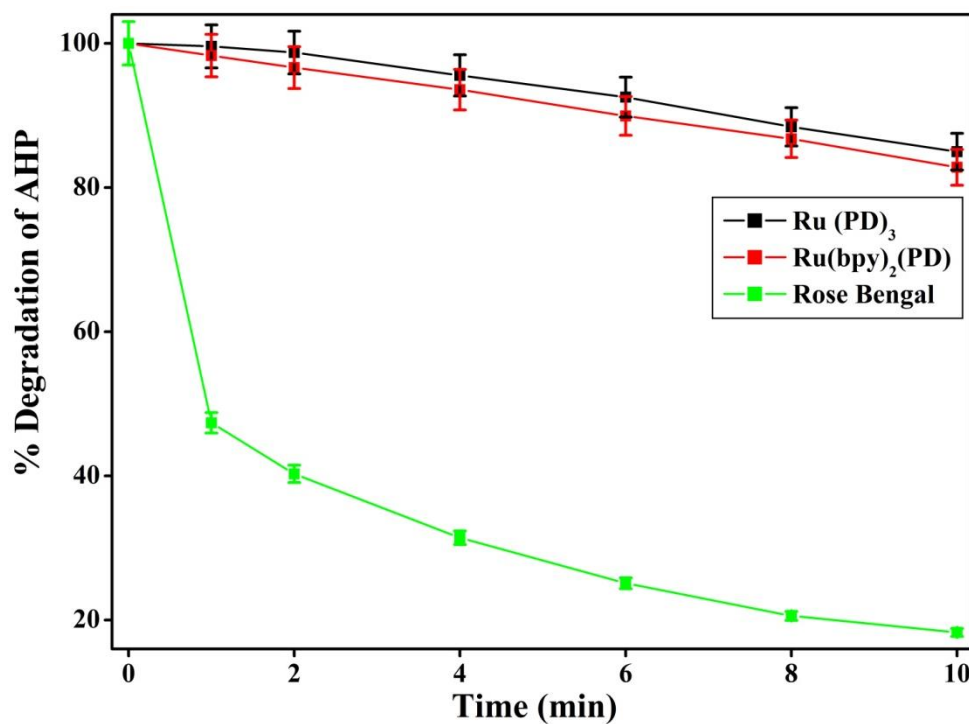
Figure 2.10: Photodegradation of singlet oxygen ($^1O_2$) scavenger, 2-amino-3-hydroxypyridine (AHP) (200 μM) in presence of [Ru(bpy)$_2$(phendione)]$^{2+}$ (10 μM), [Ru(phendione)$_3$]$^{2+}$ (10 μM) and rose bengal (10 μM).
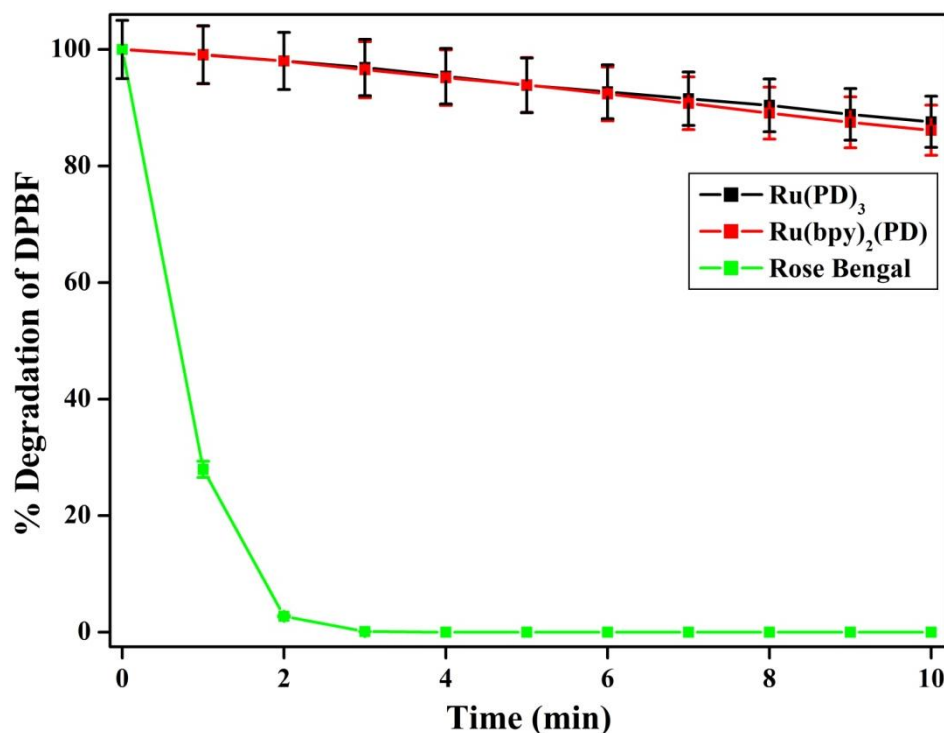
Figure 2.11: Photodegradation of singlet oxygen ($^1O_2$) scavenger, 1,3-diphenylisobenzofuran (DPBF) (50 μM) in presence of [Ru(bpy)$_2$(phendione)]$^{2+}$ (10 μM), [Ru(phendione)$_3$]$^{2+}$ (10 μM) and rose bengal (10 μM).

Photoinactivation of *E. coli* by [Ru(bpy)$_2$(phendione)]$^{2+}$ (10 μM), and [Ru(phendione)$_3$]$^{2+}$ (10 μM) was investigated in presence of mannitol (25 mM), which is known to scavenge highly reactive hydroxyl radicals [Tavares et al., 2011, Cormick et al., 2011, Maisch et al., 2005]. In presence of mannitol no growth inhibition was observed for [Ru(bpy)$_2$(phendione)]$^{2+}$, and only partial growth inhibition was observed for [Ru(phendione)$_3$]$^{2+}$ (Figure 2.8 (A)). Photolysis of *E. coli* with mannitol (25 mM) alone had no effect on cell viability. Moreover, on incubation of cells in presence of [Ru(bpy)$_2$(phendione)]$^{2+}$, and [Ru(phendione)$_3$]$^{2+}$ with mannitol under dark conditions, also had no effect on viability of *E. coli* (Figure 2.8 (A), 2.9 (B)). These results indicated that hydroxyl radicals are scavenged by mannitol, and therefore inhibit photoinactivation leading to growth of cells. Earlier, it has been reported that irradiation of Ru(II) polypyridyl complexes highly reactive hydroxyl radicals that cause non specific DNA damage [Yavin et al., 2004]. Thus, photolysis of [Ru(bpy)$_2$(phendione)]$^{2+}$ and [Ru(phendione)$_3$]$^{2+}$ cause oxidative damage to *E. coli*, leading to loss of cell integrity.

2.3.3. Cell integrity analysis:

LIVE/DEAD® *Bac*light™ assay was performed to determine cell integrity [Salmi et al., 2008]. Cells incubated with [Ru(bpy)$_2$(phendione)]$^{2+}$, and [Ru(phendione)$_3$]$^{2+}$ under dark conditions showed green fluorescence (Figure 2.12) due to uptake of membrane permeable SYTO9® dye and its binding to nucleic acids, indicating the cells were unaffected. On the other hand, cells incubated with [Ru(bpy)$_2$(phendione)]$^{2+}$, and [Ru(phendione)$_3$]$^{2+}$ and photolysed, showed red fluorescence due to PI®. PI can enter only those cells in which membranes are damaged, and competitively bind to nucleic acids to produce bright red fluorescence [Salmi et al., 2008] (Figure 2.12). Thus, these results clearly indicated that cell membrane was damaged, resulting in loss of cell integrity on exposure to light in presence of [Ru(bpy)$_2$(phendione)]$^{2+}$, and [Ru(phendione)$_3$]$^{2+}$. SEM analysis also revealed extensive membrane damage and deformation of cells, on photolysis in presence of [Ru(bpy)$_2$(phendione)]$^{2+}$, and [Ru(phendione)$_3$]$^{2+}$ (Figure 2.13). In addition, loss of genomic DNA upon photoinactivation in presence of [Ru(bpy)$_2$(phendione)]$^{2+}$, and [Ru(phendione)$_3$]$^{2+}$ was also observed (Figure 2.14). This result indicated that membrane damage leads to loss of DNA. Earlier, such loss of DNA was observed during photoinactivation of *E. coli* by porphyrin and phthalocyanine [Caminos et al., 2008, Spesia et al., 2009].

Dark **Light**

Ru(bpy)₃(PD)

Ru(PD)₃
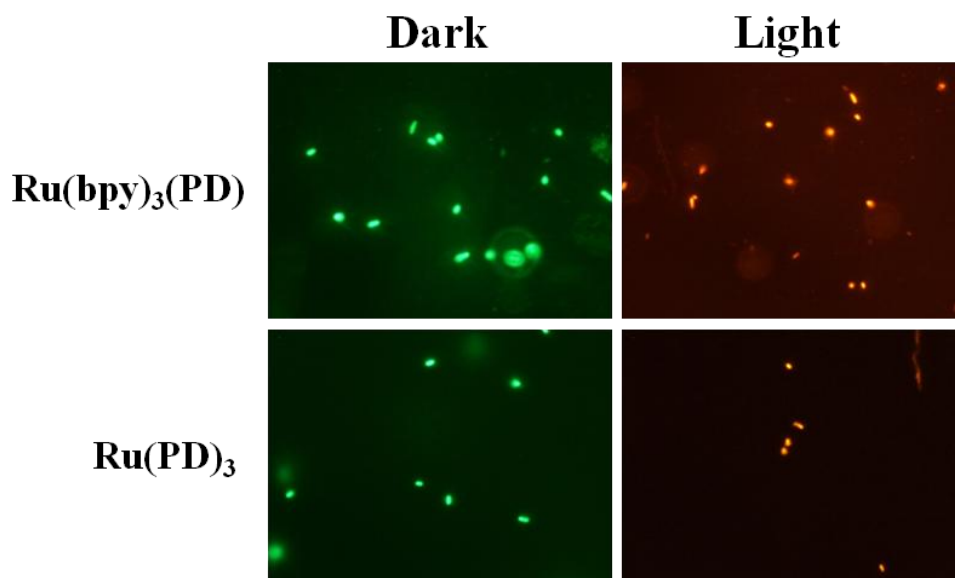
Figure 2.12: Fluorescence analysis of *E. coli* cells incubated with [Ru(bpy)$_2$(phendione)]$^{2+}$ (10 μM) and [Ru(phendione)$_3$]$^{2+}$ (10 μM) under dark and light conditions (120 minutes) using LIVE/DEAD® *Bac*light™ assay.

Control **Ru(bpy)₃(PD)** **Ru(PD)₃**
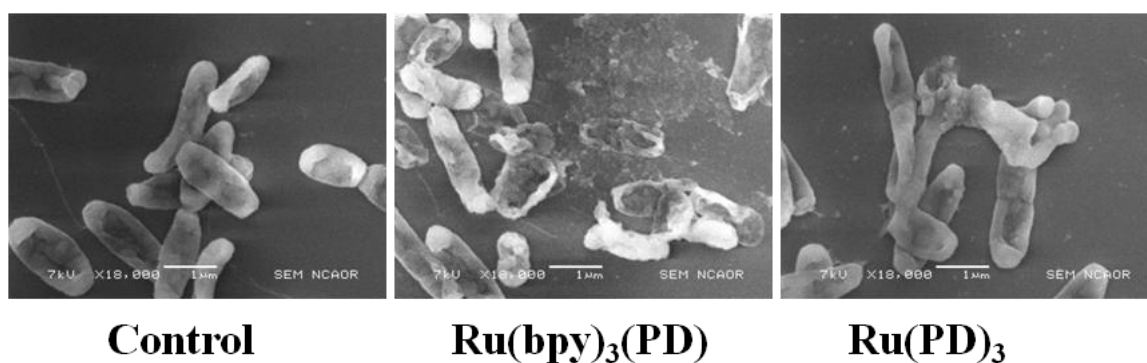
Figure 2.13: SEM analysis of *E. coli* (control) and *E. coli* cells photolysed with [Ru(bpy)$_2$(phendione)]$^{2+}$ (10 μM) and [Ru(phendione)$_3$]$^{2+}$ (10 μM), (120 minutes) (Magnification= 18,000 X).

1 **2** **3**
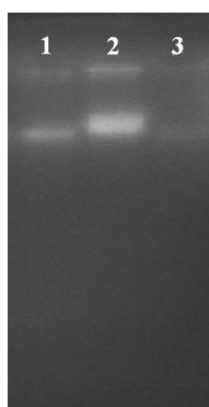
Figure 2.14: Loss of genomic DNA of *E. coli* on photolysis in presence of [Ru(bpy)$_2$(phendione)]$^{2+}$ (10 μM), and [Ru(phendione)$_3$]$^{2+}$ (10 μM). Lane no. 1 = [Ru(bpy)$_2$(phendione)]$^{2+}$ (Light), 2 = Light control, 3 = [Ru(phendione)$_3$]$^{2+}$ (Light).

48

2.3.4. Adsorption of complexes by activated carbon and silica:

Addition of [Ru(bpy)$_2$(phendione)]$^{2+}$ (C$_o$ = 10 μM) to activated carbon (1.5 mg/ml) resulted in about 98% adsorption, and rate of adsorption was determined to be 5.95 x10^{-2} s^{-1} (Figure 2.15 (A), 2.17 (A)) (Table 2.3). In case of [Ru(phendione)$_3$]$^{2+}$ (C$_o$ = 10 μM), percentage and rate of adsorption to activated carbon were determined to be ~94% and 5.81 x10^{-2} s^{-1}, respectively (Figure 2.15 (B), 2.17 (B)) (Table 2.3). Adsorption was found to depend on initial concentration (C$_o$) of complex as well as amount of activated carbon (Table 2.3).The results were analysed by Freundlich adsorption isotherms (Figure 2.15 (A, B)) (Table 2.2). Freundlich adsorption capacity, K$_F$ values for [Ru(bpy)$_2$(phendione)]$^{2+}$ and [Ru(phendione)$_3$]$^{2+}$ were determined to be 22.74 and 8.26, respectively (Table 2.2). This result showed that adsorption of [Ru(bpy)$_2$(phendione)]$^{2+}$ by activated carbon was better than adsorption of [Ru(phendione)$_3$]$^{2+}$. Adsorption capacity values determined in present investigation were close to values obtained for molecules such as phenols, metal ions and other metal complexes reported earlier [Gonzalez-Serrano et al., 2004, Jusoh et al., 2005, Kim, 2004, Aksu et al., 1999].

Adsorption of complexes was also studied using silica [Zaporozhets et al., 1999]. Addition of [Ru(bpy)$_2$(phendione)]$^{2+}$ (C$_o$ = 10 μM) to silica (1.5 mg/ml) resulted in about 88% adsorption, and rate of adsorption was determined to be ~9.64 x10^{-3} s^{-1} (Figure 2.16 (B), 2.18 (A)) (Table 2.4). In case of [Ru(phendione)$_3$]$^{2+}$, it was observed that ~47% of [Ru(phendione)$_3$]$^{2+}$ (C$_o$ = 10 μM) binds to 1.5 mg/ml silica (Figure 2.16 (B), 2.18 (B)) (Table 2.4). Percentage and rate of adsorption were found to depend on initial concentration (C$_o$) of complex as well as amount of silica (Table 2.4). K$_F$ values, for [Ru(bpy)$_2$(phendione)]$^{2+}$ and [Ru(phendione)$_3$]$^{2+}$ were determined to be 3.62 and 0.57, respectively (Table 2.2). This result also revealed that adsorption of [Ru(bpy)$_2$(phendione)]$^{2+}$ by silica was more effective than adsorption of [Ru(phendione)$_3$]$^{2+}$. All the above results revealed that adsorption of complexes by activated carbon was more effective that adsorption by silica.
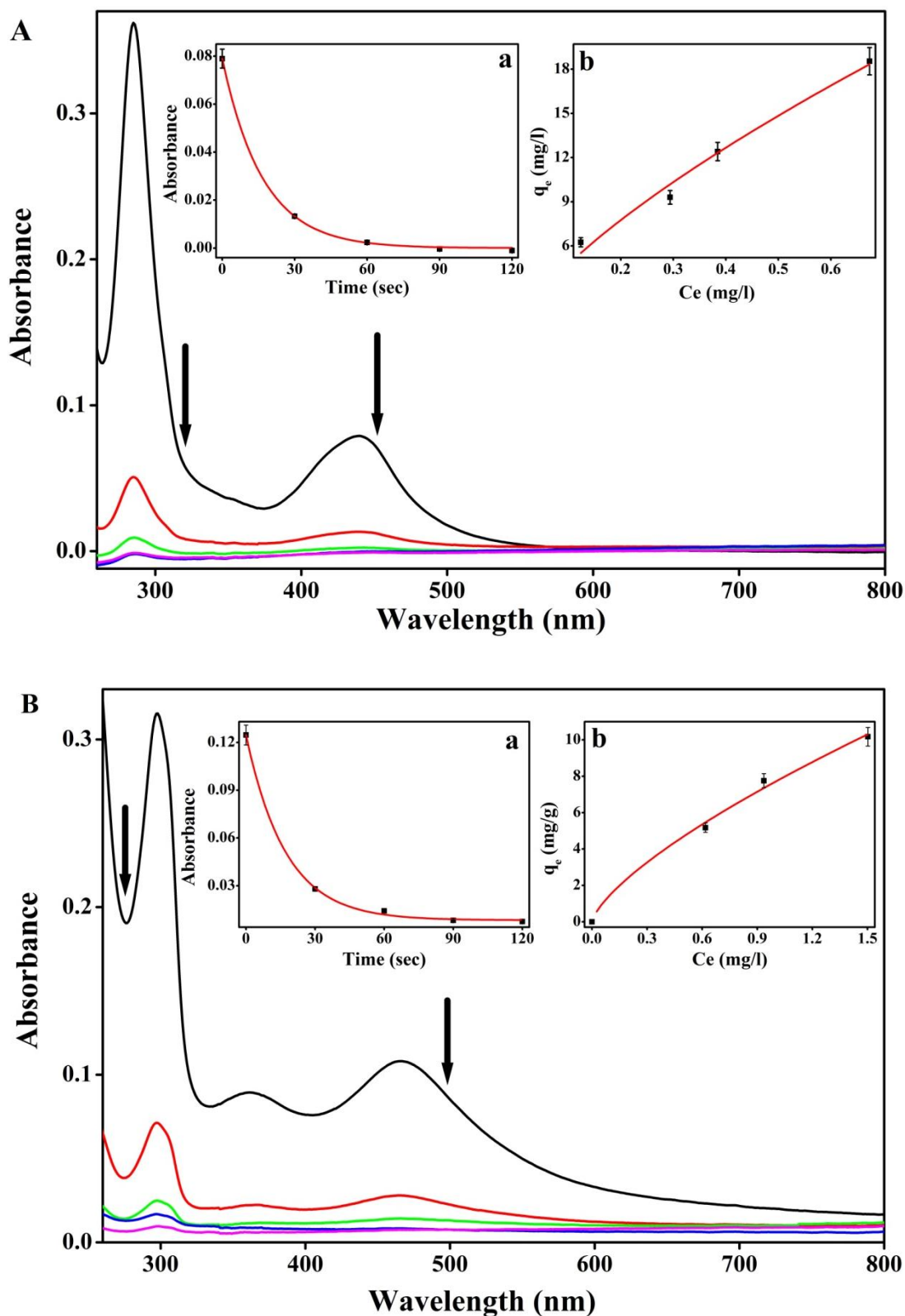
Figure 2.15: Absorption spectral changes of (A) $[Ru(bpy)_2(phendione)]^{2+}$ (C_o = 10 μM), and (B) $[Ru(phendione)_3]^{2+}$ (C_o = 10 μM) on adsorption by activated carbon (1.5 mg/ml). Inset a: Absorption decrease monitored at 440 nm and 466 nm for $[Ru(bpy)_2(phendione)]^{2+}$ and $[Ru(phendione)_3]^{2+}$, respectively, and kinetics of adsorption of complexes with first order fit. Inset b: C_e (mg/l) Vs q_e (mg/g) adsorption isotherm with non-linear curve fit.
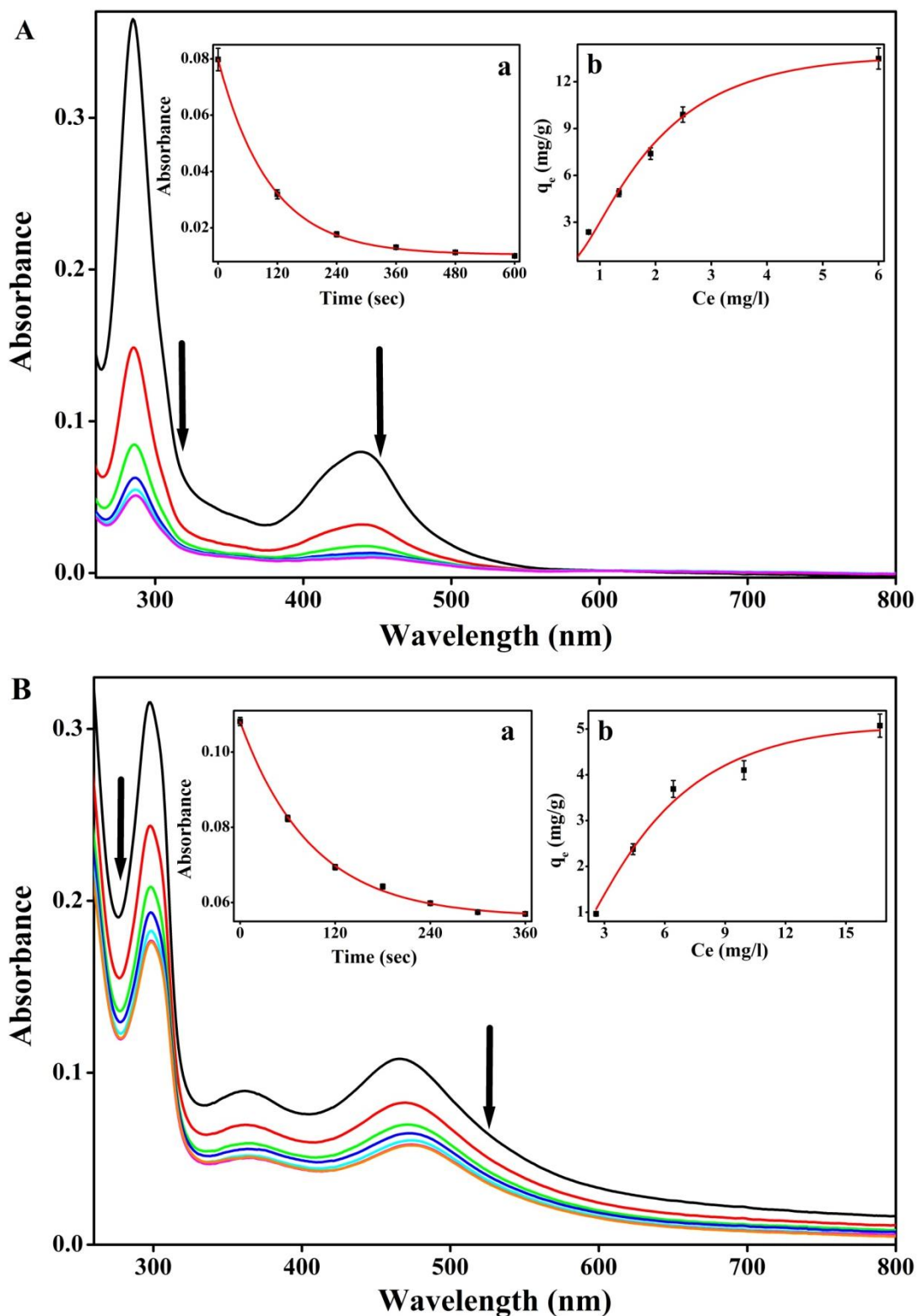
Figure 2.16: Absorption spectral changes of (A) $[Ru(bpy)_2(phendione)]^{2+}$ ($C_o = 10$ μM), and (B) $[Ru(phendione)_3]^{2+}$ ($C_o = 10$ μM) on adsorption by silica (1.5 mg/ml). Inset a: Absorption decrease monitored at 440 nm and 466 nm for $[Ru(bpy)_2(phendione)]^{2+}$ and $[Ru(phendione)_3]^{2+}$, respectively, and kinetics of adsorption of complexes with first order fit. Inset b: C_e (mg/l) Vs q_e (mg/g) adsorption isotherm with non-linear curve fit.

Table 2.2: Isotherm fitting parameters. Adsorption capacity, K_F and adsorption intensity, n of activated carbon and silica for $[Ru(bpy)_2(phendione)]^{2+}$, and $[Ru(phendione)_3]^{2+}$.

Adsorbent	Complex	$K_F{}^a$	n	1/n	$R^{2\,b}$	$R^{2\,c}$
Activated carbon	$[Ru(bpy)_2(phendione)]^{2+}$	22.74	1.55	0.64	0.98676	0.98345
	$[Ru(phendione)_3]^{2+}$	8.26	1.01	0.99	0.94307	0.97859
Silica	$[Ru(bpy)_2(phendione)]^{2+}$	3.62	1.17	0.85	0.94931	0.99534
	$[Ru(phendione)_3]^{2+}$	0.57	1.17	0.85	0.93141	0.93495

^{a} C_e is expressed in mg/l and in q_e mg/g. ^{b} goodness of fit for linear curve fitting.

^{c} goodness of fit for non-linear curve fitting.
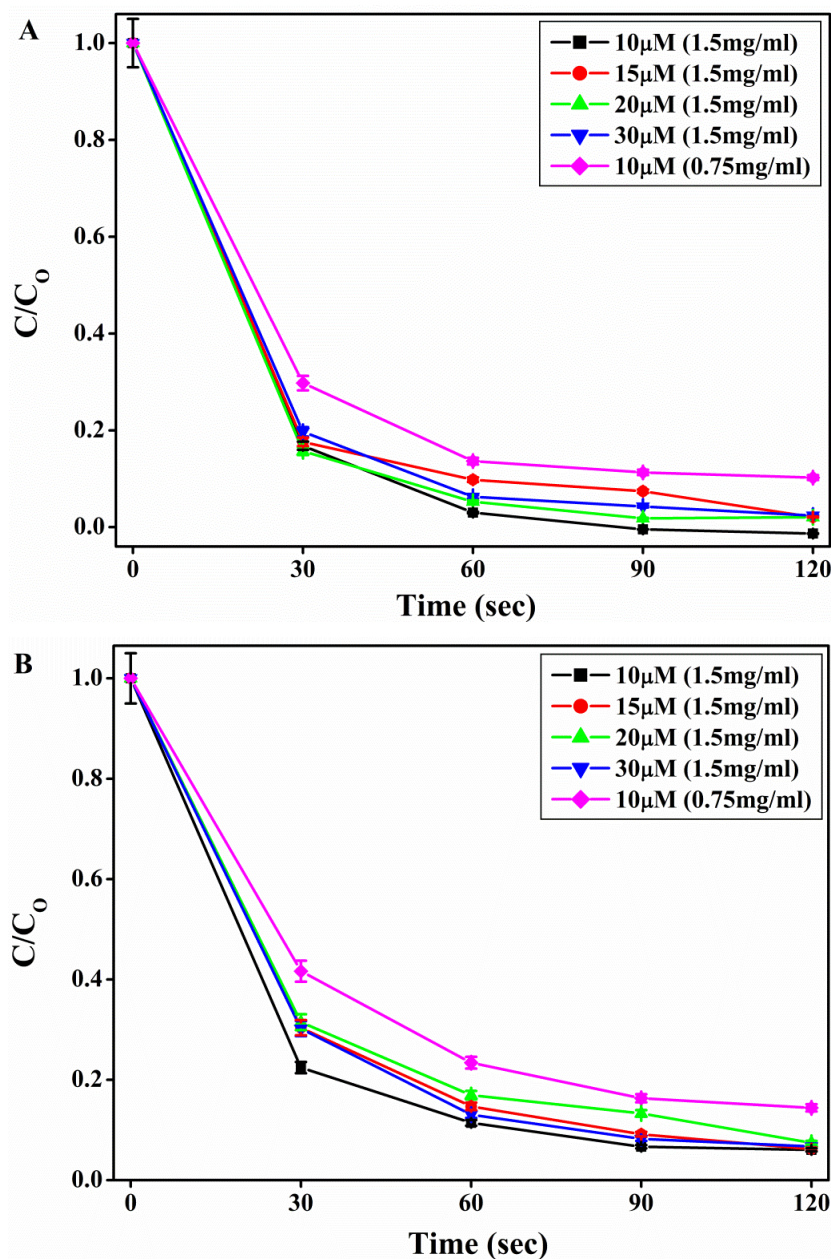
Figure 2.17: C/C_o Vs time plot for adsorption of (A) $[Ru(bpy)_2(phendione)]^{2+}$ by activated carbon, (B) $[Ru(phendione)_3]^{2+}$ by activated carbon.

52
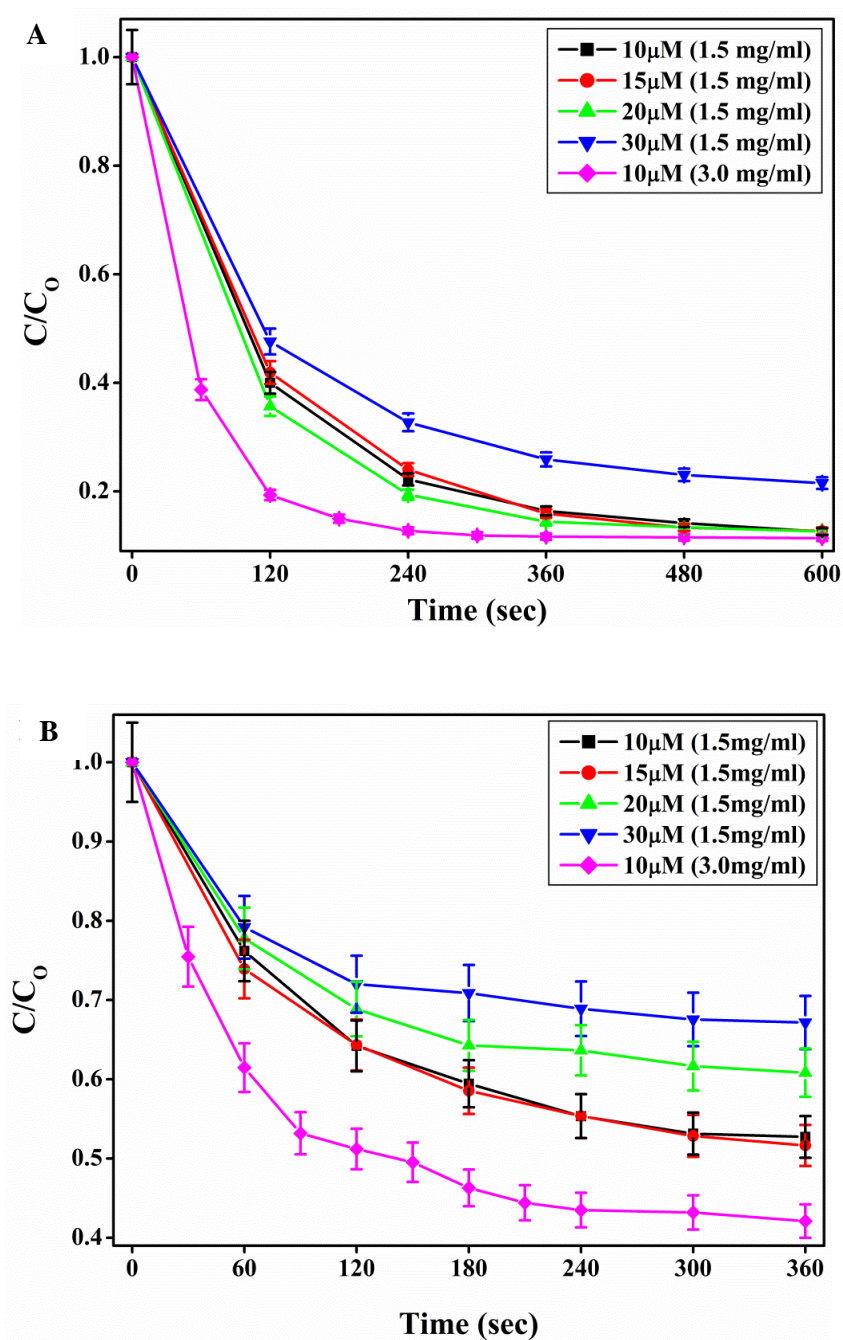
Figure 2.18: C/C$_o$ Vs time plot for adsorption of (A) [Ru(bpy)$_2$(phendione)]$^{2+}$ by silica, (B) [Ru(phendione)$_3$]$^{2+}$ by silica.

Table 2.3: Rate and percentage of adsorption of $[Ru(bpy)_2(phendione)]^{2+}$ and $[Ru(phendione)_3]^{2+}$, by activated carbon.

Condition		$[Ru(bpy)_2(phendione)]^{2+}$		$[Ru(phendione)_3]^{2+}$	
[Complex] (μM)	Carbon (mg/ml)	Rate (s^{-1})	% Adsorbed	Rate (s^{-1})	% Adsorbed
10	0.75	5.09×10^{-2}	89.75	3.71×10^{-2}	85.59
10	1.5	5.95×10^{-2}	98.68	5.81×10^{-2}	93.98
15	1.5	5.21×10^{-2}	97.92	3.47×10^{-2}	93.82
20	1.5	5.97×10^{-2}	97.94	4.37×10^{-2}	92.55
30	1.5	5.20×10^{-2}	97.59	4.47×10^{-2}	93.29

Table 2.4: Rate and percentage of adsorption of $[Ru(bpy)_2(phendione)]^{2+}$ and $[Ru(phendione)_3]^{2+}$, by silica.

Condition		$[Ru(bpy)_2(phendione)]^{2+}$		$[Ru(phendione)_3]^{2+}$	
[Complex] (μM)	Silica (mg/ml)	Rate (s^{-1})	% Adsorbed	Rate (s^{-1})	% Adsorbed
5	1.5	1.94×10^{-2}	83.54	9.61×10^{-3}	42.95
10	1.5	9.64×10^{-3}	87.42	1.11×10^{-2}	47.28
15	1.5	8.87×10^{-3}	87.29	1.17×10^{-2}	48.35
20	1.5	1.12×10^{-2}	87.39	1.38×10^{-2}	39.17
30	1.5	8.94×10^{-3}	78.49	1.67×10^{-2}	32.83
10	3.0	1.99×10^{-2}	88.34	1.91×10^{-2}	56.51

Importantly, visible light inactivation of bacteria in combination with adsorption is important condition for water disinfection using photosensitizers [Kuznetsova et al., 2007]. The present investigation reveals that $[Ru(bpy)_2(phendione)]^{2+}$ and $[Ru(phendione)_3]^{2+}$ have the ability to photoinactivate bacteria, as well as could be effectively removed from aqueous systems using adsorbents such as activated carbon.

Effective photoinactivation of fish pathogens in aquaculture systems by homogenous cationic porphyrin has been reported recently [Arrojado et al., 2011]. The authors of this report have suggested that immobilization/adsorption of cationic porphyrin on adsorbents has to be performed to avoid its release into the environment [Arrojado et al., 2011]. Recently, Ru(II) polyazaheterocyclic complexes immobilized on silicone have

been shown to cause visible light inactivation of bacteria [Manjon et al, 2009, Manjon et al, 2010]. Adsorption of bacteria on silicone during photoinactivation may occur and it was suggested that photosensitizer loaded silicone system may require autoclaving which could cause leaching of the photosensitizer and affect the durability of the material [Manjon et al, 2009]. These facts indicate that final treatment of aqueous media with adsorbents is required to remove the leached complexes and/or photobleached products. To the best of our knowledge, the present investigation is the first report which shows that simple water soluble $[Ru(bpy)_2(phendione)]^{2+}$ and $[Ru(phendione)_3]^{2+}$ are promising candidates for visible light inactivation of bacteria, with effective adsorption onto activated carbon in aqueous media for easy removal.

2.3.5. Desorption of complexes:

Incubation of silica adsorbed with complexes in 100 mM KCl solution showed increase in absorbance of complexes (Figure 2.19). This result revealed desorption of complexes. Desorption of $[Ru(bpy)_2(phendione)]^{2+}$ was more effective in presence of 100 mM KCl than in presence of 10 mM KCl (Table 2.5). Desorption of $[Ru(bpy)_2(phendione)]^{2+}$ was not effective on reducing pH to 4 compared to 100 mM KCl (Table 2.5). On the other hand, desorption of $[Ru(phendione)_3]^{2+}$ from silica was found to be almost similar under all the three tested conditions (Table 2.5). The results implied that $[Ru(phendione)_3]^{2+}$ tends to get desorbed more than $[Ru(bpy)_2(phendione)]^{2+}$ at lower KCl concentration and pH 4. In case of activated carbon, desorption of complexes was not effective under the above mentioned conditions, indicating that activated carbon is more suitable for adsorption of $[Ru(bpy)_2(phendione)]^{2+}$ and $[Ru(phendione)_3]^{2+}$ than silica in aqueous media.

Table 2.5: Percentage desorption of $[Ru(bpy)_2(phendione)]^{2+}$ (m_a = 8.8 μM), and $[Ru(phendione)_3]^{2+}$ (m_a = 4.7 μM) from silica (1.5 mg/ml).

Eluent	Desorption ratio (%)	
	$[Ru(bpy)_2(phendione)]^{2+}$	$[Ru(phendione)_3]^{2+}$
100 mM KCl	73.70	59.14
10 mM KCl	25.00	51.34
pH 4 (HCl)	25.79	56.01
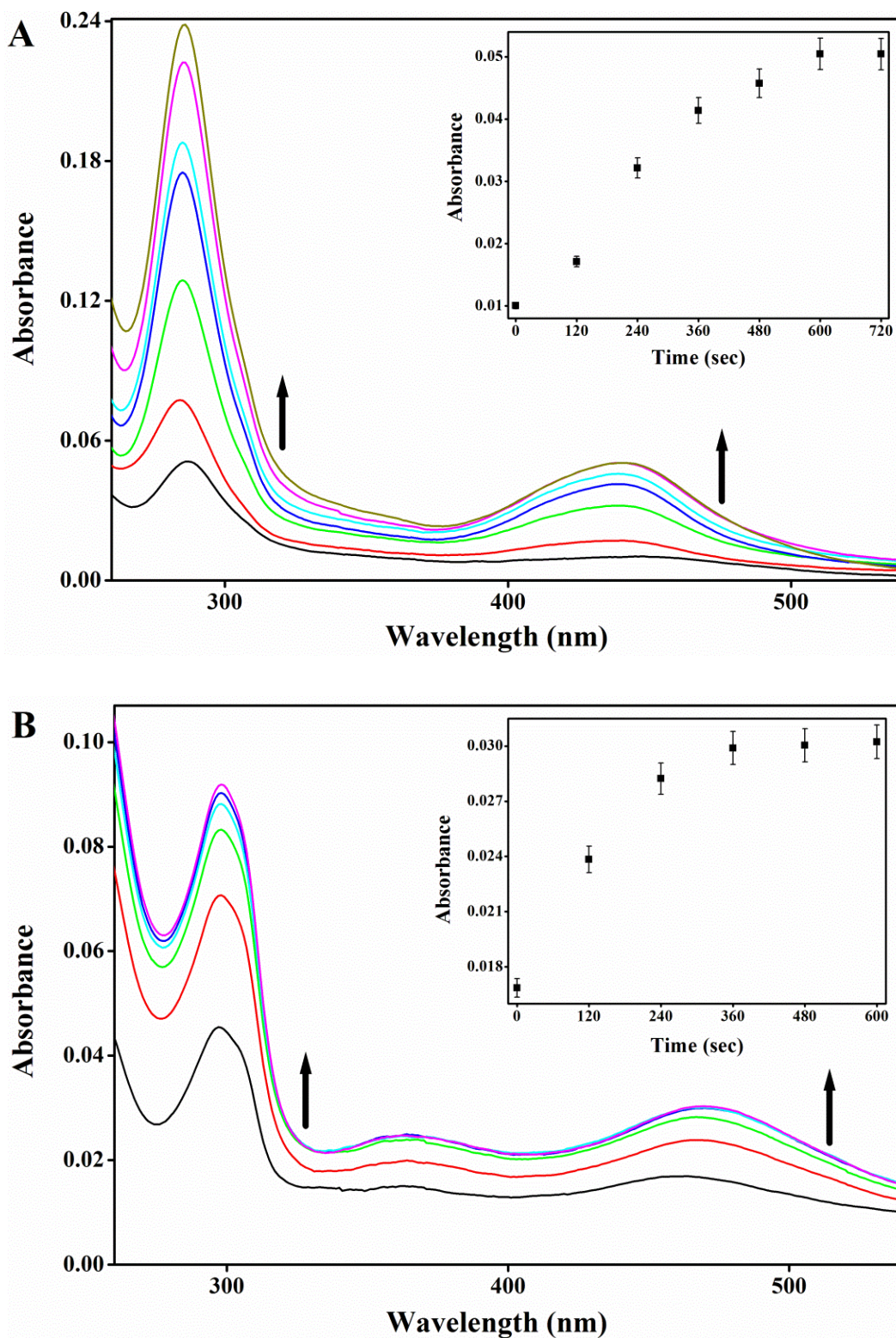
Figure 2.19: Absorption spectral changes (every 2 minutes) during desorption of (A) [Ru(bpy)$_2$(phendione)]$^{2+}$ (m$_a$ = 8.8 µM) and, (B) [Ru(phendione)$_3$]$^{2+}$ (m$_a$ = 4.7 µM) from silica (1.5 mg/ml) in presence of KCl (100 mM). Inset: Kinetics of desorption monitored at 440 nm for [Ru(bpy)$_2$(phendione)]$^{2+}$ and 466 nm for [Ru(phendione)$_3$]$^{2+}$.

2.4. Conclusions:

Micromolar concentrations of $[Ru(bpy)_2(phendione)]^{2+}$ and $[Ru(phendione)_3]^{2+}$ were effective for complete visible light inactivation of both Gram positive and negative bacteria. Gram positive bacteria were found to be more susceptible than Gram negative towards photoinactivation by complexes. LED array was used as visible light source for photoinactivation of bacteria. Radical quenching, fluorescence microscopic, SEM and genomic DNA isolation results revealed that photolysis of $[Ru(bpy)_2(phendione)]^{2+}$ and $[Ru(phendione)_3]^{2+}$, caused oxidative stress and damage to *E. coli*, with significant cell membrane damage and loss of DNA, leading to cell death. $[Ru(bpy)_2(phendione)]^{2+}$ and $[Ru(phendione)_3]^{2+}$ are better adsorbed by activated carbon as compared to silica. Importantly, activated carbon is an extensively used adsorbent in water purification. The study reveals that $[Ru(bpy)_2(phendione)]^{2+}$ and $[Ru(phendione)_3]^{2+}$ have the ability to cause visible light inactivation of bacteria, as well as they could also be effectively adsorbed by activated carbon. These results imply that $[Ru(bpy)_2(phendione)]^{2+}$ and $[Ru(phendione)_3]^{2+}$ are promising photosensitizers for visible light water disinfection.

Chapter 3

Effective water photodisinfection using ruthenium polypyridyl complexes adsorbed onto activated carbon

Highlights:

1. Complete photoinactivation of bacteria by ruthenium polypyridyl complexes adsorbed onto activated carbon.

2. Visible light LED used for photoinactivation.

3. No leaching of complexes from the composition.

4. Work in both PBS and SGW.

5. Works efficiently for at least five cycles.

6. Promising heterogeneous photosensitizers for visible light water disinfection.

Graphical abstract figure:
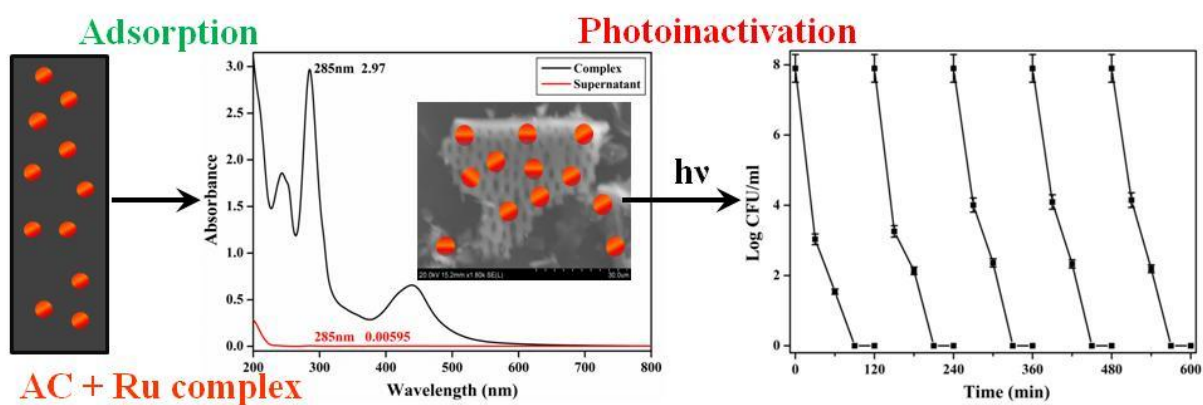
3.1. Background:

The availability of clean drinking water is one of the most important problems of the modern world and especially to India. About 1.2 billion people around the world lack access to clean water [Kemper, 2004, Coetser et al., 2007, Weber et al., 2002]. Ground and surface water are easily contaminated with bacteria in many parts of the world [Montgomery and Elimelech, 2007, Shannon et al., 2008]. Conventional methods of disinfection of bacteria have their advantages and disadvantages as discussed in chapter 1. Visible light active photosensitizers (PSs) have high quantum yields of $^1O_2$ generation and have been reported to inactivate bacteria. However, a few organic dyes have poor thermal and photochemical stability [DeRosa et al., 2002]. On the other hand, as discussed in chapter 2, ruthenium polypyridyl complexes are promising PSs for homogeneous water disinfection, and can be easily removed from water by adsorption on activated carbon. Importantly, ability of ruthenium polypyridyl complexes adsorbed onto AC to kill bacteria in water has not been studied. PS complexes adsorbed onto solid supports have the advantage of easy removal from water. Heterogeneous PSs that are photostable, and does not leach into water are desirable. All these facts prompted us to investigate the heterogenization of ruthenium polypyridyl complexes via adsorption onto activated carbon (AC), and their effect on visible light water disinfection. In this chapter, $[Ru(bpy)_2(phendione)]^{2+}$, and $[Ru(bpy)_3]^{2+}$ were adsorbed onto AC, are designated as $AC/[Ru(bpy)_2(phendione)]^{2+}$ and $AC/[Ru(bpy)_3]^{2+}$, respectively and were used for photoinactivation of bacteria in water.

3.2. Materials and methods:

3.2.1. Materials:

Chemicals were procured from SD Fine Chemicals Limited and Sigma Aldrich, India. Details are mentioned in chapter 2 section 2.2.1.

3.2.2. Complex preparation:

$[Ru(bpy)_2(phendione)](PF_6)_2.2H_2O$ and $[Ru(bpy)_3](PF_6)_2.2H_2O$ were prepared and characterised spectrophotometrically (JASCO V-570 UV/Vis/NIR Spectrophotometer), as reported earlier [Goss et al., 1985, Gao et al., 2000].

3.2.3. Visible light source:

LED array was used as visible light source, purchased from Kwality Photonics, Hyderabad, India. Details are as mentioned in chapter 2 Section 2.2.3.

3.2.4. Loading of $[Ru(bpy)_2(phendione)]^{2+}$ and $[Ru(bpy)_3]^{2+}$ onto activated carbon:

Activated carbon (20 mg) was added to 2 ml of complex solution (50, 100, 200, 300 µM) in DW and magnetically stirred for 1 hr. Resulting suspension was centrifuged at 10,000 rpm for 10 min at 20 °C. Absorbance of supernatant was recorded to find amount of remaining complex after the adsorption. Pellet was washed five times with DW by centrifugation. After five washes, the resulting pellet of $AC/[Ru(bpy)_2(phendione)]^{2+}$ and $AC/[Ru(bpy)_3]^{2+}$ was dried under vacuum at 40 °C for 1 hr. Absorbance of supernatant was recorded after every wash.

Stability of $AC/[Ru(bpy)_2(phendione)]^{2+}$ and $AC/[Ru(bpy)_3]^{2+}$ in PBS:

5 mg of optimised sample was stirred in 2 ml of 10 mM phosphate buffered saline (PBS) for ~ 2hr and centrifuged. Absorbance of supernatant was recorded to study stability of samples and leaching of complexes in the working solution used for antimicrobial studies.

3.2.5. Scanning Electron Microscopy and Energy Dispersive X-ray Spectroscopy (SEM and EDS):

The samples were analysed by SEM and EDS using FE-SEM (Hitachi 4800 Type-1). X-max silicon drift X-ray detector with a slit of 20 mm^2 was used. Small amount of samples were placed on a double sided carbon tape. No coating was done. The voltage was in the range 1- 30 kV. The working distance (WD) was set around 15 mm to get all the counts in EDS. Magnification, kV and WD was same for SEM and EDS. At least 1000 counts were taken for EDS. Surface area = 248.8 m^2/g, pore size = 3.5 nm.

3.2.6. Inductively coupled plasma atomic emission spectroscopy (ICP-OES):

In order to determine ruthenium concentration, ICP – OES using ETHOS high performance microwave digestion system was used. Solid samples (~ 10 mg) were weighed in Teflon tubes and then 1 ml H_2O_2, 2 ml HCl, 7 ml HNO_3 were added to it and tubes were placed in sample holders. The program was set such that the temperature increased from 0 to 200 °C in 20 minutes and stayed at 200 °C for next 20 minutes. After that, it came down to room temperature in 15 minutes. Therefore, a total of 55 minutes were required to complete the program for microwave digestion. Then the

digester was opened and ~ 40 ml water was added to increase the volume. For the liquid samples the probes were dipped in the solution and readings were taken directly i.e. no digestion was done.

3.2.7. Antibacterial activity:

Antibacterial activity of ruthenium polypyridyl complexes adsorbed to activated carbon was studied against *E. coli* (model Gram negative) and *S. aureus* (model Gram positive). The bacterial cells were grown in NB broth to attain log phase. The cells were harvested by centrifugation at 1000 g for 15 min at 25 °C. Cell pellet was resuspended in PBS and used as stock. In pre-sterilized 10 mm quartz cuvettes, containing 2 ml of 10^8 CFU/ml cell suspension in phosphate buffer saline (PBS), required amount of AC/[Ru(bpy)$_2$(phendione)]$^{2+}$ or AC/[Ru(bpy)$_3$]$^{2+}$ or AC (control) were added and magnetically stirred in dark for 30 min and then irradiated with light for 120 min. For dark controls, the cuvettes were covered with aluminium foil and placed in front of the light source. Temperature was 35 °C ± 2 °C. *E. coli* and *S. aureus* were exposed to light at fluence rate of 95 mW/cm^2. Under these irradiation conditions the light alone had no effect on cell viability. Reaction mix was withdrawn every 30 min, serially diluted and plated on NB agar plates. Colonies were counted after incubating plates at 37 °C for 24 hours to estimate log reductions of the bacterial count over the time. The effect of dosage of AC/[Ru(bpy)$_2$(phendione)]$^{2+}$ and AC/[Ru(bpy)$_3$]$^{2+}$ for photo bactericidal action was investigated. All the tests were done in triplicates.

To reuse the composition of invention, AC/[Ru(bpy)$_2$(phendione)]$^{2+}$ and AC/[Ru(bpy)$_3$]$^{2+}$ was removed from disinfected PBS. AC/[Ru(bpy)$_2$(phendione)]$^{2+}$ and AC/[Ru(bpy)$_3$]$^{2+}$ pellet obtained by centrifugation was resuspended in 2 ml of 10^8 CFU/ml cell suspension in PBS, and the photo bactericidal experiment was performed, as mentioned above. The reuse experiments were performed five times (five cycles). One cycle was performed each day. During the cycles, the pellet was always soaked in PBS, which was removed just before the next cycle. No autoclaving of pellet was required. After five cycles the pellet was kept soaked in PBS for another five days at room temperature. Then the suspension was centrifuged and pellet was reused for the 10th day experiment.

3.2.8. Effect in simulated ground water:

Photoinactivation of bacteria (*E. coli* and *S. aureus*) by ruthenium polypyridyl complexes adsorbed onto activated carbon was also studied using simulated ground water (SGW) as medium, under optimized conditions of AC/[Ru(bpy)$_2$(phendione)]$^{2+}$ and AC/[Ru(bpy)$_3$]$^{2+}$. To reuse the composition of invention, AC/[Ru(bpy)$_2$(phendione)]$^{2+}$ and AC/[Ru(bpy)$_3$]$^{2+}$ was removed from disinfected SGW. AC/[Ru(bpy)$_2$(phendione)]$^{2+}$ and AC/[Ru(bpy)$_3$]$^{2+}$ pellet obtained by centrifugation was resuspended in 2 ml of 108 CFU/ml cell suspension in SGW, and the photo bactericidal experiment was performed similar to that in section 3.2.7. The reuse experiments were performed five times (five cycles). One cycle was performed each day. During the cycles, the pellet was always soaked in SGW, which was removed just before the next cycle. No autoclaving of pellet was required. After five cycles the pellet was kept soaked in SGW for another five days at room temperature. Then the suspension was centrifuged and pellet was reused for the 10th day experiment. SGW contained a defined composition of inorganic and organic matter. SGW was prepared by addition of the following components to DW: Fe(NO$_3$)$_3$.9H$_2$O (0.24 μM), NaHCO$_3$ (1.2 mM), Na$_2$SO$_4$ (0.34 mM), Na$_2$HPO$_4$ (0.28 mM), NaCl (0.86 mM) and resorcinol (9.0 μM) [Gokulakrishnan et al., 2013].

3.3. Results and Discussions:

3.3.1. Loading of [Ru(bpy)$_2$(phendione)]$^{2+}$ and [Ru(bpy)$_3$]$^{2+}$ onto activated carbon:

The UV-Vis absorption spectrophotometer results reveal that 50 and 100 μM complexes [Ru(bpy)$_2$(phendione)]$^{2+}$, [Ru(bpy)$_3$]$^{2+}$) were adsorbed completely onto 20 mg of activated carbon (AC) (Figure 3.1 (A), 3.2 (A), 3.3 (A), 3.4 (A)). These loaded complexes onto AC are designated as AC/[Ru(bpy)$_2$(phendione)]$^{2+}$ and AC/[Ru(bpy)$_3$]$^{2+}$. No leaching of the complex from AC/[Ru(bpy)$_2$(phendione)]$^{2+}$ and AC/[Ru(bpy)$_3$]$^{2+}$ was observed during washing (Figure 3.1 (B), 3.2 (B), 3.3 (B), 3.4 (B)). 20 mg of AC loaded with relatively higher concentration (200 and 300 μM) of complexes showed leaching during washing of the ruthenium loaded samples (Figure 3.5 (B), 3.6 (B), 3.7 (B), 3.8 (B)). Therefore, 100 μM complex adsorbed onto 20 mg of AC (0.95% loading AC/[Ru(bpy)$_2$(phendione)]$^{2+}$, 0.86% loading AC/[Ru(bpy)$_3$]$^{2+}$), that was not leaching during the washing was used for photoinactivation of bacteria in water.
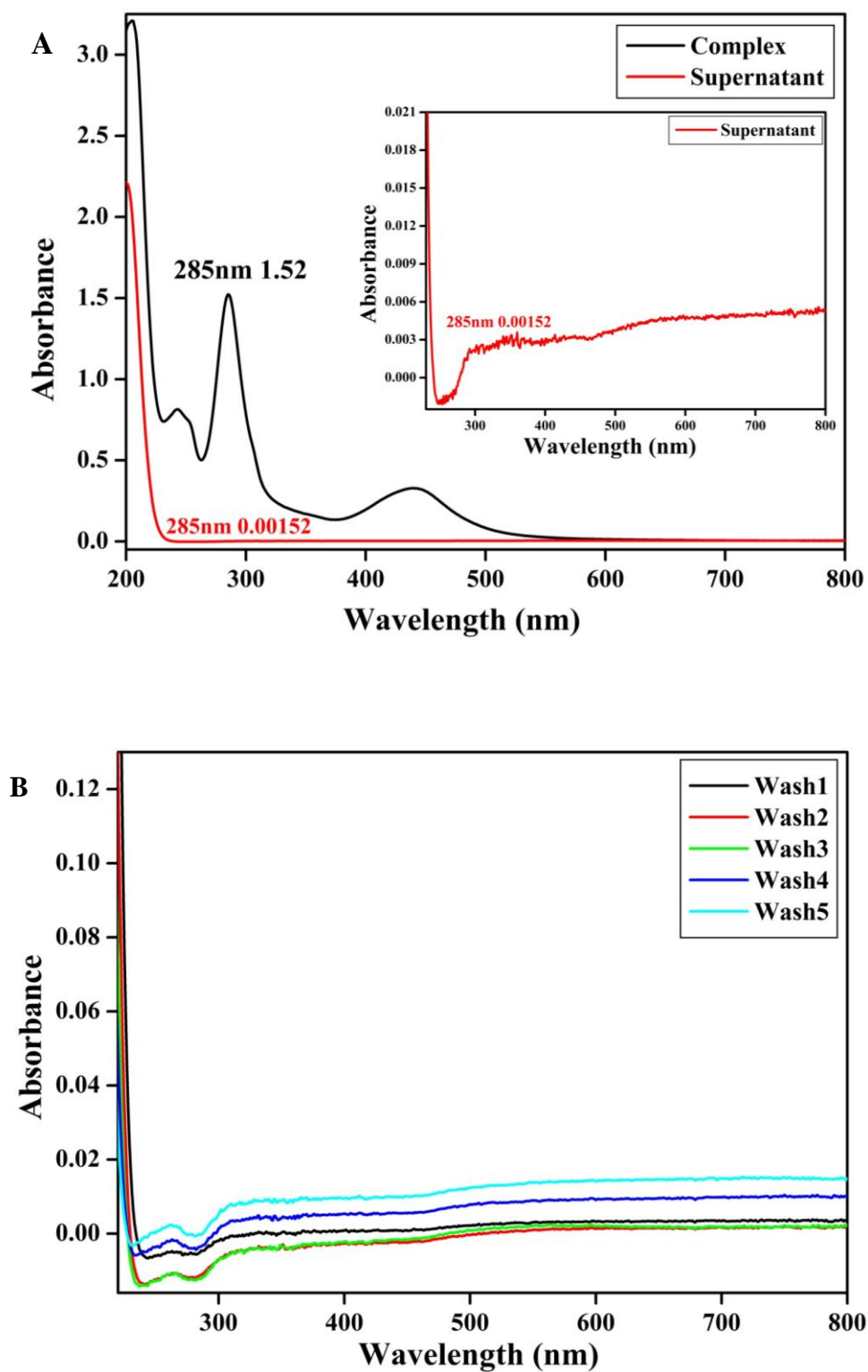
Figure 3.1: (A) UV-Vis spectra of [Ru(bpy)$_2$(phendione)]$^{2+}$ (50 µM) before and after treatment (1 hr) with activated carbon (20 mg). (B) Absorbance of supernatant of [Ru(bpy)$_2$(phendione)]$^{2+}$ after each washing (by centrifugation) with distilled water.
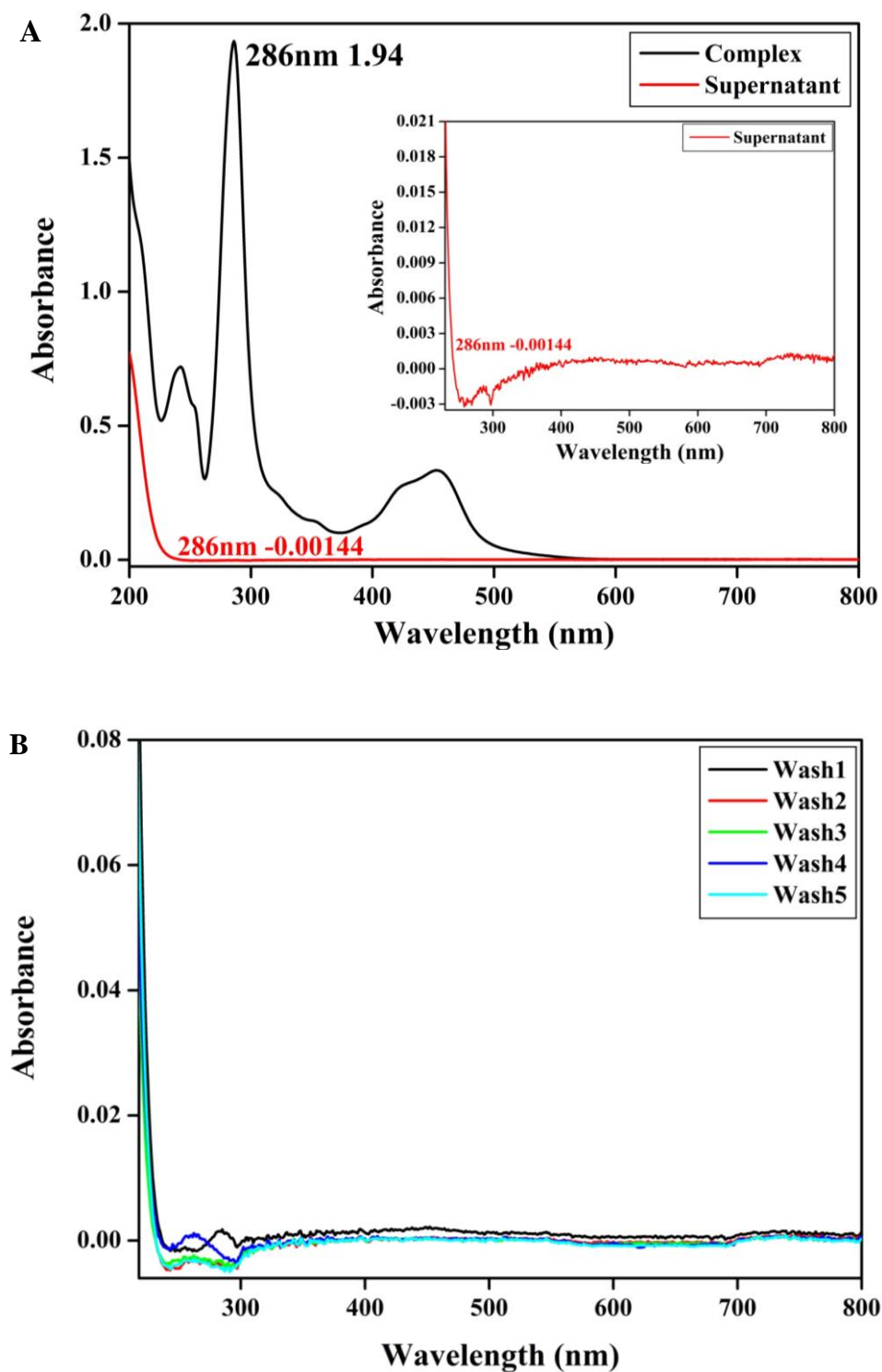
Figure 3.2: (A) UV-Vis spectra of $[Ru(bpy)_3]^{2+}$ (50 µM) before and after treatment (1 hr) with activated carbon (20 mg). (B) Absorbance of supernatant of $[Ru(bpy)_3]^{2+}$ after each washing (by centrifugation) with distilled water.
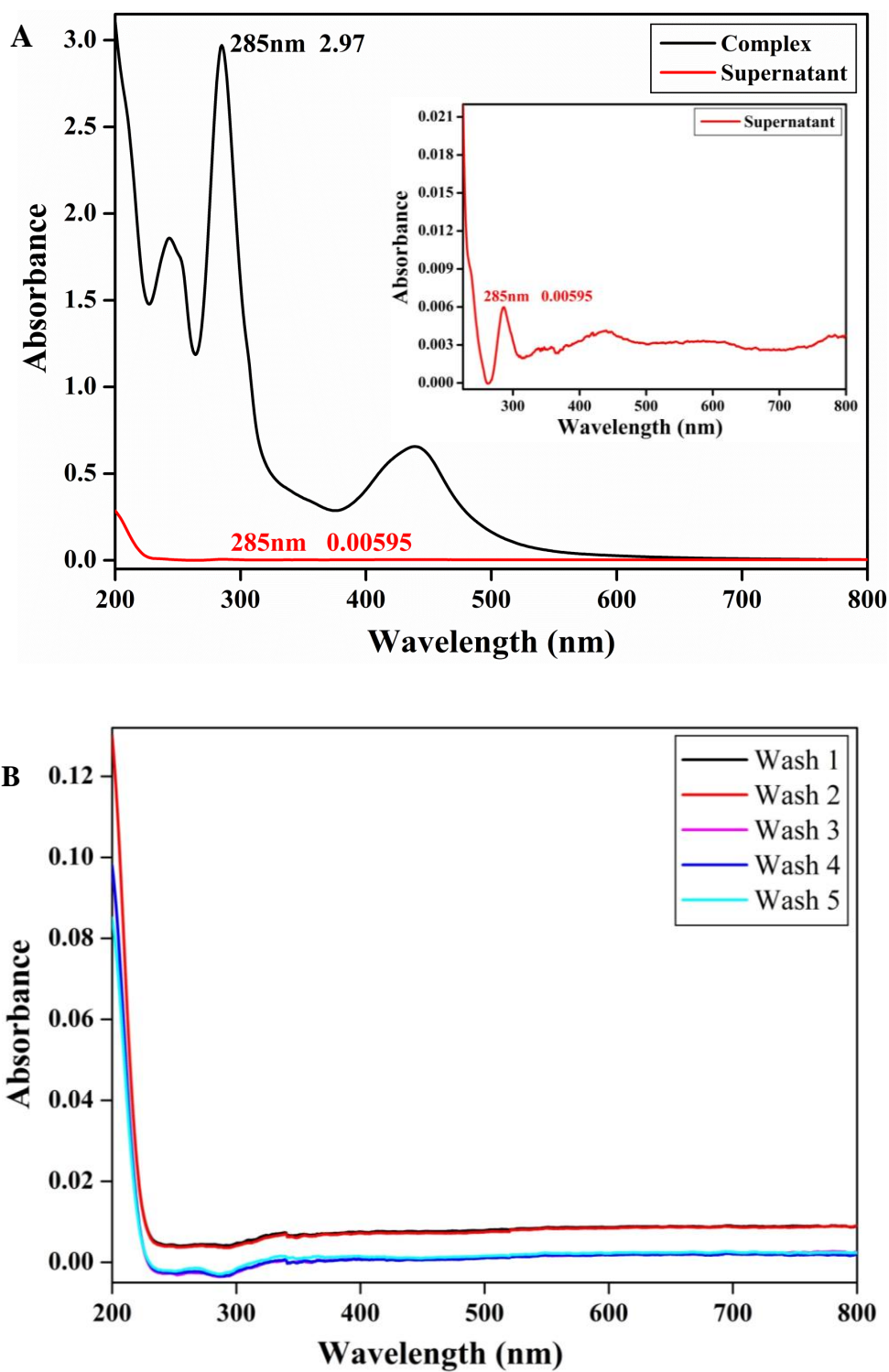
Figure 3.3: (A) UV-Vis spectra of [Ru(bpy)$_2$(phendione)]$^{2+}$ (100 µM) before and after treatment (1 hr) with activated carbon (20 mg). (B) Absorbance of supernatant of [Ru(bpy)$_2$(phendione)]$^{2+}$ after each washing (by centrifugation) with distilled water.
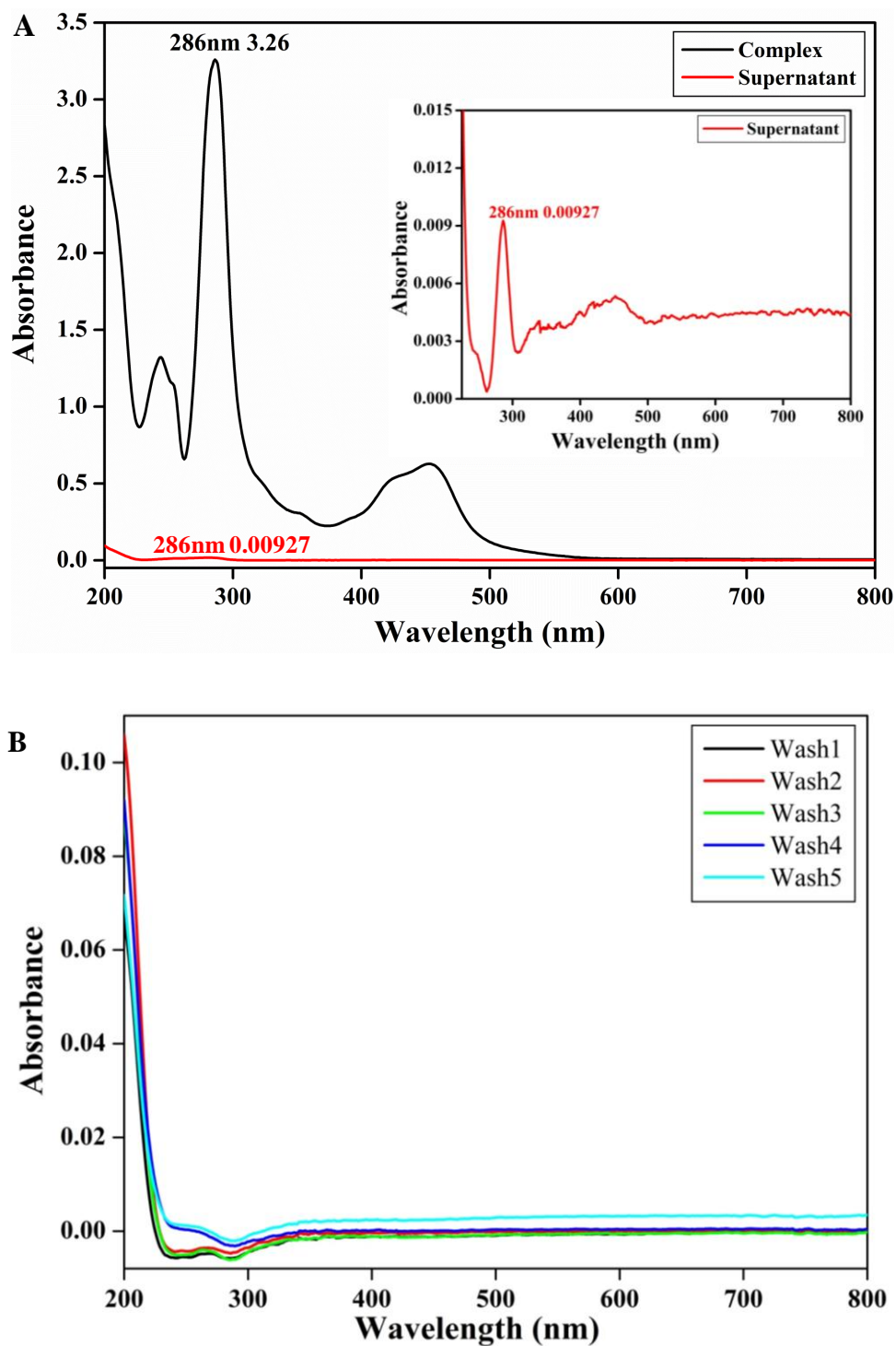
Figure 3.4: (A) UV-Vis spectra of $[Ru(bpy)_3]^{2+}$ (100 µM) before and after treatment (1 hr) with activated carbon (20 mg). (B) Absorbance of supernatant of $[Ru(bpy)_3]^{2+}$ after each washing (by centrifugation) with distilled water.
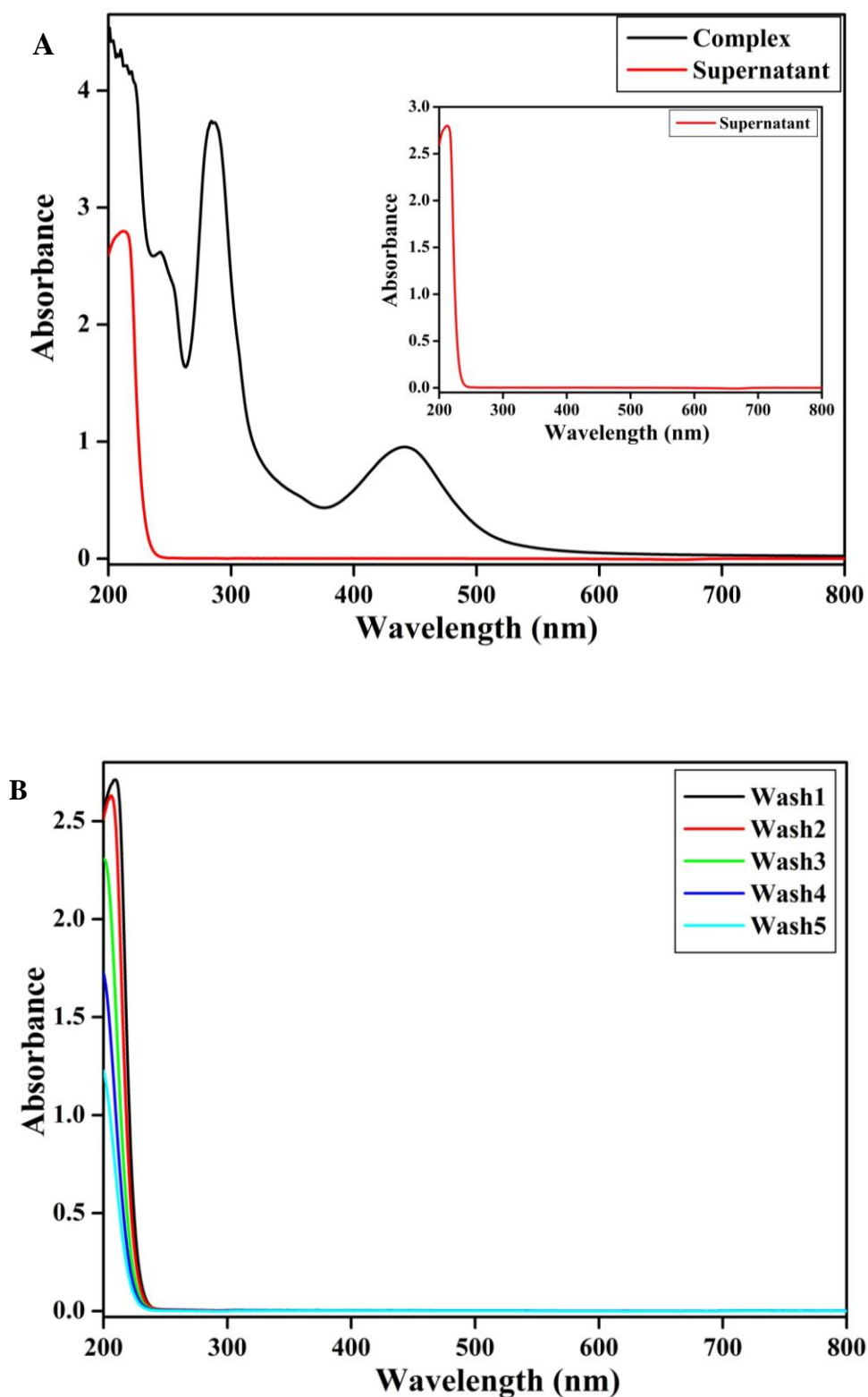
Figure 3.5: (A) UV-Vis spectra of $[Ru(bpy)_2(phendione)]^{2+}$ (200 μM) before and after treatment (1 hr) with activated carbon (20 mg). (B) Absorbance of supernatant of $[Ru(bpy)_2(phendione)]^{2+}$ after each washing (by centrifugation) with distilled water.
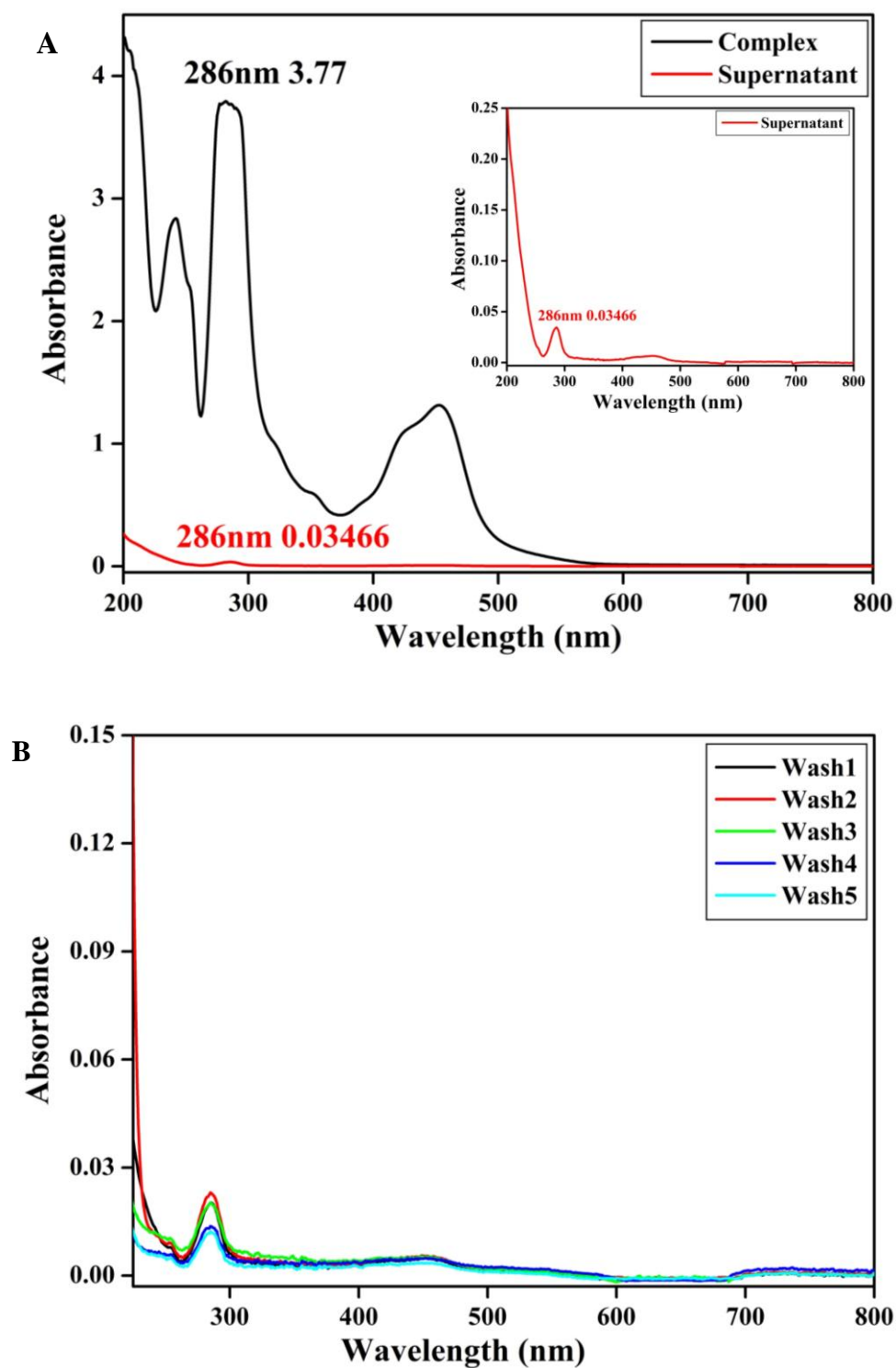
Figure 3.6: (A) UV-Vis spectra of $[Ru(bpy)_3]^{2+}$ (200 μM) before and after treatment (1 hr) with activated carbon (20 mg). (B) Absorbance of supernatant of $[Ru(bpy)_3]^{2+}$ after each washing (by centrifugation) with distilled water.
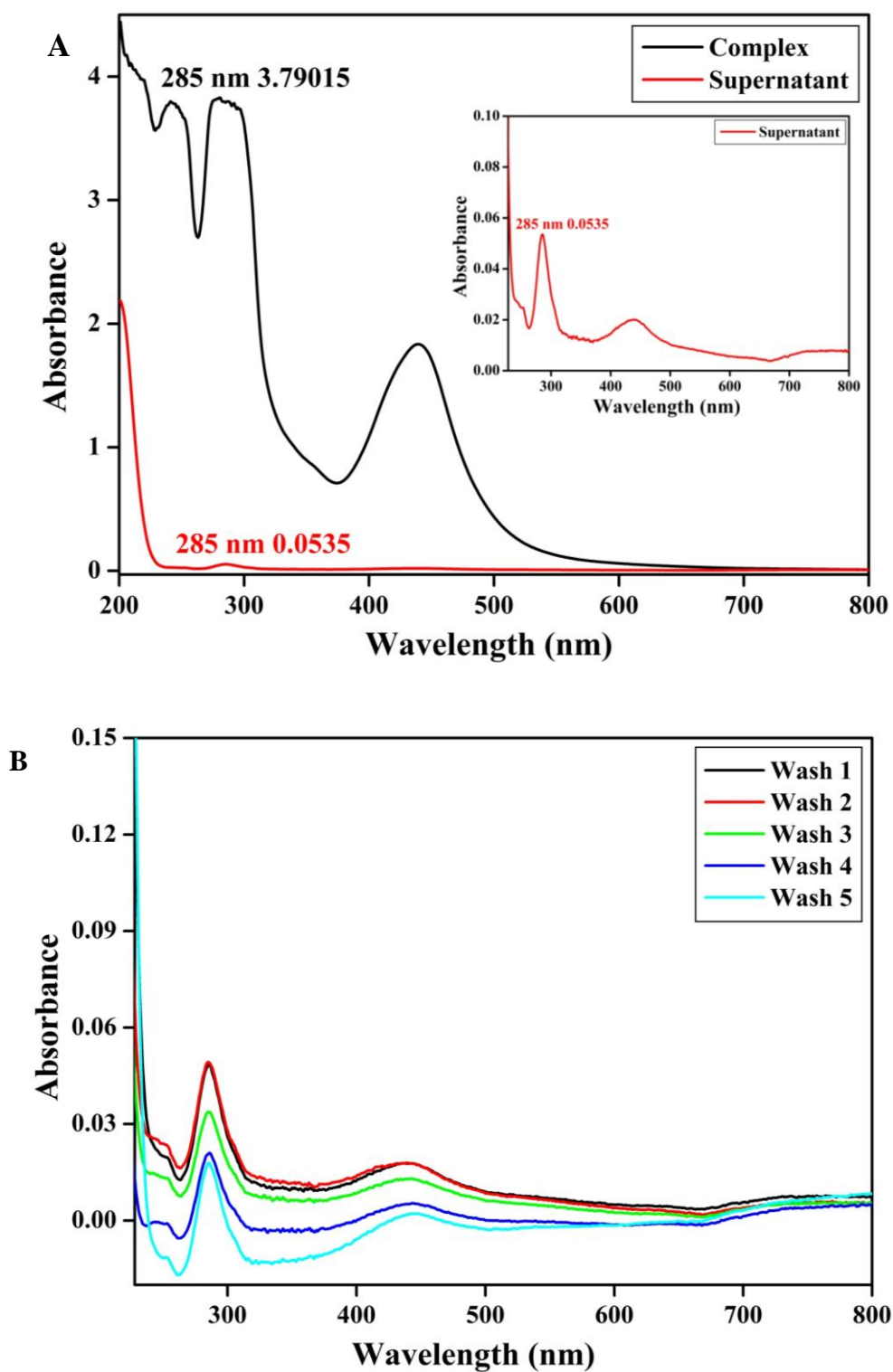
Figure 3.7: (A) UV-Vis spectra of [Ru(bpy)$_2$(phendione)]$^{2+}$ (300 μM) before and after treatment (1 hr) with activated carbon (20 mg). (B) Absorbance of supernatant of [Ru(bpy)$_2$(phendione)]$^{2+}$ after each washing (by centrifugation) with distilled water.
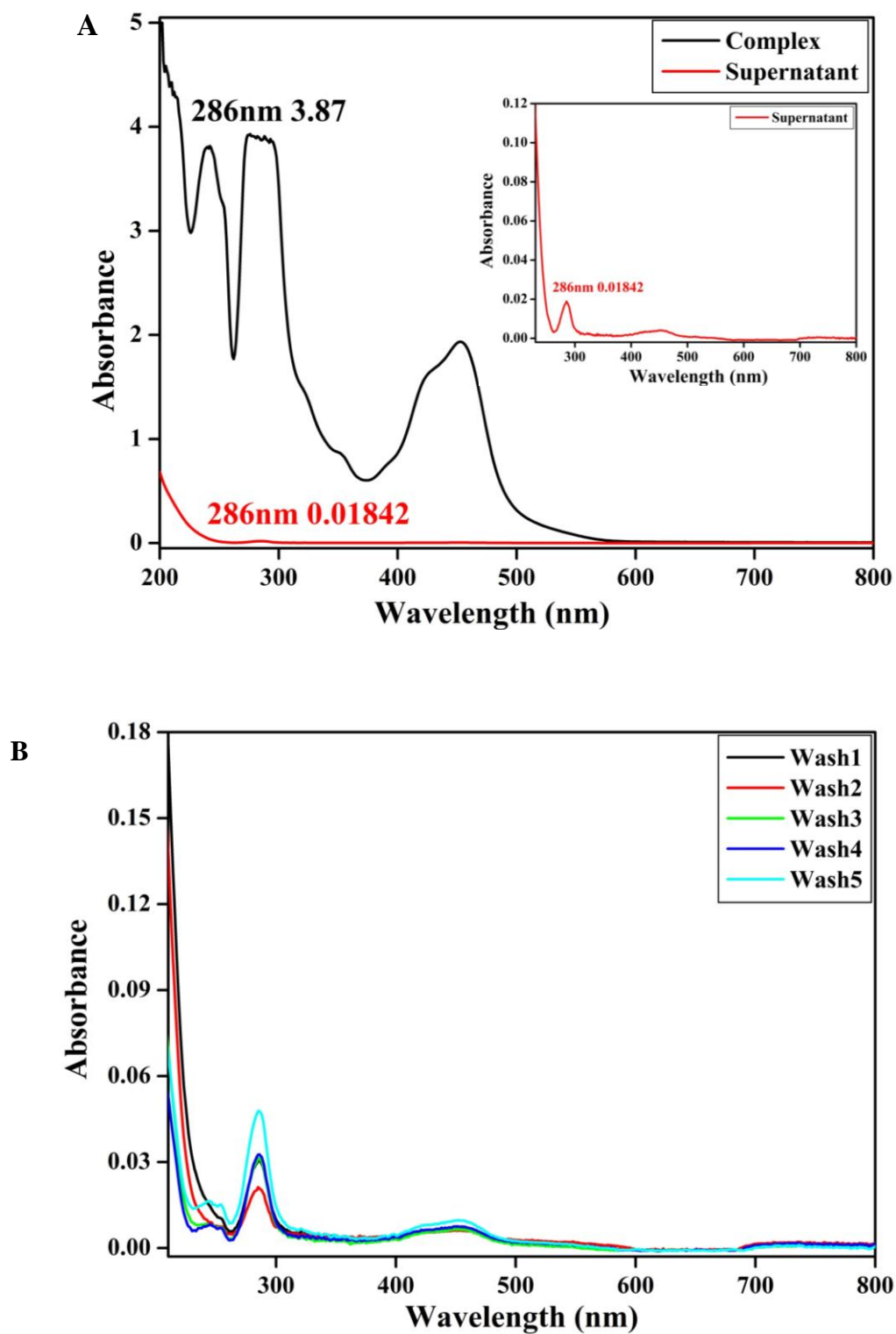
Figure 3.8: (A) UV-Vis spectra of [Ru(bpy)$_3$]$^{2+}$ (300 µM) before and after treatment (1 hr) with activated carbon (20 mg). (B) Absorbance of supernatant of [Ru(bpy)$_3$]$^{2+}$ after each washing (by centrifugation) with distilled water.

3.3.2. Stability of AC/[Ru(bpy)$_2$(phendione)]$^{2+}$ and AC/[Ru(bpy)$_3$]$^{2+}$ in PBS:

Absorbance of supernatant showed no feature of complex spectra after washing AC/[Ru(bpy)$_2$(phendione)]$^{2+}$ and AC/[Ru(bpy)$_3$]$^{2+}$ in PBS for 2 hr (Figure 3.9). This further emphasised that there was no leaching for the optimized condition (100 μM complex adsorbed onto 20 mg of AC), and the adsorbed complexes were stable at given conditions. These results indicated that AC/[Ru(bpy)$_2$(phendione)]$^{2+}$ (0.95% loading) and AC/[Ru(bpy)$_3$]$^{2+}$ (0.86% loading) could be used as supported solid photosensitizers for photoantibacterial studies.
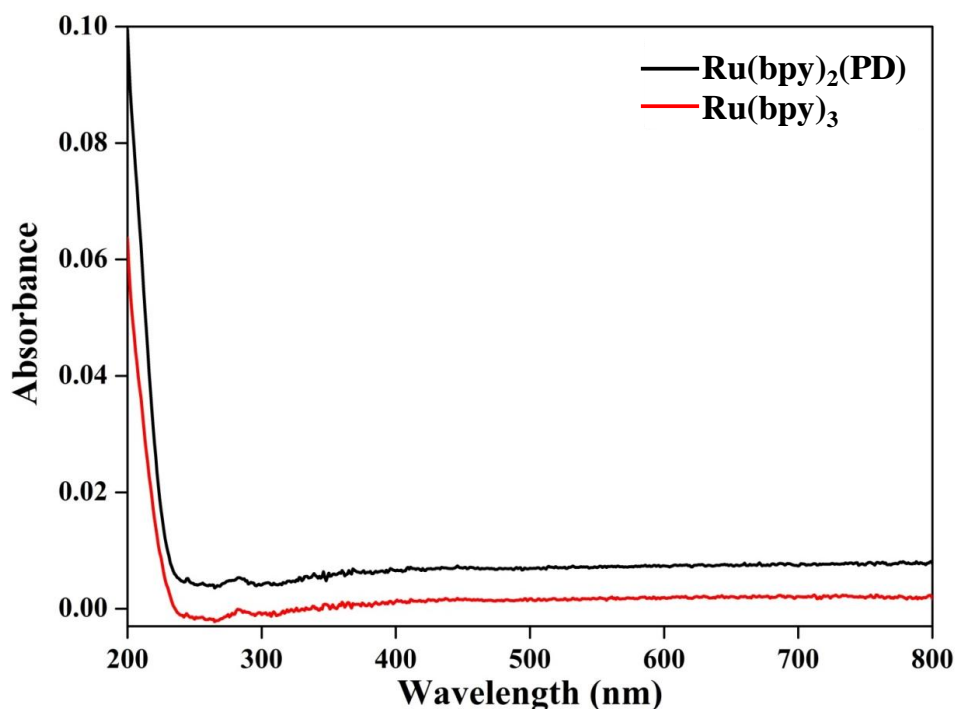
Figure 3.9: Absorbance of supernatant showing stability of samples and no leaching of complexes in working solution (PBS) for bactericidal studies.

Further, ICP-OES analysis for the supernatant and washed solutions of the optimized condition (100 μM complex adsorbed onto 20 mg of AC) showed no ruthenium content.

3.3.3. Characterization of AC/[Ru(bpy)$_2$(phendione)]$^{2+}$ and AC/[Ru(bpy)$_3$]$^{2+}$ using SEM:

SEM analysis of activated carbon showed highly porous structures Figure 3.10 (A). The material was porous even after adsorption of complexes as shown in Figure 3.10 (B, C).
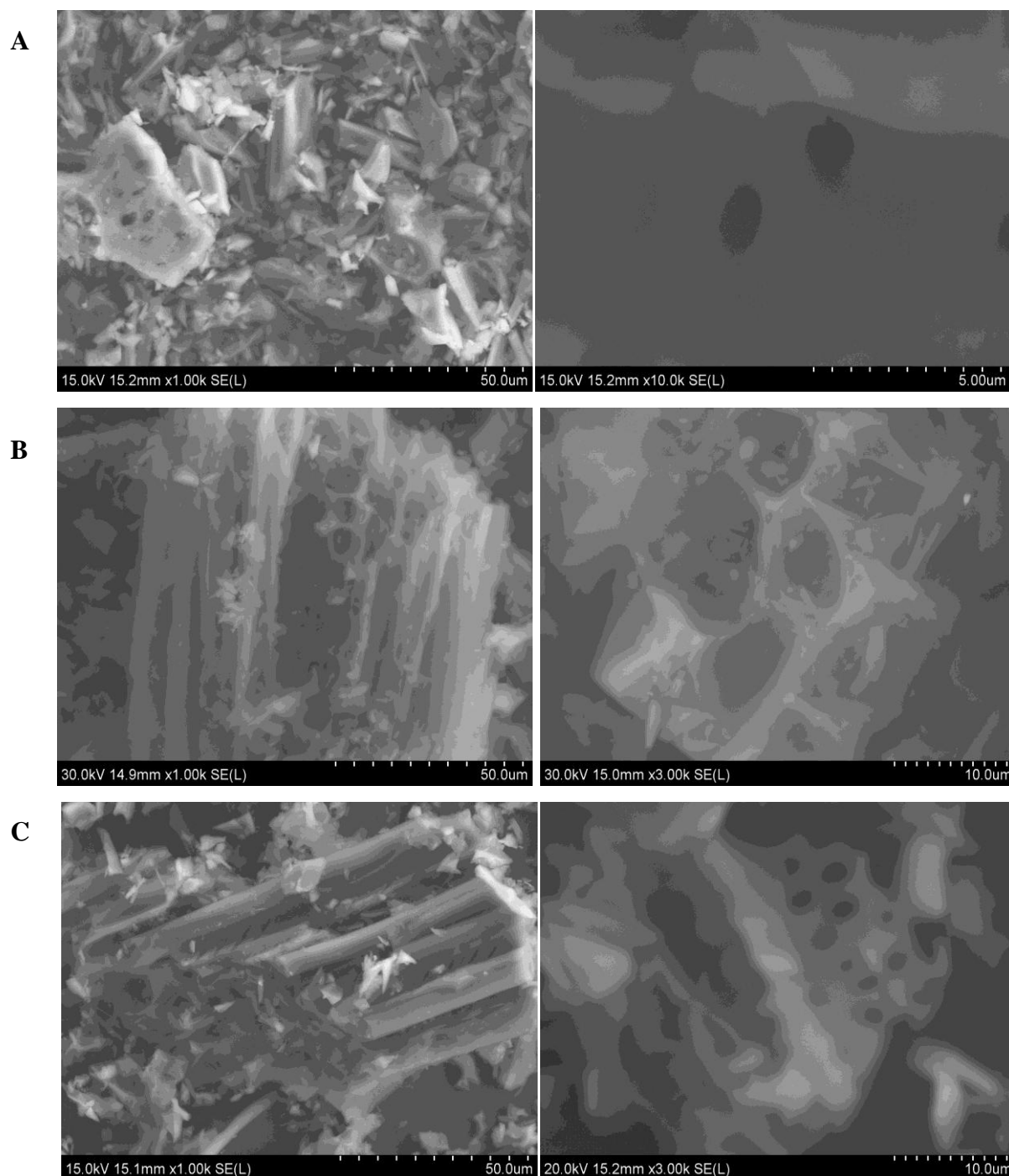
Figure 3.10: SEM analysis of (A) only Activated carbon, (B) AC/[Ru(bpy)$_2$(phendione)]$^{2+}$ and (C) AC/[Ru(bpy)$_3$]$^{2+}$.

3.3.4. Characterization of AC/[Ru(bpy)$_2$(phendione)]$^{2+}$ and AC/[Ru(bpy)$_3$]$^{2+}$ using EDS:

A

Spectrum	C	O	Total
Spectrum 1	93.50	6.50	100.00
Mean	93.50	6.50	100.00
Std. deviation	0.00	0.00	
Max.	93.50	6.50	
Min.	93.50	6.50	
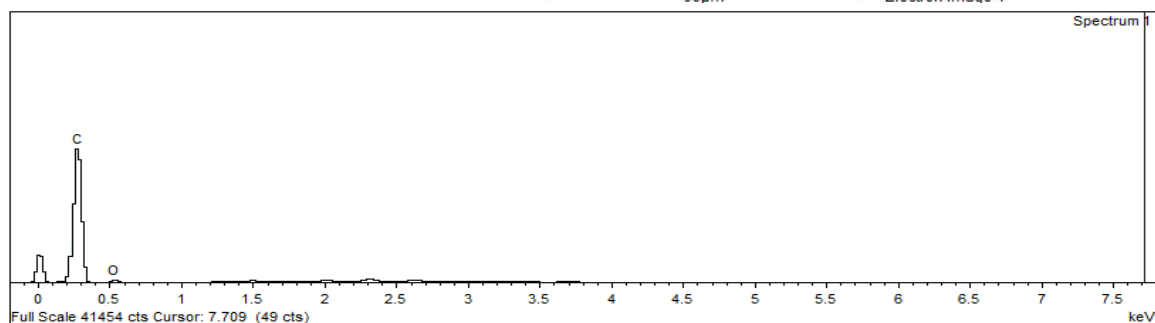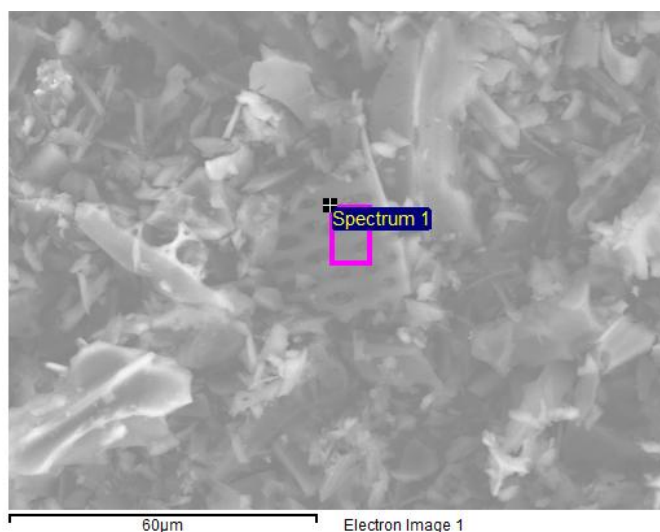
B

Spectrum	C	O	Total
Spectrum 1	91.12	8.88	100.00
Mean	91.12	8.88	100.00
Std. deviation	0.00	0.00	
Max.	91.12	8.88	
Min.	91.12	8.88	

73

C

Spectrum	C	O	Total
Spectrum 1	91.79	8.21	100.00
Spectrum 2	90.43	9.57	100.00
Mean	91.11	8.89	100.00
Std. deviation	0.80	0.96	
Max.	91.79	9.57	
Min.	90.43	8.21	
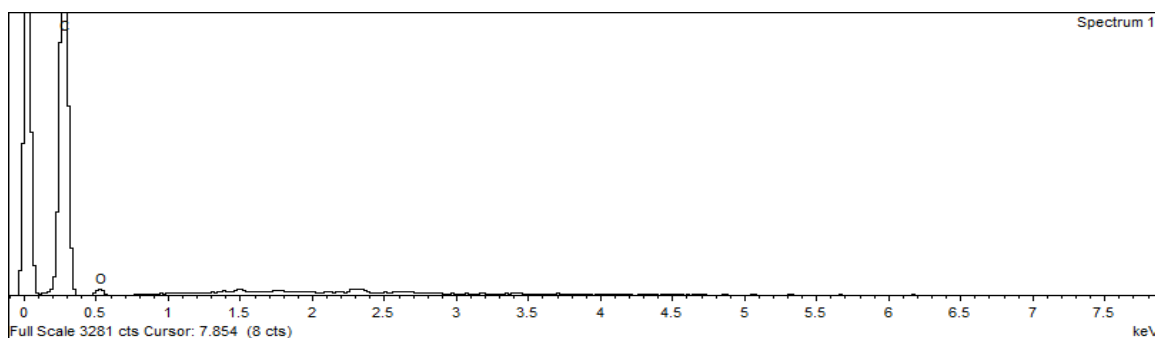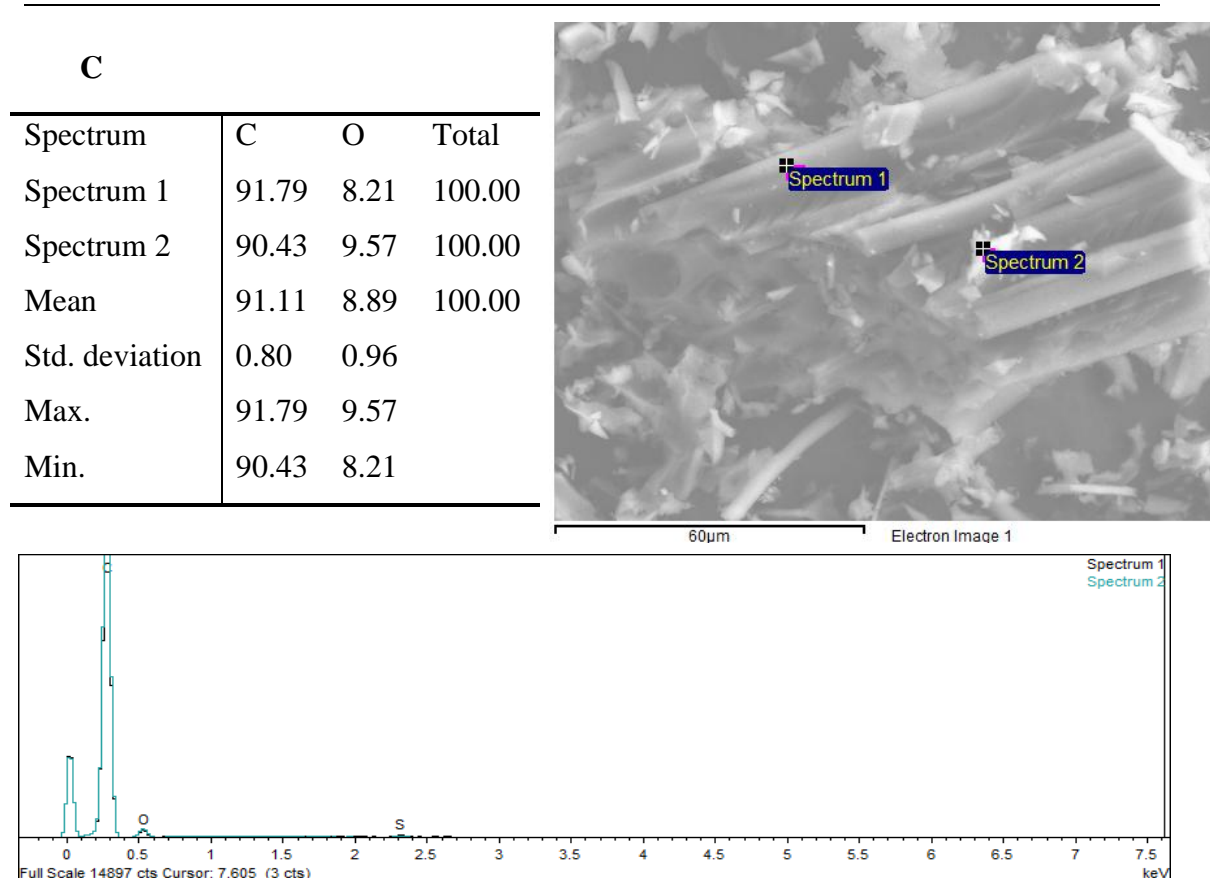
Figure 3.11: EDS spectra of (A) only Activated carbon, (B) AC/[Ru(bpy)$_2$(phendione)]$^{2+}$ and (C) AC/[Ru(bpy)$_3$]$^{2+}$.

EDS analysis of only activated carbon confirmed the presence of only carbon and oxygen elements, with carbon being 93.85 weight% and oxygen 6.50 weight% (Figure 3.11 (A)). Peak around 2.6 keV corresponding to X-ray energy of Ru(II) was not detected as loading was less than 1% in AC/[Ru(bpy)$_2$(phendione)]$^{2+}$ and AC/[Ru(bpy)$_3$]$^{2+}$. The samples mainly contain carbon (~90%) and oxygen (~8%) (Figure 3.11 (B, C))

3.3.5. Photoantibacterial activity in PBS:

Visible light photoantimicrobial activity of Ru(II) polypyridyl complexes adsorbed onto activated carbon was studied against *E. coli* (model Gram-negative bacteria) and *S. aureus* (model Gram-positive bacteria). 2.5 mg/ml of AC/[Ru(bpy)$_2$(phendione)]$^{2+}$ (0.95% loading) showed 8 log reduction of *E. coli* cell viability within 90 min, under visible light irradiation (Figure 3.12). Similar results were obtained in the case of AC/[Ru(bpy)$_3$]$^{2+}$ (0.86% loading) (Figure 3.13). Under dark conditions AC/[Ru(bpy)$_2$(phendione)]$^{2+}$ and AC/[Ru(bpy)$_3$]$^{2+}$ had no effect on cell viability (Figure

3.14 (A)). These results reveal that both AC/[Ru(bpy)$_2$(phendione)]$^{2+}$ and AC/[Ru(bpy)$_3$]$^{2+}$ are effective for visible light photoinactivation of bacteria. On reducing the dose of AC/[Ru(bpy)$_2$(phendione)]$^{2+}$ and AC/[Ru(bpy)$_3$]$^{2+}$, the ability to photoinactivate bacteria also reduced (Figure 3.12, 3.13). Further, on reducing the loading of complexes (i.e., 0.48% for [Ru(bpy)$_2$(phendione)]$^{2+}$ and 0.43% for [Ru(bpy)$_3$]$^{2+}$), a reduction in inactivation efficiency was also observed (Figure 3.12, 3.13).

No growth inhibition of *E. coli* was observed on irradiation of AC/[Ru(bpy)$_2$(phendione)]$^{2+}$ in presence of mannitol, indicating presence of hydroxyl radicals. Significant growth inhibition of *E. coli* was observed on irradiation of AC/[Ru(bpy)$_2$(phendione)]$^{2+}$ in presence of sodium azide, indicating that singlet oxygen may not be the major species produced on irradiation of AC/[Ru(bpy)$_2$(phendione)]$^{2+}$. Earlier, ruthenium complexes containing phendione ligands have been shown to produce charge-separated excited species that undergo fast radiation-less decay to ground state resulting in quenching or reduced MLCT luminescence [Zhou et al., 2010 (ii), Chouai et al., 2005], which is not favourable for the formation of singlet oxygen [Garcìa-Fresnadillo et al., 1996, Zhou et al., 2010 (ii), Chouai et al., 2005, DeRosa et al., 2002]. In case of AC/[Ru(bpy)$_3$]$^{2+}$, partial growth inhibition of *E. coli* was observed in presence of mannitol as well as in presence of sodium azide, indicating that both hydroxyl radicals and singlet oxygen are involved on irradiation of AC/[Ru(bpy)$_3$]$^{2+}$ [Tavares et al., 2011, Cormick et al., 2011, Maisch et al., 2005]. [Ru(bpy)$_3$]$^{2+}$ is known to produce both hydroxyl radicals and singlet oxygen on irradiation [DeRosa et al., 2002].

Furthermore, 10^8 *S. aureus* cells were completely photoinactivated within 120 min in presence of AC/[Ru(bpy)$_2$(phendione)]$^{2+}$ (0.95% loading) and AC/[Ru(bpy)$_3$]$^{2+}$ (0.86% loading). Under dark conditions AC/[Ru(bpy)$_2$(phendione)]$^{2+}$ and AC/[Ru(bpy)$_3$]$^{2+}$ had no effect on cell viability (Figure 3.14 (B)). These results reveal that AC/[Ru(bpy)$_2$(phendione)]$^{2+}$ and AC/[Ru(bpy)$_3$]$^{2+}$, has the ability to photoinactivate both Gram-positve and Gram-negative bacteria.
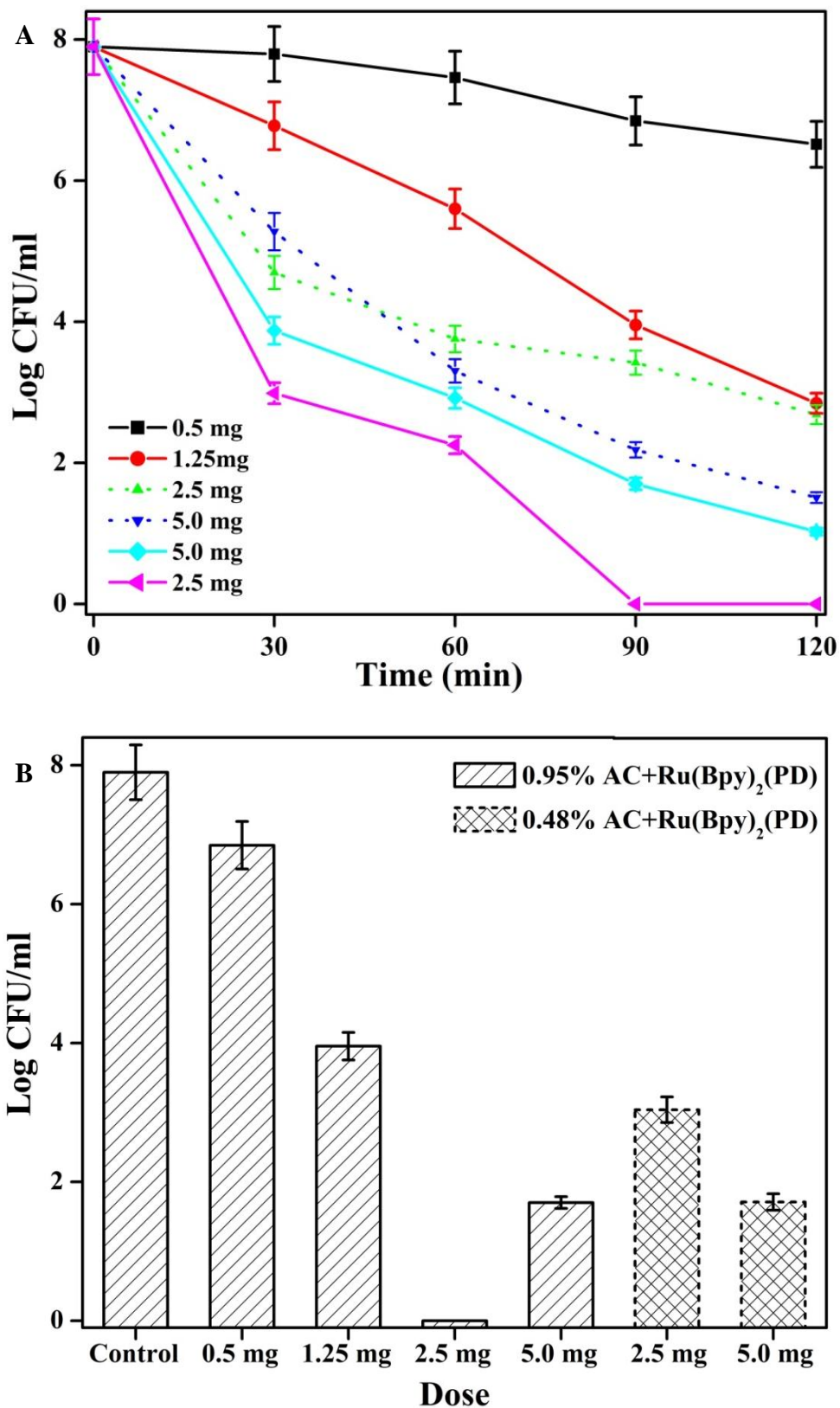
Figure 3.12: Photo bactericidal activity with respect to dose of AC/[Ru(bpy)$_2$(phendione)]$^{2+}$ against *E. coli*, in PBS. (A) Kinetics of bacterial inactivation at different doses of 0.95% loaded sample (solid lines) and 0.48% loaded sample (dotted lines). (B) Comparison of cell viability at 90 min of irradiation for the 0.95% loaded sample and 0.48% loaded sample.
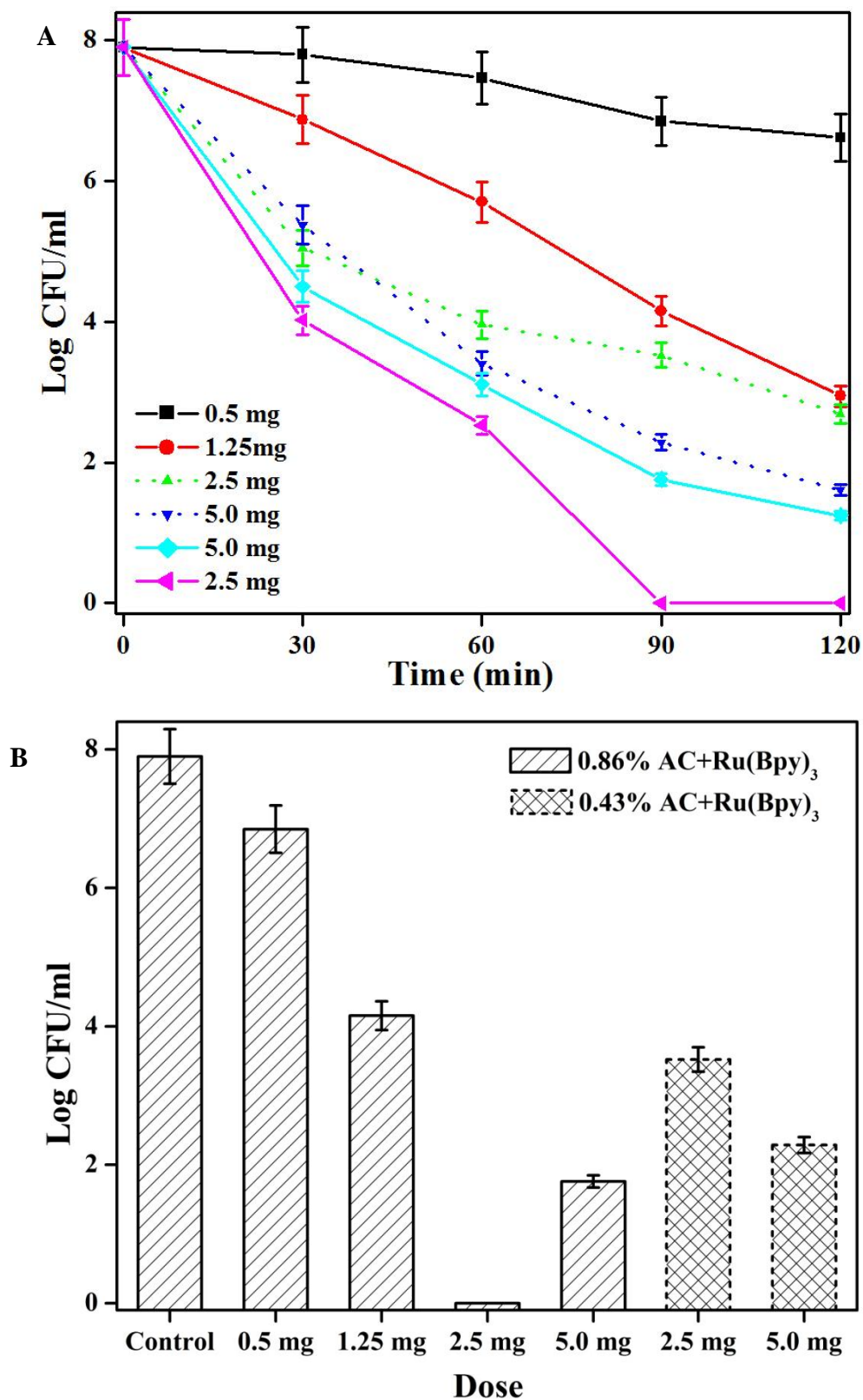
Figure 3.13: Photo bactericidal activity with respect to dose of AC/[Ru(bpy)$_3$]$^{2+}$ against *E. coli*, in PBS. (A) Kinetics of bacterial inactivation at different doses of 0.86% loaded sample (solid lines) and 0.43% loaded sample (dotted lines). (B) Comparison of cell viability at 90 min of irradiation for the 0.86% loaded sample and 0.43% loaded sample.
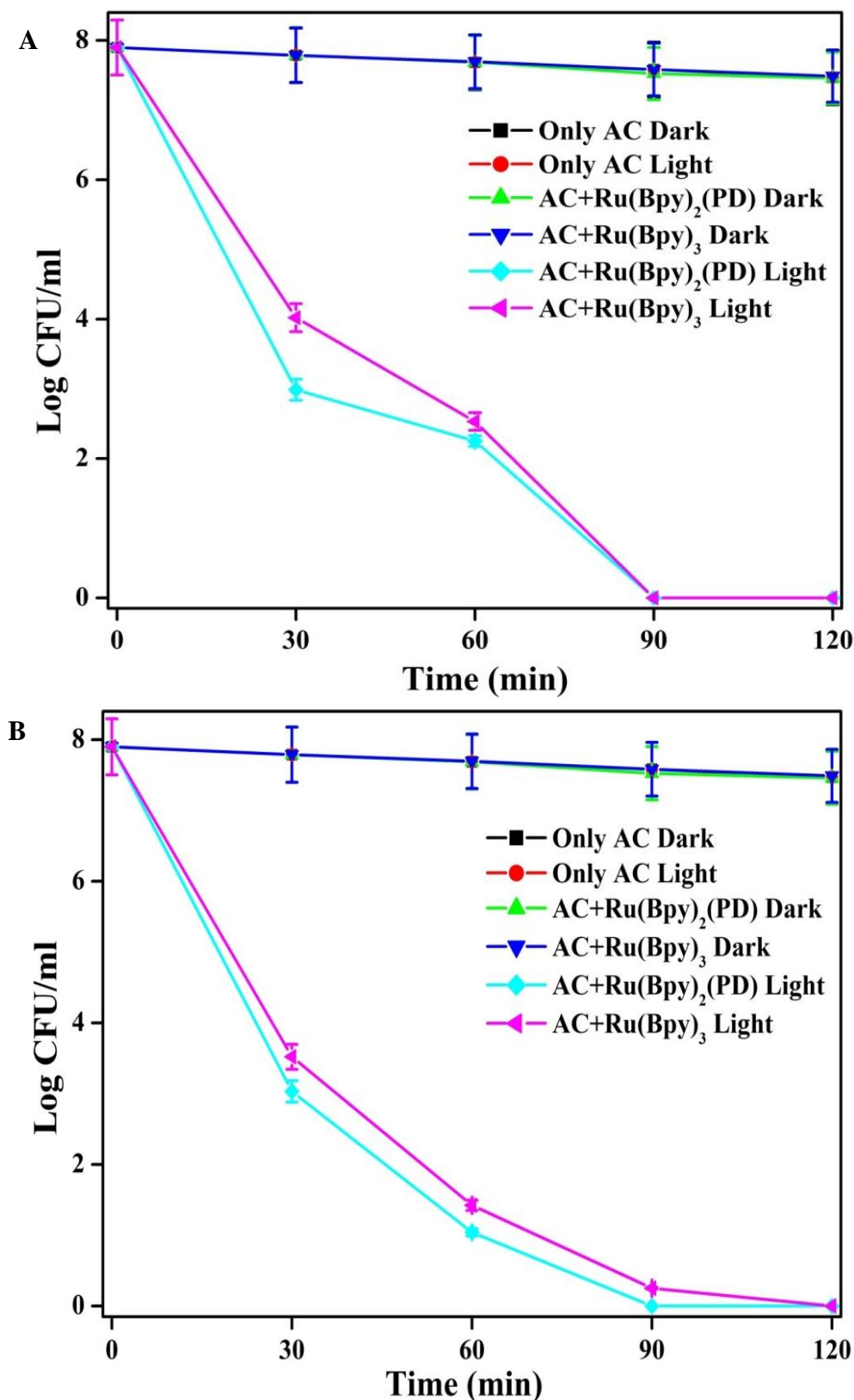
Figure 3.14: Bactericidal activity of optimized compositions against (A) *E. coli* and (B) *S. aureus* under light and dark conditions with PBS as medium.

Effect of initial cell concentration on photoinactivation of *E. coli* by AC/[Ru(bpy)$_2$(phendione)]$^{2+}$ and AC/[Ru(bpy)$_3$]$^{2+}$:

Effect of initial concentration of cells on photoinactivation of *E. coli* by AC/[Ru(bpy)$_2$(phendione)]$^{2+}$ (0.95% loading) and AC/[Ru(bpy)$_3$]$^{2+}$ (0.86% loading) revealed that complete inactivation was achieved within 90 minutes when initial concentration was 10^7 or 10^8 CFU/ml cells (Figure 3.15). The time for complete inactivation was reduced to 60 minutes on decreasing the initial concentration to 10^3 CFU/ml cells (Figure 3.15). These results reveal that the complexes are promising photosensitizers for inactivation of *E. coli*.

Reuse of AC/[Ru(bpy)$_2$(phendione)]$^{2+}$ and AC/[Ru(bpy)$_3$]$^{2+}$:

Importantly, AC/[Ru(bpy)$_2$(phendione)]$^{2+}$ and AC/[Ru(bpy)$_3$]$^{2+}$ showed photobactericidal activity for a few cycles i.e. 5 consecutive cycles, one cycle per day for 5 days totally and the final assay at the 10th day (Figure 3.16). These results indicate that AC/[Ru(bpy)$_2$(phendione)]$^{2+}$ (0.95% loading) and AC/[Ru(bpy)$_3$]$^{2+}$ (0.86% loading), can be reused. Further, ICP-OES results also indicate no leaching of complexes from AC/[Ru(bpy)$_2$(phendione)]$^{2+}$ (0.95% loading) and AC/[Ru(bpy)$_3$]$^{2+}$ (0.86% loading) and disinfected aqueous medium (PBS) is free of ruthenium.
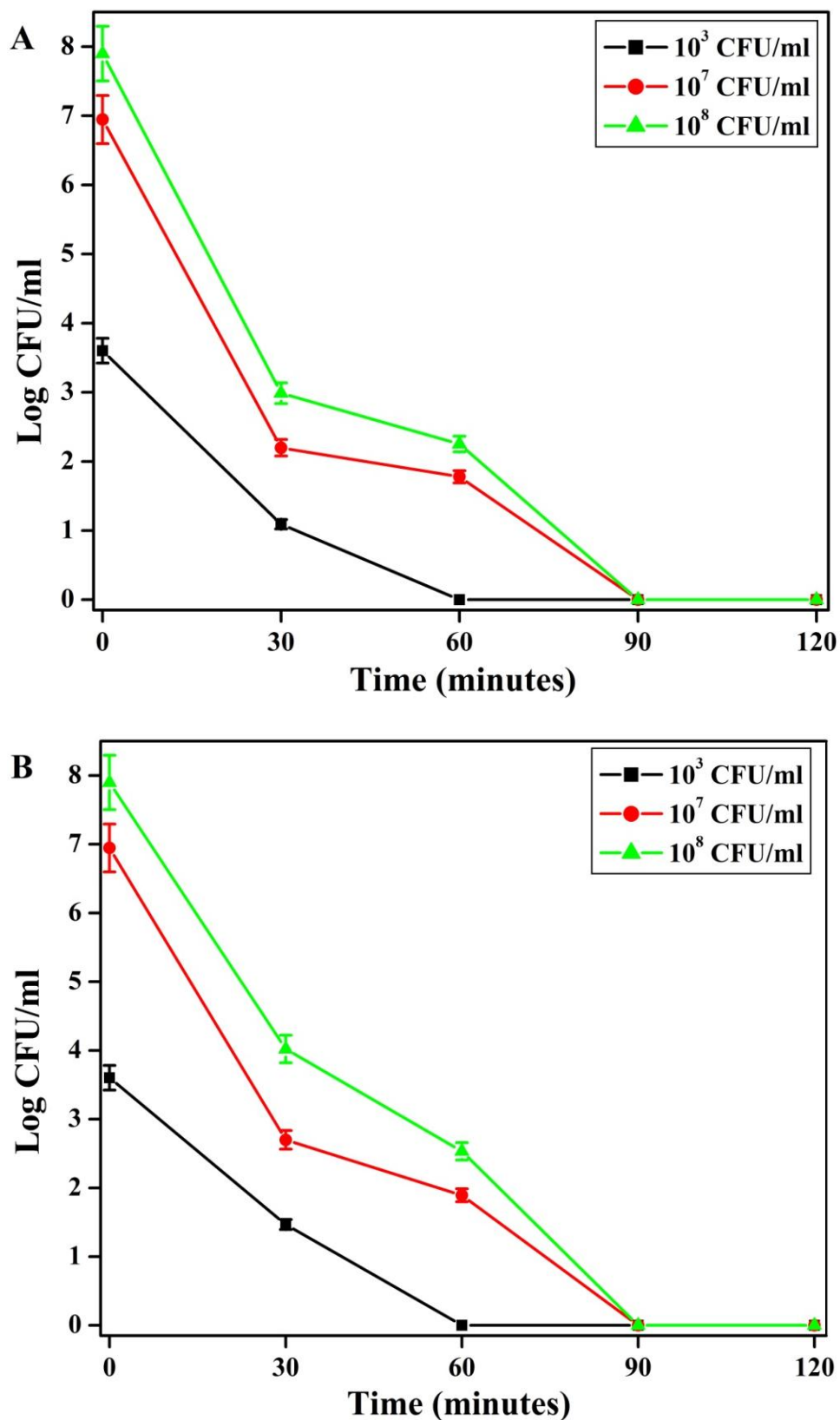
Figure 3.15: Dependence of photoinactivation of *E. coli*, in presence of (A) AC/[Ru(bpy)$_2$(phendione)]$^{2+}$ (0.95% loading) and (B) AC/[Ru(bpy)$_3$]$^{2+}$ (0.86% loading) on cell concentration.
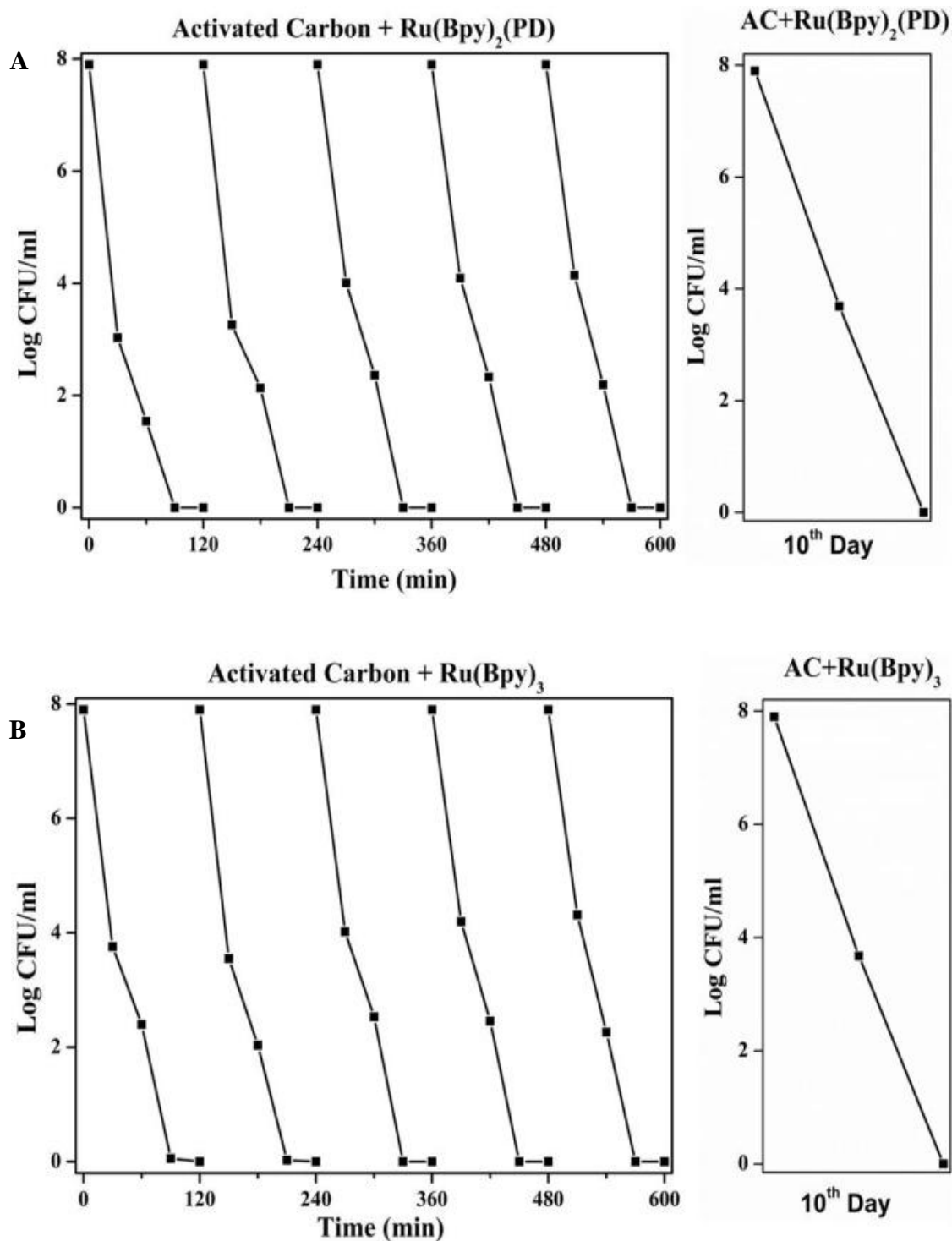
Figure 3.16: Photo-bactericidal activity of optimized compositions with PBS as medium under light irradiation for a few cycles (A) shows bactericidal activity of AC/[Ru(bpy)$_2$(phendione)]$^{2+}$ and (B) shows bactericidal activity of AC/[Ru(bpy)$_3$]$^{2+}$.

3.3.6. Photoantibacterial activity in simulated ground water:

AC/[Ru(bpy)$_2$(phendione)]$^{2+}$ (0.95% loaded) and AC/[Ru(bpy)$_3$]$^{2+}$ (0.86% loaded) also caused photoinactivation when simulated ground water was used as medium, under visible light irradiation. Complete photoinactivation of 10^8 cells was observed within 120 min, under optimized conditions (Figure 3.17). Importantly, photo bactericidal activity of AC/[Ru(bpy)$_2$(phendione)]$^{2+}$ and AC/[Ru(bpy)$_3$]$^{2+}$ was observed for a few cycles i.e. 5 consecutive cycles, one cycle per day for 5 days totally and the final assay at the 10th day with SGW as medium under light irradiation (Figure 3.18). Further, ICP-OES results also indicate no leaching of complexes from AC/[Ru(bpy)$_2$(phendione)]$^{2+}$ (0.95% loading) and AC/[Ru(bpy)$_3$]$^{2+}$ (0.86% loading) and disinfected aqueous medium (SGW) is free of ruthenium.
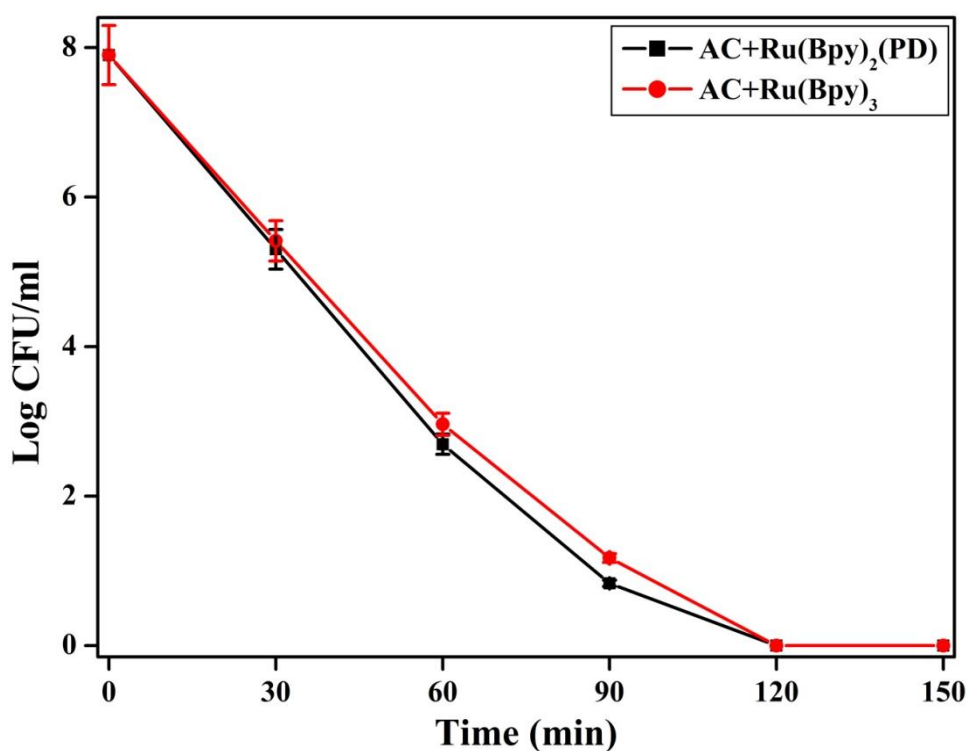
Figure 3.17: Time taken for bacterial inactivation by the composition of the invention when simulated ground water (SGW) is used as a medium.
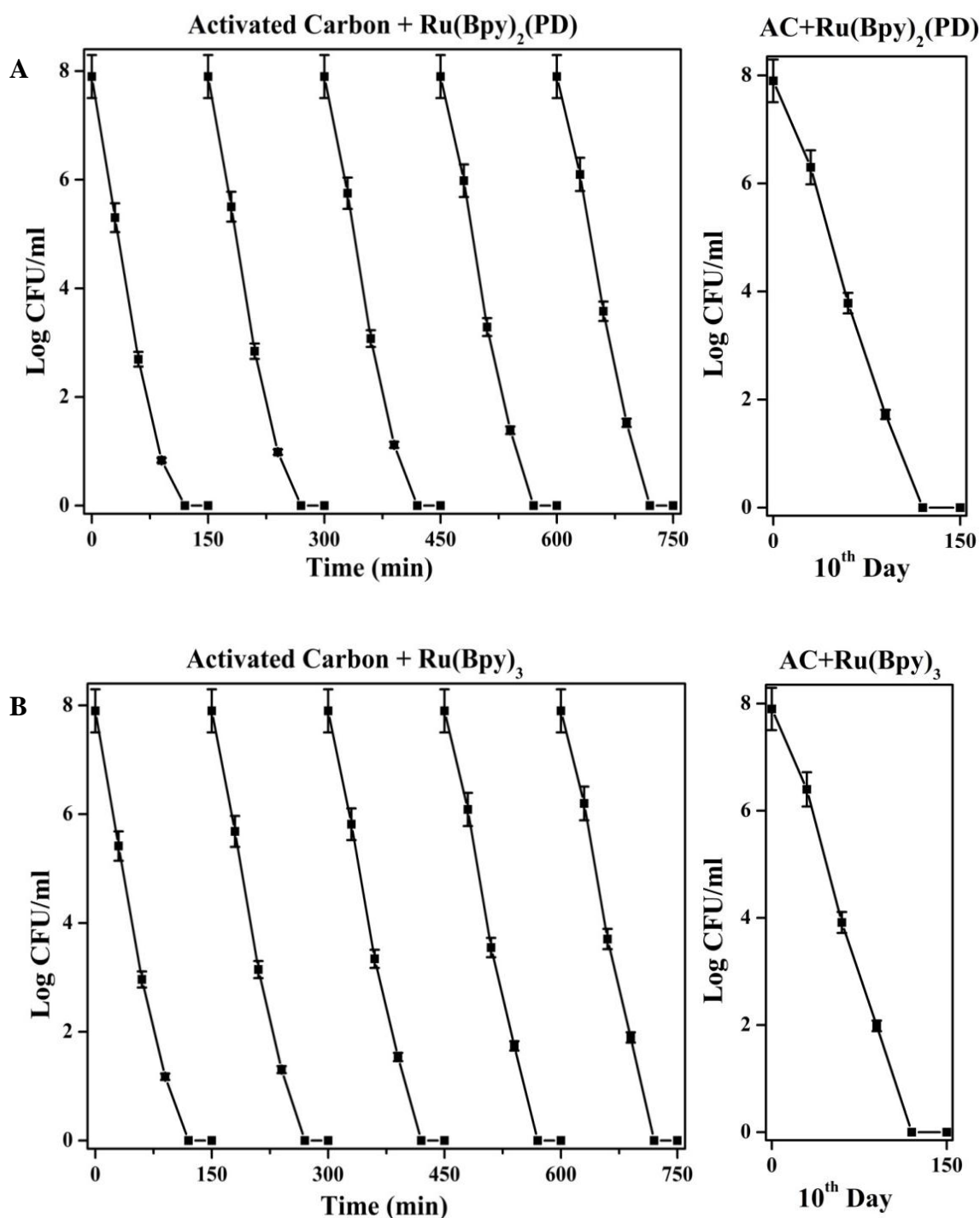
Figure 3.18: Photo-bactericidal activity of optimized compositions with SGW as medium under light irradiation for a few cycles (A) shows bactericidal activity of AC/[Ru(bpy)$_2$(phendione)]$^{2+}$ and (B) shows bactericidal activity of AC/[Ru(bpy)$_3$]$^{2+}$.

All the above results indicate that photoactive ruthenium polypyridyl complexes adsorbed to activated carbon as heterogeneous photosensitizers can be used as effective water disinfection agents under visible light irradiation. The results also show that the

complexes can be reused. Recently, Manjon et al., reported water disinfection using Ru complexes supported on porous silicones. However, the supported systems had to be autoclaved prior to next use, and the complexes leached from the supports during autoclaving process [Manjon et al., 2009]. In the present investigation it was observed that AC/[Ru(bpy)$_2$(phendione)]$^{2+}$ (0.95% loading) and AC/[Ru(bpy)$_3$]$^{2+}$ (0.86% loading) can be reused without the requirement to autoclave.

3.4. Conclusions:

2.5 mg/ml of AC/[Ru(bpy)$_2$(phendione)]$^{2+}$ comprising 23.7 µg of [Ru(bpy)$_2$(phendione)]$^{2+}$ (0.95% loading), and 2.5 mg/ml of AC/[Ru(bpy)$_3$]$^{2+}$ comprising 21.5 µg of [Ru(bpy)$_3$]$^{2+}$ (0.86% loading) was able to completely inactivate 10^8 bacteria in PBS under visible light irradiation within 90 min. The above composition was also able to completely photoinactivate 10^8 bacteria in SGW within 120 min. Importantly, AC/[Ru(bpy)$_2$(phendione)]$^{2+}$ and AC/[Ru(bpy)$_3$]$^{2+}$ could also cause complete photoinactivation for 5 consecutive cycles in both PBS and SGW. These results indicate that AC/[Ru(bpy)$_2$(phendione)]$^{2+}$ and AC/[Ru(bpy)$_3$]$^{2+}$ can be promising visible light water disinfection agents.

Chapter 4

Enhanced photoantibacterial activity of [Ru(bpy)₃]²⁺ complex in presence of glutathione coated silver nanoparticles

Highlights:

1. Complete photoinactivation of bacteria by $[Ru(bpy)_3]^{2+}$ complex and Ag-GSH NPs.

2. Visible light emitting diode array used for photoinactivation of bacteria.

3. Loss of cell integrity due to membrane damage on photolysis.

4. Photobactericidal efficiency of $[Ru(bpy)_3]^{2+}$ complex is significantly improved.

Graphical abstract figure:
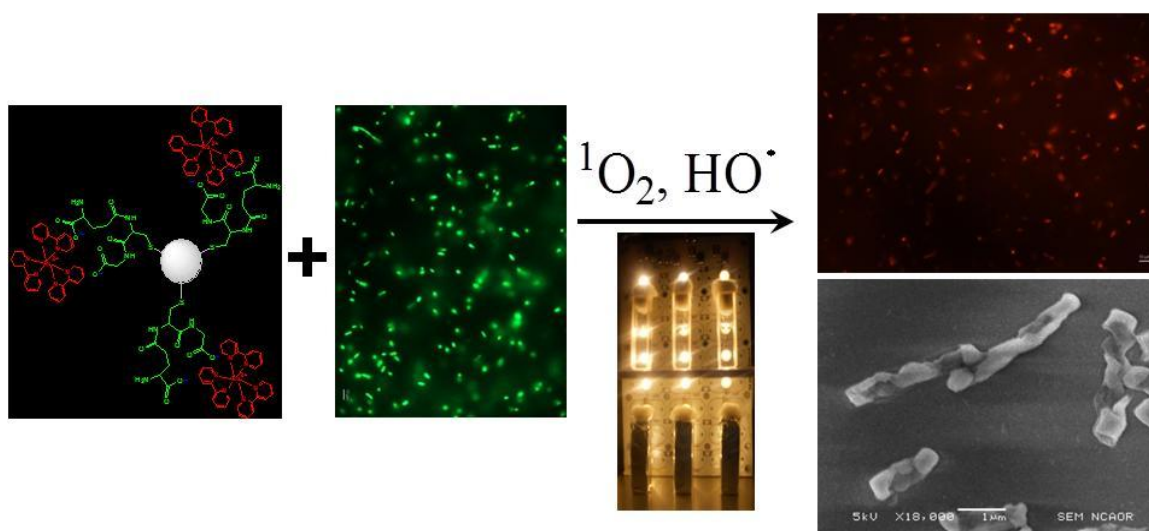
4.1. Background:

Murphy et al., used porphyrin based photosensitizers to obtain prophyrin-silver nanoparticles (Ag NPs) hybrid structures, where photoinduced electron transfer between the porphyrin and Ag NPs was observed [Murphy et al., 2011]. Pramod et al., employed ruthenium trisbypyridine complex as photosensitizer to obtain ruthenium complex-Au NPs hybrid systems [Pramod et al., 2006]. Glomm et al., have reported that the MLCT photoexcitation of $[Ru(bpy)_3]^{2+}$ adsorbed onto Ag NPs, resulted in energy and electron transfer from $[Ru(bpy)_3]^{2+}$ to Ag NPs. The electron transfer is represented in scheme 1 [Glomm et al., 2005].

$$[Ru(bpy)_3]^{2+} - Ag\ NP \xrightarrow{h\nu} [\ Ru(bpy)_3*]^{2+}\ (MLCT) - Ag\ NP \longrightarrow$$

$$[Ru(bpy)_3]^{3+} - Ag\ NP^- \longrightarrow [Ru(bpy)_3]^{2+} - Ag\ NP$$
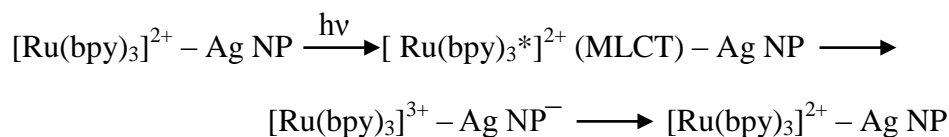
Scheme 1: Electron transfer between $[Ru(bpy)_3]^{2+}$ and Ag NP.

Importantly, photoexcited states and charge-separated states in nano hybrid systems may produce photosensitised ROS in presence of dissolved oxygen that cause cell death. Nevertheless, study on the ability of MLCT photoexcitation of $[Ru(bpy)_3]^{2+}$ adsorbed onto Ag NPs to generate ROS and induce inactivation of bacteria has not been studied. Moreover, it has been reported that Ag NP capped with glutathione peptide (Ag-GSH) was stable, and bind to the bacterial surface membrane, but the antibacterial action was significantly reduced due the glutathione coating and other factors such as prevention of the release of Ag^+ ions [Taglietti et al., 2012, Amato et al., 2011, Pallavicini et al., 2010]. Thus, Ag-GSH may be useful as carrier of cationic photosensitizer, such as $[Ru(bpy)_3]^{2+}$, towards the bacterial membrane, and may enhance the photoinactivation of bacteria by $[Ru(bpy)_3]^{2+}$ complex.

These reports indicate that nano hybrid systems consisting of a photo-donor bound to Ag NP may act as effective PACT agent. All the above facts prompted us to investigate the ability of $[Ru(bpy)_3]^{2+}$ to photoinactivate bacteria in presence of stable Ag-GSH nanoparticle (Ag-GSH-Ru nano hybrid systems) under visible light irradiation condition.

4.2. Materials and methods:

4.2.1. Materials:

Silver nitrate, sodium borohydride, trisodium citrate were purchased from S D Fine Chemicals Limited, India. L-glutathione reduced (GSH) was purchased from Sigma Aldrich, India. Details are as mentioned in chapter 2, section 2.2.1. Double distilled water (DW) was used for all experiments.

4.2.2. Complex preparation:

$[Ru(bpy)_3](PF_6)_2.2H_2O$ was prepared and characterised spectrophotometrically (JASCO V-570 UV/Vis/NIR Spectrophotometer), as reported earlier [Gao et al., 2000]. Appropriate amount of $[Ru(bpy)_3]^{2+}$ was dissolved in DW to get stock solution.

4.2.3. Visible light source:

LED array was used as visible light source, purchased from Kwality Photonics, Hyderabad, India. As mentioned in chapter 2, section 2.2.3.

4.2.4. Synthesis of Ag NP coated with GSH:

Ag NP coated with GSH was prepared as reported earlier [Taglietti et al., 2012, Amato et al., 2011]. All the glasswares were acid washed and rinsed thrice with DW before using. The procedure is briefly described below.

Ag NP preparation:

To 100 mL of ice cooled DW the following ice-cooled solutions were added in sequence under vigorous stirring: 1 mL of 1% (w/v) $AgNO_3$ solution (10 mg in 1mL DW), after one minute 1ml of 1% (w/v) sodium citrate (10 mg in 1mL DW) and, after 1 more minute, 0.75 mL of a mixture of 0.075%w $NaBH_4$ and 1%w sodium citrate (10 mg sodium citrate + 0.75 mg $NaBH_4$ in 1 mL DW). After the last addition of mixture, stirring was immediately stopped, in order to avoid coagulation.

Coating Ag NP with GSH (Ag-GSH):

Coated NPs solutions were prepared by adding the capping agent, GSH to the synthesized citrate-capped NPs suspension, followed by centrifugation at the appropriate pH. During titration of GSH against Ag-citrate capped nanoparticle, the localized surface plasmon resonance (LSPR shift) (395 to 400 nm) was observed at approximately 0.03 equivalents of GSH with respect to $[Ag^+]$. This indicated that 0.03 equivalents of GSH with respect to $[Ag^+]$ bind to the Ag nanoparticle, as reported earlier

[Amato et al., 2011]. The slight shift to 398 nm on further increasing the concentration of GSH is attributed to the formation of complex of excess GSH with Ag^+ in the solution. Thus, 0.03 equivalents of GSH with respect to the total silver concentration were added. 102.75 mL of the above prepared Ag-citrate capped nanoparticle suspension ($[Ag^+]$ = 572.9 μM) was rapidly added to 0.54 mg of soild GSH (17.187 μM). The solution was kept at room temperature (25 °C) for about 15 min and the pH of the solution was manually set to 3 by adding standard HNO_3 (1 M) before centrifugation. Ag-GSH was precipitated by centrifugation at 8000 rpm for 15 min. The obtained pellet was washed three times with DW. The washed pellet was dried at 30 °C for 10 min under vacuum.

4.2.5. Preparation of nano hybrid systems of ruthenium adsorbed Ag NP solution:

Earlier, nano hybrid systems were prepared by mixing the appropriate concentrations of PS with NPs [Murphy et al., 2011, Glomm et al., 2002]. Briefly, aqueous solutions of $[Ru(bpy)_3]^{2+}$ complex and Ag-GSH were thoroughly mixed with appropriate concentrations to obtain the Ag-GSH-Ru nano hybrid systems. Ag-GSH-Ru nano hybrid was also freshly prepared in PBS with bacteria for antibacterial experiments under dark and light conditions.
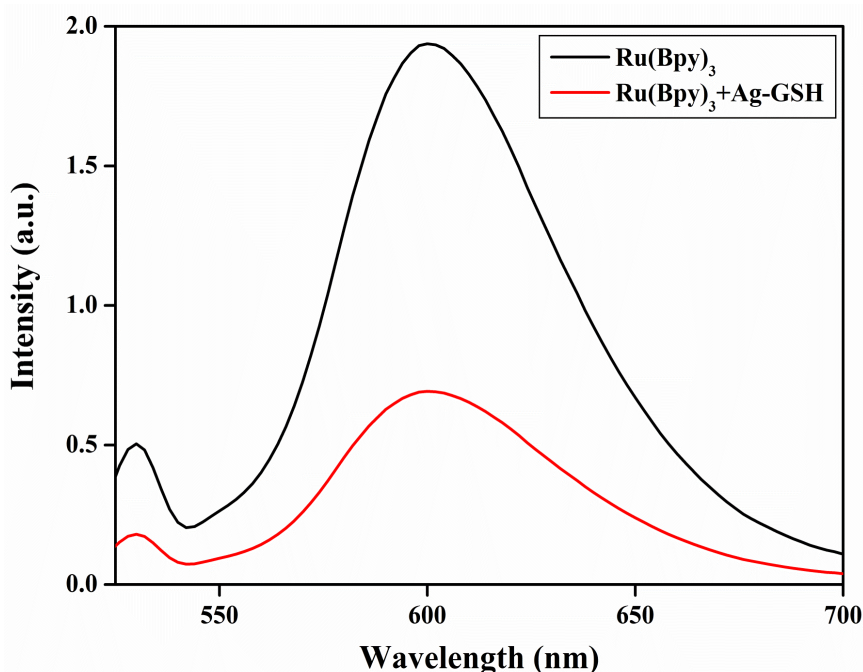
Figure 4.1: Fluorescence measurement of $[Ru(bpy)_3]^{2+}$ (0.5 μM) and Ag-GSH-Ru (Ag-GSH (10 μg/ml) + $[Ru(bpy)_3]^{2+}$ (0.5 μM)).

Fluorescence of $[Ru(bpy)_3]^{2+}$ (0.5 µM) alone and $[Ru(bpy)_3]^{2+}$ (0.5 µM) mixed with Ag-GSH (10 µg/ml) was measured at λ_{ex} = 450 nm in PBS using JASCO FP 6300 spectrofluorometer. The fluorescence of $[Ru(bpy)_3]^{2+}$ complex in the nao hybrid was significantly quenched as compared to free complex (Figure 4.1). Earlier, quenching of luminescence by nanoparticles has been shown for systems such as citrate-capped Au and Ag nanoparticles, and Ru(II) and Os(II) complexes [Huang and Murray, 2002, Glomm et al., 2002].

4.2.6. Antibacterial activity of Ag-GSH-Ru and Ag-GSH:

The bacterial cells were grown in NB broth to attain log phase. The cells were harvested by centrifugation at 1000 g for 15 min at 25 °C. Cell pellet was resuspended in PBS. Ag-GSH was suspended in PBS and $[Ru(bpy)_3]^{2+}$ dissolved in sterilised DW. Required volumes of Ag-GSH suspension and $[Ru(bpy)_3]^{2+}$ solution were mixed to obtain Ag-GSH-Ru nano hybrid systems in a pre-sterilized 10 mm quartz cuvettes containing 10^8 CFU/ml cell suspension in PBS. The total volume was 2 ml. The cuvettes were kept in dark for 30 min and then irradiated with light for 90 min. For dark controls, the cuvettes were covered with aluminium foil and placed in front of the light source. Temperature was maintained at 35 °C ± 2 °C. The reaction mix was withdrawn every 30 min, serially diluted and plated on NB agar plates.

Colonies were counted after incubating the plates at 37 °C for 24 hours. All the tests were done in triplicates. To study the effect of dose of Ag-GSH and $[Ru(bpy)_3]^{2+}$ on bacteria, different $[Ru(bpy)_3]^{2+}$ and Ag-GSH concentrations were used. 10 µg/ml of Ag-GSH and 0.5 µM $[Ru(bpy)_3]^{2+}$ was fixed as the optimised concentration/ combination and were used for experiments such as scavenging, fluorescence microscopic and SEM analysis. Effect of bacterial cell concentration (10^3 - 10^8 CFU/ml) on photoinactivation of *E. coli* by 10 µg/ml of Ag-GSH and 0.5 µM $[Ru(bpy)_3]^{2+}$ was also studied. Earlier 15 µg/ml Ag-GSH alone was shown to cause 3 log reduction on incubation for ~20 hours [Amato et al., 2011]. Also it is not desirable to use high concentration of Ag NP. Based on these facts the maximum concentration of Ag-GSH was fixed at 10 µg/ml at which Ag-GSH has no effect on bacterial viability.

Intensity of light was optimised by adjusting the distance between light source and surface of quartz cuvette containing bacterial cell suspension. *E. coli* and *S. aureus* were

exposed to light at the fluence rate of 95 mW/cm^2 and 60 mW/cm^2, respectively. Under these photolytic conditions the light alone had no effect on cell viability.

4.2.7. Membrane binding of Ag-GSH-Ru, Ag-GSH and [Ru(bpy)$_3$]$^{2+}$ to *E. coli* cells:

Membrane binding of Ag-GSH-Ru, Ag-GSH and [Ru(bpy)$_3$]$^{2+}$ to *E. coli* cells was spectrophotometrically followed by recording absorption spectra. Briefly, 10^8 CFU/ml *E. coli* cells in PBS containing 10 µg/ml of Ag-GSH or 10 µM of [Ru(bpy)$_3$)]$^{2+}$ were incubated for 120 minutes. Absorption spectra of these suspensions were taken after filtering through 0.45 µm PTFE filter. It was observed that complex did not adsorb to this filter.

4.2.8. Effect of singlet oxygen quencher and hydroxyl radical scavenger on bacterial inactivation:

Sodium azide and D-mannitol were used as singlet oxygen quencher and hydroxyl radical scavenger, respectively to study their effect on antibacterial activity of Ag-GSH-Ru. 25 mM of the quencher, 10 µg/ml Ag-GSH, 0.5 µM [Ru(bpy)$_3$]$^{2+}$ and 10^8 CFU/ml cells were suspended in PBS and incubated in dark for 30 min and then irradiated for 90 min. Dark controls were covered with aluminium foil and placed in front of the light source. The reaction mix was withdrawn after 90 min irradiation, serially diluted and plated on NB agar plates. Colonies were counted after incubating plates at 37 °C for 24 hours.

4.2.9. Analysis of cell integrity:

E. coli cells in PBS were irradiated with and without (control) Ag-GSH-Ru. Cells with Ag-GSH-Ru were covered with aluminium foil as dark controls. Details are as mentioned in chapter 2, section 2.2.7.

4.2.10. Scanning Electron Microscopy (SEM) analysis:

E. coli cells in PBS were irradiated with and without (control) Ag-GSH-Ru and complex. Cells with Ag-GSH-Ru were covered with aluminium foil as dark controls. Details are as mentioned in chapter 2, section 2.2.8.

4.3. Results and discussions:

4.3.1. Photoinactivation of bacteria by Ag-GSH-Ru nano hybrid:

Visible light irradiation of 10^8 Gram-negative (*E. coli*) bacterial cells in presence of Ag-GSH-Ru (Ag-GSH (10 µg/ml) and [Ru(bpy)$_3$]$^{2+}$ (0.5 µM)) caused complete inactivation

of bacteria within 90 min (Figure 4.2 (A), 4.3 (A)). On the other hand, visible light irradiation of 10^8 Gram-positive (*S. aureus*) bacterial cells in presence of Ag-GSH-Ru (Ag-GSH (10 µg/ml) and $[Ru(bpy)_3]^{2+}$ (0.5 µM)) caused complete inactivation of bacteria within 60 min (Figure 4.2 (B), 4.3 (B)). Ag-GSH (10 µg/ml) in combination with complex (10 µM) had no effect no cell viability under dark conditions (Figure 4.2, 4.3). Moreover, Ag-GSH (10-200 µg/ml) alone had no effect on cell viability under light and dark conditions, on both *E. coli* and *S. aureus* (Figure 4.4). Importantly, $[Ru(bpy)_3]^{2+}$ (20 µM) alone also had no effect on cell viability under dark conditions, on both *E. coli* and *S. aureus* (Figure 4.5). Thus, all the above results reveal that the hybrid system i.e., the combination of Ag-GSH and Ru complex, and light has the ability to photoinactivate both Gram-positive and Gram-negative bacteria in water.

The effect of the amount of Ag-GSH and $[Ru(bpy)_3]^{2+}$ on photoinactivation was studied. Varying the Ag-GSH concentration between 1 and 10 µg/ml with concentration of Ag-GSH maintained at 10 µg/ml, also showed an increase in log reduction of *E. coli* from 5 to 8 was observed within 90 min (Figure 4.2 (A)). Similarly, for *S. aureus* within 60 min, an increase in log reduction from 5 to 8 was observed (Figure 4.2 (B)). Moreover, varying the $[Ru(bpy)_3]^{2+}$ concentration between 0.1 and 0.5 µM with concentration of Ag-GSH maintained at 10 µg/ml, showed an increase in log reduction of *E. coli* from 6 to 8 was observed within 90 min (Figure 4.3 (A)). Similar trend was observed for *S. aureus* within 60 min (Figure 4.3 (B)).

Earlier, Lie et al., have shown that Ru complexes alone can act as a PS for inactivation of bacteria [Lei et al., 2011]. In the present investigation, we have found that concentration as high as 10 µM of PS $[Ru(bpy)_3]^{2+}$ alone was able to completely photoinactivate *E. coli* in water within 120 min (Figure 4.5 (A)). It is important to note that, the effective concentration of the PS $[Ru(bpy)_3]^{2+}$ required for photoinactivation was reduced to ~20 times in the presence of Ag-GSH (Figure 4.2 (A), 4.3 (A)). In case of *S. aureus*, 5 µM of $[Ru(bpy)_3]^{2+}$ alone was able cause complete photoinactivation within 90 min (Figure 4.5 (B)). However, the effective concentration of $[Ru(bpy)_3]^{2+}$ required for photoinactivation was reduced to ~10 times in the presence of Ag-GSH (Figure 4.2 (B), 4.3 (B)). Thus, the results reveal that *S. aureus* is more susceptible towards photoinactivation than *E. coli* in presence of Ag-GSH-Ru. Earlier, such susceptibility of Gram-positive bacteria during photoinactivation have been explained

by differences in membrane compositions between Gram-positive and Gram-negative bacteria, as discussed in chapter 1 section 1.6, and chapter 2 section 2.3.1.
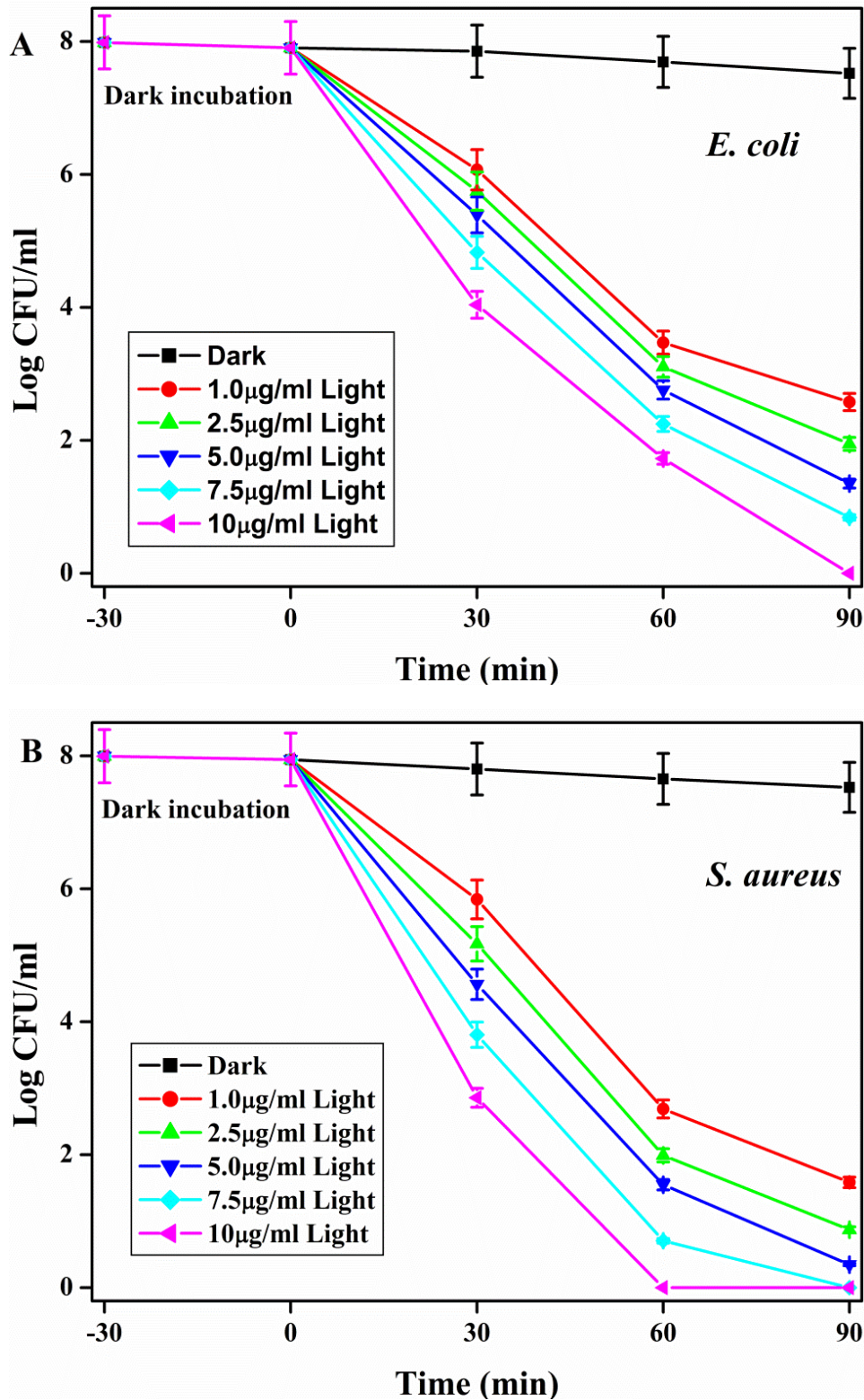
Figure 4.2: Antimicrobial activity of Ag-GSH-Ru at variable Ag-GSH (1-10 µg/ml) and fixed complex concentration (0.5 µM) under dark and light conditions against (A) *E. coli* and (B) *S. aureus*.
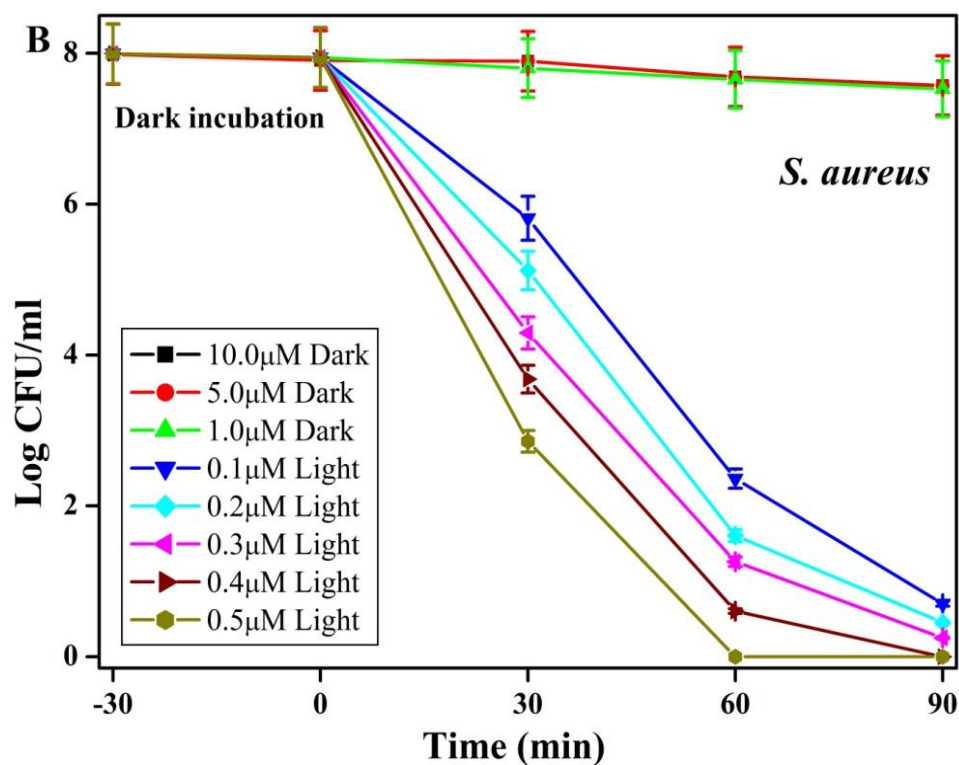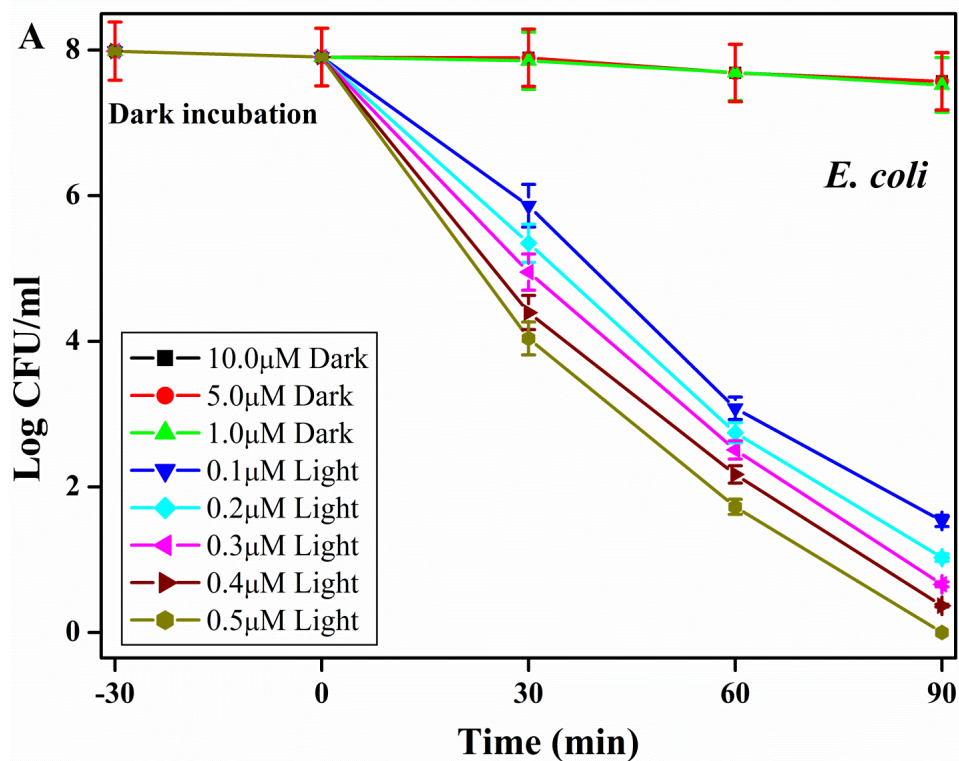
Figure 4.3: Antimicrobial activity of Ag-GSH-Ru at fixed Ag-GSH (10 µg/ml) and variable complex concentration (0.1 µM to 0.5 µM) under dark and light conditions against (A) *E. coli* and (B) *S. aureus*.
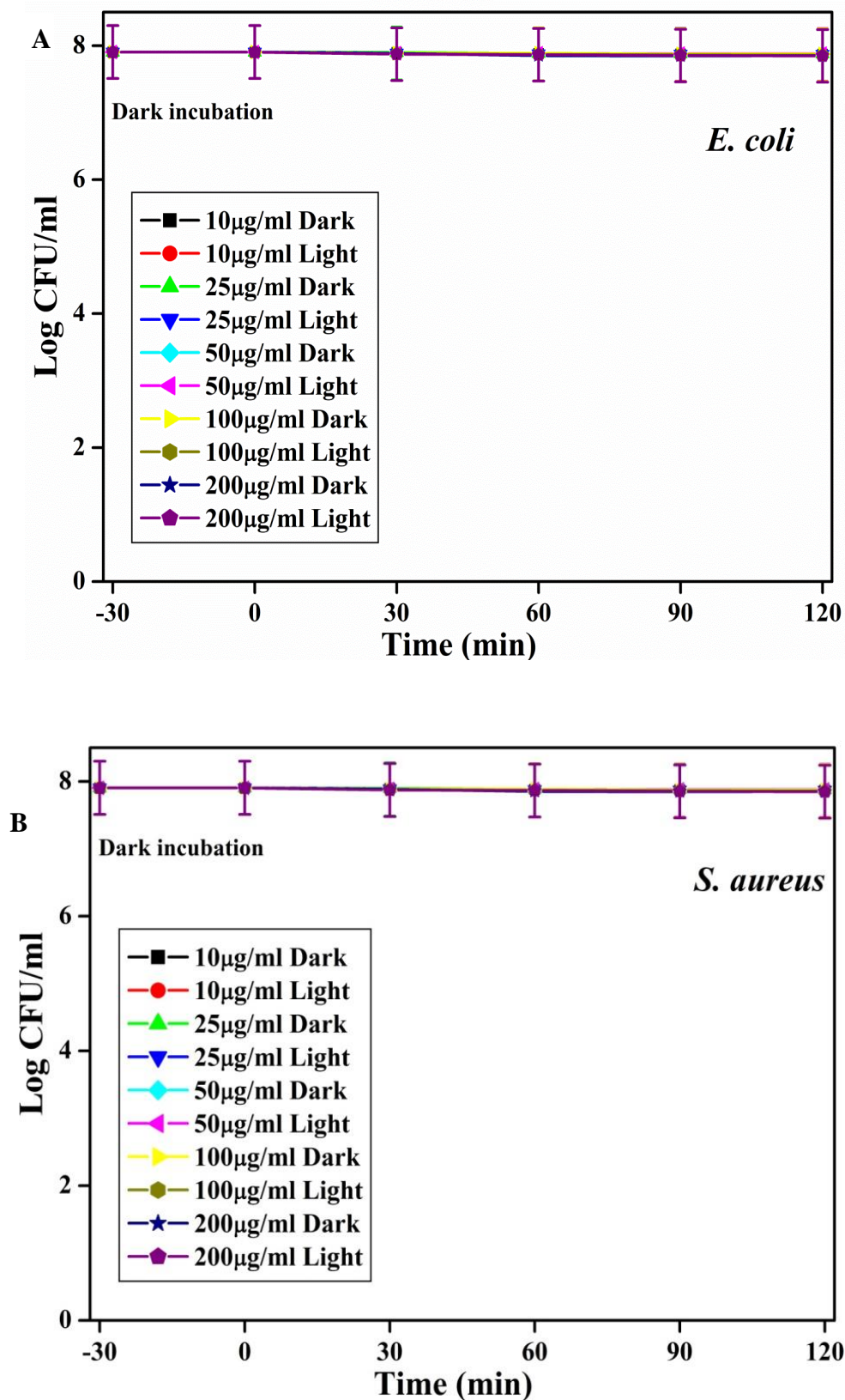
Figure 4.4: Antimicrobial activity of Ag-GSH alone under dark and light conditions against (A) *E. coli* and (B) *S. aureus*.
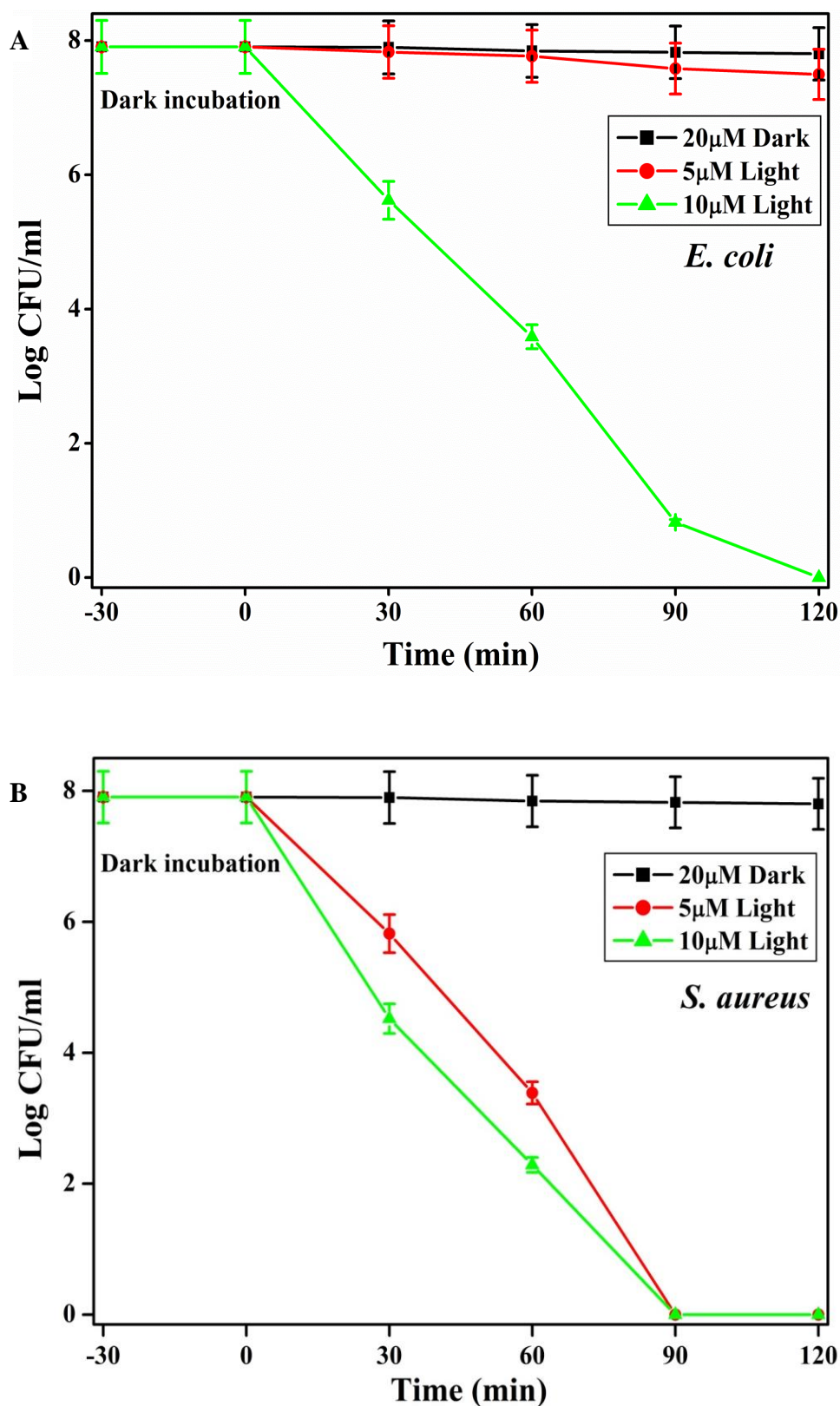
Figure 4.5: Antimicrobial activity of $[Ru(bpy)_3]^{2+}$ alone under dark and light conditions against (A) *E. coli* and (B) *S. aureus*.

Effect of initial cell concentration on photoinactivation of *E. coli* by Ag-GSH and [Ru(bpy)$_3$]$^{2+}$:

Effect of initial concentration of cells on photoinactivation of *E. coli* by Ag-GSH-Ru (Ag-GSH (10 µg/ml) + [Ru(bpy)$_3$]$^{2+}$ (0.5 µM)) revealed that complete inactivation was achieved within 90 minutes when initial concentration was 10^7 or 10^8 CFU/ml cells (Figure 4.6). The time for complete inactivation was reduced to 60 minutes on decreasing the initial concentration to 10^3 CFU/ml cells (Figure 4.6). These results reveal that the complexes are promising photosensitizers for inactivation of *E. coli*.

It has been shown that electron transfer (from MLCT state of complex to surface of nanoparticle) occurs between plasmon of Ag NP (acceptor) and ruthenium complex (donor) (scheme 1) under visible light irradiation [Franzen et al., 2002]. Thus, the present results indicate that the Ag-GSH-Ru hybrid system formed may generate ROS under visible light irradiation could kill bacteria. The effect of scavengers on photoantibacterial activity was studied and the results are presented in section 4.3.2.
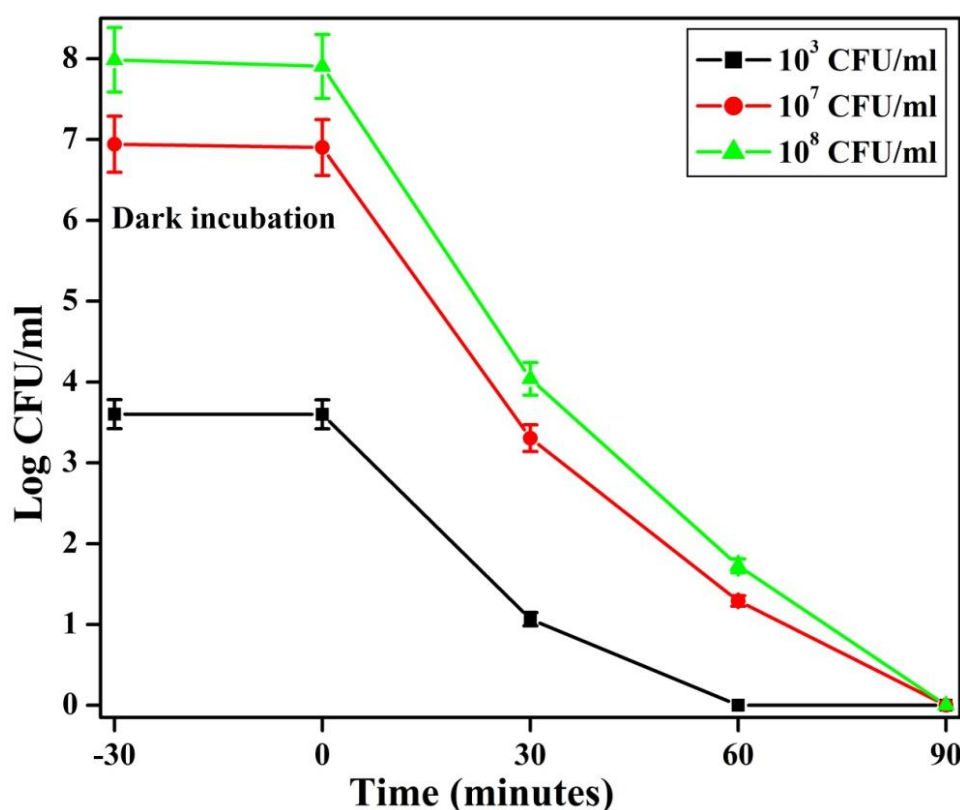
Figure 4.6: Dependence of photoinactivation of *E. coli*, in presence of Ag-GSH-Ru (Ag-GSH (10 µg/ml) + [Ru(bpy)$_3$]$^{2+}$ (0.5 µM)) on cell concentration.

Membrane binding of Ag-GSH-Ru, Ag-GSH and [Ru(bpy)$_3$]$^{2+}$ to *E. coli* cells:

The absorbance of Ag-GSH-Ru nano hybrid (Ag-GSH (10 µg/ml) and [Ru(bpy)$_3$]$^{2+}$ (0.5 µM)) decreased on incubating it with *E. coli* for 120 min (Figure 4.7 (A), 4.8). Similarly, the absorbance of Ag-GSH (10 µg/ml) also decreased on incubating it with *E. coli* for 120 min (Figure 4.7 (B), 4.8). On the other hand, the absorbance of [Ru(bpy)$_3$]$^{2+}$ (10 µM) did not significantly reduce as compared to Ag-GSH-Ru and Ag-GSH, on incubation with *E. coli* for 120 min (Figure 4.7(C), 4.8). These results indicate that Ag-GSH-Ru nano hybrid and Ag-GSH have the ability to bind bacterial membrane, whereas [Ru(bpy)$_3$]$^{2+}$ binding was insignificant. Earlier, it has been reported that Ag-GSH has the ability to bind bacterial membrane [Amato et al., 2011]. Decrease in the absorbance for both, Ag-GSH-Ru and Ag-GSH, was almost similar, indicating that the adsorption of [Ru(bpy)$_3$]$^{2+}$ onto Ag-GSH did not alter the membrane binding affinity of Ag-GSH (Figure 4.8).

4.3.2. Effect of singlet oxygen quencher and hydroxyl radical scavenger on bacterial inactivation:

Effect of singlet oxygen quencher and hydroxyl radical scavenger on bacterial inactivation was studied using sodium azide and mannitol respectively [Tavares et al., 2011, Cormick et al., 2011, Maisch et al., 2005]. Growth was observed in presence of both, indicating that both singlet oxygen and hydroxyl radicals are responsible for photoinactiavtion of bacteria (Figure 4.9). The quencher/scavenger alone under dark and light conditions and, quencher/scavenger in presence of Ag-GSH-Ru did not affect cell viability under dark conditions. [Ru(bpy)$_3$]$^{2+}$ is a well known photosensitizer that generates both singlet oxygen and hydroxyl radicals on irradiation [DeRosa et al., 2001].
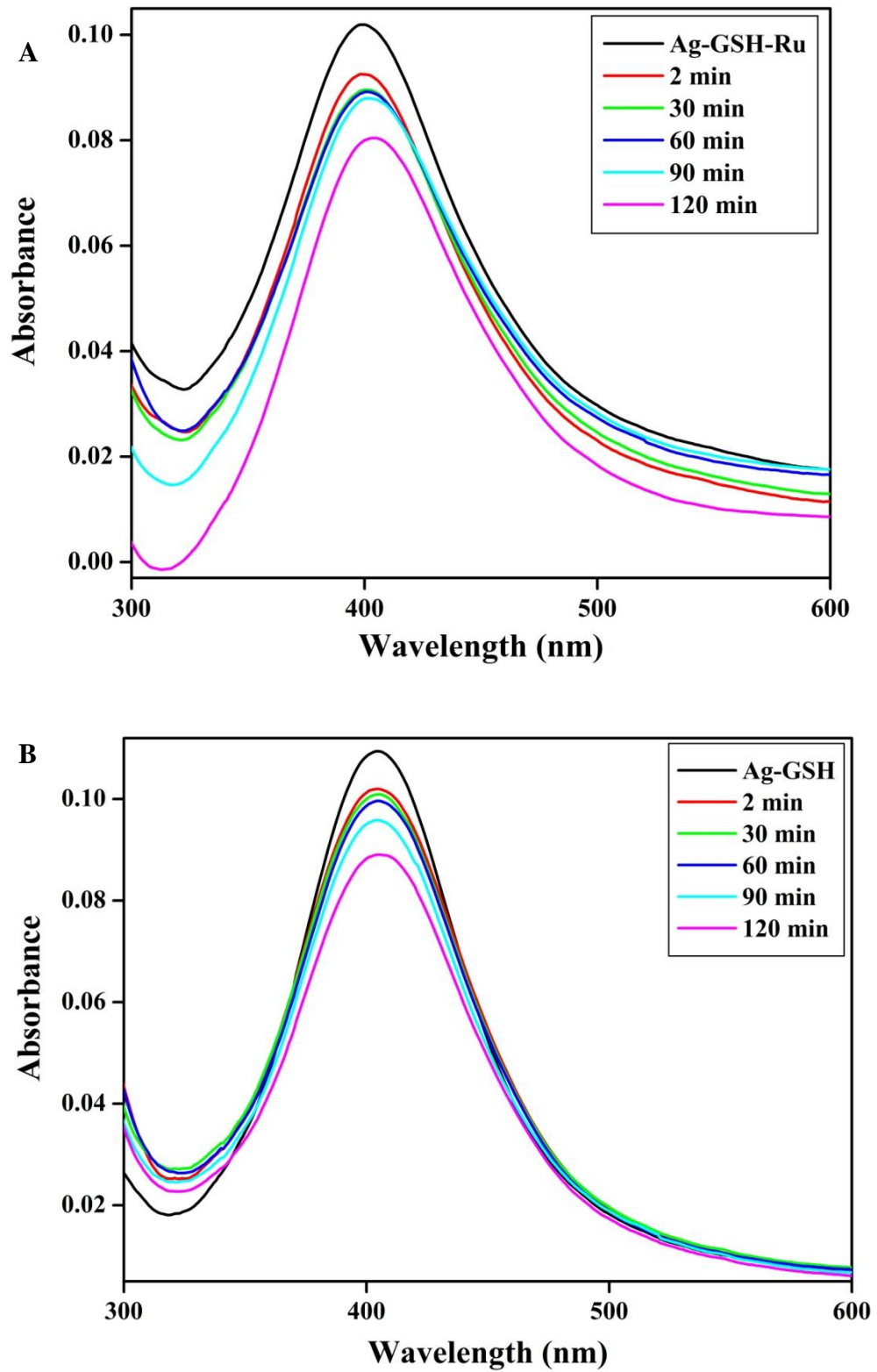
Figure 4.7: Membrane binding of (A) Ag-GSH-Ru and (B) Ag-GSH to *E. coli* cells.
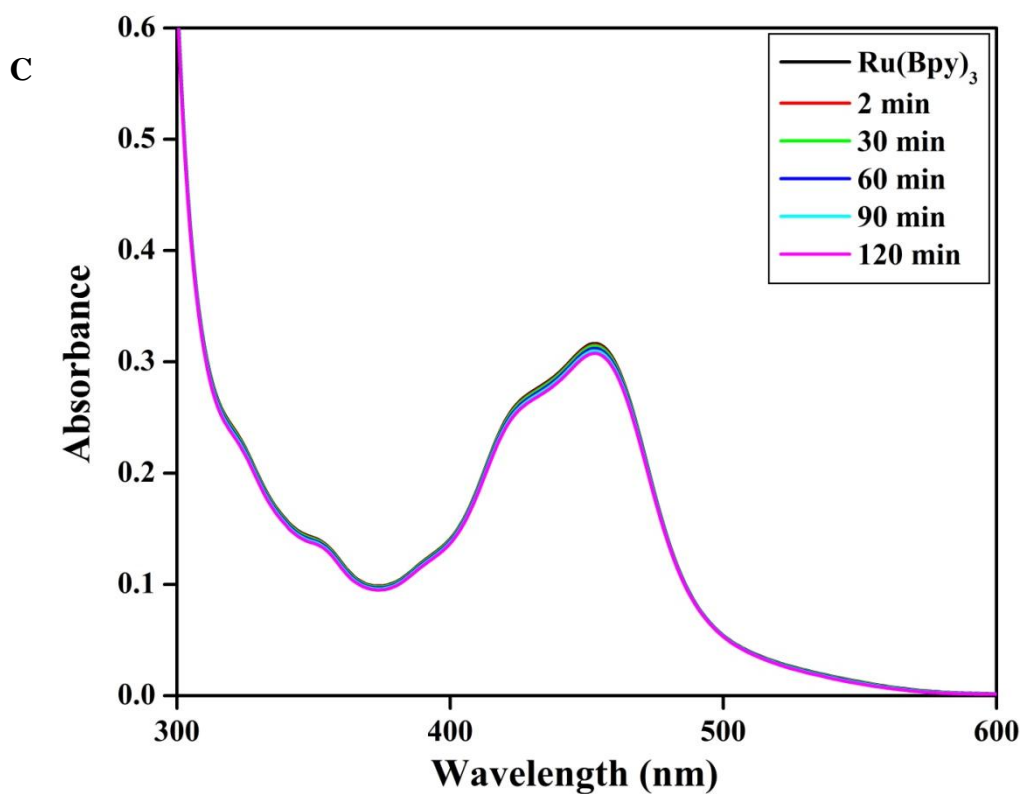
Figure 4.7: Membrane binding of (C) $[Ru(bpy)_3]^{2+}$ to *E. coli* cells.
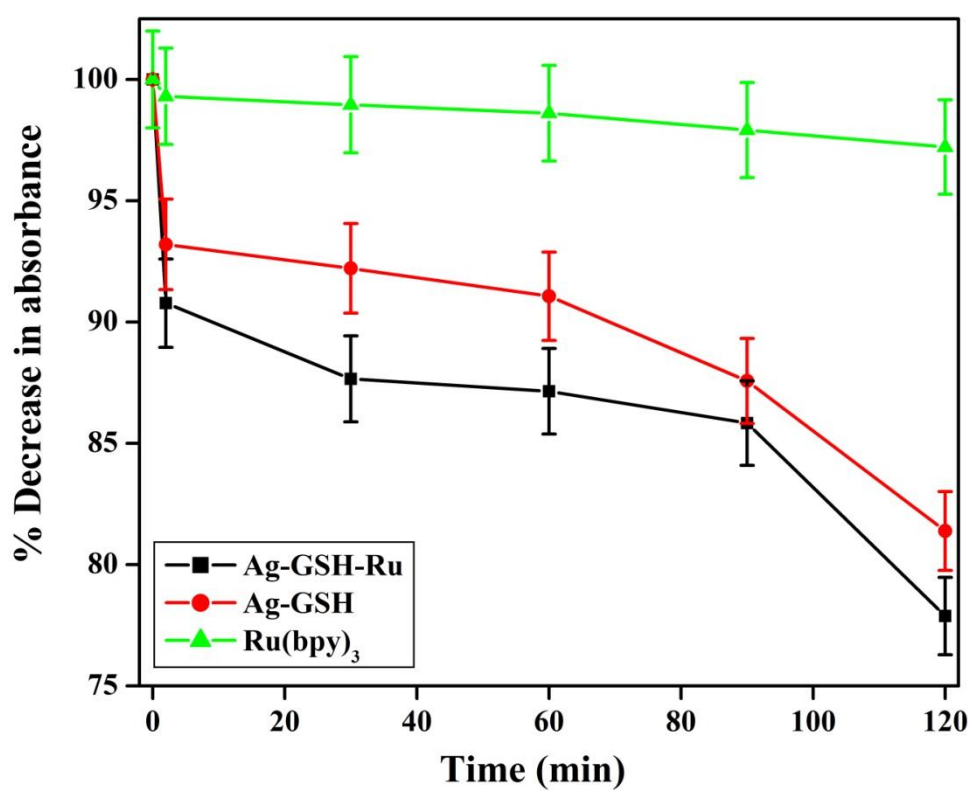
Figure 4.8: Percentage decrease in absorbance of Ag-GSH-Ru, Ag-GSH and $[Ru(bpy)_3]^{2+}$, monitored at 398 nm, 405 nm and 452 nm respectively.
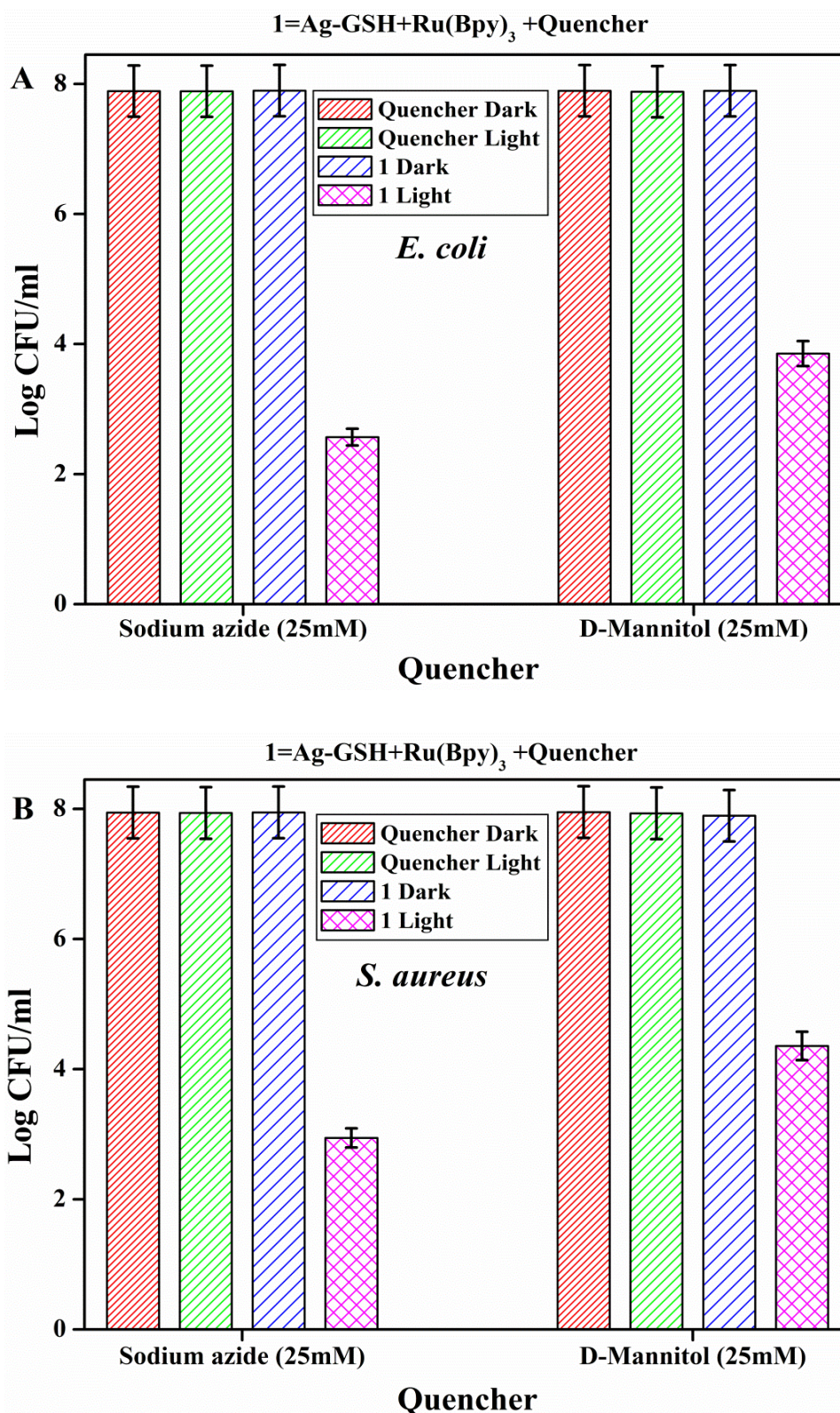
Figure 4.9: Effect of singlet oxygen quencher and hydroxyl radical scavenger on antibacterial activity of Ag-GSH-Ru (Ag-GSH (10 μg/ml) + [Ru(bpy)$_3$]$^{2+}$ (0.5 μM)) under dark and light conditions against (A) *E. coli* and (B) *S. aureus*.

4.3.3. Cell integrity analysis:

LIVE/DEAD® *Bac*light™ assay and SEM analyses were performed to determine cell integrity [Salmi et al., 2008]. Only cells irradiated with light, and cells in presence of Ag-GSH-Ru under dark conditions showed green fluorescence due to uptake of membrane permeable SYTO9® dye, indicating live cells. Cells irradiated in presence of Ag-GSH-Ru showed red fluorescence due to PI®, indicating membrane damage and loss of cell integrity (Figure 4.10). SEM analysis also revealed extensive membrane damage, on irradiation of cells with visible light in presence of Ag-GSH-Ru (Figure 4.11). The results indicate that singlet oxygen and other ROS are produced during irradiation of $[Ru(bpy)_3]^{2+}$ with visible light, and damage cell membrane and lead to cell death. Earlier, Ag-GSH has also been shown to penetrate cells and interact with cell components and cause cell damage [Amato et al., 2011]. Thus, a combined effect of the two components of the system studied here, leads to effective photoinactivation of bacteria. Additionally, the combination considerably reduced the amount of both Ag-GSH and $[Ru(bpy)_3]^{2+}$ used, and time involved for complete photoinactivation.

Control **Dark** **Light**
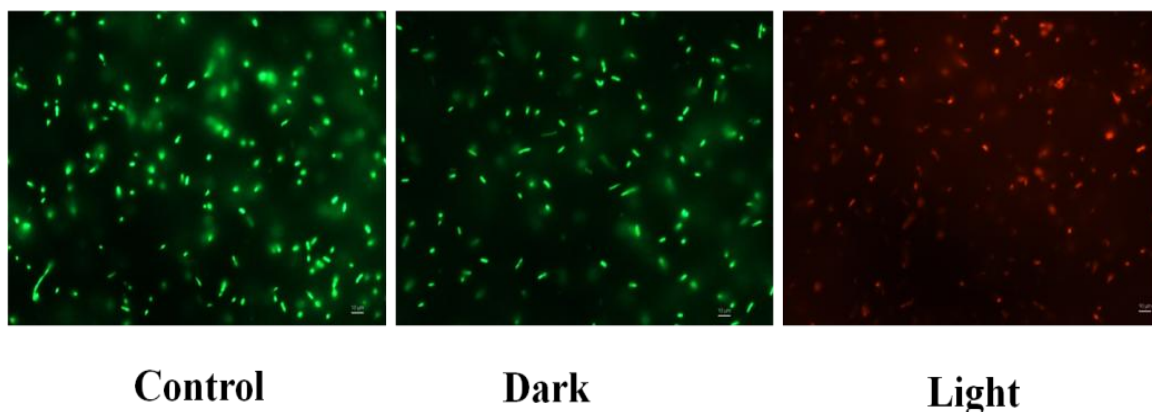
Figure 4.10: Fluorescence microscopic analysis of membrane damage by Live/Dead Baclight kit using SYTO9 and Propidium iodide against *E. coli* by Ag-GSH-Ru (Ag-GSH (10 µg/ml) + $[Ru(bpy)_3]^{2+}$ (0.5 µM)). Green Fluorescence = Live cells, Red Fluorescence = Dead Cells.
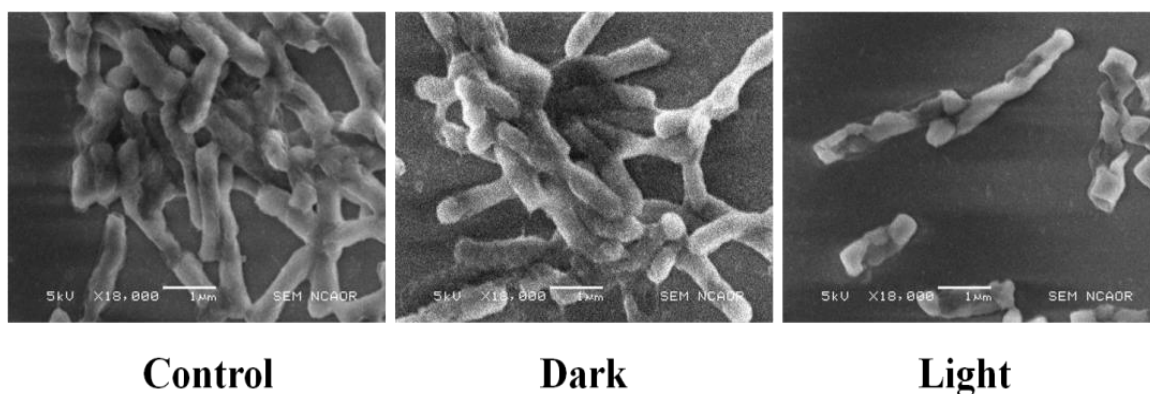
Figure 4.11: Scanning electron microscopic analysis of membrane damage against *E. coli* by Ag-GSH-Ru (Ag-GSH (10 µg/ml) + [Ru(bpy)$_3$]$^{2+}$ (0.5 µM)).

4.4. Conclusions:

It has been demonstrated that the combination of 0.5 µM of [Ru(bpy)$_3$]$^{2+}$ and 10 µg/ml of Ag-GSH was effective for killing 10^8 bacterial cells within 90 min, under visible light irradiation using LED array as light source. The Ag-GSH hybrid systems i.e., the combination of positively charged ruthenium complex and negatively charged Ag-GSH caused complete photoinactivation of both Gram-negative and Gram-positive bacteria in water. Scavenging, fluorescence microscopic and SEM results reveal that ROS generated during irradiation, cause significant cell membrane damage and lead to cell death. The effective concentration of [Ru(bpy)$_3$]$^{2+}$ for photoinactivation of bacteria was significantly reduced (~10 time for *S. aureus* and ~20 times for *E. coli*) in presence of Ag-GSH.

Chapter 5

Photo antibacterial activity of [RuCl(bpy)$_2$(ATPh)]Cl

Highlights:

1. Complete photoinactivation of bacteria by [RuCl(bpy)$_2$ATPh]$^+$.

2. Visible light emitting diode array used for photoinactivation of bacteria.

3. Visible light photoinactivation of both Gram-positive and Gram-negative bacteria.

4. Photo generated singlet oxygen and hydroxyl radicals kill bacteria.

Graphical abstract figure:
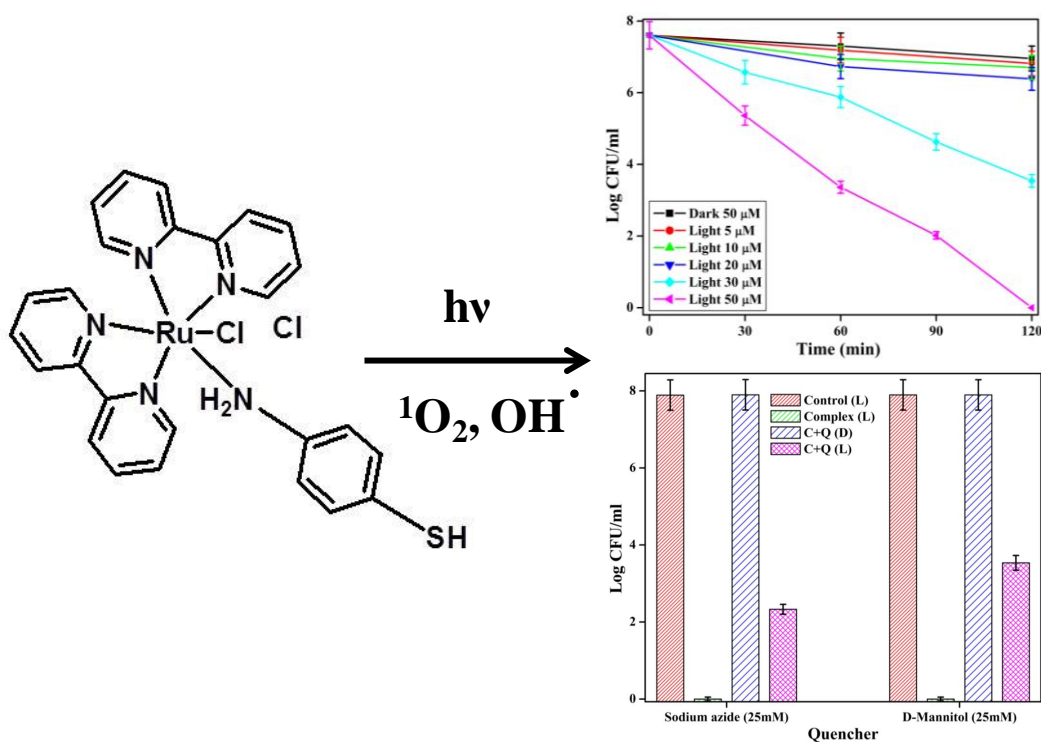
5.1. Background:

Ruthenium complexes are known as effective visible light active photosensitizers [Lei et al., 2011]. Earlier, it has been shown that $[RuCl(bpy)_2ATPh]^+$ complex (Figure 5.1) bound to gold nanoparticle could be used as fluorescent probe for NO that is important in biological systems [Diaz-Garcia et al., 2009].
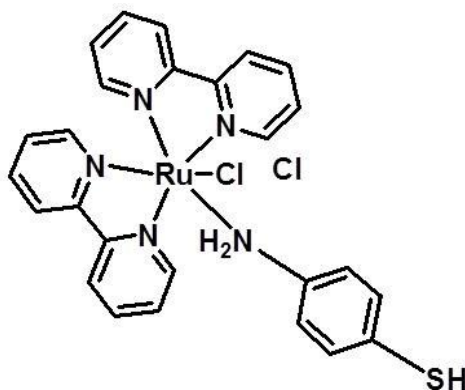
Figure 5.1: Structure of $[RuCl(bpy)_2ATPh]Cl$.

The $[RuCl(bpy)_2ATPh]^+$ complex may generate ROS on visible light irradiation. Thus, we aimed to study the photoantibacterial effects of $[RuCl(bpy)_2ATPh]^+$ in water.

5.2. Materials and methods:

5.2.1. Materials:

4-Aminothiophenol (ATPh) and L-glutathione reduced (GSH) were purchased from Sigma Aldrich, India. Other details are as mentioned in chapter 2, section 2.2.1. Double distilled water was used for all experiments.

5.2.2. Complex preparation:

Briefly for $[RuCl(bpy)_2ATPh]^+$, commercial $RuCl_3.3H_2O$ (780 mg, 2.98 mmol), bipyridine (936 mg, 6 mmol), and LiCl (840 mg, 20 mmol) were heated at reflux and stirred magnetically in reagent grade dimethylformamide (25 ml) for 8 hours. After the reaction mixture was cooled to room temperature, 100 ml of reagent grade acetone was added and the resultant solution cooled at 0°C overnight. The solution was filtered to yield a red to red-violet solution and a dark green-black microcrystalline product. The solid was washed three times with 5-ml portions of water followed by three 5-ml portions of diethyl ether, and then it was dried by suction to obtain $[Ru(bpy)_2Cl_2].2H_2O$.

[Ru(bpy)$_2$Cl$_2$].2H$_2$O and ATPh were dissolved in methanol in 1:1 molar ratio and magnetically stirred for 2 hrs. The reaction resulted in a precipitate. The precipitate was centrifuged at 5000 rpm for 5 min and supernatant discarded. The pellet obtained was washed thrice with cold distilled water. The washed pellet was then dried under vacuum at 40 ºC for about 1.5 hrs. The dried dark-violet [RuCl(bpy)$_2$ATPh]Cl (Figure 5.1) thus obtained was kept in a closed microfuge tube.

5.2.3. FTIR analysis:

FTIR spectrum of [Ru(bpy)$_2$]$^{2+}$ and [RuCl(bpy)$_2$ATPh]$^+$ has been recorded using IR Affinity-1 Shimadzu by press pellet technique. The samples were mixed with activated KBr and pellet was made.

Coordination of ATPh ligand to [Ru(bpy)$_2$]$^{2+}$ was studied by FTIR spectroscopy. Appearance of the two IR bands in the range 2500–2700 cm^{-1} indicates the presence of SH group of the attached ATPh ligand. The appearance of broad NH-stretching vibrations at 3432 cm^{-1} and NH-bending band at 1627 cm^{-1} (Figure 5.2) indicates the amino group of ATPh ligand. The band at 1319 cm^{-1}, indicates C-N stretching in primary-amine of ATPh ligand. These IR results are in accordance with earlier reports [Diaz-Garcia et al., 2009, Al Abdel Hamid et al., 2011].
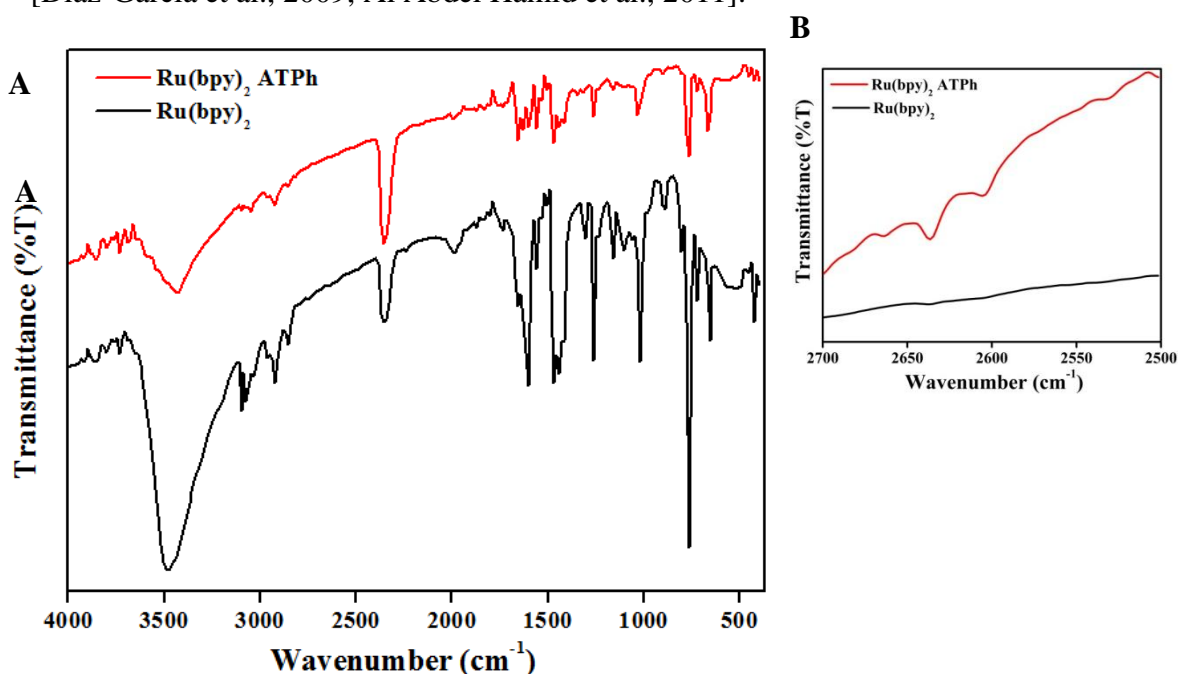
Figure 5.2: (A) Comparative FTIR spectrum of [Ru(bpy)$_2$]$^{2+}$ and [RuCl(bpy)$_2$ATPh]$^+$. (B) Inset: Enlargement of the SH bands in [RuCl(bpy)$_2$ATPh]$^+$ in the frequency range 2500–2700cm^{-1}.

5.2.4. Visible light source:

LED array was used as visible light source, purchased from Kwality Photonics, Hyderabad, India. Details are as mentioned in chapter 2 Section 2.2.3.

5.2.5. Antibacterial studies:

Antibacterial activity of $[RuCl(bpy)_2ATPh]^+$ was studied against *E. coli* (model Gram-negative) and *S. aureus* (model Gram-positive). Details are as mentioned in chapter 2, section 2.2.4.

5.2.6. Effect of singlet oxygen quencher and hydroxyl radical scavenger on bacterial inactivation:

ROS quenching experiments using sodium azide (singlet oxygen) and mannitol (hydroxyl radical) [Tavares et al., 2011, Cormick et al., 2011, Maisch et al., 2005] were performed against *E. coli*. Details are as mentioned in chapter 2, section 2.2.5.

5.2.7. Detection of singlet oxygen:

Spectrophotometric detection of singlet oxygen was done as reported, using AHP [Komagoe et al., 2001, Amat-Guerri et al., 1999, Gomes et al., 2013]. Details are as mentioned in chapter 2, section 2.2.6, using AHP as probe.

5.3. Results and discussions:

5.3.1. Photoantibacterial activity:

Visible light irradiation of 10^8 *E. coli* cells using LED array in presence of $[RuCl(bpy)_2ATPh]^+$ (50 µM) resulted in complete inactivation of *E. coli* within 120 min (Figure 5.3 (A)). On reducing the concentration of $[RuCl(bpy)_2ATPh]^+$, photoinactivation efficiency was reduced (Figure 5.3 (A)). $[RuCl(bpy)_2ATPh]^+$ had no effect on cell viability under dark conditions. Additionally, complete inactivation of 10^8 *S. aureus* cells was also observed within 90 min for 50 µM of $[RuCl(bpy)_2ATPh]^+$ on visible light irradiation (Figure 5.3 (B)). On reducing the concentration of $[RuCl(bpy)_2ATPh]^+$, photoinactivation efficiency was reduced (Figure 5.3 (B)). It is evident that Gram-positive bacteria, *S. aureus* is more susceptible towards photoinactivation in presence of $[RuCl(bpy)_2ATPh]^+$ as compared to Gram-negative bacteria, *E. coli*. Such differences in susceptibility of Gram-negative and Gram-positive bacteria have been reported earlier, and are discussed in chapters 1, 2 and 4. Thus, these

results indicate that $[RuCl(bpy)_2ATPh]^+$ has the ability to inactivate both Gram-negative and Gram-positive bacteria in water under visible light irradiation.

Effect of initial cell concentration on photoinactivation of *E. coli* by $[RuCl(bpy)_2ATPh]^+$:

Effect of initial concentration of cells on photoinactivation of *E. coli* by $[RuCl(bpy)_2ATPh]^+$ (50 μM) revealed that complete inactivation was achieved within 120 minutes when initial concentration was 10^7 or 10^8 CFU/ml cells (Figure 5.4). The time for complete inactivation was reduced to 90 minutes on decreasing the initial concentration to 10^3 CFU/ml cells (Figure 5.4). These results reveal that the complexes are promising photosensitizers for inactivation of *E. coli*.

5.3.2. Effect of singlet oxygen quencher and hydroxyl radical scavenger on photoantibacterial activity:

Photoinactivation of *E. coli* (model organism) by $[RuCl(bpy)_2ATPh]^+$ (50 μM) was carried out in presence of sodium azide (singlet oxygen quencher) and D-mannitol (hydroxyl radical scavenger) (each 25 mM) [Tavares et al., 2011, Cormick et al., 2011, Maisch et al., 2005]. Partial growth inhibition was observed for both sodium azide and D-mannitol (Figure 5.5). Furthermore, AHP was used as probe to detect singlet oxygen generation on visible light irradiation in presence of $[RuCl(bpy)_2ATPh]^+$ [Komagoe et al., 2001, Amat-Guerri et al., 1999]. There was ~10% decrease in absorbance of the probe on photolysis in presence of $[RuCl(bpy)_2ATPh]^+$ as compared to ~80% in presence of standard singlet oxygen generator, rose bengal (Figure 5.6). The above results indicate that both singlet oxygen and hydroxyl radicals are responsible for killing bacterial cells on visible light irradiation in presence of $[RuCl(bpy)_2ATPh]^+$.
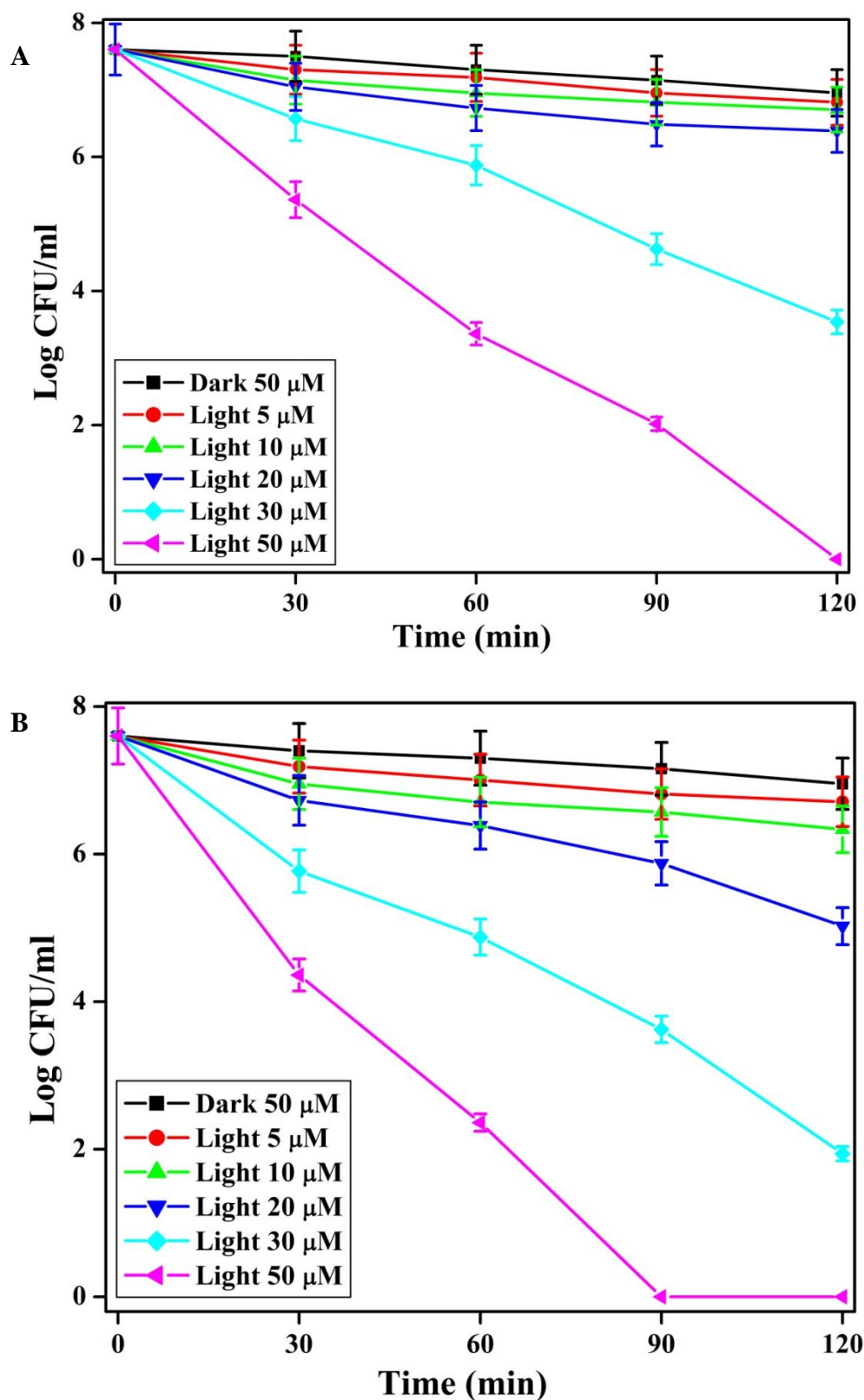
Figure 5.3: Antimicrobial activity of the [RuCl(bpy)$_2$ATPh]$^+$ against (A) *E. coli* and (B) *S. aureus* under dark and visible light irradiation.
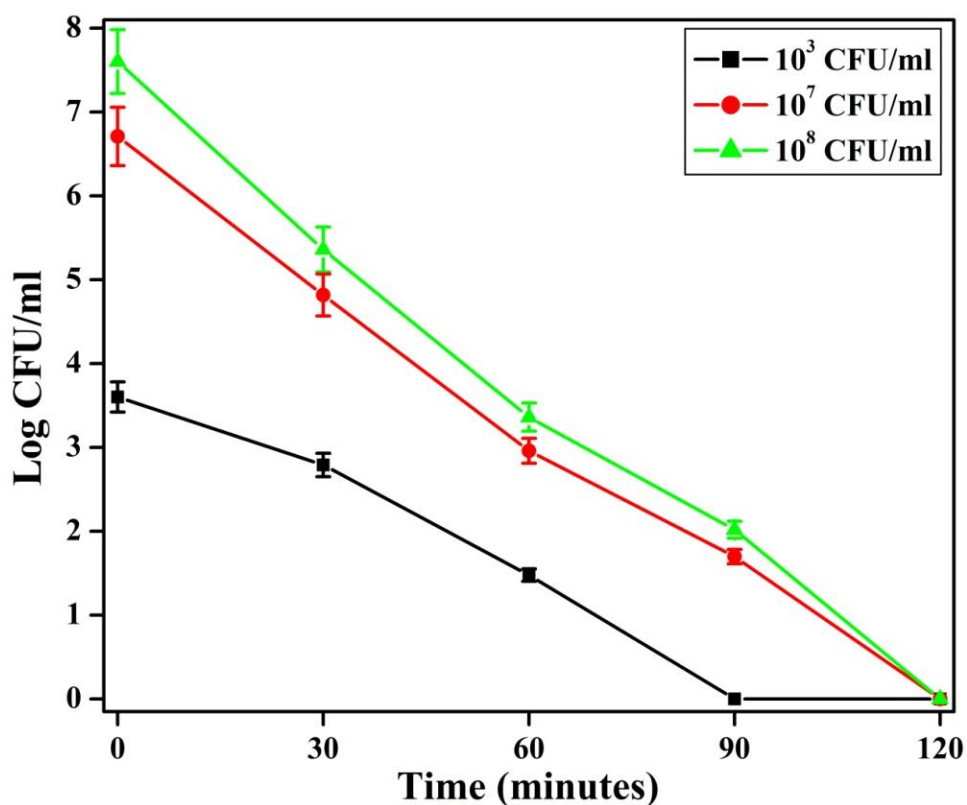
Figure 5.4: Dependence of photoinactivation of *E. coli*, in presence of [RuCl(bpy)$_2$ATPh]$^+$ on cell concentration.
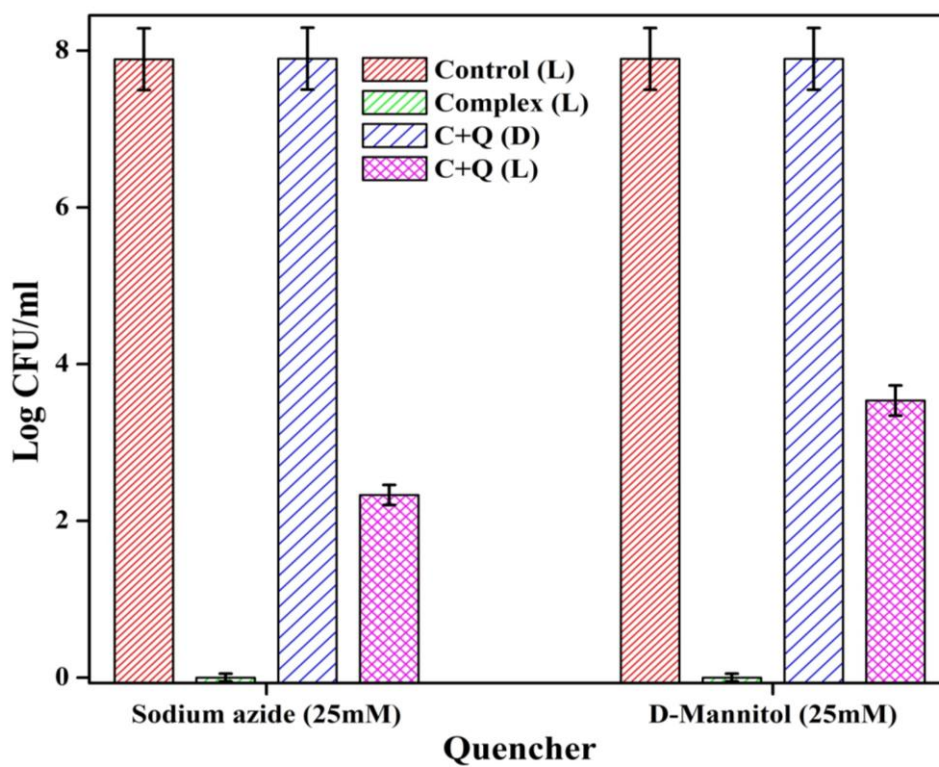
Figure 5.5: Effect of singlet oxygen quencher (Q) and hydroxyl radical scavenger (Q) on photoinactivation of *E. coli* by [RuCl(bpy)$_2$ATPh]$^+$ (C).
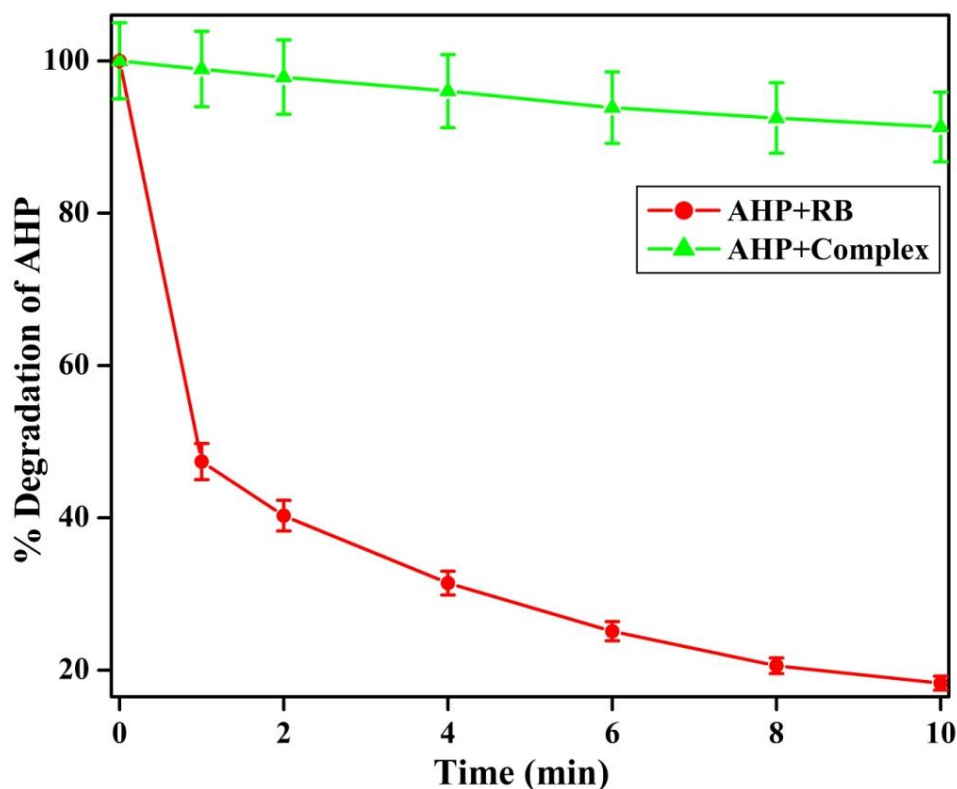
Figure 5.6: Photodegradation of singlet oxygen ($^1O_2$) scavenger, 2-amino-3-hydroxypyridine (AHP) (200 μM) in presence of [RuCl(bpy)$_2$ATPh]$^+$ and rose bengal, monitored at 318 nm.

5.4. Conclusions:

50 μM of [RuCl(bpy)$_2$ATPh]$^+$ kills 8 log *E. coli* cells within 120 min under visible light irradiation. Additionally, 50 μM of [RuCl(bpy)$_2$ATPh]$^+$ also kills 8 log *S. aureus* cells within 90 min under visible light irradiation. Scavenging experiments indicate that both singlet oxygen and hydroxyl radicals are responsible for photoinactivation of bacteria. Comparison of [RuCl(bpy)$_2$ATPh]$^+$ with other investigated ruthenium complexes reveal that the [RuCl(bpy)$_2$ATPh]$^+$ with ATPh ligand require higher dosage for complete inactivation of bacteria. The results reveal that [RuCl(bpy)$_2$ATPh]$^+$ has the ability to completely inactivate both Gram-negative and Gram-positive bacteria under visible light irradiation using LED as light source.

Chapter 6

Heterogenized methylene blue on hydrogen titanate nanosheets as effective visible light active photosensitizer for water disinfection

Highlights:

1. Complete photoinactivation of bacteria by MB+HTNS and MB+FHTNS.

2. Visible light emitting diode array used for photoinactivation of bacteria.

3. MB+FHTNS can be used efficiently for at least five cycles.

4. Photo generated singlet oxygen and hydroxyl radicals kill bacteria.

5. Promising heterogeneous photosensitizer for visible light water disinfection.

Graphical abstract figure:

_____
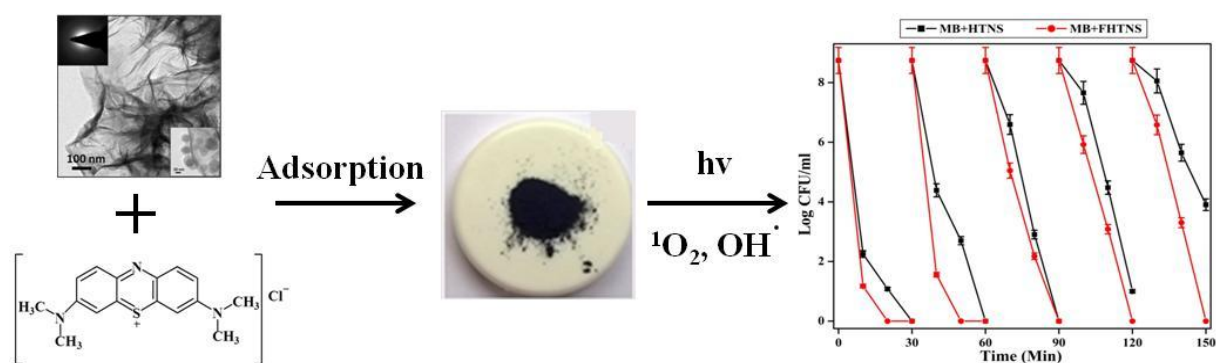
6.1. Background:

Heterogeneous photosensitizers (PSs) for water disinfection are gaining attention in recent years [Manjon et al., 2009]. Heterogeneous PSs are easy to remove from disinfected water, thereby causing minimum secondary pollution [Kuznetsova et al., 2007]. Earlier, hydrogen titanate ($H_2Ti_3O_7$) nanosheets (HTNS), has been shown to adsorb and effectively remove methylene blue (MB) from water [Hareesh et al., 2012]. HTNS was prepared by hydrothermal treatment in an autoclave [Hareesh et al., 2012]. Organic PS like MB is known to generate singlet oxygen and hydroxyl radicals on visible light irradiation, and kill bacteria [DeRosa et al., 2002]. However, the effect of heterogeneous PS, (MB is adsorbed onto HTNS) on photoinactivation of bacteria, has not been studied. HTNS can be integrated with iron to form magnetic nano sheets (FHTNS) (5 wt% of γ-Fe_2O_3). FHTNS can be easily removed from water by applying magnetic field. Earlier, as discussed in chapter 3, inorganic ruthenium based metal complexes adsorbed onto activated carbon, were shown to be efficient water disinfection agents. Here we investigated the effect of an organic PS as heterogeneous PS (MB+HTNS and MB+FHTNS) on visible light inactivation of bacteria in water.

6.2. Materials and methods:

6.2.1. Materials:

MB was purchased from Sigma Aldrich, India. Details are as mentioned in chapter 2, section 2.2.1. Double distilled water was used for all experiments. HTNS ($H_2Ti_3O_7$) and FHTNS (5 wt% of γ-Fe_2O_3) were prepared as reported earlier [Hareesh et al., 2012]. BET specific surface-area of HTNS is 402 m^2 g^{-1} and FHTNS is 300 m^2 g^{-1}. Pore volume of HTNS is 0.34 cm^3 g^{-1} and FHTNS is 0.33 cm^3 g^{-1}. Saturation magnetization of FHTNS is 3.9 emu g^{-1}.

6.2.2. Loading of MB on HTNS and FHTNS:

10 mg of either HTNS or FHTNS was added to 10 ml of MB solution (100 μM) in DW and magnetically stirred for 1 hour. Resulting suspension was centrifuged at 5,000 rpm for 5 min at 20 °C. The obtained pellet was dried overnight at 60 °C. Absorbance of supernatant was recorded to find the amount of MB remaining after the reaction. The percentage loading obtained was 3.07% for MB+HTNS and 2.77% for MB+FHTNS.

6.2.3. Visible light source:

LED array was used as visible light source, purchased from Kwality Photonics, Hyderabad, India. As mentioned in chapter 2 Section 2.2.3.

6.2.4. Antibacterial studies:

Photoinactivation of bacteria by MB+HTNS (3.07% loaded) and MB+FHTNS (2.77% loaded), was studied using PBS as medium. Details are as mentioned in chapter 2, section 2.2.4 and chapter 3, section 3.2.7.

6.2.5. Effect of singlet oxygen quencher and hydroxyl radical scavenger on photoantibacterial activity:

ROS quenching experiments using sodium azide (singlet oxygen) and mannitol (hydroxyl radical) [Tavares et al., 2011, Cormick et al., 2011, Maisch et al., 2005] were performed against *E. coli*. Details are as mentioned in chapter 2, section 2.2.5.

6.2.6. Detection of singlet oxygen:

Spectrophotometric detection of singlet oxygen was done as reported, using AHP [Komagoe et al., 2001, Amat-Guerri et al., 1999, Gomes et al., 2013]. Details are as mentioned in chapter 2, section 2.2.6, using AHP as probe.

6.2.7. Effect in simulated ground water:

Photoinactivation of bacteria by MB+HTNS (3.07% loaded) and MB+FHTNS (2.77% loaded), was also studied using SGW as medium, under optimized conditions. Details are as mentioned in chapter 2, section 2.2.4 and chapter 3, section 3.2.7.

6.3. Results and discussions:

6.3.1. Loading of MB on HTNS and FHTNS:

The UV-Vis absorption spectrophotometer results reveal that 95.799 μM MB was adsorbed onto HTNS, and 86.495 μM MB was adsorbed onto FHTNS (Figure 6.1). Importantly, these loaded samples designated as MB+HTNS (3.07% loaded) and MB+FHTNS (2.77% loaded), showed no leaching on washing indicating that these heterogenized samples can be used for photoinactivation of bacteria in water.
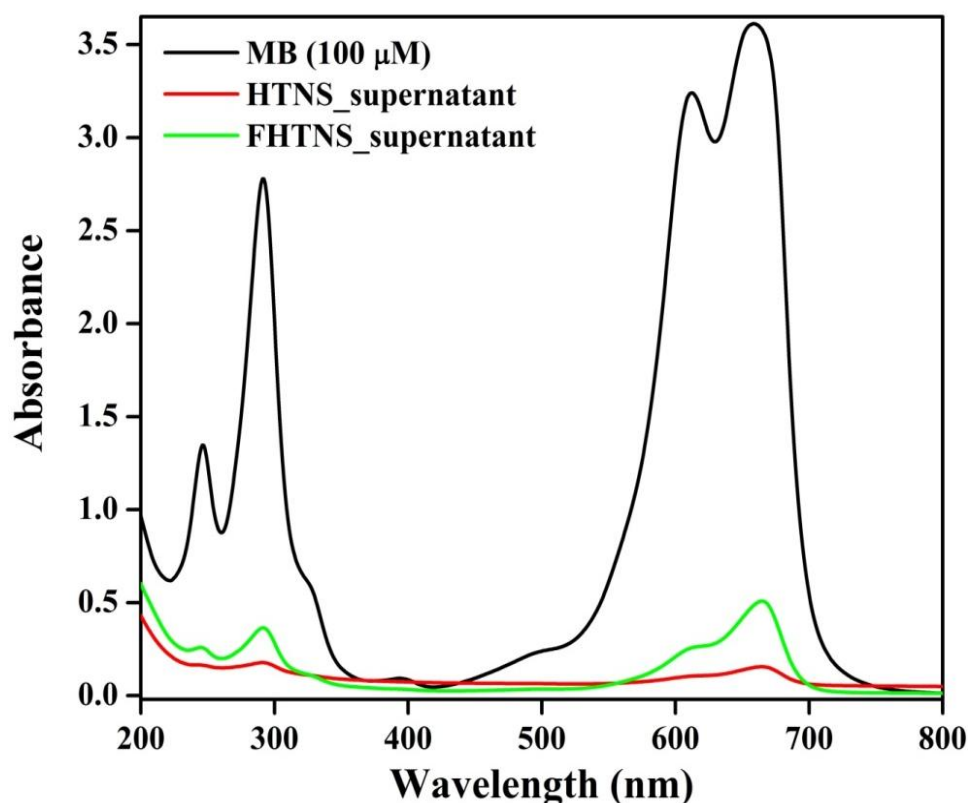
Figure 6.1: UV-Vis spectra of MB (100 μM) before and after treatment (1 hr) with HTNS (10 mg) and FHTNS (10 mg). Absorbance of supernatant was recorded after centrifugation.

6.3.2. Photoantibacterial activity:

Visible light photoantibacterial activity of MB adsorbed onto HTNS or FHTNS was studied against *E. coli* (model Gram-negative bacteria). 1 mg/ml of MB+HTNS (3.07% loaded) showed 8 log reduction of cell viability within 30 min and, 1 mg/ml of MB+FHTNS (2.77% loaded) showed 8 log reduction of cell viability within 20 min (Figure 6.2). HTNS and FHTNS alone under light and dark conditions had no effect on cell viability (Figure 6.2). Moreover, MB+HTNS, and MB+FHTNS also had no effect on cell viability under dark conditions (Figure 6.2). These results reveal that MB+HTNS, and MB+FHTNS are effective for visible light photoinactivation of bacteria. On reducing the dose of MB+HTNS, and MB+FHTNS, the ability to photoinactivate bacteria also reduced (Figure 6.3). 10 μM and 20 μM of MB alone caused 8 log reduction in cell viability within 20 min. On reducing the concentration of MB alone to 5 μM and 2.5 μM, the time required for 8 log reduction in cell viability increased to 40 min (Figure 6.4).

114
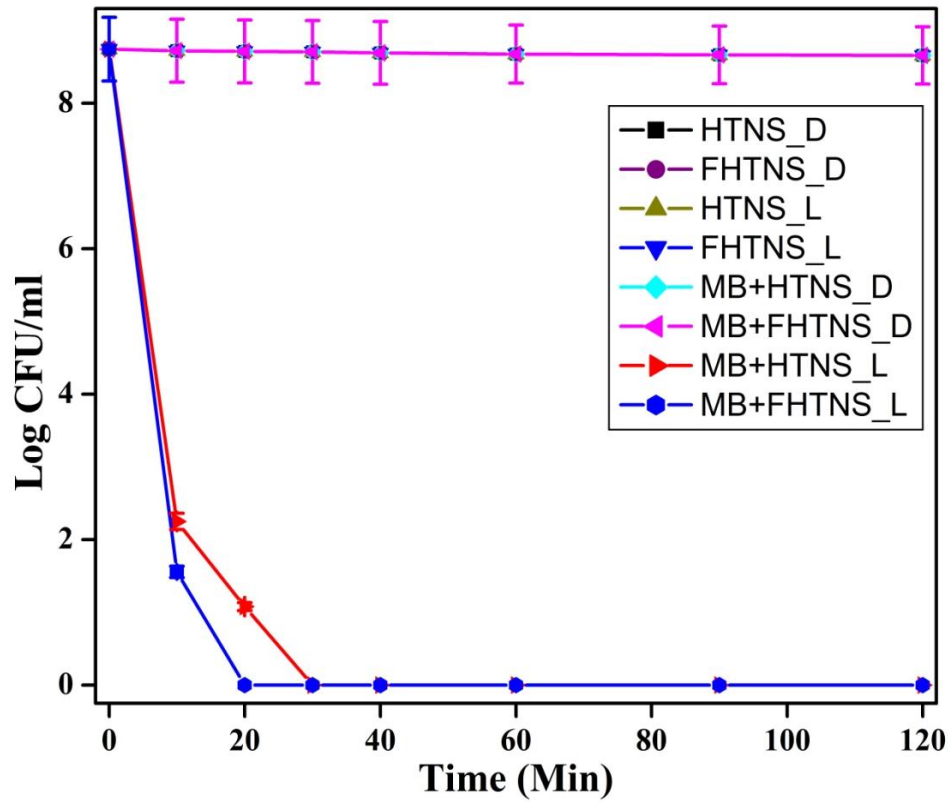
Figure 6.2: Bactericidal activity of MB+HTNS, and MB+FHTNS against *E. coli* under light and dark conditions.
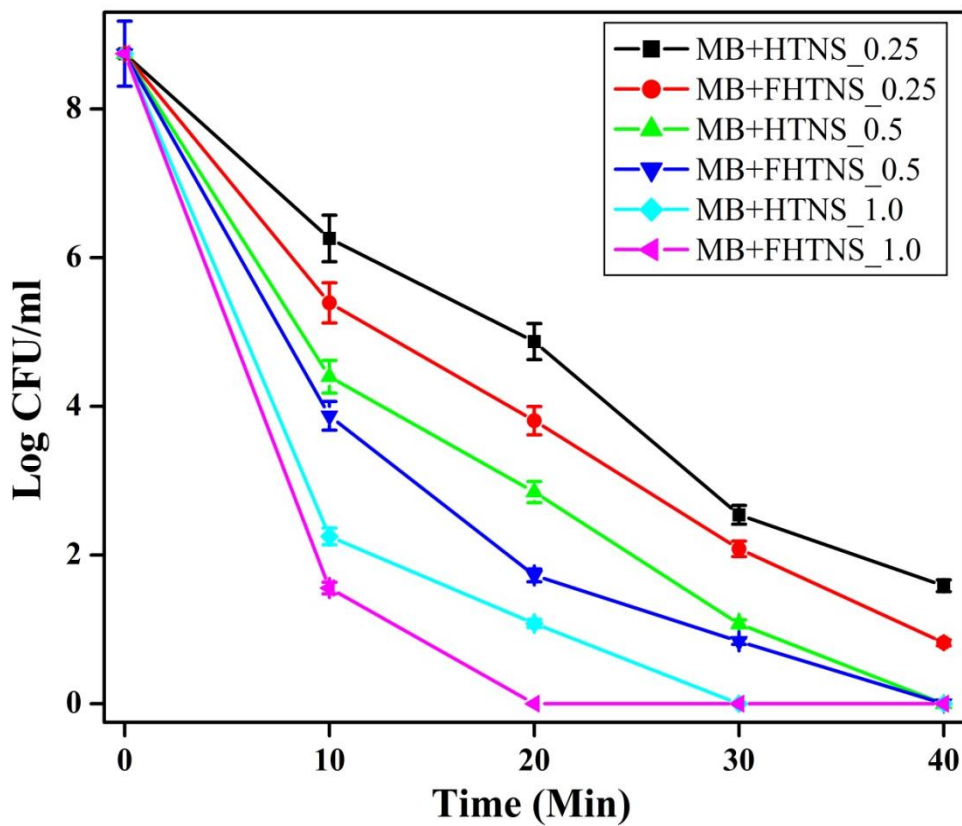
Figure 6.3: Photo bactericidal activity with respect to dose of MB+HTNS, and MB+FHTNS against *E. coli*.
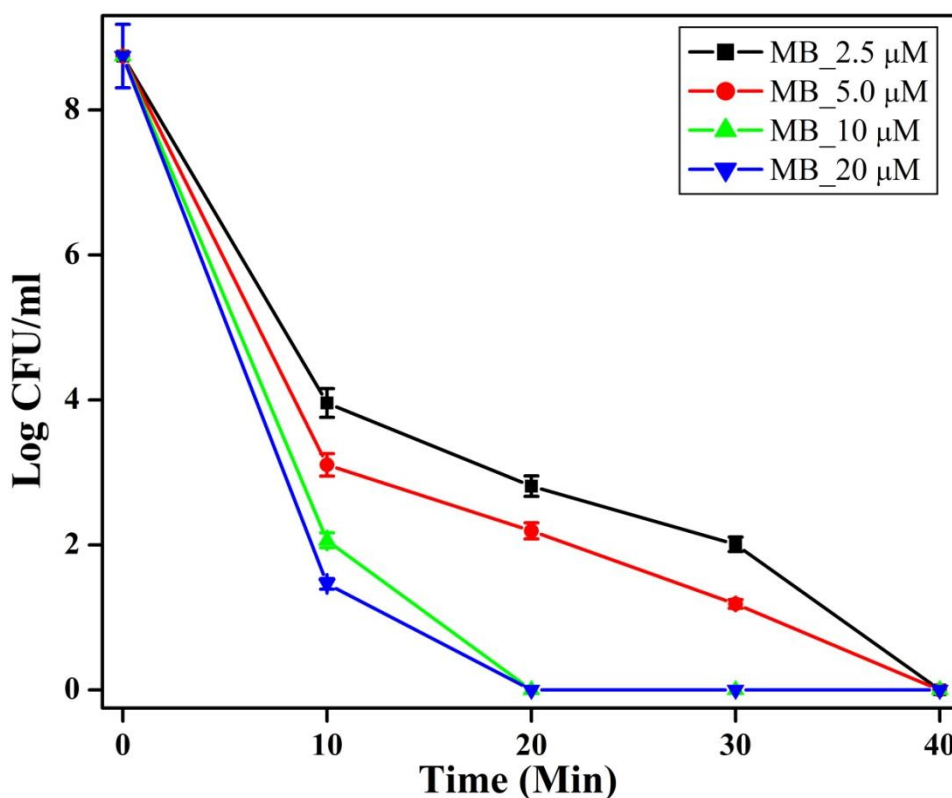
Figure 6.4: Photo bactericidal activity with respect to dose of MB against *E. coli*.

Effect of initial cell concentration on photoinactivation of *E. coli* by MB+HTNS, and MB+FHTNS:

Effect of initial concentration of cells on photoinactivation of *E. coli* by MB+HTNS (3.07% loaded) revealed that complete inactivation was achieved within 30 minutes when initial concentration was 10^7 or 10^8 CFU/ml cells (Figure 6.5 (A)). The time for complete inactivation was reduced to 20 minutes on decreasing the initial concentration to 10^3 CFU/ml cells (Figure 6.5 (A)). Similarly, effect of initial concentration of cells on photoinactivation of *E. coli* by MB+FHTNS (2.77% loaded) revealed that complete inactivation was achieved within 20 minutes when initial concentration was 10^7 or 10^8 CFU/ml cells (Figure 6.5 (B)). The time for complete inactivation was reduced to 10 minutes on decreasing the initial concentration to 10^3 CFU/ml cells (Figure 6.5 (B)).These results reveal that the complexes are promising photosensitizers for inactivation of *E. coli*.
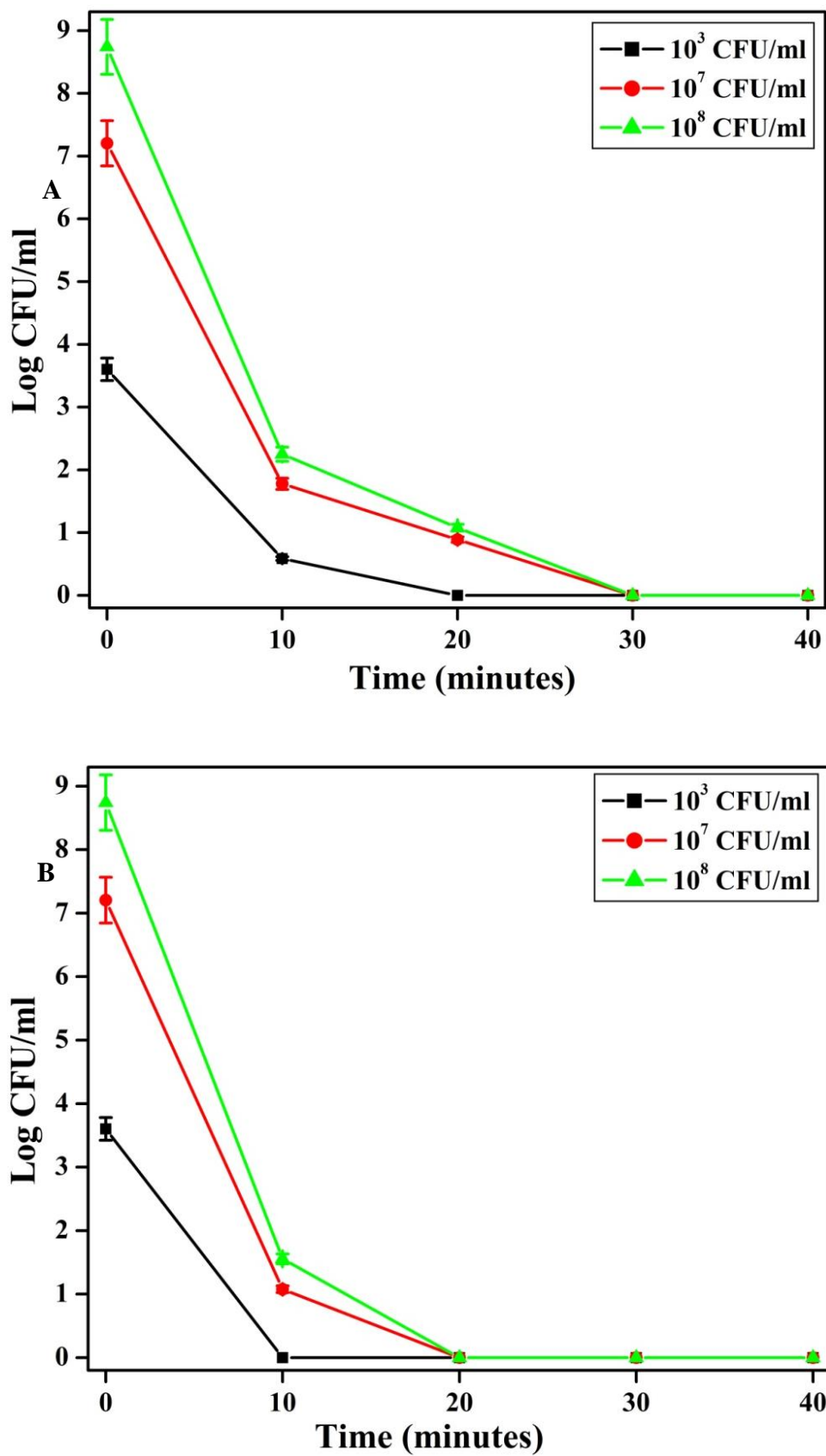
Figure 6.5: Dependence of photoinactivation of *E. coli*, in presence of (A) MB+HTNS and (B) MB+FHTNS on cell concentration.

Reuse of MB+HTNS, and MB+FHTNS:

Importantly, MB+FHTNS showed photobactericidal activity for 5 consecutive cycles (Figure 6.6) and MB+HTNS showed photobactericidal activity for 3 cycles (Figure 6.6). These results indicate that MB+HTNS, and MB+FHTNS, can be reused.
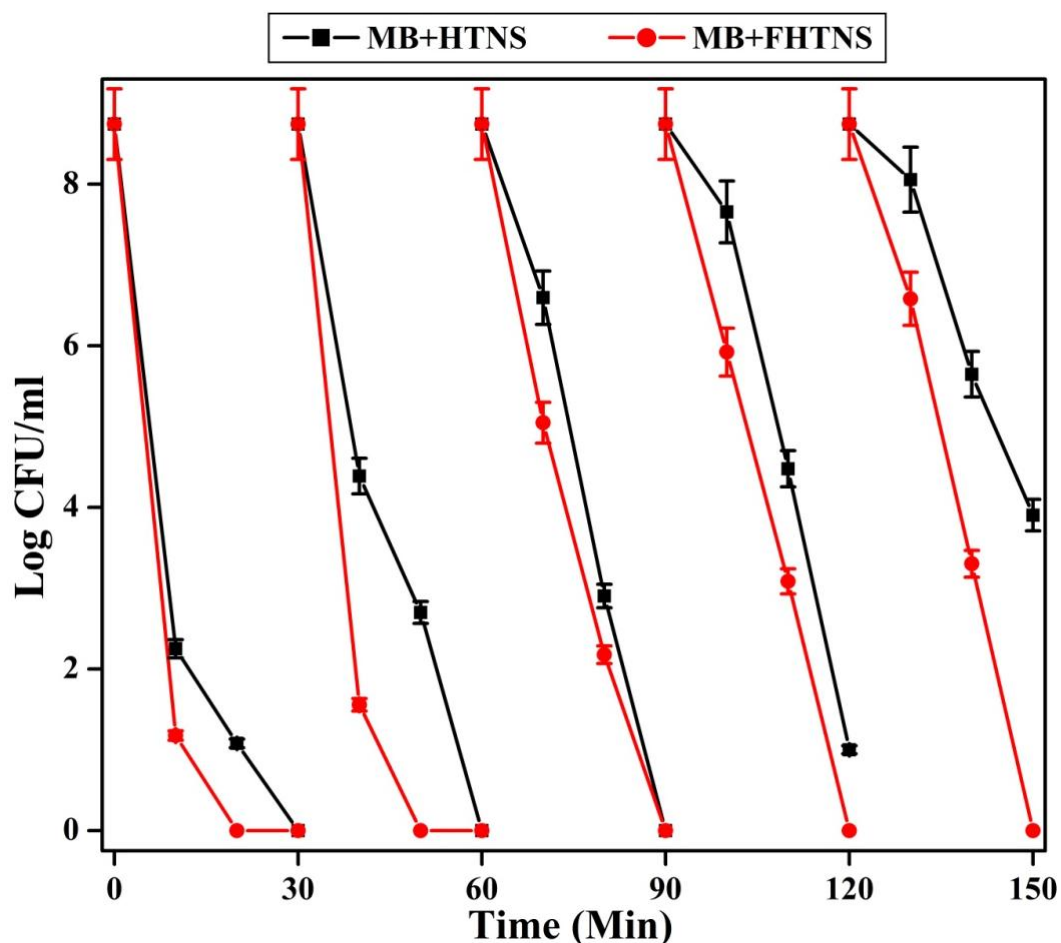
Figure 6.6: Photo-bactericidal activity of MB+HTNS, and MB+FHTNS at optimized conditions under light irradiation for 5 cycles in PBS.

6.3.3. Effect of singlet oxygen quencher and hydroxyl radical scavenger on photoantibacterial activity:

Effect of quenchers/scavengers was studied using sodium azide and mannitol [Tavares et al., 2011, Cormick et al., 2011, Maisch et al., 2005]. Cell growth was observed in presence of both the quenchers, indicating that both singlet oxygen and hydroxyl radicals are involved in the photoinactiavtion of bacteria (Figure 6.7). The scavengers alone and, scavengers in presence of MB+HTNS, and MB+FHTNS had no effect on cell viability under dark conditions. MB is a well known photosensitizer that generates both singlet oxygen and hydroxyl radicals [DeRosa et al., 2001]. Furthermore, AHP was used

as probe to detect singlet oxygen generation on visible light irradiation in presence of MB and MB+FHTNS [Komagoe et al., 2001, Amat-Guerri et al., 1999]. There was ~55% decrease in absorbance of the probe on photolysis in presence of MB+FHTNS as compared to ~90% in presence of MB alone (Figure 6.8). The above results further indicate that both singlet oxygen and hydroxyl radicals are responsible for killing bacterial cells on visible light irradiation in presence of MB+FHTNS.
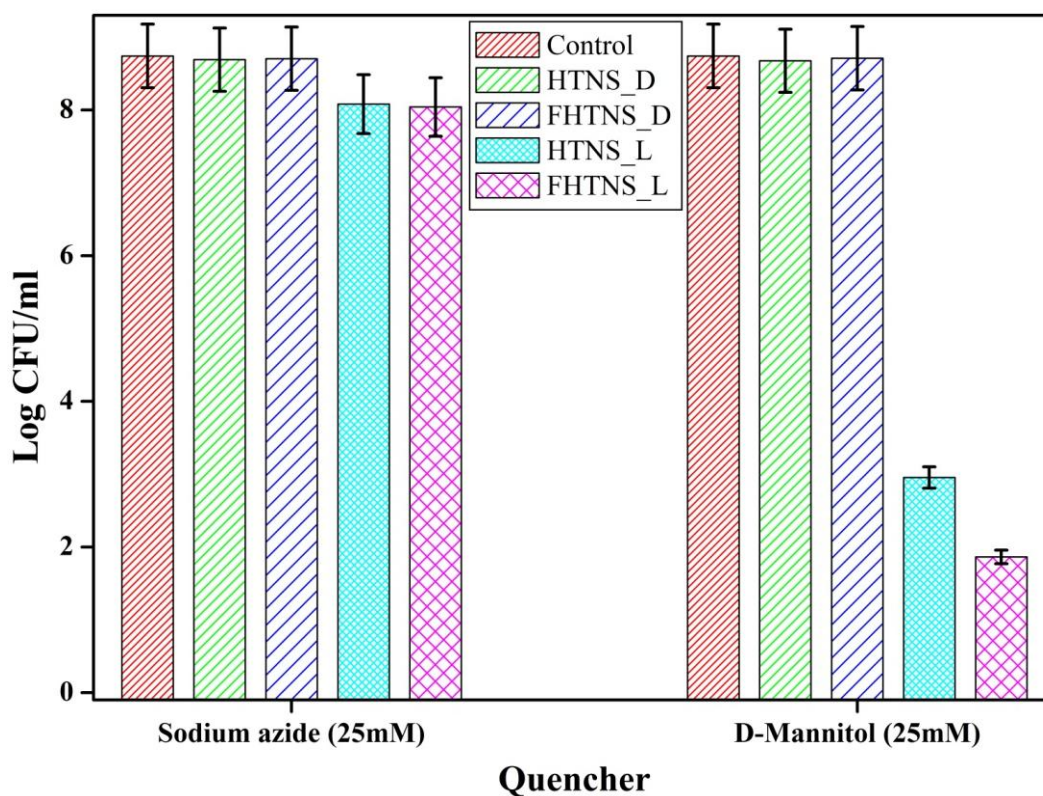
Figure 6.7: Effect of scavengers on antibacterial activity of MB+HTNS, and MB+FHTNS under dark and light conditions against *E. coli*.

6.3.4. Photoantibacterial activity in simulated ground water:

MB+HTNS (3.07% loaded) and MB+FHTNS (2.77% loaded) also caused photoinactivation when simulated ground water (SGW) was used as medium, under visible light irradiation. Complete photoinactivation of 10^8 cells was observed within 40 min, under optimized conditions (Figure 6.9). Importantly, photo bactericidal activity of MB+HTNS (3.07% loaded) and MB+FHTNS (2.77% loaded) was observed for 5 consecutive cycles, with SGW as medium under light irradiation (Figure 6.10).
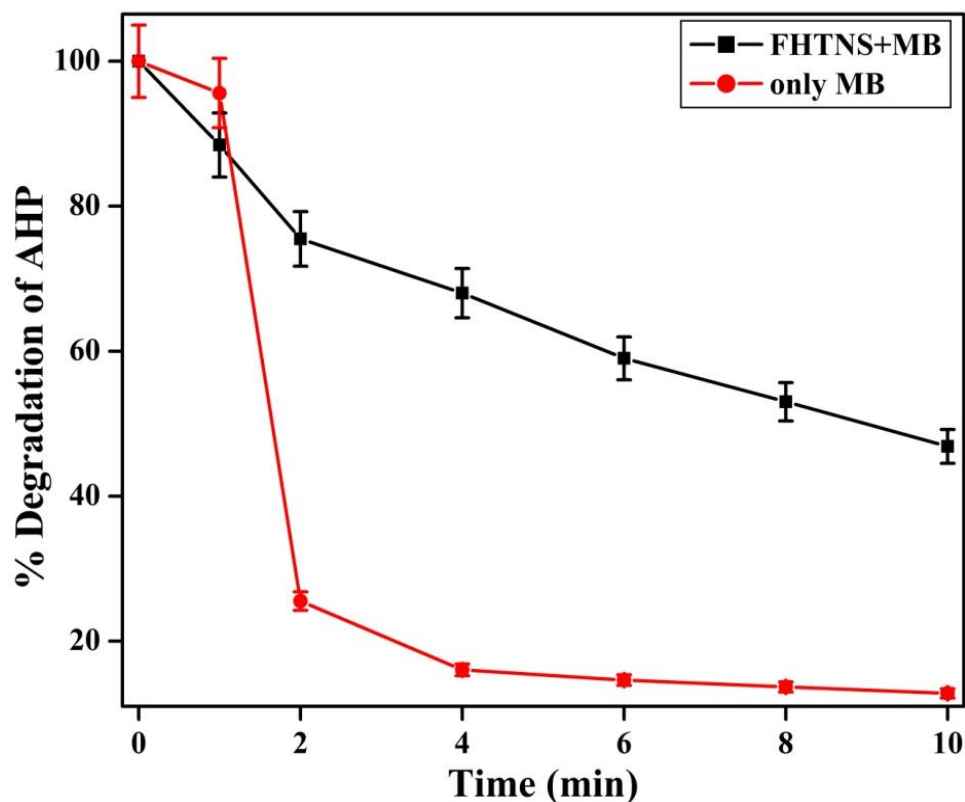
Figure 6.8: Photodegradation of singlet oxygen ($^1O_2$) scavenger, 2-amino-3-hydroxypyridine (AHP) (200 μM) in presence of MB and MB+FHTNS, monitored at 318 nm.
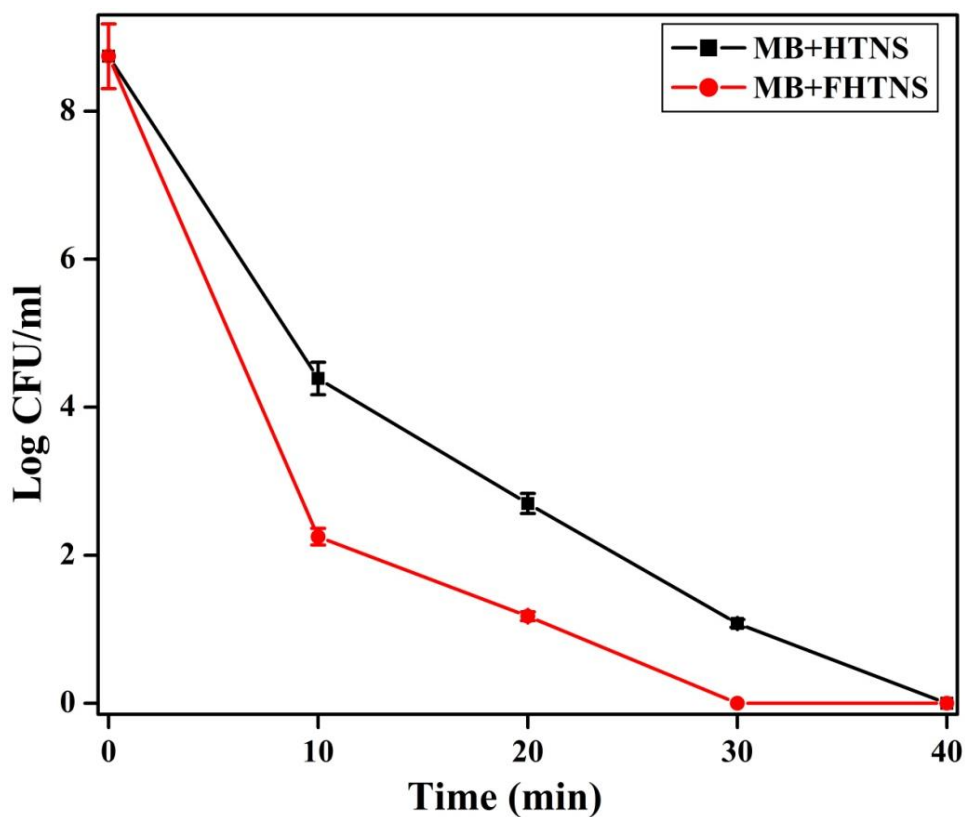
Figure 6.9: Photo-bactericidal activity of MB+HTNS, and MB+FHTNS at optimized conditions under light irradiation in SGW.
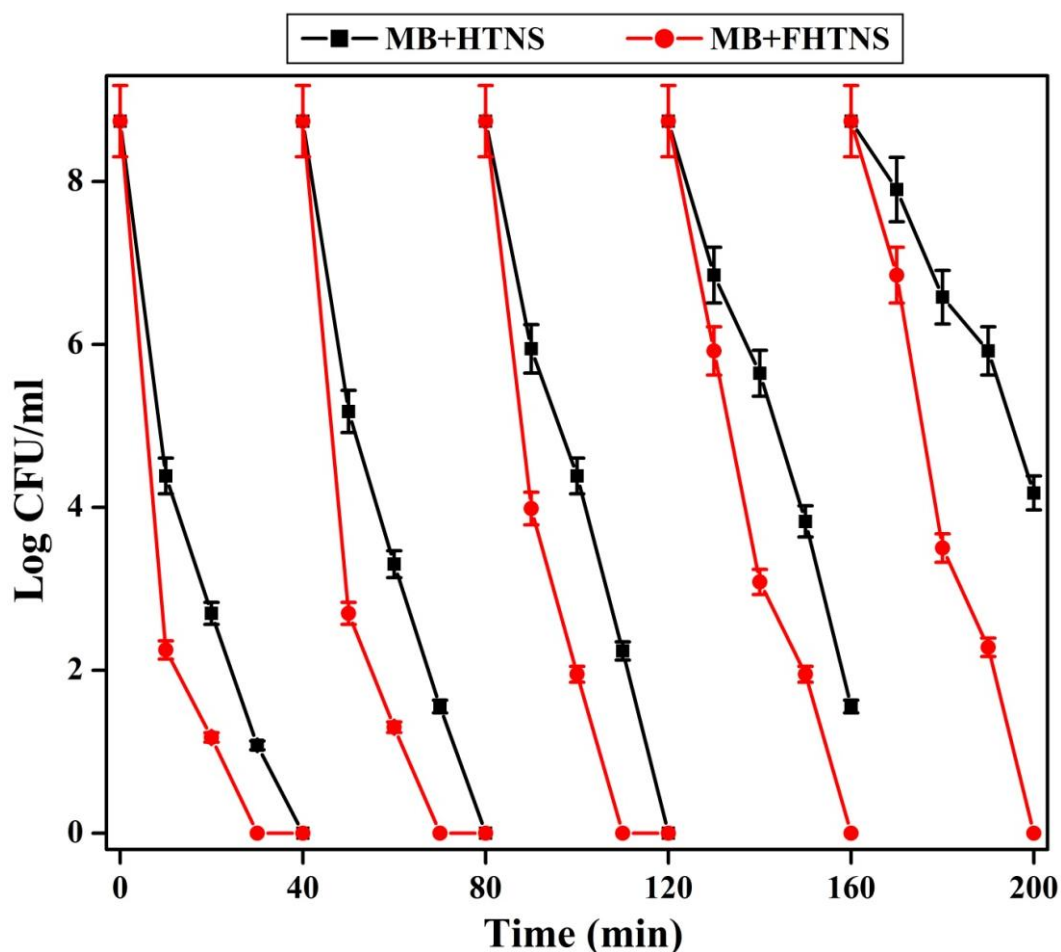
Figure 6.10: Photo-bactericidal activity of MB+HTNS, and MB+FHTNS at optimized conditions under light irradiation for 5 cycles in SGW.

6.4. Conclusions:

MB adsorbed onto HTNS and FHTNS had the ability to photoinactivate bacteria under visible light irradiation by LED array. 1 mg/ml of MB+HTNS (3.07% loaded) and 1 mg/ml of MB+FHTNS (2.77% loaded) completely inactivated 10^8 CFU/ml cells within 30 and 20 min, respectively. Importantly, MB+FHTNS was also able to cause photoinactivation for 5 continuous cycles. Scavenging results showed that both singlet oxygen and hydroxyl radicals are responsible for photoinactivation of bacteria. These results reveal that MB+FHTNS is a promising heterogeneous PS for visible light water disinfection, and can be reused.

Conclusions

Visible light active photosensitizers (PSs) are actively studied in the field of photodynamic therapy (PDT) and photodynamic antimicrobial chemotherapy (PACT). Recent studies reveal that the PSs, which act as PDT or PACT agents, can also be applied for environmental purposes like water disinfection. In the present work, the ability of ruthenium polypyridyl complexes to inactivate bacteria under homogeneous and heterogeneous conditions was studied. An introduction on the current research and existing gaps on the use of visible light active PSs for inactivation of bacteria is presented in chapter 1. In chapter 1, the basics of photochemistry of PSs, generation of reactive oxygen species (ROS) by PSs and their effect on biological systems such as cell membranes, nucleus, nucleic acids, etc. have been discussed. Additionally, different PSs and their conjugates capable of generating ROS have been reviewed. Various visible light sources such as lasers, lamps and light emitting diodes (LEDs) are also discussed in chapter 1.

Chapter 2 describes visible light water disinfection using simple ruthenium polypyridyl complexes ($[Ru(bpy)_2(phendione)]^{2+}$, $[Ru(phendione)_3]^{2+}$) and their effective removal from water using adsorbents such as activated carbon and silica. LED array was used as light source to kill both Gram-positive and Gram-negative bacteria. 10 µM of complex was required to completely inactivate *E. coli* within 120 min, 20 µM for *P. aeruginosa* within 140 min, 5 µM for *S. aureus* within 100 min, and 5 µM for *B. subtilis* within 80 min. ROS caused significant membrane damage and loss of DNA, leading to cell death. The study reveals the ability of ruthenium polypyridyl complexes for photoinactivation and their easy removal using adsorbents that are used in water treatment.

Chapter 3 illustrates the ability of ruthenium polypyridyl complexes ($[Ru(bpy)_2(phendione)]^{2+}$, $[Ru(bpy)_3]^{2+}$) adsorbed onto activated carbon to inactivate both Gram-positive and Gram-negative bacteria under visible light. The heterogeneous complexes (2.5 mg/ml of AC/complex1 comprising 23.7 µg of $[Ru(bpy)_2(phendione)]^{2+}$ (0.95% loading), and 2.5 mg/ml of AC/complex3 (0.86% loading) comprising 21.5 µg of $[Ru(bpy)_3]^{2+}$), were found to be reusable for at least five cycles in both phosphate buffer saline (PBS) and simulated ground water (SGW). For the first time the study reveals that photoactive ruthenium polypyridyl complexes adsorbed to activated carbon

as heterogeneous photosensitizers are promising water disinfection agents under visible light irradiation.

Chapter 4 explains the effect of Ag-GSH-Ru nano hybrid systems of $[Ru(bpy)_3]^{2+}$ and silver nanoparticle (Ag NP) on bacteria under visible light irradiation. Both Gram-positive and Gram-negative bacteria were completely killed the PS nano hybrid systems. The study reveals that effective concentration of PS ($[Ru(bpy)_3]^{2+}$) required for complete photoinactivation was considerably reduced (~10 times for *S. aureus* and ~20 times for *E. coli*) as compared to inactivation of bacteria by only PS.

Chapter 5 describes visible light antibacterial effect of $[RuCl(bpy)_2(ATPh)]^+$ complex. The scavenging experiments indicate that the $[RuCl(bpy)_2(ATPh)]^+$ can generate both singlet oxygen and hydroxyl radicals on visible light irradiation. $[RuCl(bpy)_2(ATPh)]^+$ has the ability to photoinactivate both Gram-positive and Gram-negative bacteria in water.

Chapter 6 illustrates the ability of organic PS methylene blue (MB) adsorbed onto hydrogen titania nano sheets (HTNS) (3.07% loading) for visible light photoinactivation of bacteria in water. Iron integrated HTNS (FHTNS) is magnetic. MB adsorbed onto FHTNS (MB+FHTNS) (02.27% loading) can be reused for at least five cycles for photoinactivation. The study reveals the potential of MB+FHTNS as potential visible light water disinfection agent, which could be magnetically removed after disinfection of water.

Based on all the results, the main findings of the present study are (i) Identification of ruthenium polypyridyl complexes as effective visible light active PSs for both Gram-positive and Gram-negative bacteria in water, (ii) removal of ruthenium based PSs using common adsorbents like AC and silica from disinfected water, (iii) conversion of homogeneous PSs to heterogeneous PSs by simple adsorption, (iv) identification of heterogeneous ruthenium polypyridyl complexes as effective visible light active PSs for water disinfection, (v) the ability of a nano hybrid systems as effective visible light active PS for visible light inactivation of bacteria, (vi) heterogenized MB for rapid water disinfection.

Future scope

The results presented in this thesis reveal the potential of visible light active photosensitizers (PSs) for inactivation of both Gram-positive and Gram-negative bacteria. In chapter 2, it is shown that ruthenium complexes viz., $[Ru(bpy)_2(phendione)]^{2+}$, $[Ru(phendione)_3]^{2+}$ at micromolar concentrations are effective PSs for visible light water disinfection. Chapter 2 also reveals that the trace amount of ruthenium complexes can be removed from water using simple adsorbents like activated carbon and silica that are used in water treatment. The present study indicates that ruthenium complexes are promising PS candidates for water disinfection. The photoinactivation of other bacterial species by ruthenium complexes can be studied. Recently magnetic adsorbent has been used in water treatment. The removal of ruthenium complexes by magnetic adsorbents may be attempted for easy removal of PS by application of magnetic field. Heteronuclear polypyridyl ruthenium complexes have also been reported and their photoantibacterial activities could be studied.

One major finding of this thesis is that the photoactive ruthenium polypyridyl complexes ($[Ru(bpy)_2(phendione)]^{2+}$, $[Ru(bpy)_3]^{2+}$) adsorbed onto activated carbon as heterogeneous PSs, can be used as effective water disinfection agents under visible light irradiation (chapter 3) and these complexes were reusable. The photodynamic inactivation of other microbes in water by these heterogenized complexes can be studied for household point of use (POU) application.

Chapter 4 reveals that Ag-GSH-Ru nano hybrid systems of $[Ru(bpy)_3]^{2+}$ and Ag NP significantly reduces the effective concentration of PS ($[Ru(bpy)_3]^{2+}$) required for complete photoinactivation (~10 times for *S. aureus* and ~20 times for *E. coli*) as compared to photoinactivation of bacteria by only PS. The potential of the nano hybrid systems as visible light PACT agent for selective killing of bacteria in presence of other cell lines may be evaluated.

Chapter 5 reveals the ability of $[RuCl(bpy)_2(ATPh)]^+$ to photoinactivate both Gram-positive and Gram-negative bacteria in water. The thiol group of ATPh provides opportunity to functionalize the ruthenium complex to thiol binding NPs. Thus, additional research could be carried out to form a nano hybrid between negatively

charged Ag-GSH and positively charged $[RuCl(bpy)_2(ATPh)]^+$. The effect of the nano hybrid on visible light inactivation on bacteria will be studied.

Chapter 6 reveals the ability of MB adsorbed onto FHTNS as heterogeneous PS for complete photoinactivation of bacteria in water. The heterogeneous PS was reusable. The photoinactivation ability of the heterogeneous PSs can be studied to develop POU water treatment for house hold applications.

All the chapters implied the use of LED array as visible light source for photoinactivation of bacteria. These results highlight the potential for future research on the design and development of LED arrays for photoinactivation of microbes.

References

1. Abdel-Shafi, A. A., Worrall, D. R., Ershov, A. Y., Photosensitized generation of singlet oxygen from ruthenium(II) and osmium(II) bipyridyl complexes, Dalton Transactions, 1 (2004) 30–36.

2. Acher, A. J., Juven, B. J., Destruction of coliforms in water and sewage water by dye-sensitized photooxidation, Applied Environmental Microbiology, 33 (1977) 1019–1022.

3. Ahmed, M. N., Ram, R. N., Removal of basic dye from waste-water using silica as adsorbent, Environmental Pollution, 77 (1992) 79–86.

4. Aksu, Z., Calik, A., Adsorption of iron(III)-cyanide complex ions to granular activated carbon, Journal of Environmental Science and Health. Part A, Toxic/Hazardous Substances & Environmental Engineering, 34 (1999) 2087–2103.

5. Al Abdel Hamid, A. A., Al-Khateeb, M., Tahat, Z. A., Qudah, M., Obeidat, S. M., Rawashdeh, A. M., A selective chemosensor for mercuric ions based on 4-aminothiophenol-ruthenium (II) bis (bipyridine) complex, International Journal of Inorganic Chemistry, 2011 (2011).

6. Ali, H., van Lier, J. E., Metal complexes as photo- and radiosensitizers, Chemical Reviews, 99 (1999) 2379–2450.

7. Amat-Guerri, F., Pajares, A., Gianotti, J., Haggi, E., Stettler, G., Bertolotti, S., Miskoski, S., Garcia, N. A., Singlet molecular oxygen-mediated photooxidation of 2-substituted 3-hydroxypyridines, Journal of Photochemistry and Photobiology A, 126 (1999) 59–64.

8. Amato, E., Diaz-Fernandez, Y. A., Taglietti, A., Pallavicini, P., Pasotti, L., Cucca, L., Milanese, C., Grisoli, P., Dacarro, C., Fernandez-Hechavarria, J. M., Necchi, V., Synthesis, characterization and antibacterial activity against gram-positive and gram-negative bacteria of biomimetically coated silver nanoparticles, Langmuir, 27 (2011) 9165–9173.

9. Arrojado, C., Pereira, C., Tome, J. P. C., Faustino, M. A. F., Neves, M. G. P. M. S., Tome, A. C., Cavaleiro, J. A. S., Cunha, A., Calado, R., Gomes, N. C. M., Almeida, A., Applicability of photodynamic antimicrobial chemotherapy as an alternative to inactivate fish pathogenic bacteria in aquaculture systems, Photochemical & Photobiological Sciences, 10 (2011) 1691–1700.

10. Atkins, P., de Paula, J., Elements of physical chemistry, Fifth edition, Oxford University Press, USA, 2013, 425–430.

11. Bachowski, G. J., Korytowski, W., Girotti, A. W., Characterization of lipid hydroperoxides generated by photodynamic treatment of leukemia cells, Lipids, 29 (1994) 449–459.

12. Bachowski, G. J., Pintar, T. J., Girotti, A. W., Photosensitized lipid peroxidation and enzyme inactivation by membrane-bound merocyanine 540: reaction mechanisms in the absence and presence of ascorbate, Photochemistry and Photobiology, 53 (1991) 481–491.

13. Badawy, A. M. El, Silva, R. G., Morris, B., Scheckel, K. G., Suidan, M. T., Tolaymat, T. M., Surface charge-dependent toxicity of silver nanoparticles, Environmental Science & Technology, 45 (2011) 283–287.

14. Balzani, V., Credi, A., Venturi, M., Photochemistry and photophysics of coordination compounds: An extended view, Coordination Chemistry Reviews, 171 (1998) 3–16.

15. Balzani, V., Juris, A., Venturi, M., Luminescent and redox-active polynuclear transition metal complexes, Chemical Reviews, 96 (1996) 759–833.

16. Balzani. V., Juris. A., Photochemistry and photophysics of Ru(II)-polypyridine complexes in the Bologna group. From early studies to recent developments, Coordination Chemistry Reviews, 211 (2001) 97–115.

17. Bansal, R. K., Organic reaction mechanisms, Tata McGraw-Hill Education, third edition, 1998.

18. Barazzouk, S., Kamat, P. V., Hotchandani, S., Photoinduced electron transfer between chlorophyll a and gold nanoparticles, The Journal of Physical Chemistry B, 109 (2004) 716–723.

19. Bensasson, R. V., Advanced course in photobiology and photomedicine, Sarna, T., Ed. Jagiellonian University: Krakow, U.J. Press, 1999.

20. Bilski, P., Motten, A. G., Bilska, M., Chignell, C. F., The photooxidation of diethylhydroxylamine by rose bengal in micellar and nonmicellar aqueous solutions, Photochemistry and Photobiology, 58 (1993) 11–18.

21. Blanco, J., Malato, S., Fernandez-Ibanez, P., Alarcon, D., Gernjak, W., Maldonado, M. I., Review of feasible solar energy applications to water processes, Renewable and Sustainable Energy Reviews, 13 (2009) 1437–1445.

22. Boyle, M., Sichel, C., Fernandez-Ibanez, P., Arias-Quiroz, G. B., Iriarte-Puna, M., Mercado, A., Ubomba-Jaswa, E., McGuigan, K. G., Bactericidal effect of solar water disinfection under real sunlight conditions, Applied and Environmental Microbiology, 74 (2008) 2997–3001.

23. Buchko, G. W., Cadet, J., Ravanat, J. L., Labataille, P., Isolation and characterization of a new product produced by ionizing irradiation and type I photosensitization of 2′-deoxyguanosine in oxygen-saturated aqueous solution: (2S)-2,5′-anhydro-1-(2′-deoxy-beta-d-erythro-pentofuranosyl)-5-guanidinylidene-2-hydroxy-4-oxoimidazolidine, International Journal of Radiation Biology, 63 (1993) 669–676.

24. Buchko, G. W., Wagner, J. R., Cadet, J., Raoul, S., Weinfeld, M., Methylene blue-mediated photooxidation of 7,8-dihydro-8-oxo-2′-deoxyguanosine, Biochimica et Biophysica Acta, 1263 (1995) 17–24.

25. Busscher, H. J., Dijkstra, R. J. B., Engels, E., Langworthy, D. E., Collias, D. I., Bjorkquist, D. W., Mitchell, M. D., van der Mei, H. C., Removal of two waterborne pathogenic bacterial strains by activated carbon particles prior to and after charge modification, Environmental Science & Technology, 40 (2006) 6799–6804.

26. Cahan, R., Friman, H., Nitzan, Y., Antibacterial activity of Cyt1Aa from *Bacillus thuringiensis* subsp. *israelensis*, Microbiology, 154 (2008) 3529–3536.

27. Calin, M. A., Parasca, S. V., Light sources for photodynamic inactivation of bacteria, Lasers in Medical Science, 24 (2009) 453–460.

28. Caminos, D. A., Spesia, M. B., Pons, P., Durantini, E. N., Mechanisms of *Escherichia coli* photodynamic inactivation by an amphiphilic tricationic porphyrin and 5,10,15,20-tetra(4-N,N,N-trimethylammoniumphenyl) porphyrin, Photochemical & Photobiological Sciences, 7 (2008) 1071–1078.

29. Campagna, S., Serroni, S., Bodige, S., MacDonnell, F. M., Absorption spectra, photophysical properties, and redox behavior of stereochemically pure dendritic ruthenium(II) tetramers and related dinuclear and mononuclear complexes, Inorganic Chemistry, 38 (1999) 692–701.

30. Carlson, B., Phelan, G. D., Kaminsky, W., Dalton, L., Jiang, X., Liu, S., Jen, A. K.-Y., Divalent osmium complexes: synthesis, characterization, strong red phosphorescence, and electrophosphorescence, Journal of American Chemical Society, 124 (2002) 14162–14172.

31. Castano, A. P., Demidova, T. N., Hamblin, M. R., Mechanisms in photodynamic therapy: part one—photosensitizers, photochemistry and cellular localization, Photodiagnosis and Photodynamic Therapy, 1 (2004) 279–293.

32. Chaidez, C., Gerba, C. P., Comparison of the microbiologic quality of point-of-use (POU)-treated water and tap water, International Journal of Environmental Health Research, 14 (2004) 253−260.

33. Chatterjee, D. K., Fong, L. S., Zhang, Y., Nanoparticles in photodynamic therapy: an emerging paradigm, Advanced Drug Delivery Reviews, 60 (2008) 1627−1637.

34. Chen, G., Dussert, B. W., Suffet, I. H., Evaluation of granular activated carbons for removal of methylisoborneol to below odor threshold concentration in drinking water, Water Research, 31 (1997) 1155–1163.

35. Chen, J., Jarvi, M., Lo, P. C., Stefflova, K., Wilson, B. C., Zheng, G., Using the singlet oxygen scavenging property of carotenoid in photodynamic molecular beacons to minimize photodamage to non-targeted cells, Photochemical & Photobiological Sciences, 6 (2007) 1311−1317.

36. Chen, Y., Lu, A., Li, Y., Yip, H. Y., An, T., Li, G., Jin, P., Wong, P.-K., Photocatalytic inactivation of *Escherichia coli* by natural sphalerite suspension: Effect of spectrum, wavelength and intensity of visible light, Chemosphere, 84 (2011) 1276–1281.

37. Chouai, A., Wicke, S. E, Turro, C., Bacsa, J., Dunbar, K. R., Wang, D., Thummel, R. P., Ruthenium(II) complexes of 1,12-Diazaperylene and their interactions with DNA, Inorganic Chemistry, 44 (2005) 5996–6003.

38. Ciesla, P., Kocot, P., Mytych, P., Stasicka, Z., Homogeneous photocatalysis by transition metal complexes in the environment, Journal of Molecular Catalysis A: Chemical 224 (2004) 17–33.

39. Coetser, S. E., Heath, R. G. M., Ndombe, N., Diffuse pollution associated with the mining sectors in South Africa: a first-order assessment, Water Science and Technology, 55 (2007) 9–16.

40. Concepcion, J. J., Brennaman, M. K., Deyton, J. R., Lebedeva, N. V., Forbes, M. D. E., J. Papanikolas, M., Meyer, T. J., Excited-state quenching by proton-coupled electron transfer, Journal of the American Chemical Society, 129 (2007) 6968–6969.

41. Cooper, A. T., Goswami, D. Y., Evaluation of methylene blue and rose bengal for dye sensitized solar water treatment, Journal of Solar Energy Engineering, 124 (2002) 305–310.

42. Cormick, M. P., Quiroga, E. D., Bertolotti, S. G., Alvarez, M. G., Durantini, E. N., Mechanistic insight of the photodynamic effect induced by tri- and tetra-cationic porphyrins on *Candida albicans* cells, Photochemical & Photobiological Sciences, 10 (2011) 1556–1561.

43. Coutier, S., Bezdetnaya, L., Marchal, S., Melnikova, V., Belitchenko, I., Merlin, J. L., Guillemin, F., Foscan®(mTHPC) photosensitized macrophage activation: enhancement of phagocytosis, nitric oxide release and tumour necrosis factor-alpha-mediated cytolytic activity, British Journal of Cancer, 81 (1999) 37–42.

44. Dahl, T. A., Midden, W. R., Neckers, D. C., Comparison of photodynamic action by rose bengal in gram-positive and gram-negative bacteria, Photochemistry and Photobiology, 48 (1988) 607–612.

45. Dash, B. P., Chaudhari, S., Electrochemical denitrificaton of simulated ground water, Water Research, 39 (2005) 4065–4072.

46. Daud, W. M. A. W., Houshamnd, A. H., Textural characteristics, surface chemistry and oxidation of activated carbon, Journal of Natural Gas Chemistry, 19 (2010) 267–279.

47. Demas, J. N., DeGraff, B. A., Design and applications of highly luminescent transition metal complexes, Analytical Chemistry, 63 (1991) 829 A–837A.

48. Demidova, T. N., Hamblin, M. R., Effect of cell-photosensitizer binding and cell density on microbial photoinactivation, Antimicrobial Agents and Chemotherapy, 49 (2005) 2329–2335.

49. Demidova, T. N., Hamblin, M. R., Photodynamic therapy targeted to pathogens, International Journal of Immunopathology and Pharmacology, 17 (2004) 245–254.

50. DeRosa, M. C., Crutchley, R. J., Photosensitized singlet oxygen and its applications, Coordination Chemistry Reviews, 233-234 (2002) 351–371.

51. Detty, M. R., Gibson, S. L., Wagner, S. J., Current clinical and preclinical photosensitizers for use in photodynamic therapy, Journal of Medicinal Chemistry, 47 (2004) 3897–3915.

52. Diaz-Garcia, A. M., Fernandez-Oliva, M., Ortiz, M., Cao, R., Interaction of nitric oxide with gold nanoparticles capped with a ruthenium(II) complex, Dalton Transactions, 38 (2009) 7870–7872.

53. Dror-Ehre, A., Mamane, H., Belenkova, T., Markovich, G., Adin, A., Silver nanoparticle- *E. coli* colloidal interaction in water and effect on *E. coli* survival, Journal of Colloid and Interface Science, 339 (2009) 521–526.

54. Eckhardt, S., Brunetto, P. S., Gagnon, J., Priebe, M., Giese, B., Fromm, K. M., Nanobio silver: its interactions with peptides and bacteria, and its uses in medicine, Chemical Reviews, 113 (2013) 4708–4754.

55. Egger, S., Lehmann, R. P., Height, M. J., Loessner, M. J., Schuppler, M., Antimicrobial properties of a novel silver-silica nanocomposite material, Applied and Environmental Microbiology, 75 (2009) 2973–2976.

56. Elumalai, P., Atkins, P., de Paula, J., Atikns' physical chemistry, Oxford University Press, USA, 2002.

57. Feng, Q. L., Wu, J., Chen, G. Q., Cui, F. Z., Kim, T. N., Kim, J. O., A mechanistic study of the antibacterial effect of silver ions on *Escherichia coli* and *Staphylococcus aureus*, Journal of Biomedical Materials Research, 52 (2000) 662–668.

58. Fewtrell, L., Kaufmann, R. B., Kay, D., Enanoria, W., Haller, L., Colford Jr., J. M., Water, sanitation, and hygiene interventions to reduce diarrhoea in less developed countries: a systematic review and meta-analysis, The Lancet Infectious Diseases, 5 (2005) 42–52.

59. Filho, N. L. D., do Carmo, D. R., Adsorption at silica, alumina, and related surfaces, Encyclopedia of Surface and Colloid Science, volume 2, second edition, P. Somasundaran, 2006, 209–228.

60. Francis, P. D., The use of ultraviolet light and ozone to remove dissolved organic contaminants in ultra pure water. Report, M 2221, Electricity Council Research Centre, Capenhurst: Chester, England, 1988.

61. Franzen, S., Folmer, J. C. W., Glomm, W. R., O'Neal, R., Optical properties of dye molecules adsorbed on single gold and silver nanoparticles, The Journal of Physical Chemistry A, 106 (2002) 6533–6540.

62. Gao, F. G., Bard, A. J., Solid-state organic light-emitting diodes based on tris(2,2'-bipyridine)ruthenium(II) complexes, Journal of the American Chemical Society, 122 (2000) 7426–7427.

63. Gao, F., Chao, H., Zhou, F., Yuan, Y.-X., Peng, B., Ji, L.-N., DNA interactions of a functionalized ruthenium(II) mixed-polypyridyl complex $[Ru(bpy)_2ppd]^{2+}$, Journal of Inorganic Biochemistry, 100 (2006) 1487–1494.

64. Garcìa-Fresnadillo, D., Georgiadou, Y., Orellana, G., Braun, A. M., Oliveros, E., Singlet-oxygen ($^1\Delta_g$) production by ruthenium(II) complexes containing polyazaheterocyclic ligands in methanol and in water, Helvetica Chimica Acta, 79 (1996) 1222–1238.

65. Gariépy, J., The use of Shiga-like toxin 1 in cancer therapy, Critical Reviews in Oncology/Hematology, 39 (2001) 99−106.

66. Gill, M. R., Thomas, J. A., Ruthenium(II) polypyridyl complexes and DNA—from structural probes to cellular imaging and therapeutics, Chemical Society Reviews, 41 (2012) 3179–3192.

67. Girotti, A. W., Lipid hydroperoxide generation, turnover, and effector action in biological systems, Journal of Lipid Research, 39 (1998) 1529–1542.

68. Girotti, A. W., Mechanisms of lipid peroxidation, Journal of Free Radicals in Biology & Medicine, 1 (1985) 87–95.

69. Girotti, A. W., Mechanisms of photosensitization, Photochemistry and Photobiology, 38 (1983) 745–51.

70. Girotti, A. W., Photosensitized oxidation of membrane lipids: reaction pathways, cytotoxic effects, and cytoprotective mechanisms, Journal of Photochemistry and Photobiology B: Biology, 63 (2001) 103–113.

71. Girotti, A. W., W. Korytowski, Cholesterol as a singlet oxygen detector in biological systems, Methods in Enzymology, 319 (2000) 85–100.

72. Glomm, W. R., Moses, S. J., Brennaman, M. K., Papanikolas, J. M., Franzen, S., Detection of adsorption of Ru(II) and Os(II) polypyridyl complexes on gold and silver nanoparticles by single-photon counting emission measurements, The Journal of Physical Chemistry B, 109 (2005) 804–810.

73. Gokulakrishnan, S., Parakh, P., Prakash, H., Photodegradation of methyl orange and photoinactivation of bacteria by visible light activation of persulphate using a tris(2,2'-bipyridyl)ruthenium(II) complex, Photochemical & Photobiological Sciences, 12 (2013) 456–466.

74. Gomes, M. C., Silva, S., Faustino, M. A. F., Neves, M. G. P. M. S., Almeida, A., Cavaleiro, J. A. S., Tome, J. P. C., Cunha, A., Cationic galactoporphyrin photosensitisers against UV-B resistant bacteria: oxidation of lipids and proteins by $^1O_2$, Photochemical & Photobiological Sciences, 12 (2013) 262–271.

75. Gonzalez-Serrano, E., Cordero, T., Rodriguez-Mirasol, J., Cotoruelo, L., Rodriguez, J. J., Removal of water pollutants with activated carbons prepared from H_3PO_4 activation of lignin from kraft black liquors, Water Research, 38 (2004) 3043–3050.

76. Gopal, K., Tripathy, S. S., Bersillon, J. L., Dubey, S. P., Chlorination byproducts, their toxicodynamics and removal from drinking water, Journal of Hazardous Materials, 140 (2007) 1–6.

77. Goss, C. A., Abruna, H. D., Spectral, electrochemical and electrocatalytic properties of 1,10-phenanthroline-5,6-dione complexes of transition metals, Inorganic Chemistry, 24 (1985) 4263–4267.

78. Greco, F., Vicent, M. J., Polymer-drug conjugates: current status and future trends, Frontiers in Bioscience, 13 (2008) 2744−2756.

79. Grueso, E., Alcantara, D., Martinez, J., Mancera, M., Penades, S., Sanchez, F., Pradogotor, R., Kinetic approach for the study of noncovalent interaction between $[Ru(NH_3)_5pz]^{2+}$ and gold nanoparticles, The Journal of Physical Chemistry A, 111 (2007) 9769–9774.

80. Grune, T., Klotz, L. O., Gieche, J., Rudeck, M., Sies, H., Protein oxidation and proteolysis by the nonradical oxidants singlet oxygen or peroxynitrite, Free Radical Biology and Medicine, 30 (2001) 1243–1253.

81. Guo, Y., Rogelj, S., Zhang, P., Rose bengal-decorated silica nanoparticles as photosensitizers for inactivation of Gram-positive bacteria, Nanotechnology, 21 (2010) 65102–65108.

82. Gupta. V. K., Carrott. P. J. M., Ribeiro Carrott. M. M. L., Suhas, Low-cost adsorbents: growing approach to wastewater treatment-a review, Critical Reviews in Environmental Science and Technology, 39 (2009) 783–842.

83. Gurzadyan, G. G., Gorner, H., Schulte-Frohlinde, D., Ultraviolet (193, 216 and 254 nm) photoinactivation of *Escherichia coli* strains with different repair deficiencies, Radiation Research, 141 (1995) 244–251.

84. Haas, K. L., Franz, K. J., Application of metal coordination chemistry to explore and manipulate cell biology, Chemical Reviews, 109 (2009) 4921–4960.

85. Hajipour, M. J., Fromm, K. M., Akbar Ashkarran, Jimenez de Aberasturi, A., D., Larramendi, I. R. d., Rojo, T., Serpooshan, V., Parak, W. J., Mahmoudi, M., Antibacterial properties of nanoparticles, Trends in Biotechnology, 30 (2012) 499–511.

86. Hamblin, M. R., Hasan, T., Photodynamic therapy: a new antimicrobial approach to infectious disease?, Photochemical & Photobiological Sciences, 3 (2004) 436–450.

87. Hamblin, M. R., Jori, G., Ed, Comprehensive series in photochemistry and photobiology–Volume 11, Photodynamic inactivation of microbial pathogens: medical and environmental applications, European Society for Photobiology 2011, Royal Society of Chemistry Publishing, 2011.

88. Hammarstroem, L., Johansson, O., Expanded bite angles in tridentate ligands. Improving the photophysical properties in bistridentate Ru^{II} polypyridine complexes, Coordination Chemistry Reviews, 254 (2010) 2546–2559.

89. Hareesh, P., Babitha, K. B., Shukla, S., Processing fly ash stabilized hydrogen titanate nano-sheets for industrial dye-removal application, Journal of Hazardous Materials, 229– 230 (2012) 177– 182.

90. Hashimoto, K., Hiramoto, M., Kajiwara, T., Sakata, T., Luminescence decays and spectra of $[Ru(bpy)_3]^{2+}$ adsorbed on TiO_2 *in vacuo* and in the presence of water vapour, The Journal of Physical Chemistry, 92 (1988) 4636–4640.

91. Henderson B. W., Miller A. C., Effects of scavengers of reactive oxygen and radical species on cell survival following photodynamic treatment *in vitro*: comparison to ionizing radiation, Radiation Research, 108 (1986) 196–205.

92. Hennig, H., Homogeneous photo catalysis by transition metal complexes, Coordination Chemistry Reviews, 182 (1999) 101–123.

93. Holt, K. B., Bard, A. J., Interaction of silver(I) ions with the respiratory chain of *Escherichia coli*: An electrochemical and scanning electrochemical microscopy study of the antimicrobial mechanism of micromolar Ag^+, Biochemistry, 44 (2005) 13214−13223.

94. Hu, C., Guo, J., Qu, J. H., Hu, X. X., Photocatalytic degradation of pathogenic bacteria with AgI/TiO_2 under visible light irradiation, Langmuir, 23 (2007) 4982–4987.

95. Hu, C., Lan, Y. Q., Qu, J. H., Hu, X. X., Wang, A. M., $Ag/AgBr/TiO_2$ visible light photocatalyst for destruction of azodyes and bacteria, The Journal of Physical Chemistry B, 110 (2006) 4066–4072.

96. Huang, L., Xuan, Y., Koide, Y., Zhiyentayev, T., Tanaka, M., Hamblin, M. R., Type I and type II mechanisms of antimicrobial photodynamic therapy: An *in vitro* study on Gram-negative and Gram-positive bacteria, Lasers in Surgery and Medicine, 44 (2012) 490–499.

97. Huang, T., Murray, R. W., Quenching of $[Ru(bpy)_3]^{2+}$ fluorescence by binding to Au nanoparticles, Langmuir, 18 (2002) 7077–7081.

98. Hunter, P. R., Household water treatment in developing countries: comparing different intervention types using meta-regression, Environmental Science & Technology, 43 (2009) 8991−8997.

99. Huo, Y. N., Bian, Z. F., Zhang, X. Y., Jin, Y., Zhu, J., Li, H. X., Highly active $TiO_{2-x}N_x$ visible photocatalyst prepared by N-doping in $Et_3N/EtOH$ fluid under supercritical conditions, The Journal of Physical Chemistry C, 112 (2008) 6546–6550.

100. Hussein, F. H., Alkhateeb, A. N., Photo-oxidation of benzyl alcohol under natural weathering conditions, Desalination, 209 (2007) 350–355.

101. Jablonski, A., Efficiency of anti-Stokes fluorescence in dyes, Nature, 131 (1933) 839–840.

102. Jain, J., Arora, S., Rajwade, J. M., Omray, P., Khandelwal, S., Paknikar, K. M., Silver nanoparticles in therapeutics: development of an antimicrobial gel formulation for topical use, Molecular Pharmaceutics, 6 (2009) 1388–1401.

103. Jimenez-Hernandez, M. E., Manjon, F., Garcia-Fresnadillo, D., Orellana, G., Solar water disinfection by singlet oxygen photogenerated with polymer-supported Ru(II) sensitizers, Solar Energy, 80 (2006) 1382–1387.

104. Jin, Z. L., Zhang, X. J., Li, Y. X., Li, S. B., Lu, G. X., 5.1% Apparent quantum efficiency for stable hydrogen generation over eosin-sensitized CuO/TiO_2 photocatalyst under visible light irradiation, Catalysis Communications, 8 (2007) 1267–1273.

105. Jin, Z. L., Zhang, X. J., Lu, G. X., Li, S. B., Improved quantum yield for photocatalytic hydrogen generation under visible light irradiation over eosin sensitized TiO_2—investigation of different noble metal loading, Journal of Molecular Catalysis A: Chemical, 259 (2006) 275–280.

106. Jose Ruben, M., Jose Luis, E., Alejandra, C., Katherine, H., Juan, B. K., Jose Tapia, R., Miguel Jose, Y., The bactericidal effect of silver nanoparticles, Nanotechnology, 16 (2005) 2346–2353.

107. Jusoh, A. bin, Cheng, W. H., Low, W. M., Noraaini, A., Megat, M. J., Mohd Noor, Study on the removal of iron and manganese in groundwater by granular activated carbon, Desalination, 182 (2005) 347–353.

108. Kannan, C., Sundaram, T., Palvannan, T., Environmentally stable adsorbent of tetrahedral silica and non-tetrahedral alumina for removal and recovery of malachite green dye from aqueous solution, Journal of Hazardous Materials, 157 (2008) 137–145

109. Kasaini, H., Goto, M., Furusaki, S., Selective separation of Pd(II), Rh(III), and Ru(III) ions from a mixed chloride solution using activated carbon pellets, Separation Science and Technology, 35 (2000) 1307–1327.

110. Kayser, H., Ueber die Verdichtung von Gasen an Oberflächen in ihrer Abhängigkeit von Druck und Temperatur, Annalen der Physik, 248 (1881) 526–537.

111. Kemper, K. E., Groundwater—from development to management, Hydrogeology Journal, 12 (2004) 3–5.

112. Khan, S. R., Huang, C. R., Bozzelli, J. W., Oxidation of 2-chlorophenol using ozone and ultraviolet radiation, Environmental Progress & Sustainable Energy, 4 (1985) 229–238.

113. Kim, D. S., Adsorption characteristics of Fe(III) and Fe(III) – NTA complex on granular activated carbon, Journal of Hazardous Materials, 106 (2004) 67–84.

114. Kniebühler, G., Pongratz, T., Betz, C. S., Göke, B., Sroka, R., Stepp, H., Schirra, J., Photodynamic therapy for cholangiocarcinoma using low dose mTHPC (Foscan(®)), Photodiagnosis and Photodynamic Therapy, 10 (2013) 220–228.

115. Kokura, S., Handa, O., Takagi, T., Ishikawa, T., Naito, Y., Yoshikawa, T., Silver nanoparticles as a safe preservative for use in cosmetics, Nanomedicine: Nanotechnology, Biology and Medicine, 6 (2010) 570–574.

116. Komagoe, K., Kato, H., Inoue, T., Katsu, T., Continuous real-time monitoring of cationic porphyrin-induced photodynamic inactivation of bacterial membrane functions using electrochemical sensors, Photochemical & Photobiological Sciences, 10 (2001) 1181–1188.

117. Kornblum, Z. C., Photochemistry, Encyclopedia Americana, Grolier online, 2010.

118. Kreibig, U., Vollmer, M., Optical properties of metal clusters, Springer Science & Business Media, 25, 1995.

119. Kuznetsova, N. A., Makarov, D. A., Kaliya, O. L., Vorozhtsov, G. N., Photosensitized oxidation by dioxygen as the base for drinking water disinfection, Journal of Hazardous Materials, 146 (2007) 487–491.

120. Lang, K., Schulte, K. W., Ruzicka, T., Fritsch, C., Aminolevulinic acid (Levulan) in photodynamic therapy of actinic keratoses, Skin Therapy Letters, 6 (2001) 1–2.

121. Laus, R., Costa, T. G., Szpoganicz, B., Favere, V. T., Adsorption and desorption of Cu(II), Cd(II) and Pb(II) ions using chitosan crosslinked with epichlorohydrin-triphosphate as the adsorbent, Journal of Hazardous Materials, 183 (2010) 233–241.

122. Lee, H. Y., Park, H. K., Lee, Y. M., Kim, K., Park, S. B., A practical procedure for producing silver nanocoated fabric and its antibacterial evaluation for biomedical applications, Chemical Communications, 28 (2007) 2959–2961.

123. Legrini, O., Oliveros, E., Braun, A. M., Photochemical processes for water treatment, Chemical Reviews, 93 (1993) 671–698.

124. Lei, W., Zhou, Q., Jiang, G., Zhang, B., Wang, X., Photodynamic inactivation of *Escherichia coli* by Ru(II) complexes, Photochemical & Photobiological Sciences, 10 (2011) 887–890.

125. Leung, J. W. C., Lau, G. T. C., Sung, J. J. Y., Costerton, J. W., Decreased bacterial adherence to silver-coated stent material: an *in vitro* study, Gastrointestinal Endoscopy, 38 (1992) 338–340.

126. Li, G. S., Yu, J. C., Zhang, D. Q., Hu, X. L., Lau, W. M., A mesoporous $TiO_{2-x}N_x$ photocatalyst prepared by sonication pretreatment and *in situ* pyrolysis, Separation and Purification Technology, 67 (2009) 152–157.

127. Li, J., Wang, X., Jiang, H., Lu, X., Zhub, Y., Chen, B., New strategy of photodynamic treatment of TiO_2 nanofibers combined with celastrol for HepG2 proliferation *in vitro*, Nanoscale, 3 (2011) 3115–3122.

128. Liu, F. T., Rabinovich, G. A., Galectins as modulators of tumour progression, Nature Reviews Cancer, 5 (2005) 29−41.

129. Loeb, S., Hofmann, R., Kim, J-H., Beyond the pipeline: assessing the efficiency limits of advanced technologies for solar water disinfection, Environmental Science & Technology Letters, 3 (2016) 73−80.

130. Lui, G. Y., Roser, D., Corkish, R., Ashbolt, N. J., Stuetz, R., Point-of-use water disinfection using ultraviolet and visible light-emitting diodes, Science of the Total Environment, 553 (2016) 626–635.

131. Ma, J., Jiang, L., Photogeneration of singlet oxygen ($^1O_2$) and free radicals (Sen$^{\bullet-}$, $O_2^{\bullet-}$) by tetrabrominated hypocrellin B derivative, Free Radical Research, 35 (2001) 767–77.

132. Maclean, M., MacGregor, S. J., Anderson, J. G., Woolsey, G., Inactivation of bacterial pathogens following exposure to light from a 405-nanometer light-emitting diode array, Applied and Environmental Microbiology, 75 (2009) 1932–1937.

133. Magaraggia, M., Coppellotti, O., Fabris, C., Guidolin, L., Jori, G., Inactivation of microbial pathogens by photosensitized processes: environmental applications, in Photodynamic inactivation of microbial pathogens: medical and environmental applications, ed. Hamblin, M. R., Jori, G., European Society for Photobiology 2011, Royal Society of Chemistry, 403–423.

134. Mahmoudi, M., Serpooshan, V., Silver-coated engineered magnetic nanoparticles are promising for the success in the fight against antibacterial resistance threat, ACS Nano, 6 (2012) 2656–2664.

135. Maisch, T., Bosl, C., Szeimies, R. M., Lehn, N., Abels, C., Photodynamic effects of novel XF porphyrin derivatives on prokaryotic and eukaryotic cells, Antimicrobial Agents and Chemotherapy, 49 (2005) 1542–1552.

136. Malik, Z., Ladan, H., Nitzan, Y., Photodynamic inactivation of Gram-negative bacteria: problems and possible solutions, Journal of Photochemistry and Photobiology B: Biology, 14 (1992) 262–266.

137. Manjon, F., Garcia-Fresnadillo, D., Orellana, G., Water disinfection with Ru(II) photosensitisers supported on ionic porous silicones, Photochemical & Photobiological Sciences, 8 (2009) 926–932.

138. Manjon, F., Santana-Magana, M., Garcia-Fresnadillo, D., Orellana, G., Singlet oxygen sensitizing materials based on porous silicone: photochemical characterization, effect of dye reloading and application to water disinfection with solar reactors, Photochemical & Photobiological Sciences, 9 (2010) 838–845.

139. Manjon, F., Villen, L., Garcia-Fresnadillo, D., Orellana, G., On the factors influencing the performance of solar reactors for water disinfection with

photosensitized singlet oxygen, Environmental Science & Technology, 42 (2008) 301–307.

140. Matés, J. M., Segura, J. A., Alonso, F. J., Marquez, J., Sulphur-containing non enzymatic antioxidants: therapeutic tools against cancer, Frontiers in Bioscience, 4 (2012) 722–748.

141. Meierhofer, R., Wegelin, M., Solar water disinfection: A guide for the application of SODIS; No. 06/02; SANDEC (Water & Sanitation in Developing Countries) at EAWAG (Swiss Federal Institute for Environmental Science and Technology): Duebendorf, Switzerland, 2002, 1−88.

142. Michaeli, A., Feitelson, J., Reactivity of singlet oxygen toward amino acids and peptides, Photochemistry and Photobiology, 59 (1994) 284–289.

143. Midden, W. R., Dahl, T. A., Biological inactivation by singlet oxygen: distinguishing $O_2(^1\Delta_g)$ and $O_2(^1\Sigma^+_g)$, Biochimica et Biophysica Acta, 1117 (1992) 216–222.

144. Milgrom, L. R., The colours of life, Oxford University Press: Oxford, 1997.

145. Mirjalili, M., Yaghmaei, N., Mirjalili, M., Antibacterial properties of nano silver finish cellulose fabric, Journal of Nanostructure in Chemistry, 3 (2013) 43–47.

146. Miyauchi, M., Ikezawa, A., Tobimatsu, H., Irie, H., Hashimoto, K., Zeta potential and photocatalytic activity of nitrogen doped TiO_2 thin films, Physical Chemistry Chemical Physics, 6 (2004) 865–870.

147. Mohan, D., Pittman Jr., C. U., Activated carbons and low cost adsorbents for remediation of tri- and hexavalent chromium from water, Journal of Hazardous Materials, 137 (2006) 762–811.

148. Montgomery, M. A., Elimelech, M., Water and sanitation in developing countries: including health in the equation, Environmental Science & Technology, 41 (2007) 17–24.

149. Moreno-Castilla, C., Adsorption of organic molecules from aqueous solutions on carbon materials, Carbon, 42 (2004) 83–94.

150. Mulazzani, Q. G., Sun, H., Hoffman, M. Z., Ford, W. E., Rodgers, M. A. J., Quenching of the excited states of ruthenium(II)-diimine complexes by oxygen, The Journal of Physical Chemistry, 98 (1994) 1145–1150.

151. Murata, A., Suenaga, H., Hideshima, S., Tanaka, Y., Kato, F., Hydroxyl radical as the reactive species in the inactivation of phages by ascorbic acid, Agricultural and Biological Chemistry, 50 (1986) 1481–1487.

152. Murphy, S., Huang, L., Kamat, P. V., Charge-transfer complexation and excited-state interactions in porphyrin-silver nanoparticle hybrid structures, The Journal of Physical Chemistry C, 115 (2011) 22761–22769.

153. Neyens, E., Baeyens, J., A review of classic Fenton's peroxidation as an advanced oxidation technique, Journal of Hazardous Materials, B98 (2003) 33–50.

154. Nikolaeva, I. A., Misharin, A. Y., Ponomarev, G. V., Timofeev, V. P., Tkachev, Y. V., Chlorin e6-cholesterol conjugate and its copper complex. Simple synthesis and entrapping in phospholipid vesicles, Bioorganic & Medicinal Chemistry Letters, 20 (2010) 2872−2875.

155. Nyman, E. S., Hynninen, P. H., Research advances in the use of tetrapyrrolic photosensitizers for photodynamic therapy, Journal of Photochemistry and Photobiology B: Biology, 73 (2004) 1–28.

156. Ogura, S., Yazaki, K., Yamaguchi, K., Kamachi, T., Okura, I., Localization of poly-L-lysine-photosensitizer conjugate in nucleus, Journal of Controlled Release, 103 (2005) 1−6.

157. Pallavicini, P., Taglietti, A., Dacarro, G., Diaz-Fernandez, Y. A., Galli, M., Grisoli, P., Patrini, M., De Magistris, G. S., Zanoni, R., Self-assembled monolayers of silver nanoparticles firmly grafted on glass surfaces: low Ag^+ release for an efficient antibacterial activity, Journal of Colloid and Interface Science, 350 (2010) 110–116.

158. Pandey, S. K., Zheng, X., Morgan, J., Purpurinimide carbohydrate conjugates: effect of the position of the carbohydrate moiety in photosensitizing efficacy, Molecular Pharmaceutics, 4 (2007) 448−464.

159. Paramonova, E., Zerfoss, E. L., Logan, B. E., Measurement of biocolloid collision efficiencies for granular activated carbon by use of a two-layer filtration model, Applied And Environmental Microbiology, 72 (2006) 5190–5196.

160. Pavoni, B., Drusian, D., Giacometti, A., Zanette, M., Assessment of organic chlorinated compound removal from aqueous matrices by adsorption on activated carbon, Water Research, 40 (2006) 3571–3579.

161. Peri, J. B., Hensley Jr., A. L., The surface structure of silica gel, The Journal of Physical Chemistry, 72 (1968) 2926–2933.

162. Perotti, C., Fukuda, H., Casas, A., Batlle, A. M. d. C., Scavengers protection of cells against ALA-based photodynamic therapy-induced damage, Lasers in Medical Science, 17 (2002) 222–229.

163. Pia Donzello, M., Viola, E., Giustini, M., Ercolani, C., Monacelli, F., Tetrakis(thiadiazole)porphyrazines. 8. Singlet oxygen production, fluorescence response and liposomal incorporation of tetrakis(thiadiazole)porphyrazine

macrocycles [TTDPzM] (M = $Mg^{II}(H_2O)$, Zn^{II}, $Al^{III}Cl$, $Ga^{III}Cl$, Cd^{II}, Cu^{II}, $2H^{I}$), Dalton Transactions, 41 (2012) 6112–6121.

164. Pignatello, J. J., Oliveros, E., MacKay, A., Advanced oxidation processes for organic contaminant destruction based on the Fenton reaction and related chemistry, Critical Reviews in Environmental Science and Technology, 36 (2006) 1–84.

165. Polo, L., Valduga, G., Jori, G., Reddi, E., Low-density lipoprotein receptors in the uptake of tumour photosensitizers by human and rat transformed fibroblasts, The International Journal of Biochemistry & Cell Biology, 34 (2002) 10−23.

166. Pramod, P., Sudeep, P. K., George Thomas, K., Kamat, P. V., Photochemistry of ruthenium trisbipyridine functionalized on gold nanoparticles, The Journal of Physical Chemistry B Letters, 110 (2006) 20737-20741.

167. Prat, C., Vicente, M., Esplugas, S., Ozone and ozone/UV decolorization of bleaching waters of the paper industry, Industrial & Engineering Chemistry Research, 29 (1990) 349–355.

168. Ragas, X., Sanchez-Garcia, D., Ruiz-Gonzalez, R., Dai, T., Agut, M., Hamblin, M. R., Nonell, S., Cationic porphycenes as potential photosensitizers for antimicrobial photodynamic therapy, Journal of Medicinal Chemistry, 53 (2010) 7796–7803.

169. Ravanat, J. L., Cadet, J., Reaction of singlet oxygen with 2′-deoxyguanosine and DNA. Isolation and characterization of the main oxidation products, Chemical Research in Toxicology, 8 (1995) 379–88.

170. Ravanat, J.-L., Mascio, P. Di, Martinez, G. R., Medeiros, M. H. G., Cadet, J., Singlet oxygen induces oxidation of cellular DNA, Journal of Biological Chemistry, 275 (2000) 40601–40604.

171. Reiter R., Tsan D., Osuna C., Gitto E., Actions of melatonin in the reduction of oxidative stress: a review, Journal of Biomedical Science, 7 (2000) 444–458.

172. Rengifo-Herrera, J. A., Mielczarski, E., Mielczarski, J., Castillo, N. C., Kiwi, J., Pulgarin, C., *Escherichia coli* inactivation by N, S co-doped commercial TiO_2 powders under UV and visible light, Applied Catalysis B: Environmental, 84 (2008) 448–456.

173. Rengifo-Herrera, J. A., Sanabria, J., Machuca, F., Dierolf, C. F., Pulgarin, C., Orellana, G., A comparison of solar photocatalytic inactivation of waterborne *E. coli* using Tris (2,2'-bipyridine)ruthenium(II), rose bengal, and TiO_2, Journal of Solar Energy Engineering, 129 (2007) 135–140.

174. Repo, E., Kurniawan, T. A., Warchol, J. K., Sillanpaa, M. E. T., Removal of Co(II) and Ni(II) ions from contaminated water using silica gel functionalized with

EDTA and/or DTPA as chelating agents, Journal of Hazardous Materials, 171 (2009) 1071–1080.

175. Rezzoug, H., Bezdetnaya, L., A'amar, O., Merlin, J. L., Guillemin, F., Parameters affecting photodynamic activity of Foscan® or Meta-tetra(hydroxyphenyl)chlorin (mTHPC) *in vitro* and *in vivo*, Lasers in Medical Science, 13 (1998)119–125.

176. Rivera-Utrilla, J., Bautista-Toledo, I., Ferro-Garcia, M. A., Moreno-Castilla, C., Activated carbon surface modifications by adsorption of bacteria and their effect on aqueous lead adsorption, Journal of Chemical Technology and Biotechnology, 76 (2001) 1209–1215.

177. Roe, D., Karandikar, B., Bonn-Savage, N., Gibbins, B., Roullet, J.-B., Antimicrobial surface functionalization of plastic catheters by silver nanoparticles. Journal of Antimicrobial Chemotherapy, 61 (2008) 869–876.

178. Rohatgi–Mukherjee, K. K., Fundamentals of photochemistry: Wiley Eastern Limited, revised edition, 1986.

179. Sakthivel, S., Janczarek, M., Kisch, H., Visible light activity and photoelectrochemical properties of nitrogen-doped TiO_2, The Journal of Physical Chemistry B, 108 (2004) 19384–19387.

180. Salmi, C., Loncle, C., Vidal, N., Letourneux, Y., Fantini, J., Maresca, M., Taieb, N., Pages, J.-M., Brunel, J. M., Squalamine: an appropriate strategy against the emergence of multidrug resistant Gram-negative bacteria?, PLoS ONE, 3 (2008) e2765.

181. Schäfer, M., Schmitz, C., Facius, R., Horneck, G., Milow, B., Funken, K. H., Ortner, J., Systematic study of parameters influencing the action of rose bengal with visible light on bacterial cells: comparison between the biological effect and singlet-oxygen production, Photochemistry and Photobiology, 71 (2000) 514–523.

182. Shadidi, M., Sioud, M., Selective targeting of cancer cells using synthetic peptides, Drug Resistance Updates, 6 (2003) 363−371.

183. Shannon, M. A., Bohn, P. W., Elimelech, M., Georgiadis, J. G., Marinas, B. J., Mayes, A. M., Science and technology for water purification in the coming decades, Nature, 452 (2008) 301–310.

184. Silver, S., Phung, L. T., Bacterial heavy metal resistance: new surprises, Annual Review of Microbiology, 50 (1996) 753–789.

185. Singh, S., Patel, P., Jaiswal, S., Prabhune, A. A., Ramana, C. V., Prasad, B. L. V., A direct method for the preparation of glycolipid–metal nanoparticle conjugates: sophorolipids as reducing and capping agents for the synthesis of water re-dispersible silver nanoparticles and their antibacterial activity, New Journal of Chemistry, 33 (2009) 646–652.

186. Sioi, M., Bolosis, A., Kostopoulou, E., Poulios, I., Photocatalytic treatment of coloured wastewater from medical laboratories, Journal of Photochemistry and Photobiology B: Biology, 184 (2006) 18–25.

187. Smith, A. P., Fraser, C. L., "Bipyridine ligands" in Comprehensive Coordination Chemistry II, 2003, 1–23.

188. Sondi, I., Salopek-Sondi, B., Silver nanoparticles as antimicrobial agent: a case study on *E. coli* as a model for Gram-negative bacteria, Journal of Colloid and Interface Science, 275 (2004) 177–182.

189. Song, Y. Z., An, J., Jiang, L., ESR evidence of the photogeneration of free radicals (GDHB*, O_2*) and singlet oxygen ($^1O_2$) by 15-deacetyl-13-glycine-substituted hypocrellin B, Biochimica et Biophysica Acta, 1472 (1999) 307–313.

190. Soukos, N. S., Ximenez-Fyvie, L. A., Hamblin, M. R., Socransky, S. S., Hasan, T., Targeted antimicrobial photochemotherapy, Antimicrobial Agents and Chemotherapy, 42 (1998) 2595–2601.

191. Sperandio, F. F., Huang, Y. Y., Hamblin, M. R., Antimicrobial photodynamic therapy to kill Gram-negative bacteria, Recent Patents on Anti-Infective Drug Discovery, 8 (2013) 108–120.

192. Spesia, M. B., Caminos, D. A., Pons, P., Durantini, E. N., Mechanistic insight of the photodynamic inactivation of *Escherichia coli* by a tetracationic zinc(II) phthalocyanine derivative, Photodiagnosis and Photodynamic Therapy, 6 (2009) 52–61.

193. St. Denis, T. G., Dai, T., Izikson, L., Astrakas, C., Anderson, R. R., Hamblin, M. R., Tegos, G. P., All you need is light, Antimicrobial photoinactivation as an evolving and emerging discovery strategy against infectious disease, Virulence, 2 (2011) 509–520.

194. Stark, G., Functional consequences of oxidative membrane damage, The Journal of Membrane Biology, 205 (2005) 1–16.

195. Stefflova, K., Li, H., Chen, J., Zheng, G., Peptide-based pharmacomodulation of a cancer-targeted optical imaging and photodynamic therapy agent, Bioconjugate Chemistry, 18 (2007) 379−388.

196. Stochel, G., Brindell, M., Macyk, W., Stasicka, Z., Szacilowski, K., Bioinorganic photochemistry, John Wiley & Sons Ltd., 2009.

197. Stochel, G., Wanat, A., Kulis, E., Stasicka, Z., Light and metal complexes in medicine, Coordination Chemistry Reviews, 171 (1998) 203–220.

198. Suppan, P., Chemistry and light, Royal Chemical Society: Cambridge, 1994.

199. Sykora, J., Sima, J., Photochemistry of coordination compounds, Coordination Chemistry Reviews, 107 (1990) 1–212.

200. Szaciłowski, K., Macyk, W., Drzewiecka-Matuszek, A., Brindell, M., Stochel, G., Bioinorganic photochemistry: frontiers and mechanisms, Chemical Reviews, 105 (2005) 2647–2694.

201. Szewzyk, U., Szewzyk, R., Manz, W., Schleifer, K. H., Microbiological safety of drinking water, Annual Review of Microbiology, 54 (2000) 81–127.

202. Taglietti, A., Diaz Fernandez, Y. A., Amato, E., Cucca, L., Dacarro, G., Grisoli, P., Necchi, V., Pallavicini, P., Pasotti, L., Patrini, M., Antibacterial activity of glutathione-coated silver nanoparticles against Gram-positive and Gram-negative bacteria, Langmuir, 28 (2012) 8140–8148.

203. Tarragó-Trani, M. T., Jiang, S., Harich, K. C., Storrie, B., Shiga-like toxin subunit B (SLTB)-enhanced delivery of chlorin e6 (Ce6) improves cell killing, Photochemistry and Photobiology, 82 (2006) 527−537.

204. Tavares, A., Dias, S. R., Carvalho, C. M., Faustino, M. A., Tome, J. P., Neves, M. G., Tome, A. C., Cavaleiro, J. A., Cunha, A., Gomes, N. C., Alves, E., Almeida, A., Mechanisms of photodynamic inactivation of a Gram-negative recombinant bioluminescent bacterium by cationic porphyrins, Photochemical & Photobiological Sciences, 10 (2011) 1659–1669.

205. Taylor, M. J., Richardson, T., Antioxidant activity of cysteine and protein sulfydryls in a linoleate emulsion oxidized by hemoglobin, Journal of Food Science, 45 (1980) 1223–1227.

206. Thanh, N. V. K., Phong, N. T. P., Investigation of antibacterial activity of cotton fabric incorporating nano silver colloid, Journal of Physics: Conference Series, 187 (2009) 012072–012078.

207. Tijerina, M., Kopecková, P., Kopecek, J., Correlation of subcellular compartmentalization of HPMA copolymer-Mce6 conjugates with chemotherapeutic activity in human ovarian carcinoma cells, Pharmaceutical Research, 20 (2003) 728−737.

208. Tomas, C. R., Wastewater engineering and treatment: problems and solutions, in Chemical Engineering Techniques in Biotechnology, ed. M. A. Winkler, Elsevier, Amsterdam, 1990, 23–94.

209. Tuan, T. Q., Son, N. V., Dung, H. T. K., Luong, N. H., Thuy, B. T., Thi, N., Anh, V., Hoa, N. D., Hai, N. H., Preparation and properties of silver nanoparticles loaded in activated carbon for biological and environmental applications, Journal of Hazardous Materials, 192 (2011) 1321– 1329.

210. Turro, N. J., Ramamurthy, V., Scaiano, J. C., Principles of molecular photochemistry: an introduction, University Science Books, 2009.

211. Urano, K., Yamamoto, E., Tonegawa, M., Fujie, K., Adsorption of chlorinated organic compounds on activated carbon from water, Water Research, 25 (1991) 1459–1464.

212. Varghese, S., Elfakhri, S., Sheel, D. W., Sheel, P., Bolton, F. J., Foster, H. A., Novel antibacterial silver-silica surface coatings prepared by chemical vapour deposition for infection control, Journal of Applied Microbiology, 115 (2013) 1107–1116.

213. Villen, L., Manjon, F., Garcia-Fresnadillo, D., Orellana, G., Solar water disinfection by photocatalytic singlet oxygen production in heterogeneous medium, Applied Catalysis B, 69 (2006) 1–9.

214. Vrouenraets, M. B., Visser, G. W., Loup, C., Targeting of a hydrophilic photosensitizer by use of internalizing monoclonal antibodies: a new possibility for use in photodynamic therapy, International Journal of Cancer, 88 (2000) 108−114.

215. Wachowska, M., Muchowicz, A., Firczuk, M., Gabrysiak, M., Winiarska, M., Wańczyk, M., Bojarczuk, K., Golab, J., Aminolevulinic acid (ALA) as a prodrug in photodynamic therapy of cancer, Molecules, 16 (2011) 4140–4164.

216. Wainwright, M., Photodynamic antimicrobial chemotherapy (PACT). Journal of Antimicrobial Chemotherapy, 42 (1998) 13–28.

217. Wainwright, M., Photosensitisers in biomedicine, Wiley-Blackwell, John Wiley & Sons Ltd., 2009.

218. Wan, M. T., Lin, J. Y., Current evidence and applications of photodynamic therapy in dermatology, Clinical, Cosmetic and Investigational Dermatology, 7 (2014) 145–163.

219. Wang, L., Luo, J., Shan, S., Crew, E., Yin, J., Zhong, C.-J., Wallek, B., Wong, S. S. S., Bacterial inactivation using silver-coated magnetic nanoparticles as functional antimicrobial agents, Analytical Chemistry, 83 (2011) 8688–8695.

220. Wang, M., Xu, L., Peng, J., Zhai, M., Li, J., Wei, G., Adsorption and desorption of Sr(II) ions in the gels based on polysaccharide derivates, Journal of Hazardous Materials, 171 (2009) 820–826.

221. Wang, P., Huang, B. B., Qin, X. Y., Zhang, X. Y., Dai, Y., Whangbo, M. H., Ag/AgBr/WO$_3$·H$_2$O: visible-light photocatalyst for bacteria destruction, Inorganic Chemistry, 48 (2009) 10697−10702.

222. Weber, Jr., W. J., Pirbazari, M., Melson, G. L., Biological growth on activated carbon: an investigation by scanning electron microscopy, Environment Science & Technology, 12 (1978) 817–819.

223. Weber, W. J., Distributed optimal technology networks: a concept and strategy for potable water sustainability, Water Science and Technology, 46 (2002) 241–246.

224. Wigginton, N. S., De Titta, A., Piccapietra, F., Dobias, J., Neasatyy, V. J., Suter, M. J. F., Bernier-Latmani, R., Binding of silver nanoparticles to bacterial proteins depends on surface modifications and inhibits enzymatic activity, Environmental Science and Technology, 44 (2010) 2163–2168.

225. Winter, S., Tortik, N., Kubin, A., Krammer, B., Plaetzer, K., Back to the roots: photodynamic inactivation of bacteria based on water-soluble curcumin bound to polyvinylpyrrolidone as a photosensitizer, Photochemical & Photobiological Sciences, 12 (2013) 1795–1802.

226. Wolken, J. J., Light and life processes, Van Nostrand Reinhold Co.: New York, 1998.

227. Wu, J., Hou, S. Y., Ren, D. C., Mather, P. T., Antimicrobial properties of nanostructured hydrogel webs containing silver, Biomacromolecules, 10 (2009) 2686−2693.

228. Wu, P. G., Xie, R. C., Shang, J. K., Enhanced visible-light photocatalytic disinfection of bacterial spores by palladium-modified nitrogen-doped titanium oxide, Journal of the American Ceramic Society, 91 (2008) 2957−2962.

229. Yao, K. S., Cheng, T. C., Li, S. J., Yang, L. Y., Tzeng, K. C., Chang, C. Y., Ko, Y., Comparison of photocatalytic activities of various dye-modified TiO_2 thin films under visible light, Surface and Coatings Technology, 203 (2008) 922−924.

230. Yao, K. S., Wang, D. Y., Chang, C. Y., Weng, K. W., Yang, L. Y., Lee, S. J., Cheng, T. C., Hwang, C. C., Photocatalytic disinfection of phytopathogenic bacteria by dye-sensitized TiO_2 thin film activated by visible light, Surface and Coatings Technology, 202 (2007) 1329−1332.

231. Yavin, E., Stemp, E. D. A., Weiner, L., Sagi, I., Arad-Yellin, R., Shanzer, A., Direct photo-induced DNA strand scission by a ruthenium bipyridyl complex, Journal of Inorganic Biochemistry, 98 (2004) 1750–1756.

232. Yin, R., Dai, T., Avci, P., Jorge, A. E. S., de Melo, W. C., Vecchio, D., Huang, Y-Y, Gupta, A., Hamblin, M. R., Light based anti-infectives: ultraviolet C irradiation, photodynamic therapy, blue light, and beyond, Current Opinion in Pharmacology, 13 (2013) 731–762.

233. Yoon, I., Li, J. Z., Shim, Y. K., Advance in photosensitizers and light delivery for photodynamic therapy, Clinical Endoscopy, 46 (2013) 7−23.

234. Youji, L. I., Mingyuan, M. A., Xiaohu, W., Xiaohua, W., Inactivated properties of activated carbon-supported TiO_2 nanoparticles for bacteria and kinetic study, Journal of Environmental Sciences, 20 (2008) 1527–1533.

235. Yu, J. C., Ho, W. K., Yu, J. G., Yip, H., Wong, P. K., Zhao, J. C., Efficient visible-light-induced photocatalytic disinfection on sulfur-doped nanocrystalline titania, Environmental Science & Technology, 39 (2005) 1175−1179.

236. Zaporozhets, O., Gawer, O., Sukhan, V., The interaction of Fe (II), Cu (II) and Ag (I) ions and their complexes with 1,10-phenanthroline adsorbed on silica gel, Colloids and Surfaces A, 147 (1999) 273–281.

237. Zhang, D., Li, G., Yu, J. C., Inorganic materials for photocatalytic water disinfection, Journal of Materials Chemistry, 20 (2010) 4529–4536.

238. Zhang, M., Zhang, Z., Blessington, D., Pyropheophorbide 2-deoxyglucosamide: a new photosensitizer targeting glucose transporters, Bioconjugate Chemistry, 14 (2003) 709−714.

239. Zheng, G., Li, H., Zhang, M., Lund-Katz, S., Chance, B., Glickson, J. D., Low density lipoprotein reconstituted by pyropheophorbide cholesteryl oleate as target-specific photosensitizer, Bioconjugate Chemistry, 13 (2002) 392−396.

240. Zheng, X., Morgan, J., Pandey, S. K., Conjugation of 2-(1'-hexyloxyethyl)-2-devinylpyropheophorbide-a (HPPH) to carbohydrates changes its subcellular distribution and enhances photodynamic activity *in vivo*, Journal of Medicinal Chemistry, 52 (2009) 4306−4318.

241. Zheng, X., Pandey, R. K., Porphyrin-carbohydrate conjugates: impact of carbohydrate moieties in photodynamic therapy (PDT), Anti-Cancer Agents in Medicinal Chemistry, 8 (2008) 241−268.

242. Zhou, Q.-X., Lei, W.-H., Chen, J.-R., Li, C., Hou, Y.-J., Wang, X.-S., Zhang, B.-W., A new heteroleptic ruthenium(II) polypyridyl complex with long wavelength absorption and high-singlet oxygen quantum yield, Chemistry - A European Journal, 16 (2010) 3157–3165.

243. Zhou, Q.-X., Lei, W.-H., Sun, Y., Chen, J.-R., Li, C., Hou, Y.-J., Wang, X.-S., Zhang, B.-W., $[Ru(bpy)_{3-n}(dpb)_n]^{2+}$: Unusual photophysical property and efficient DNA photocleavage activity, Inorganic Chemistry, 49 (2010) 4729–4731.

List of publications

1. **P. Parakh**, S. Gokulakrishnan, H. Prakash, Visible light water disinfection using $[Ru(bpy)_2(phendione)](PF_6)_2.2H_2O$ and $[Ru(phendione)_3]Cl_2.2H_2O$ complexes and their effective adsorption onto activated carbon, Sep. Purif. Technol. 109 (2013) 9–17. Impact Factor: 3.299, Citations: 6

2. S. Gokulakrishnan, **P. Parakh**, H. Prakash, Photodegradation of methyl orange and photoinactivation of bacteria by visible light activation of persulphate using tris(2,2′-bipyridyl)ruthenium(II) complex, Photochem. Photobiol. Sci. 12 (2013) 456–466. Cover page article. Impact Factor: 2.267, Citations: 11

3. S. Gokulakrishnan, **P. Parakh**, H. Prakash, Degradation of Malachite green by Potassium persulphate, its enhancement by 1,8-dimethyl-1,3,6,8,10,13-hexaazacyclotetradecane nickel(II) perchlorate complex, and removal of antibacterial activity, J. Hazard. Mater. 213– 214 (2012) 19– 27. Impact Factor: 4.836, Citations: 23

Communicated

1. Manu Jose, P.T. Aswathy, K. Sriram, **P. Parakh**, H. Prakash, S. Shukla, Ion-exchange bonded $H_2Ti_3O_7$ nanosheets-based magnetic nanocomposite for dye removal via adsorption and its regeneration via synergistic activation of persulfate. RSC Advances. Communicated, (under revision) RA-ART-06-2016-014902. Impact Factor: 3.289

Manuscripts under progress

1. **P. Parakh**, S. Gokulakrishnan, H. Prakash, Ruthenium tris (polypyridine)-glutathione capped silver nanoparticle hybrid systems for effective visible light driven inactivation of bacteria.

2. **P. Parakh**, J. S. Chauhan, R. Tulasi, Manu Jose, S. Shukla, H. Prakash, Heterogenized methylene blue on hydrogen titanate nanosheets as effective visible light active photosensitizer for water disinfection.

3. **P. Parakh**, H. Prakash, Water disinfection using visible light active molecular systems. A review.

Patents filed

1. **P. Parakh**, H. Prakash, S. Gokulakrishnan, P. Panzade, A bactericidal composition and a method for disinfecting water under visible light irradiation. Indian patent filed. Application no.: 201611017381. Date: 18th May, 2016.

Posters presented

1. "Visible light inactivation of bacteria by Ruthenium(II) polypyridyl complexes and effective removal of complexes by activated carbon", **P. Parakh,** S. Gokulakrishnan, H. Prakash, IISc Bangalore – 1st best poster prize.

2. "Visible light inactivation of bacteria by Ruthenium(II) polypyridyl complexes and effective removal of complexes by environment friendly adsorbents", **P. Parakh,** S. Gokulakrishnan, H. Prakash, at "ICAOP – 2012" at School Of Environmental Sciences, Mahatma Gandhi University, Kottayam – 2nd best poster prize.

Other posters presented

1. "Visible light inactivation of bacteria by activation of persulphate with [Ru(bpy)3]2+ complex", S. Gokulakrishnan, **P. Parakh,** H. Prakash, IISc Bangalore.

2. "Visible light activation of persulphate with [Ru(bpy)3]2+ complex: Degradation of organic pollutant and Inactivation of bacteria", S. Gokulakrishnan, **P. Parakh,** H. Prakash, Mahatma Gandhi University, Kottayam.

3. "Degradation of Malachite green by Potassium persulphate, its enhancement by 1,8-dimethyl-1,3,6,8,10,13-hexaazacyclotetradecane nickel(II) perchlorate complex and removal of antibacterial activity", S. Gokulakrishnan, **P. Parakh,** H. Prakash, at RAIC – 2012", Bharathidasan University, Tiruchirappalli – 1st best poster prize.

Conferences and workshops attended

1. "DBT BIRAC workshop on bio-entrepreneurship, grant-writing & intellectual property management" at BITS Pilani, K K Birla Goa Campus, February, 2016.

2. National Conference on "New Frontiers in Chemistry – From Fundamentals to Applications (NFCFA) – 2015" at BITS-Pilani, K K Birla Goa Campus, Goa

3. "Workshop on Intellectual Property Rights (IPR) Management" at BITS Pilani, K K Birla Goa Campus, March, 2015.

4. "International Workshop on Indo–UK perspective on Water Quality: Threats, Technologies and Options-2013" at IISc Bangalore JN TATA Auditorium Seminar Hall.

5. "Emerging Technologies: Micro To Nano (ETMN) – 2013" at BITS-Pilani, K K Birla Goa Campus, Goa.

6. "Second International Conference on Advanced Oxidation Processes (ICAOP) – 2012" at School of Environmental Sciences, Mahatma Gandhi University, Kottayam.

7. "Recent Advances in Inorganic Chemistry (RAIC) – 2012" at Bharathidasan University, Tiruchirappalli.

Brief Biography of the Candidate

Name   Miss Priyadarshini Parakh

Date of birth 1st May 1985

e-mail   parakhpriya85@gmail.com,

              p2010016@ @goa.bits-pilani.ac.in

Experience:

1. CSIR JRF-SRF at BITS, Pilani, K. K. Birla Goa Campus, Goa. 2010-2015, working on "Investigation on effects of metallo-peptides and complexes on microbes, DNA and environmentally persistent compounds".

2. Institute SRF at BITS, Pilani, K. K. Birla Goa Campus, Goa. 2015-2016.

Education:

Examination	Name of Examination	University / Board	Year
Master's Degree	M.Sc. (Biotechnology)	Jai Narain Vyas University, Jodhpur (Raj.)	2009
Exams Qualified	**CSIR NET LS** December 2009 **GATE 2010** (BT) Score 273 **Rajasthan State Eligibility Test** for Lectureship 2010 **CSIR JRF** June 2009 **CSIR NET LS** December 2008		
Bachelor's Degree	B.Sc. (Biotechnolgy, Botany and Zoology)	Jai Narain Vyas University, Jodhpur (Raj.)	2007
Other qualifications	7.00x: Introduction to Biology - The Secret of Life	MITx	2013
	"O" level Computer qualification "Business Professional Programmer"	DOEACC Society	2006

Research Publications: 03 Papers, 01 Patent filed.

Brief Biography of Ph. D Supervisor

Name: Prof. Halan Prakash
Associate Professor,
Department of Chemistry, BITS, Pilani K K Birla Goa Campus
E-mail: halanprakash@goa.bits-pilani.ac.in
Phone: +91-832-2580344

Education:

Master's degree (M.Sc., Chemistry) in 1997 from Bharathiar University, India
Ph.D. (Chemistry) in 2003, Department of Inorganic Chemistry and National Centre for Ultrafast Processes at the University of Madras

Postdoctoral Experience:

2006 Kyoto Pharmaceutical University and NAIST, Japan (JSPS fellowship)
2003-2005 - Tata Institute of Fundamental Research (TIFR), India.

No. of Sponsored Research Projects:

Completed: RGYI DBT (Department of Biotechnology), India, ABG (Aditya Birla Group) project, India

Honours and Awards:

Excellence in analytical chemistry (EACH), Visiting scholar, University of Tartu, Estonia, Erasmus Program, EU, 2016.
NAIST young scientist visiting fellowship, 2011
JSPS fellowship, 2006

Publications:

20 research papers, and presented work in more than 30 conferences (international and national). Received more than 200 citations, and published work as cover article in prestigious Photochemical and Photobiological Sciences, Royal Society of Chemistry.

Membership:

Member of Royal Society of Chemistry, UK, and Executive member of Society for Environmental Chemistry and Allied Sciences (SECAS), India, Indian Institute of Metals.

Reviewer for International Journals:

Reviewer for over 10 reputed journals, and received appreciation as an active reviewer from Royal Society of Chemistry, UK.

No. of PhD Students:

Guided one as supervisor, one as co-supervisor, and guiding one student as supervisor at BITS, Pilani K K Birla Goa Campus.